PART I: A CONTRIBUTION TO THE STUDY OF THE SEISMICITY OF SOUTHERN CALIFORNIA

PART II: INVERSION OF PHASE TIMES FOR HYPOCENTERS AND SHALLOW CRUSTAL VELOCITIES

Thesis by

James Alan Hileman

In Partial Fulfillment of the Requirements

for the Degree of

Doctor of Philosophy

California Institute of Technology

Pasadena, California

1978

(Submitted June 17, 1977)

ACKNOWLEDGMENTS

The work presented in this thesis was made possible by the faculty, students, and staff of the Seismological Laboratory. They have provided a stimulating environment in which to work and pursue topics of interest. I gratefully acknowledge their guidance, discussions, and constructive criticisms that contributed to this work.

Dr. Clarence Allen contributed greatly to my understanding of the seismicity topics discussed in Part I. I have enjoyed this association and learned much from him.

Dr. Bernard Minster suggested the inversion problem developed in Part II. Both he and Dr. Don Anderson provided much helpful guidance. Dr. Gary Fuis furnished data for the Galway Lake earthquakes.

The manuscript was typed with patience by Mrs. Marla Turner. Mr. Lazlo Lenches coordinated the preparation of the figures.

The seismicity data presented here are available because of the collective efforts of the staff of the Seismological Laboratory for over forty years. Significant support for this work has come from the National Science Foundation, U.S. Geological Survey, National Ocean and Atmospheric Administration, U.S. Navy, U.S. Air Force, Nuclear Regulatory Commission, California Division of Mines and Geology, California Department of Water Resources, and Western Oil and Gas Association. In addition, the Caltech Earthquake Research Affiliates, a group of private sponsors, has contributed markedly to the Laboratory's program since 1952.

The research reported here has been supported primarily by a

U.S. Geological Survey contract (14-08-0001-16603), Support of Southern California Seismic Arrays. A grant from Achievement Rewards for College Scientists is also gratefully acknowledged.

ABSTRACT

Southern California seismicity data for the period 1932 through 1975 are summarized in a series of epicenter maps. These maps show the seismic activity for one-year periods, for five-year periods, and as summaries for all earthquakes with magnitudes equal to or greater than 4, 5, and 6 respectively. Enlarged epicenter maps are given for the Los Angeles area and for the more significant aftershock sequences in the region.

A regional value of $b = 1.00 \pm .02$ ($\log N = a - bM$) is found for forty years of data. For several smaller areas in the region, b-values have a range of 0.76 - 1.00. Temporal variations of b-values (maximum likelihood estimates) for the various areas studied do not show any strong correlation with the occurence of large earthquakes. A slight increase of the regional b-value after the 1952 Kern County earthquake is suggested.

Seismicity in the Imperial Valley indicates that several faults there are susceptible to triggering, i.e. they are loosely coupled to motions of neighboring faults. Some earthquake swarms indicate this ease of triggering. A survey of the high level of swarm activity in the Imperial Valley is given. Two unusual aftershock sequences with periodic activity are described because the periodicity suggests sensitivity to some triggering phenomenon.

Some seismicity in Southern California seems to be aligned in weakly defined zones that are transverse to the general tectonic fabric. These zones are thought to reflect conditions in the lower crust or

uppermost mantle. The cause of these zones is unknown, but their trends are similar to those for the early Paleozoic continental boundary and to a recently discovered upper-mantle velocity anomaly.

Depth is usually the least-certain hypocenter parameter because it depends critically upon the accuracy of the velocity model. With enough arrival-time data, velocity estimation is feasible in addition to the usual hypocenter determinations. Linear least-squares inversion theory is adapted for the simultaneous determination of hypocenters and local velocity structure. A maximum likelihood formulation is used so that the data are weighted according to their estimated variances. A tradeoff parameter controls the relative importance of the RMS error and the amount by which the model is changed at each iteration. The inversion is also stabilized by specifying the allowed variances of each of the model parameters.

Arrival times for a set of 20 earthquakes in the central Mojave Desert were inverted to improve the local velocity model. Each of the trials indicated that shallow crustal velocities in the vicinity of Galway Lake are somewhat lower than those of the usual velocity models. The velocities were not strongly constrained by this data set. This study points out the need for several seismographic stations placed within an aftershock area for best control of velocity estimates.

TABLE OF CONTENTS

PART I.

A CONTRIBUTION TO THE STUDY OF THE SEISMICITY OF SOUTHERN CALIFORNIA

INTRODUCTION TO PART I

Studies of regional seismicity are necessarily continuing studies. Passing time may provide additional data for areas known incompletely, and advances in theory may invite reassessment of the entire seismicity record. Also, the seismic character of "well-known" areas can change with time. Our understanding of Southern California seismicity has been influenced repeatedly by new data and improved theory.

In Southern California, every historic earthquake of magnitude 6 and above has occurred in a location different from those of earlier historic events with only a few exceptions. We have yet to observe these larger earthquakes repeating along the same extent of rupture, except near Parkfield. Therefore it seems likely that most of the large earthquakes in Southern California, for at least the near future, will also occur in new locations. In the light of our current understanding of the seismicity and tectonics of Southern California, past earthquakes of moderate and larger magnitudes have occurred in geologically reasonable locations. One prime value of ongoing seismicity studies is to aid in identifying those areas which are also reasonable for future earthquakes and in assessing the potential seismic hazard for particular areas of interest because of engineering projects. Seismicity studies are equally important in contributing to our fundamental understanding of earthquake processes. These practical and theoretical aspects are often intimately related and the justification of a particular study may depend upon one's viewpoint at a given time.

Strong earthquakes in Southern California were noted by the early Spanish soldiers and missionaries. Four "violent" shocks with estimated Rossi-Forel intensities of VIII-X and numerous aftershocks which shook the Los Angeles region in July of 1769 are the earliest recorded earthquakes (Townley and Allen, 1939).

> "Friday, July 28 ... At this place we experienced a terrible earthquake which was repeated four times during the day. The first vibration or shock occurred at one o'clock in the afternoon, and was most violent; the last took place at about half-past four. ... To this place we gave the name Rio de Los Temblores." [Probably San Pedro Bay] (Wood, 1916)

Although official records, newspapers and personal diaries of the Spanish colonialists and the later American settlers record numerous accounts of shocks, the first systematic listing of seismic activity was a brief pamphlet by Edward S. Holden in 1887, "List of Recorded Earthquakes in California, Lower California, Oregon and Washington Territory". Subsequent records have become more and more accurate in fully describing the seismic activity of this region.

Holden was associated with the Lick Observatory at Mt. Hamilton in Central California, where a seismograph was set up in 1887. Interestingly, California's first seismographic instrument was not installed for the purpose of studying earthquakes but to monitor shocks that might affect the delicate adjustments of the observatory's astronomical instruments.

Holden continued to gather earthquake reports and in 1898 published a "Catalog of Earthquakes of the Pacific Coast from 1769 to 1897" under the auspices of the Smithsonian Institution. This work was extended in 1907 by A. G. McAdie of the U.S. Weather Bureau in

San Francisco, who published a catalog for the years 1897 to 1906. By 1915, there were 179 Weather Bureau observers in the state systematically reporting felt shocks (Palmer, 1916).

The best compilation of early data is the catalog of Townley and Allen (1939), who reviewed and revised the catalogs of both Holden and McAdie as well as bringing the earthquake listing up to date through the year 1928.

In 1912, the Seismographic Station of the University of California at Berkeley began to publish annual bulletins of instrumentally recorded earthquakes. The Berkeley coverage began in 1910 and included the Mt. Hamilton seismograph as well as others in the area as they were installed.

In Southern California, the populace was generally not too concerned with earthquakes. People were certainly aware of the 1906 San Francisco earthquake but chose to consider Southern California as a different province with regard to damaging earthquakes. The scientific report of the 1906 earthquake (Lawson, 1908) clearly described the San Andreas fault as it passed through Central California and into Southern California. Reports of the 1857 Fort Tejon earthquake were included. The early historical reports of Southern California shocks seem to have been ignored or rationalized as exaggerations. Robert T. Hill (1928) in discussing damage to missions by the 1812 and 1857 earthquakes argued: "In each instance, the buildings of adobe mud were inferior in construction, without proper reinforcement, if any, and of crushing and tensile strengths so low that one wonders

how they sustained the weight of their own walls." Hill recognized most of the major faults in Southern California, but he concluded that they were fundamentally different from Northern California faults and that Los Angeles was safe from major earthquakes.

In June of 1925, Santa Barbara was shaken by a moderate earthquake of magnitude 6.3, the first California shock since 1906 to strongly affect an urban area. Thirteen persons were killed (Olsen and Sylvester, 1975). This earthquake stimulated the Carnegie Institution of Washington to install the first seismographic station in Southern California at Riverside in 1926 and to initiate a cooperative program with the California Institute of Technology. By 1932, seven seismograph stations were operating (Riverside, Pasadena, Mount Wilson, Santa Barbara, Tinemaha, La Jolla, Haiwee), and the systematic location of all adequately registered earthquakes in the Southern California region began. Annual bulletins were published in a variety of formats, and in 1973 a summary catalog (Hileman et al.) was published for the years 1932 through 1972. The summary catalog has since been updated for 1973 and 1974 by Friedman et al.

Much of the work reported in the first part of this thesis developed as a part of and in parallel to the preparation of the summary catalog. Most of the seismicity maps herein have also been published in the summary catalog.

The seismicity maps and the computer codes for generating them were first conceived as a graphical means of displaying the data, but they readily became useful tools for analysis of seismological

questions. Chapter 1 presents the seismicity maps, both general and detailed, along with considerations of possible errors in the epicenter data.

Evaluation of some of the statistical parameters of Southern California's seismicity was a natural application of the computer codes mentioned above. In Chapter 2, recurrence data, showing the relationship between earthquake magnitude and frequency of occurrence, are given for the Southern California region and various selected smaller areas. These data are interpreted in terms of the usual linear relationship between magnitude and frequency and are characterized by the slope b of the recurrence curve. Studies of seismicity in certain other areas have indicated that b values can change with time. Suyehiro (1966) found variation in b between foreshocks and aftershocks in both Japan and Chile. Healy et al. (1968) found changes in b during the Denver earthquake sequence. These authors as well as others have suggested that b may show changes precursory to large earthquakes. The time variation of the parameter b is discussed herein for several Southern California areas, but no significant precursory changes have been found.

The Imperial Valley region is a unique tectonic area with a high level of seismicity. Observations there suggest that motions on some faults are unusually sensitive to slip on neighboring faults. This sensitivity is also suggested by some unusual aftershock sequences and frequent earthquake swarms. Most Southern California aftershock sequences follow expected decay behavior. But earthquakes occur

periodically in a few aftershock sequences in the Imperial Valley region. Chapter 3 reviews the swarm activity and describes the periodicity within aftershock sequences.

Examination of the seismicity maps brings to light a number of interesting seismicity trends, some of which are discussed in Chapter 4. The Ventura-Winnemucca seismic zone, which trends northeastward across Southern California, was first pointed out by Ryall et al. (1966). However, the detailed seismicity maps included herein show several faintly defined, similarly trending parallel zones. It may be significant that each of the two most apparent of these transversely aligned zones intersects the San Andreas fault in the vicinity of distinct bends in the fault trend.

One recurring theme in nearly all seismicity studies seems to be the problem of the accuracy of hypocenter estimates. Epicenter errors usually can be reduced satisfactorily for shocks which are interior to dense networks of seismographs. But depth assignments often are not well constrained. This is usually caused by uncertainties in the velocity models used in location programs. In Part II, least-squares inversion techniques are used to address the problem of improving local velocity models.

Chapter 1

DATA BASE

Introduction

This chapter presents the basic data of Southern California seismicity from 1932 through 1975 in the form of various epicenter maps and a table of the larger earthquakes — magnitude 5 and above. A complete tabular listing of all earthquake origin times and hypocentral coordinates can be found in Hileman et al. (1973) for the years 1932-1972, and in Friedman et al. (1976) for the years 1973-1974. This graphical representation of seismicity provides ready access to an otherwise overwhelming mass of data. Spatial and temporal distributions of seismic activity become more readily apparent, and the known instrumentally determined seismicity of desired areas can be ascertained quickly.

The format of the maps was chosen to be similar to that of Allen et al. (1965) to facilitate comparison with their figures showing strain release in Southern California. The maps include annual seismicity for each of the years 1932 through 1975, and 5-year summary maps for the same period. For the entire time period, maps at this scale become too crowded if all the seismicity is shown. Therefore, three maps are given which show only earthquakes of magnitudes greater than 4, 5, and 6, respectively. Finally, a number of selected areas are shown at enlarged scales.

The seismicity maps and the epicenters themselves must be used with some precautions. There are a number of limitations described below which arise because of the various location procedures used

through the years, as well as from fundamental uncertainties in the problem of locating earthquakes on the basis of observed phase-arrival times.

Location Techniques

The use of computers to determine Southern California earthquake epicenters began in 1961. Most earthquakes that occurred before that time were located using graphical or very simple analytical methods incorporating standardized regional travel-time curves (Nordquist, 1962). The graphical methods are based on the intersection of arcs of distance determined from P-minus-origin intervals. One of the typical analytical methods, described by Richter (1958, Appendix XI), adjusts a trial-and-error epicenter until the calculated travel times and observed arrival times yield consistent origin times for all stations. The first computer-derived hypocenter solutions for the Southern California seismographic network began in June, 1961, when Nordquist (1962) completed a program for the Bendix G-150 computer. The original programs have been modified and improved from time to time, and eventually replaced with the currently used program HYPO71, developed by the U.S. Geological Survey (Lee and Lahr, 1971).

Plotting Program

The computer routine, EPLOTZ, for plotting selected epicenter data on a basemap of major faults is straightforward and need not be described in great detail here. The catalog of Southern California

seismicity is stored on magnetic tape as images of epicenter data cards. EPLOTZ reads the catalog tape comparing each earthquake against specified limits for time of occurrence,magnitude and geographic location. Data meeting all of the editing specifications are stored in a temporary file and then plotted when the editing phase is completed. Faults as shown on Plate 1 of Allen et al. (1965) were digitized to form the basemap used in EPLOTZ. The program will plot at any specified enlargement or reduction of the map scale and thereby has the capability to "zoom in" on areas of particular interest. For example, Figure I-2 was plotted at 38% of full size for convenience in publication, Figure I-60 was plotted at an enlargement of 1500% to show the details of the aftershock distribution of the San Fernando earthquake.

Calculations of plotting coordinates in EPLOTZ are referenced directly to the coordinates of the original base map rather than using analytical expressions to convert geographic coordinates into map coordinates. Therefore, any errors in the drafting of the original base map and in digitizing that map persist in EPLOTZ. Such plotting errors are inconsequential--less than the line width for 100% plots. At extreme enlargements, plotting errors can become more evident but are always much less than the location uncertainties of the epicenters.

Limitations Inherent in the Epicenter Data

The most fundamental limitation of the seismicity plots is the uncertainty of the epicenter locations themselves. Some general comments can be made about location accuracies for various areas and

time periods, but each earthquake is a separate case. The accuracy of each epicenter estimate is affected by the geometry of the true epicenter relative to the seismographic stations registering useful phases, the velocity model or travel-time tables used, the velocity structure actually experienced by the seismic waves, the number of usable phases, and possible errors in identifying and timing phases. Because more stations have been incorporated into the Southern California seismographic network from time to time since 1932, and ongoing studies have continually refined the velocity models, many of the above factors have also been changing. Even temporal changes of the true velocity structure are now reported for Southern California (Whitcomb et al., 1973b; Whitcomb, 1976).

As earthquakes are located, a quality factor is assigned to each solution, and these factors are then tabulated in the seismicity catalog. The quality factors are:

A - epicenter probably within 1 km, origin time to 0.3 seconds,

B - epicenter probably within 5 km, origin time to nearest second,

C - epicenter probably within 15 km, origin time to a few seconds,

D - epicenter not known within 15 km, rough location.

For any detailed evaluation of the seismicity in a particular area, the quality factors of the individual earthquakes should be considered.

Some statistics on the qualities of Southern California epicenter estimates are given in Table I-1. In the table, the areas Southern California, Northern Mexico, and Los Angeles Area correspond to the boundaries shown in Figure I-66. For the Southern California

Table I-1

SOUTHERN CALIFORNIA

	M < 3					3 ≤ M < 4					4 ≤ M				
Time Period	Σ	A	B	C	D	Σ	A	B	C	D	Σ	A	B	C	D
1935-1939	742	0	28	68	4	758	1	32	63	4	155	16	25	49	10
1955-1959	525	2	63	32	3	622	8	59	30	2	89	45	23	27	5
1970-1974	2759	22	40	26	12	970	35	44	13	8	98	29	31	13	28
1974	668	12	59	19	9	135	36	55	4	5	10	30	50	10	10

NORTHERN MEXICO

	M < 3					3 ≤ M < 4					4 ≤ M				
	Σ	A	B	C	D	Σ	A	B	C	D	Σ	A	B	C	D
1935-1939	5	0	0	40	60	118	0	0	48	52	60	0	0	67	33
1955-1959	1	0	0	0	100	22	0	0	41	59	217	0	1	53	46
1970-1974	94	0	22	53	25	114	0	16	58	25	20	0	15	45	40
1974	58	0	14	53	33	35	0	9	51	40	6	0	0	17	83

LOS ANGELES AREA

	M < 3					3 ≤ M < 4					4 ≤ M				
	Σ	A	B	C	D	Σ	A	B	C	D	Σ	A	B	C	D
1935-1939	374	0	40	56	4	160	3	63	34	0	22	46	50	4	0
1955-1959	220	1	56	39	4	44	4	64	30	2	6	50	50	0	0
1970-1974	1481	16	31	35	19	396	41	36	10	13	63	30	19	10	41
1974	239	12	46	26	16	19	58	42	0	0	2	50	0	50	0

Some statistics on the quality of epicenter locations. The figures under the Σ columns are the total number of earthquakes for the time periods and magnitude ranges indicated. The remaining figures are percentages (rounded to nearest unit) of locations for the qualities A,B,C,D.

area prior to the 1950's, about two-thirds of the locations were of C or D quality. The seismographic network was significantly upgraded following the 1952 Kern County earthquakes, and subsequently about two-thirds of the locations have been of A or B quality. Network improvements in the 1970's have produced more A-quality locations for shocks with magnitudes less than 4. About 80% of the Northern Mexico earthquakes reported throughout the catalog have C and D qualities.

Before the use of computer solutions for earthquake epicenters, the results were usually reported to the nearest minute of longitude and latitude. The resulting seismicity maps therefore show artificial alignments of the epicenters. The distribution of aftershocks of the 1952 Kern County earthquake shows these artificial alignments clearly (Figure I-61). When computer solutions have been used, one-tenth of a minute precision has been retained in the solutions, equal to about 150 meters, but the true accuracy rarely, if ever, approached such values. Maps of the computer-generated epicenters do not show the artificial alignments due to round-off.

Another common practice before the availability of computer solutions was assignment of the main-shock epicentral coordinates to many of the aftershocks. This occurred because of the labor of manual solutions and the difficulty of picking phases when many shocks occur in close succession. For the 1933 Long Beach earthquake, over 160 aftershocks were given coordinates of the mainshock, and only about 20 aftershocks were located individually during the first two months of the sequence. Subsequent aftershocks of the series were

located individually. Similar entries in the seismicity catalog characterize many other moderate to large earthquakes. The 1940 Imperial Valley earthquake does not show an aftershock zone in Figure I-10 because the aftershocks were not located individually. For more recent earthquakes, such as 1968 Borrego Mountain (Figure I-38) and 1971 San Fernando (Figure I-41), the only aftershocks not located individually are those occurring during the very early portion of the series when successive shocks overlap on the records. Sometimes mainshock coordinates were revised, but coordinates originally assigned to unlocated aftershocks were left unchanged.

Epicenter Maps

Figures I-2 through I-57 show the seismicity of the Southern California region within the boundaries of meaningful coverage by the seismographic array. These boundaries are those adopted by Allen et al. (1965). The true limits would describe a smoother figure whose exact shape would depend on earthquake magnitudes and the amount of uncertainty allowed in one's definition of a "meaningful" epicenter location. On many of the maps, epicenters are shown outside the boundary, but the coverage outside is neither complete nor consistent. Figure I-1 is a reference map of this area showing the major faults, cities and highways; the cultural information is deleted from most of the other figures for clarity.

Every epicenter symbol on the maps represents an event in the catalog listing, or several events having the same location. The

legend on each map shows the correspondence between the size of the epicenter symbol and the range of magnitudes represented. It should be noted that before 1944, magnitudes were reported only to the nearest half-unit.

Enlarged maps of the Los Angeles area are shown in Figures I-58 and I-59 covering the seismicity up through the end of 1970. The San Fernando earthquake series beginning in February, 1971, is shown in Figure I-60. Aftershock distributions for the Kern County earthquake (1952), the Borrego Mountain earthquake (1968), the Walker Pass earthquake (1946), the Manix earthquake (1947) and the Desert Hot Springs earthquake (1948) are shown in Figures I-61 through I-65. Aftershock distributions are not given for several other large Southern California earthquakes, such as the Long Beach earthquake (1933) and the Imperial Valley earthquake (1940), because too few of the aftershocks were located individually.

At first glance, the seismicity map for 1933 (Figure I-3) seems to indicate abnormally low seismicity for the Southern California region as a whole concurrent with the Long Beach earthquake. Such an impression is incorrect. Because of the many events of the 1933 aftershock sequence, small events elsewhere around the area were not located. For much of 1933, the catalog seems to have a magnitude threshold of 3.0, particularly for shocks outside the Los Angeles area.

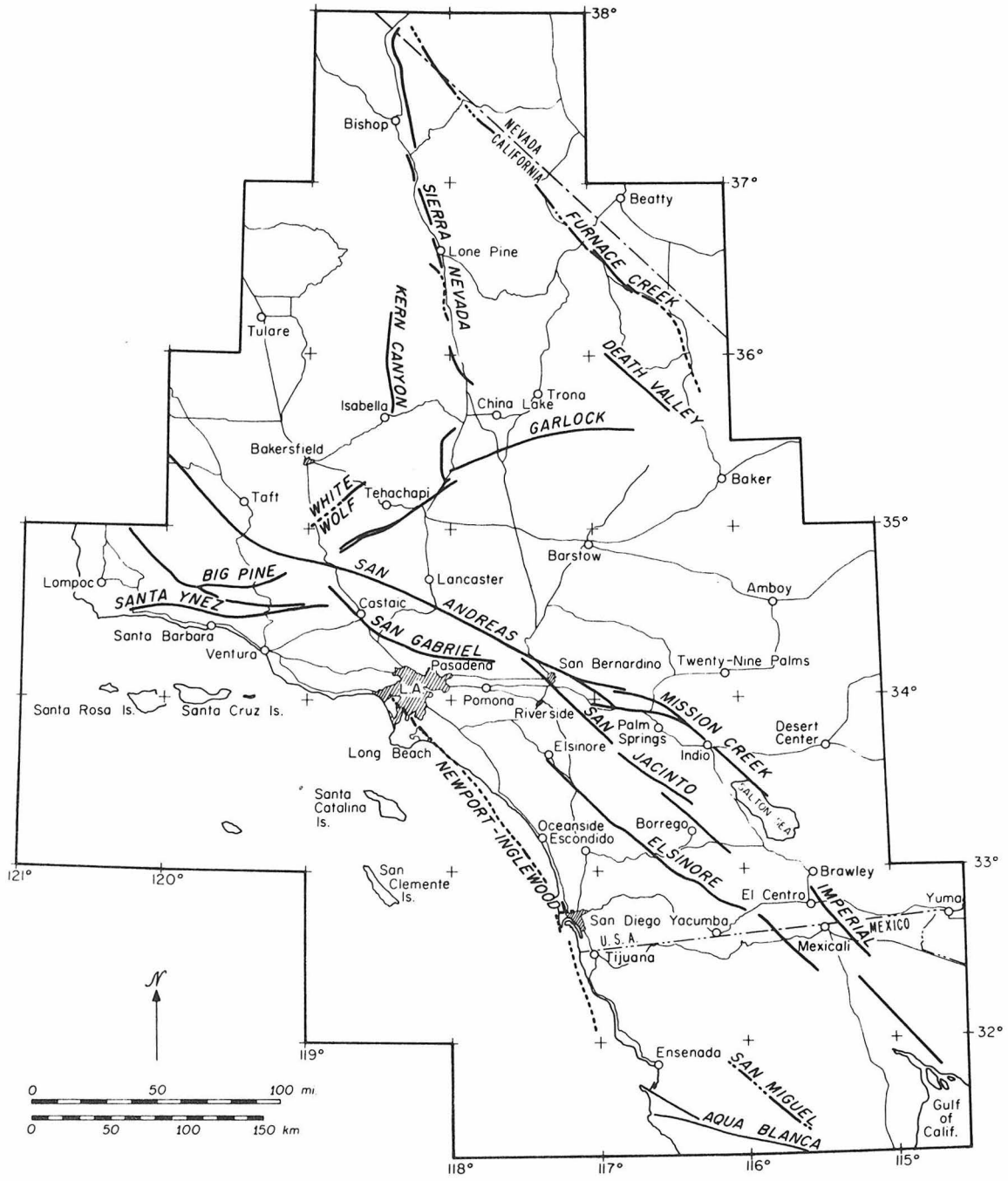

Figure I-1. Base map of Southern California region with major faults. The outline encloses the area for which network coverage is believed to be complete generally for earthquakes of $M_L \geqslant 3.0$, $M_L \geqslant 4.0$ in Mexico.

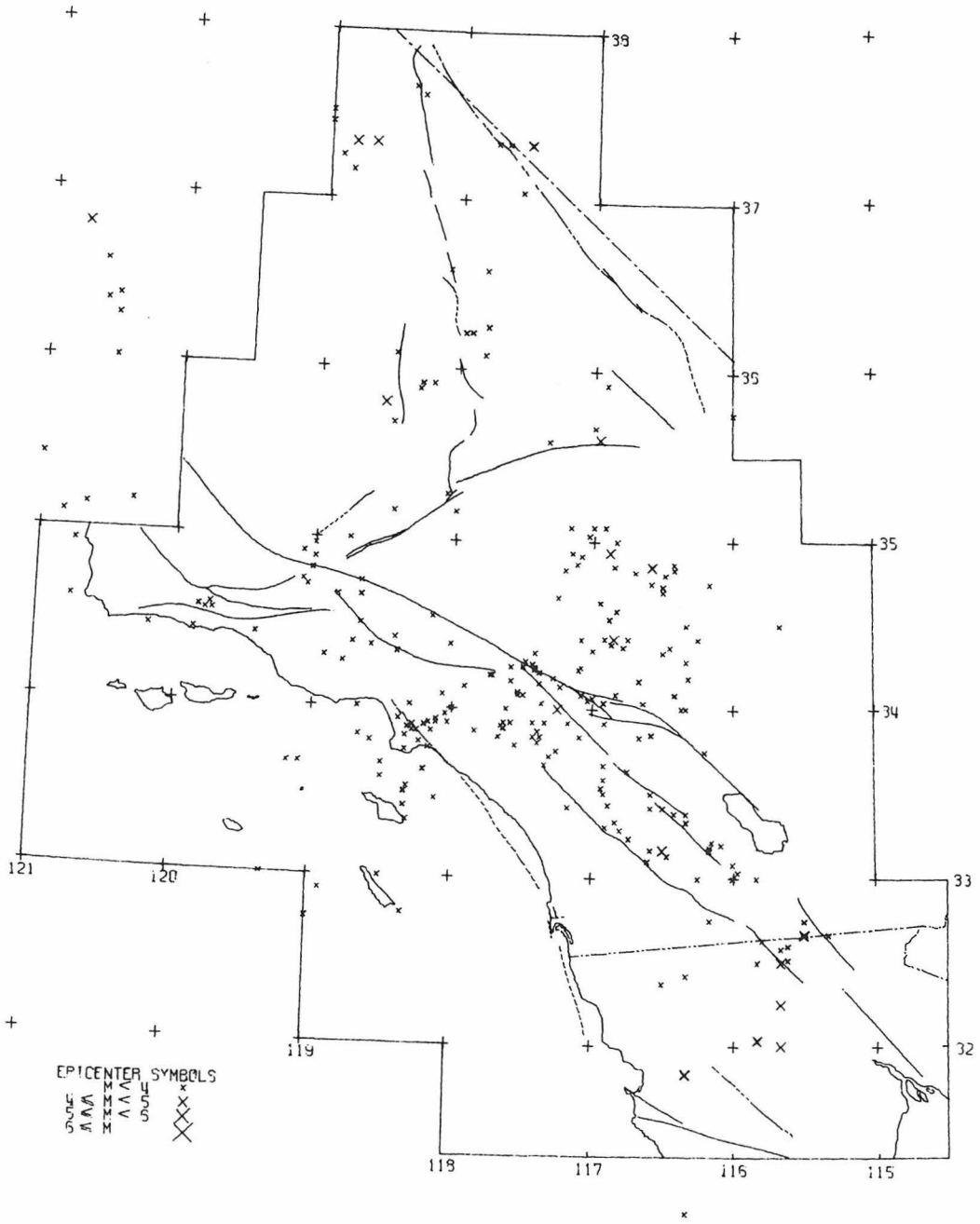

1932 ALL EVENTS

Figure I-2.

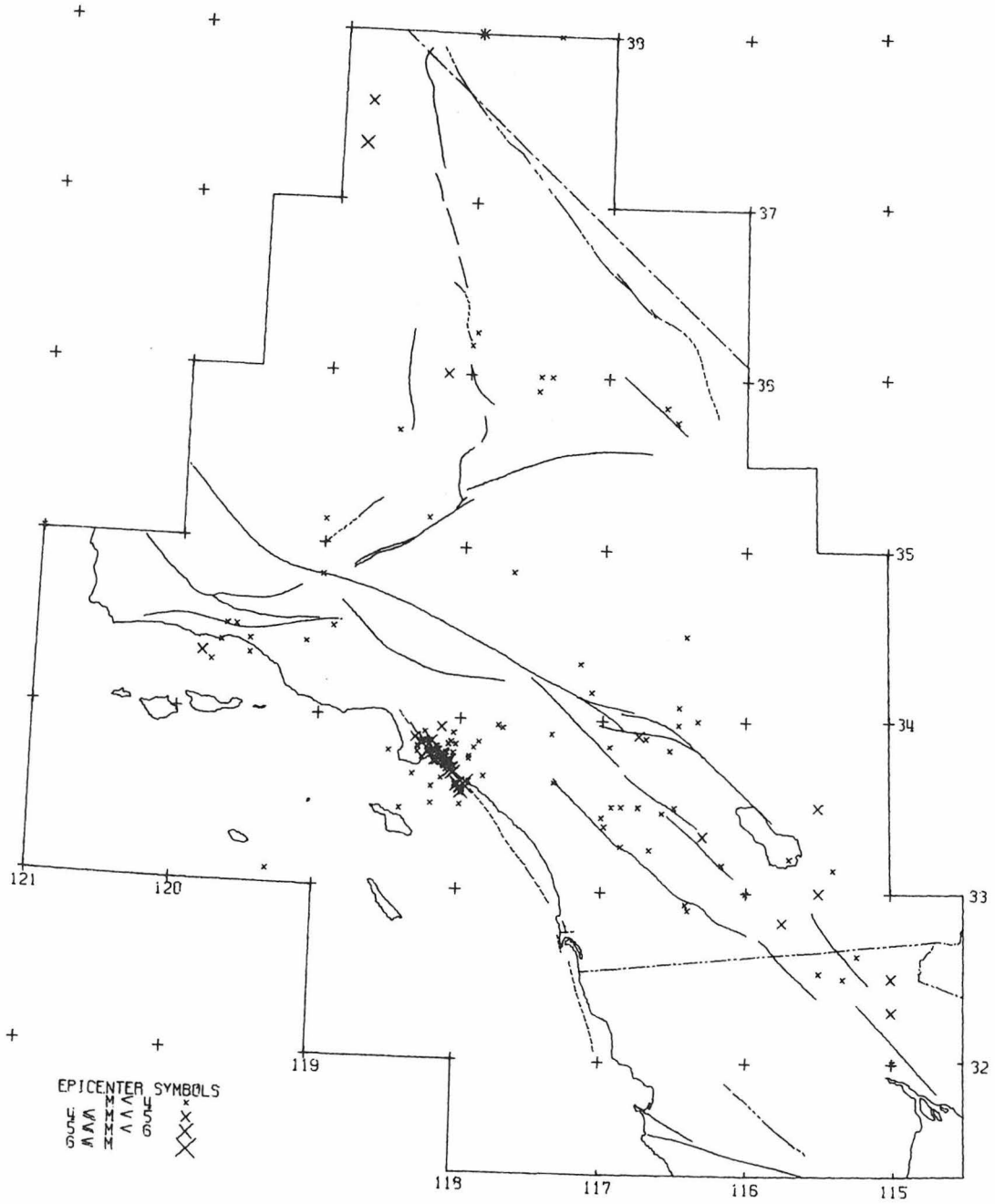

1933 ALL EVENTS

Figure I-3.

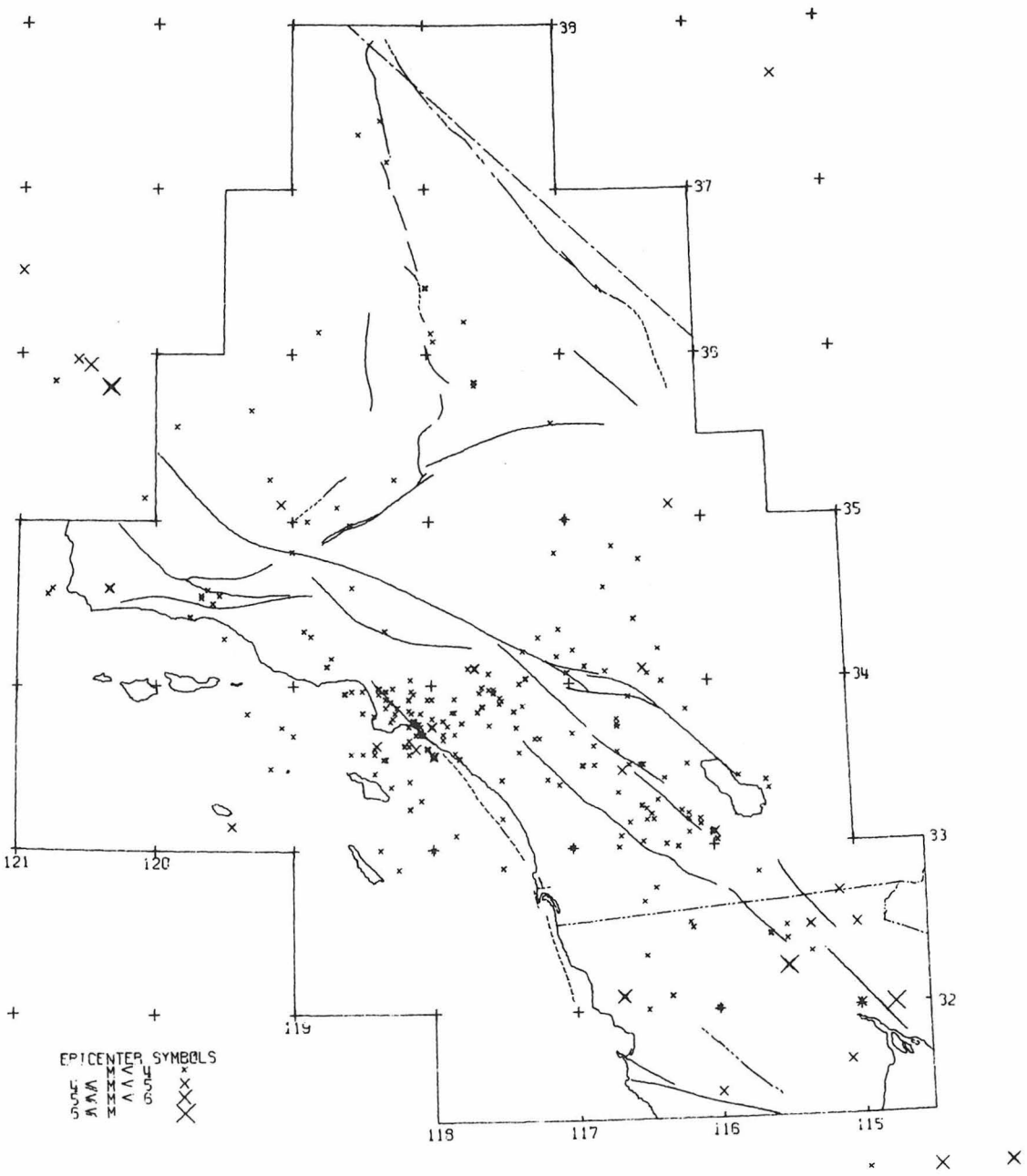

1934 ALL EVENTS

Figure I-4.

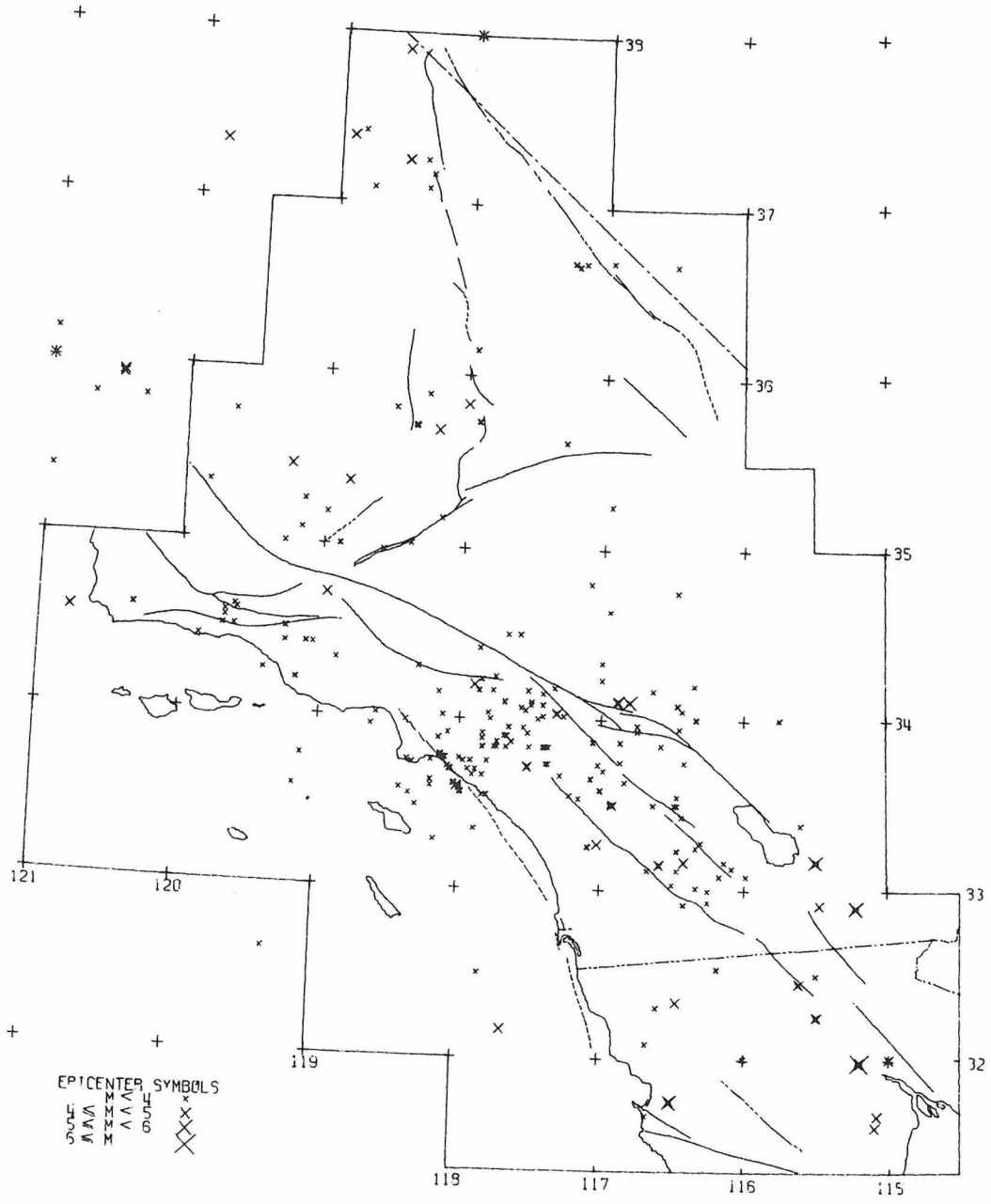

1935 ALL EVENTS

Figure I-5.

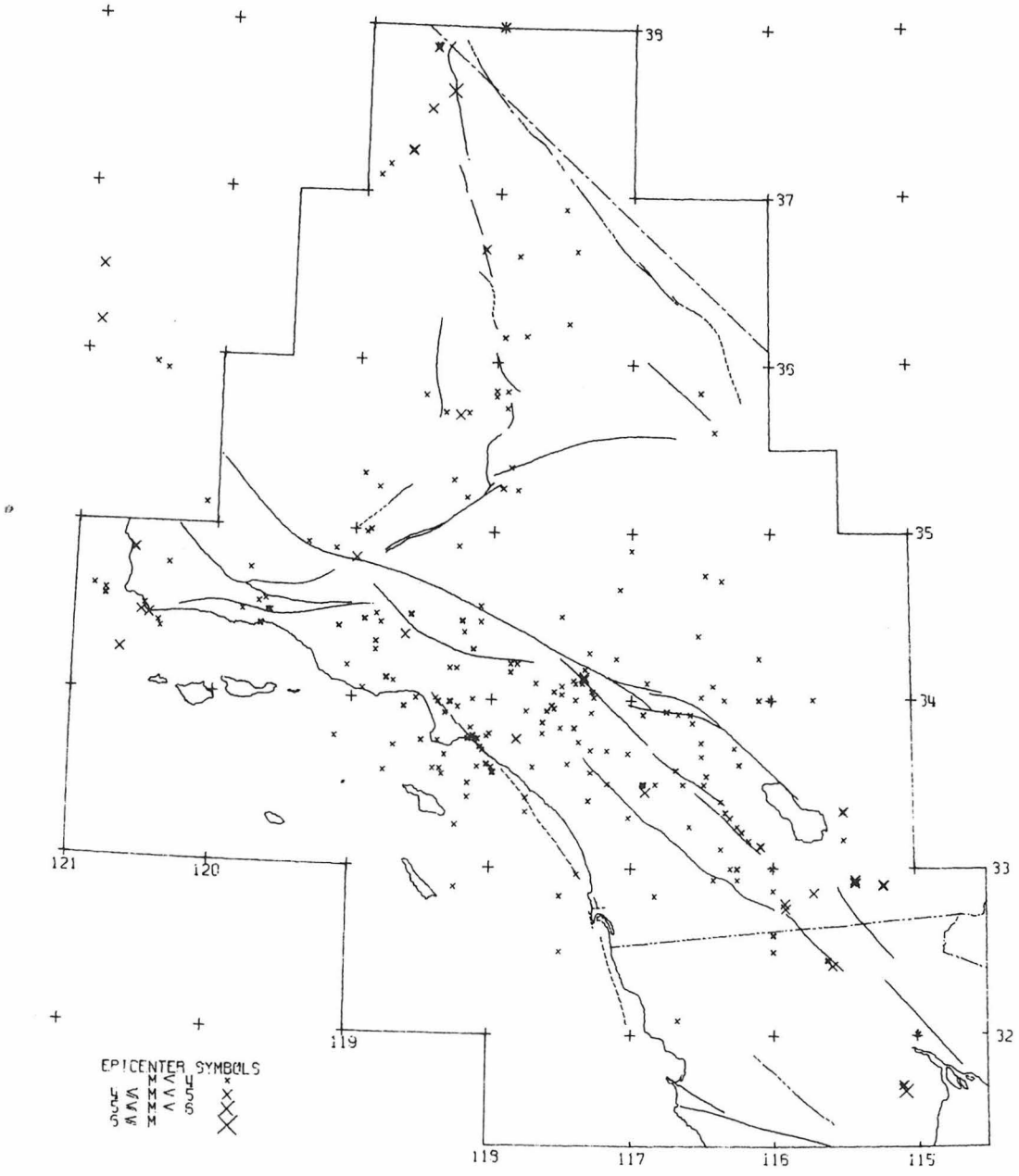

1936 ALL EVENTS

Figure I-6.

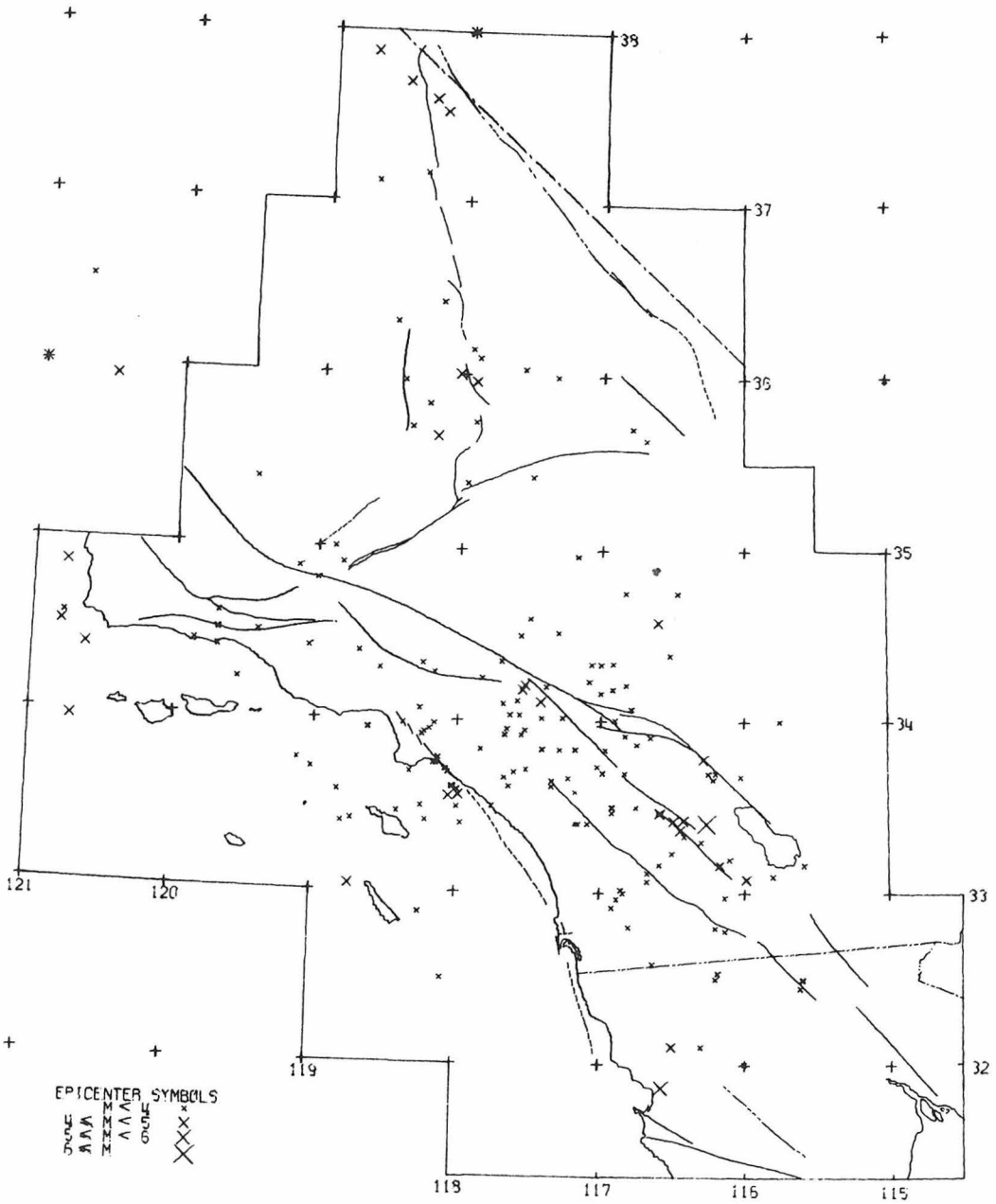

1937 ALL EVENTS

Figure I-7.

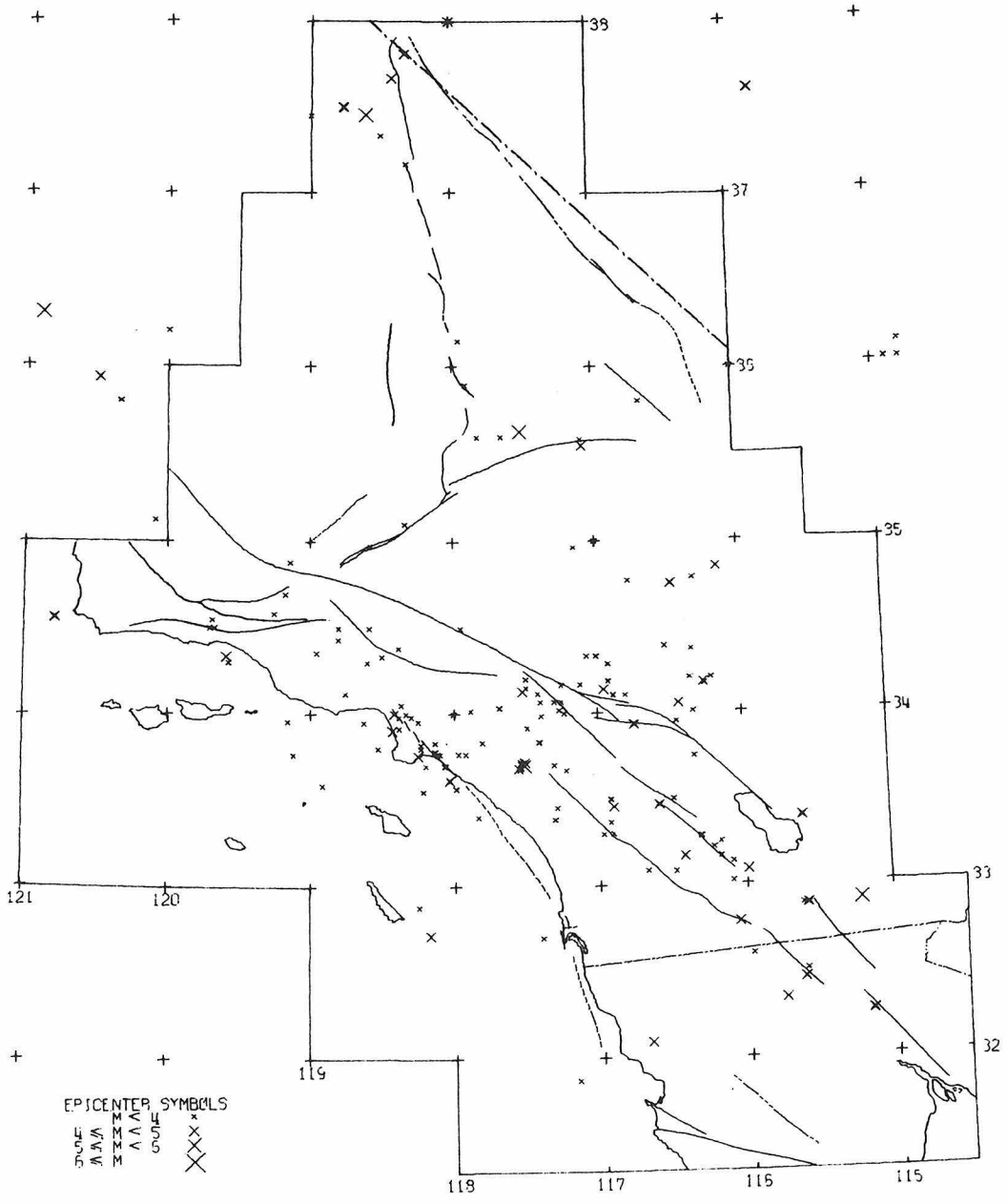

1939 ALL EVENTS

Figure I-8.

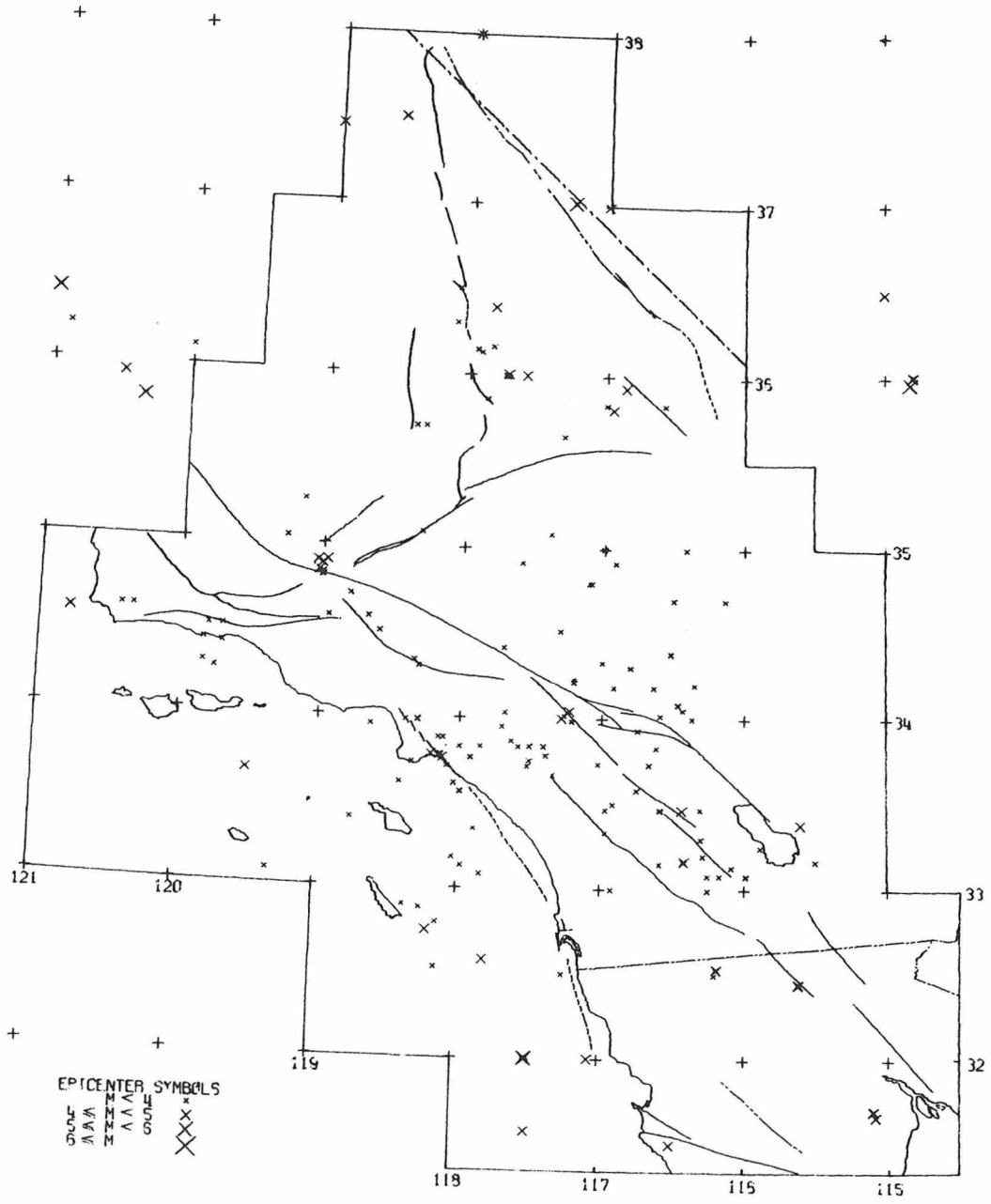

1939 ALL EVENTS

Figure I-9.

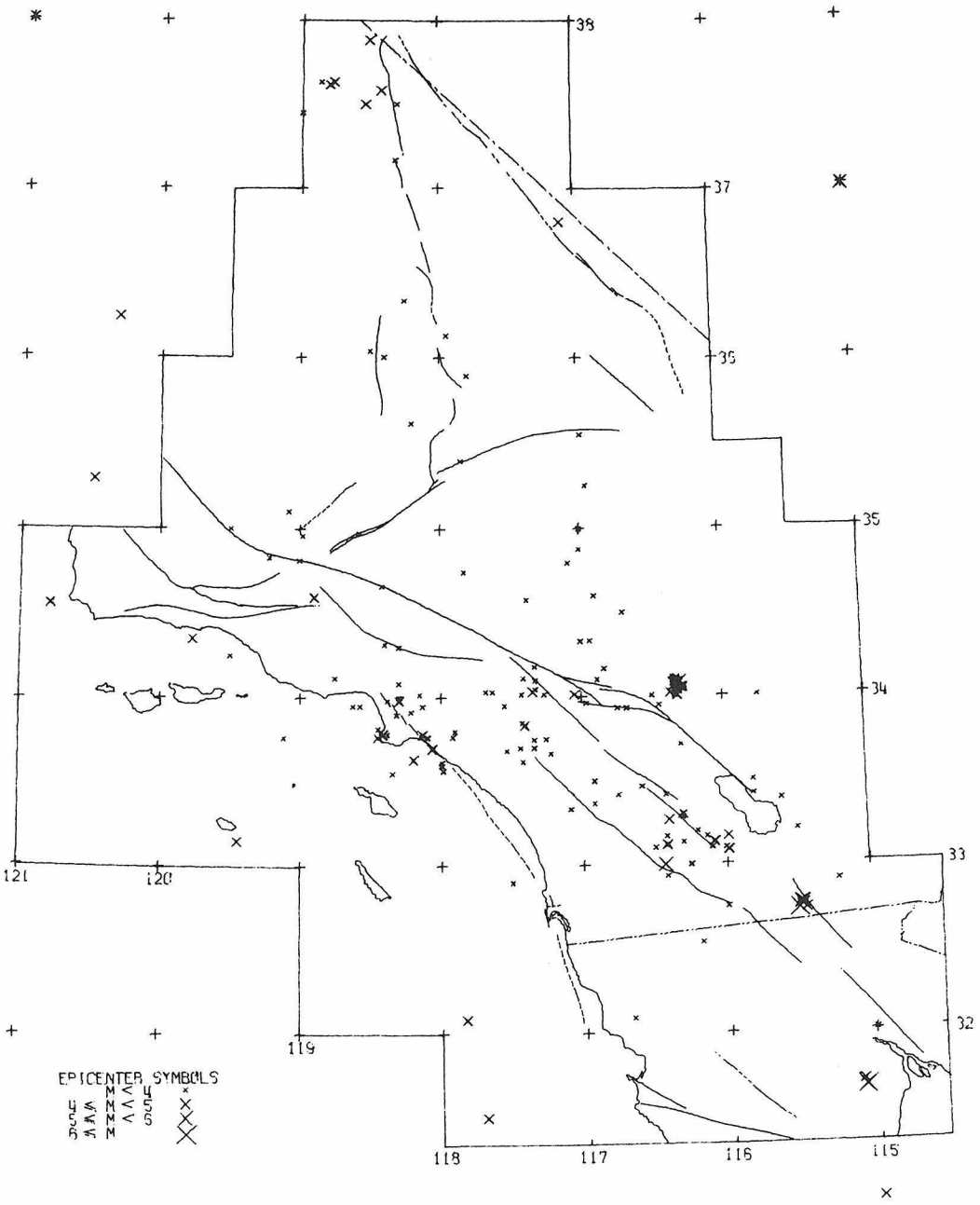

1940 ALL EVENTS

Figure I-10.

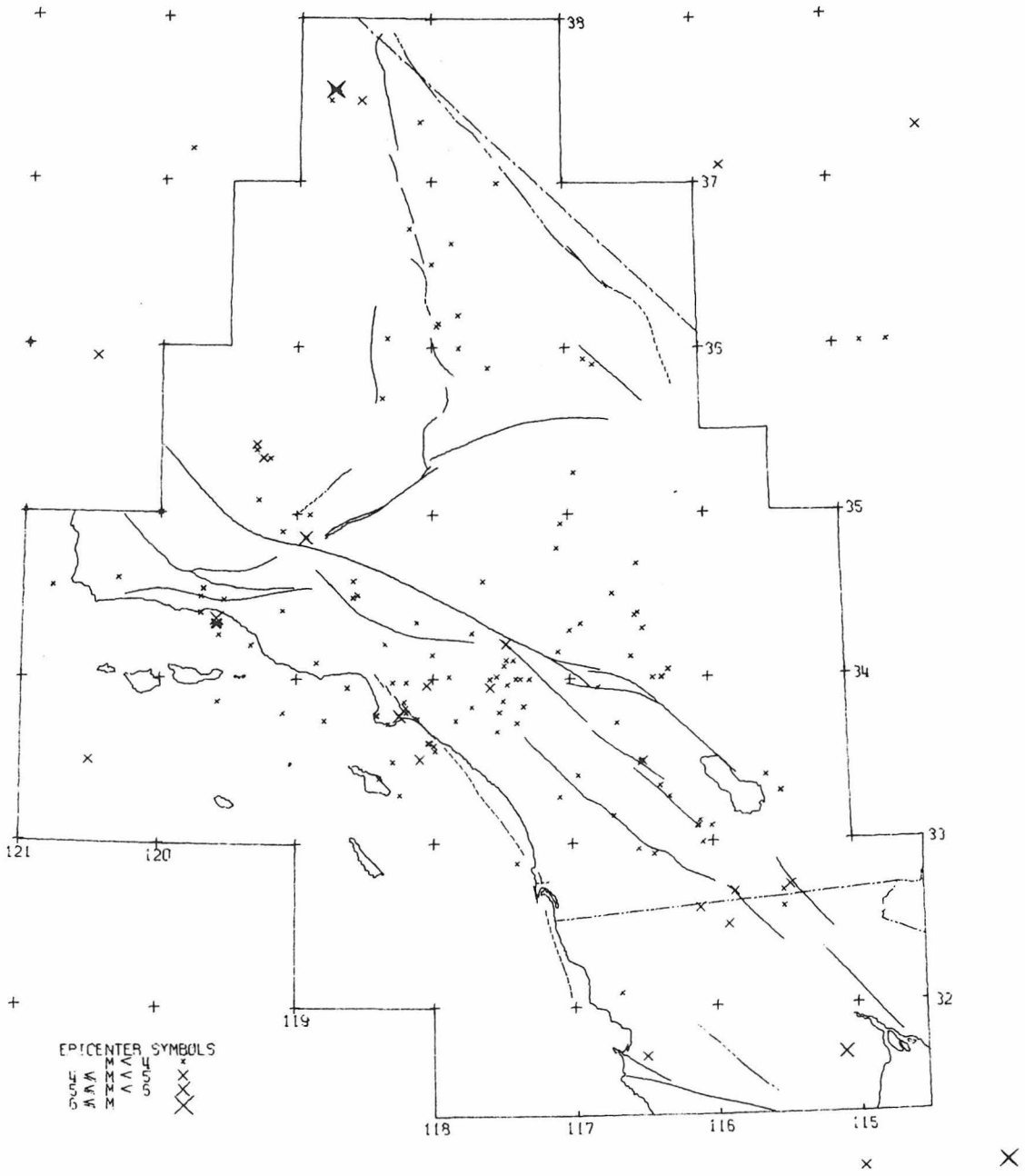

1941 ALL EVENTS

Figure I-11.

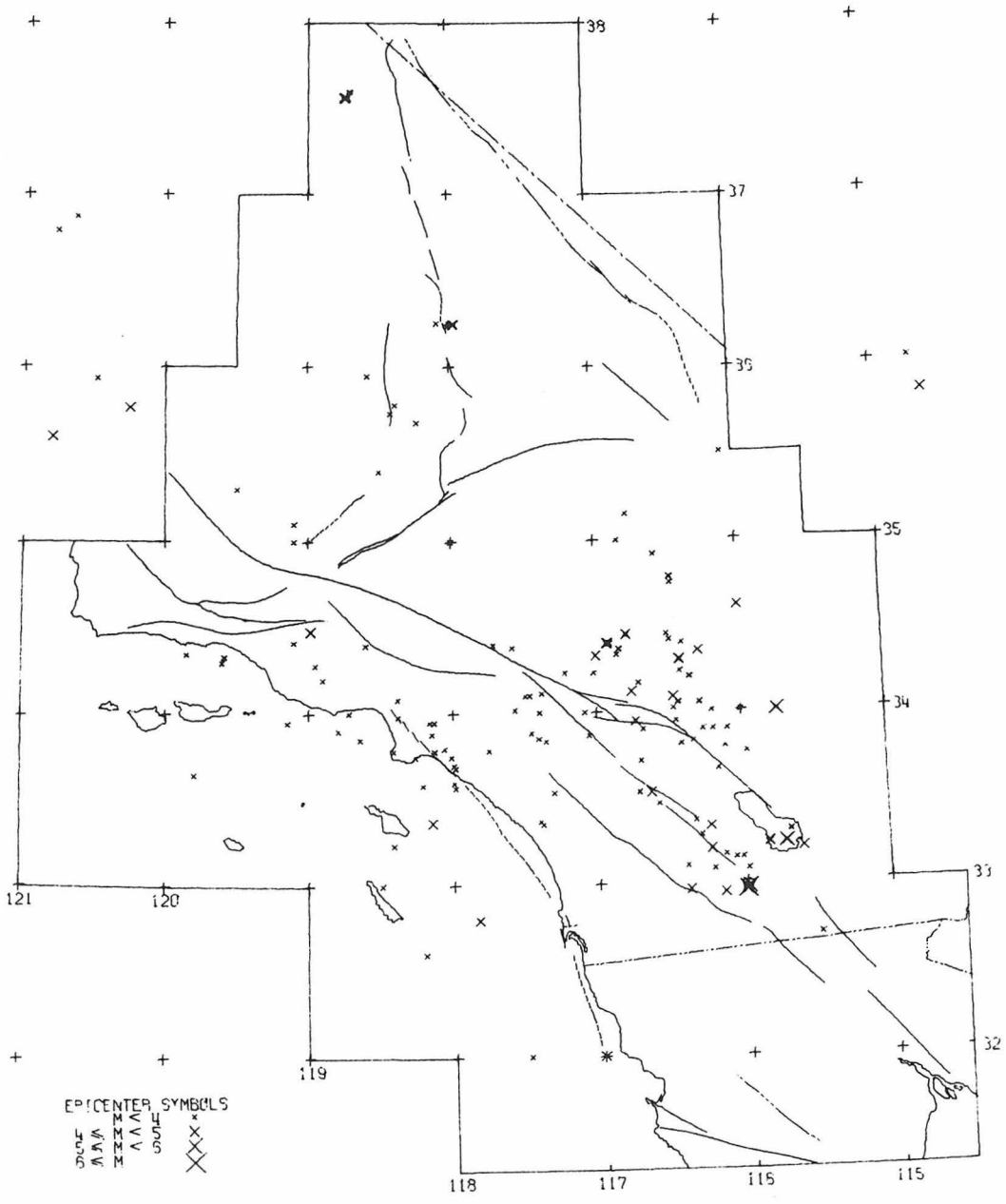

1942 ALL EVENTS

Figure I-12.

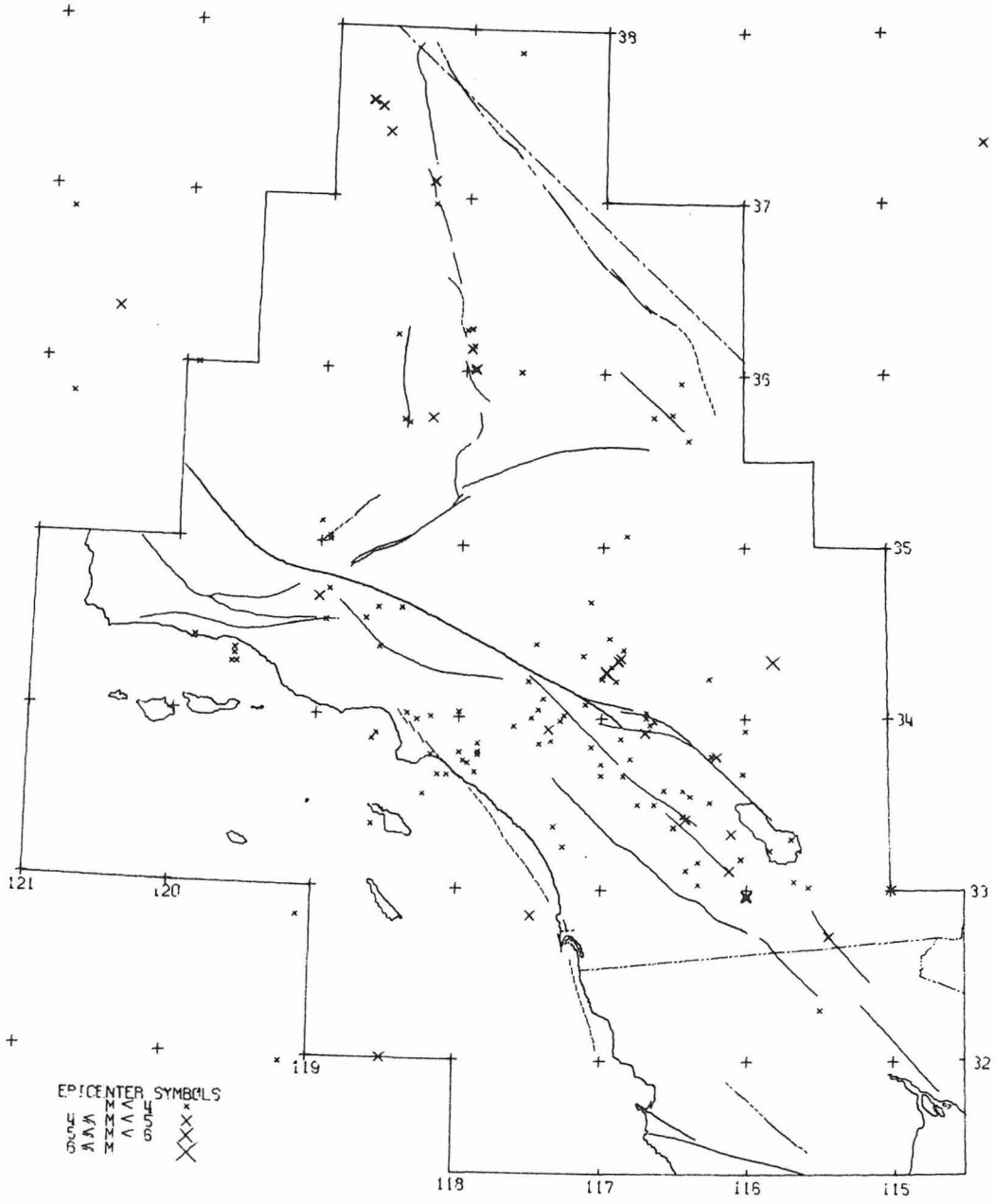

1943 ALL EVENTS

Figure I-13.

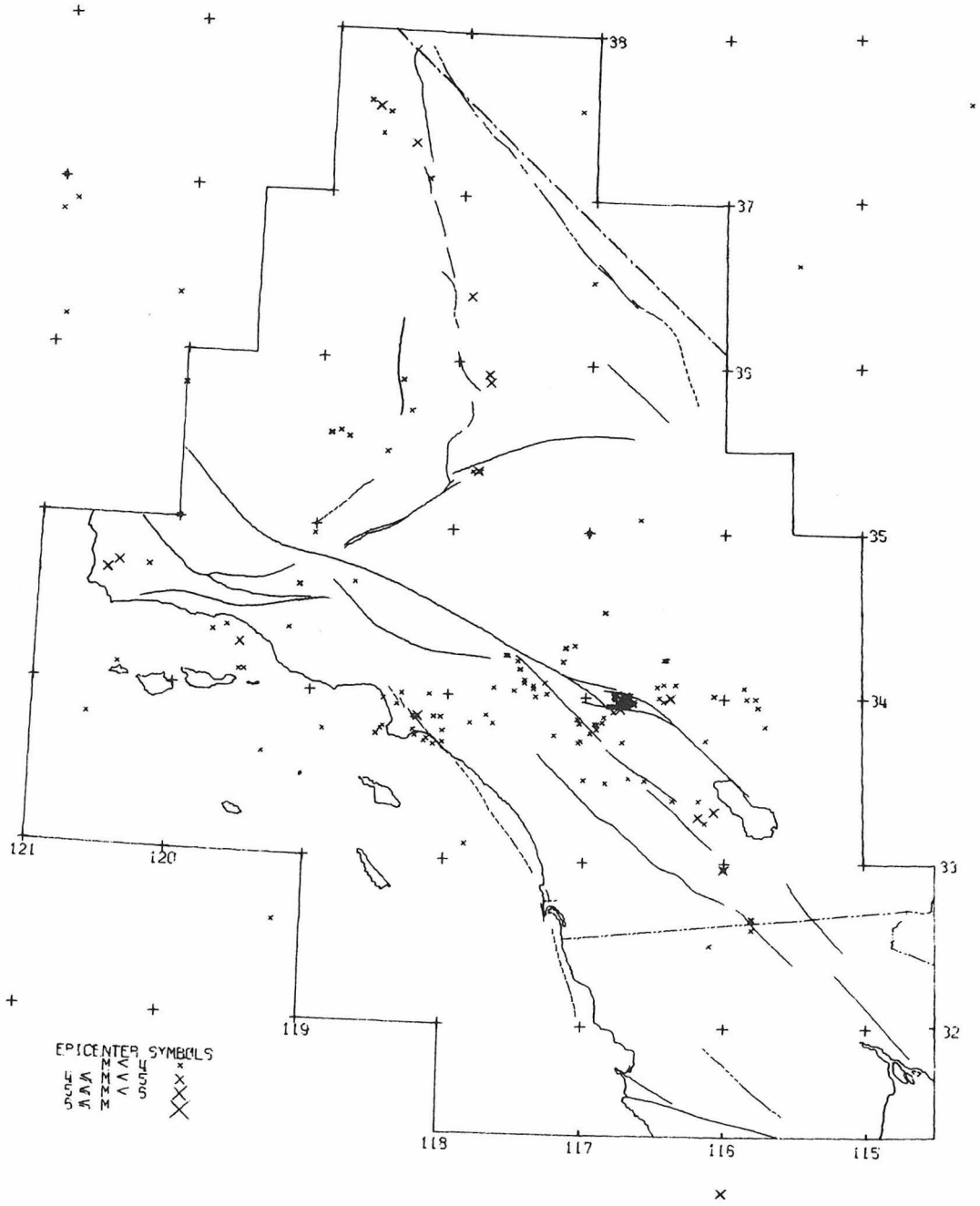

1944 ALL EVENTS

Figure I-14.

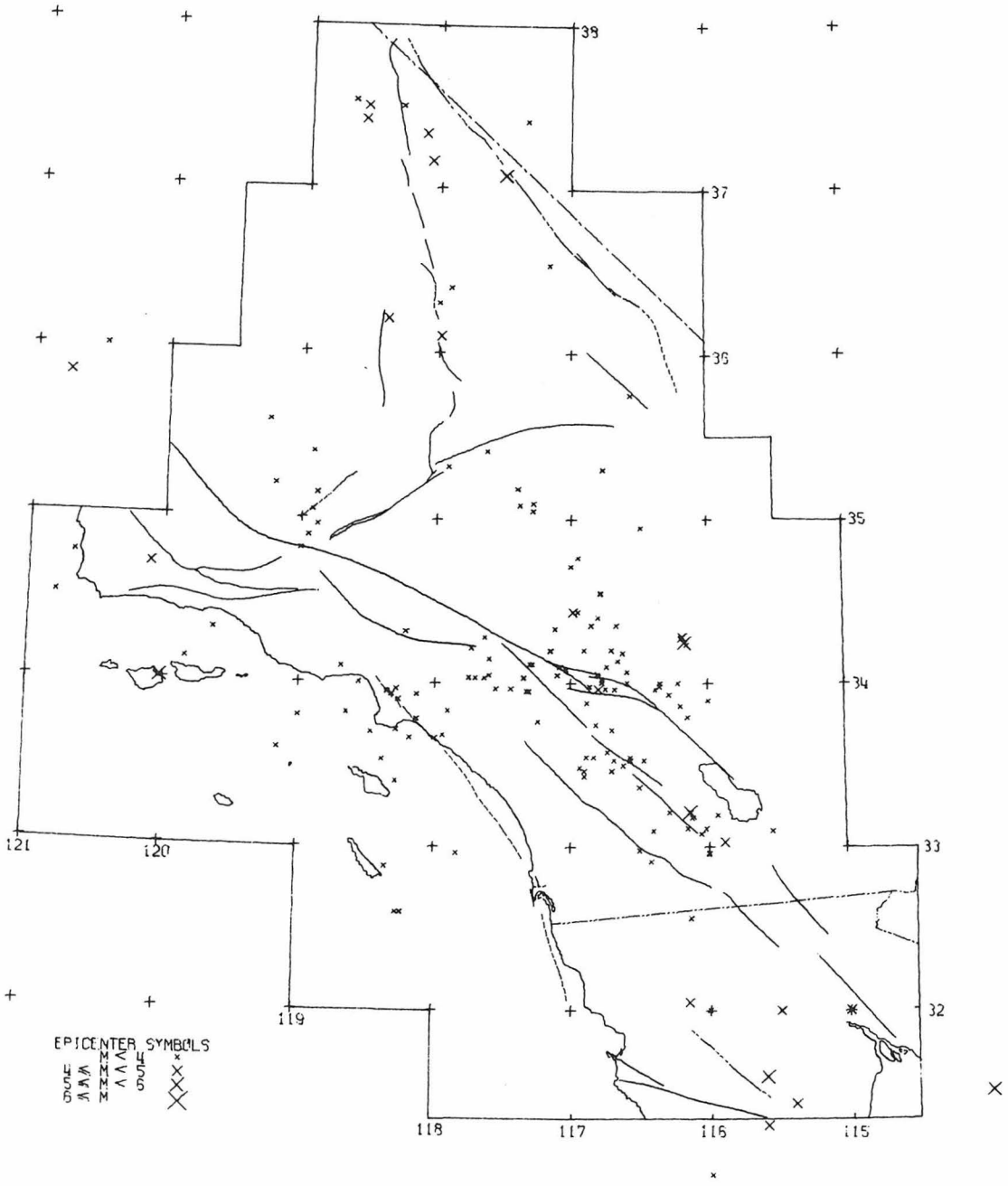

1945 ALL EVENTS

Figure I-15.

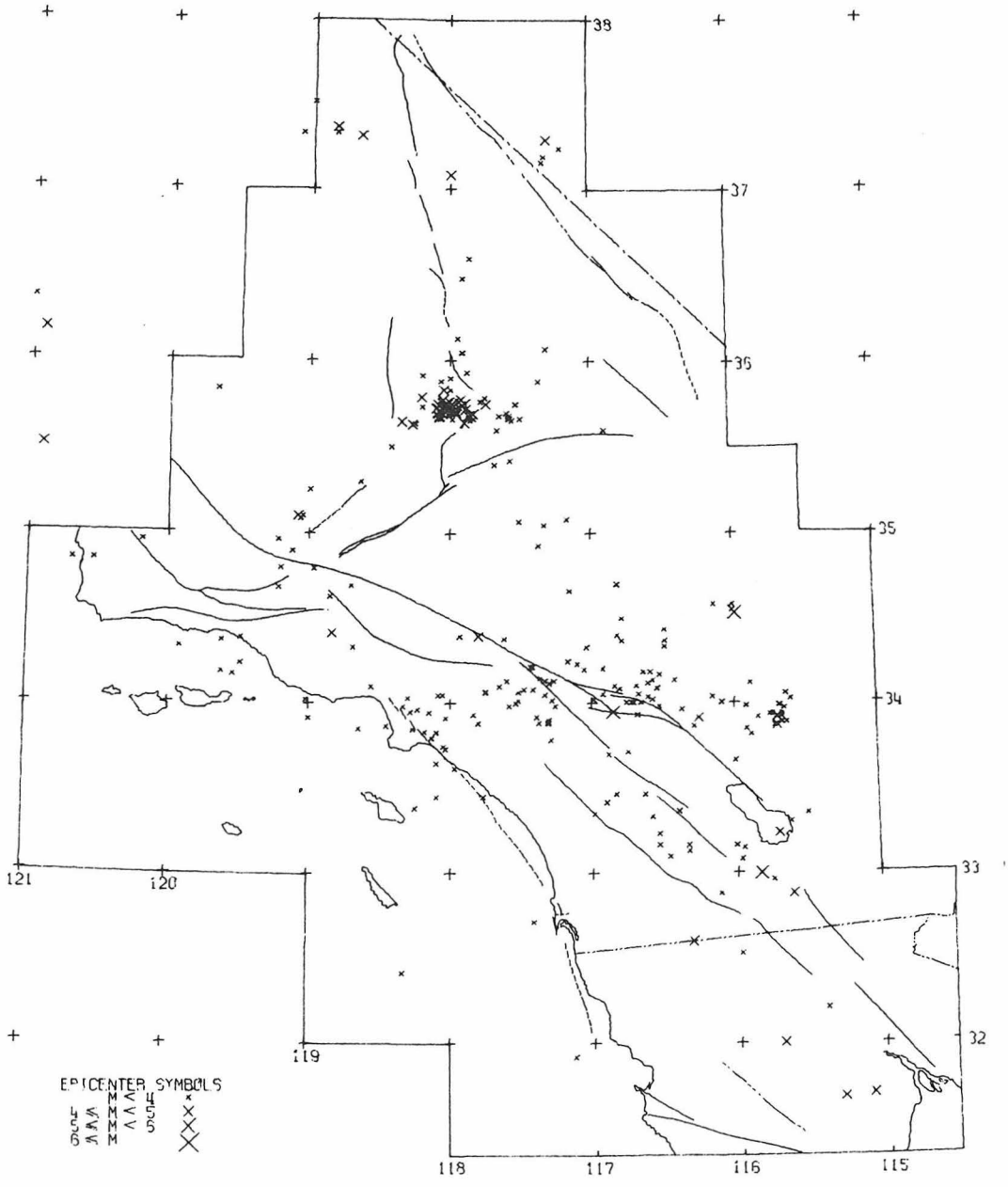

1945 ALL EVENTS

Figure I-16.

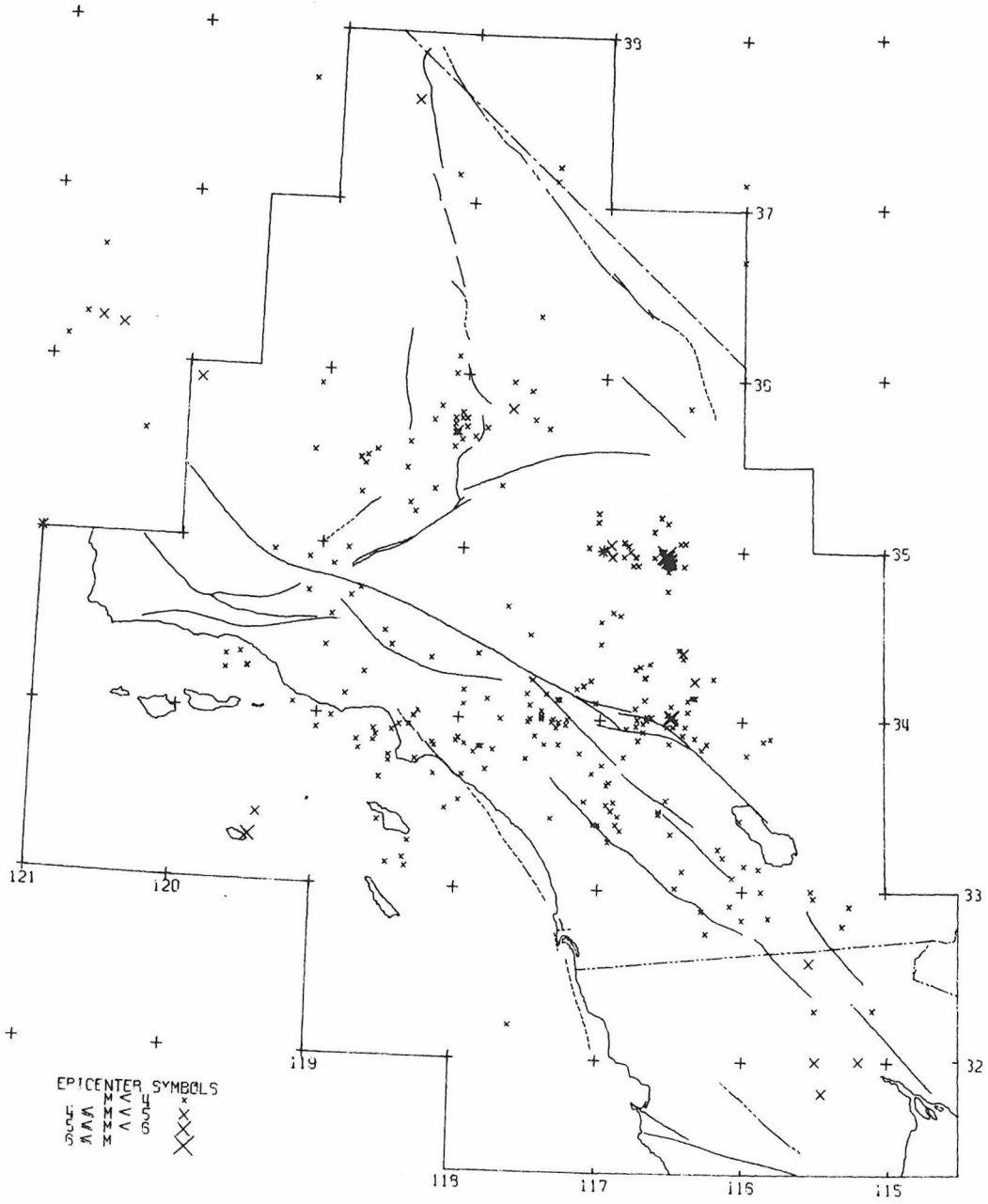

1947 ALL EVENTS

Figure I-17.

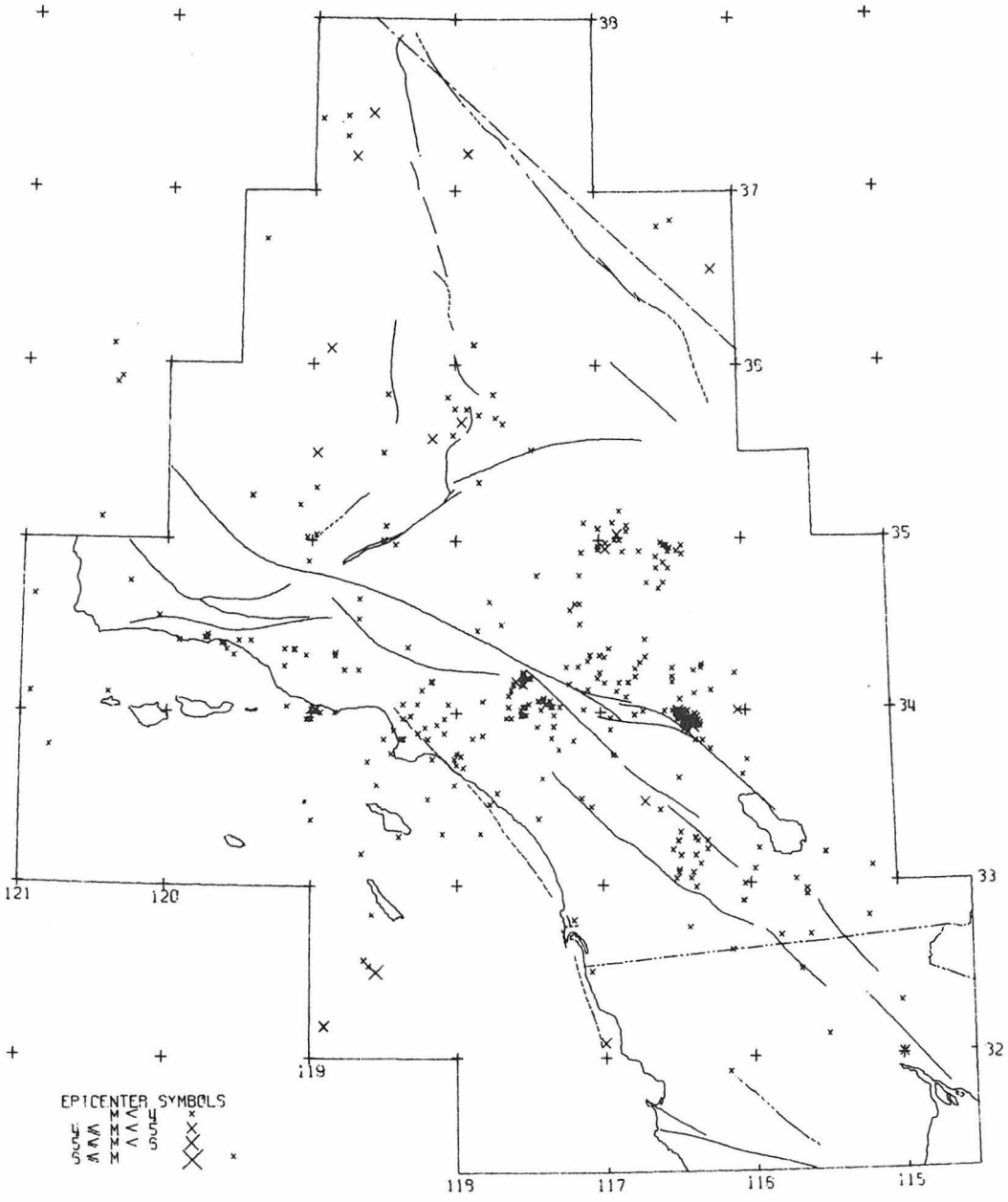

1948 ALL EVENTS

Figure I-18.

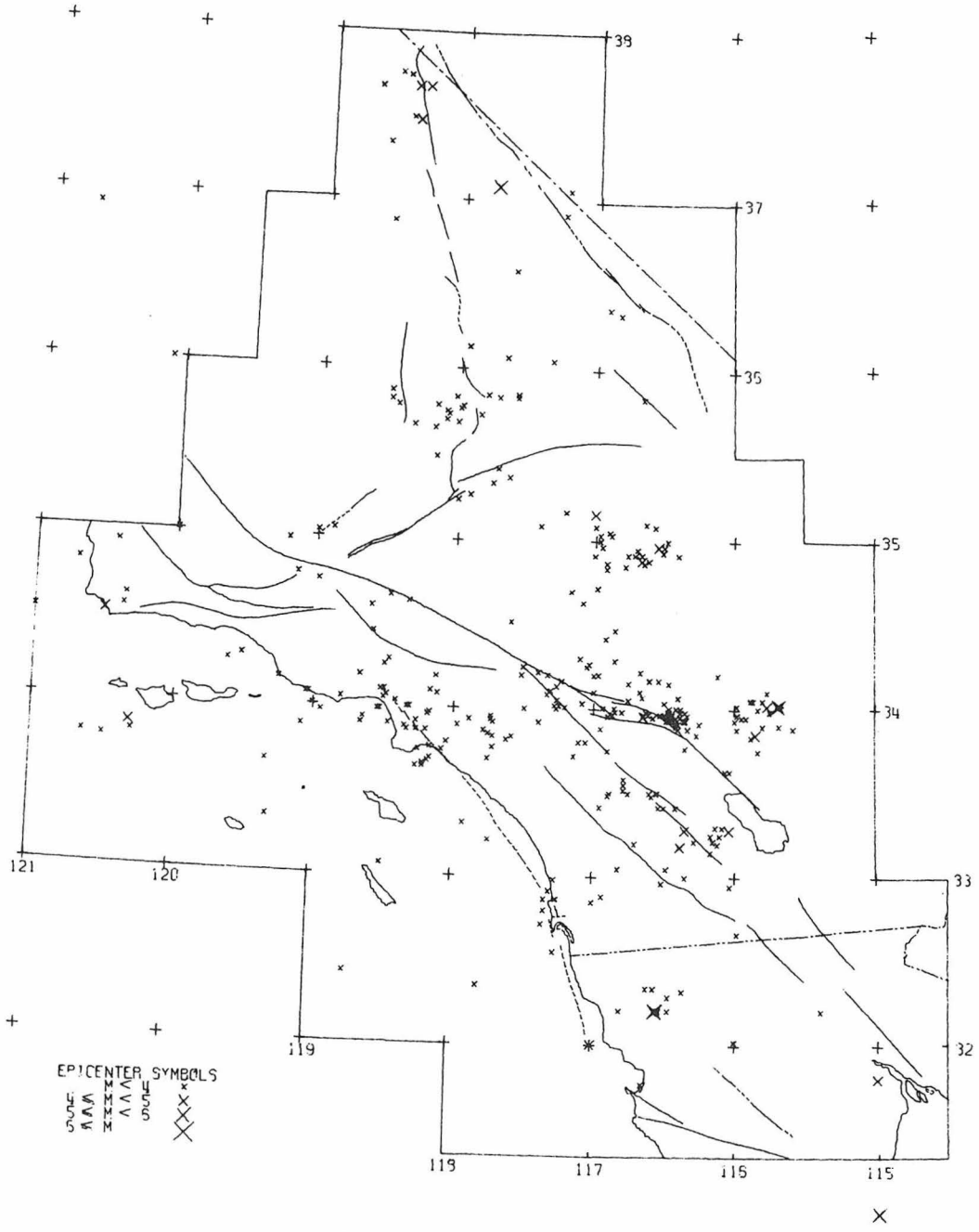

1949 ALL EVENTS

Figure I-19.

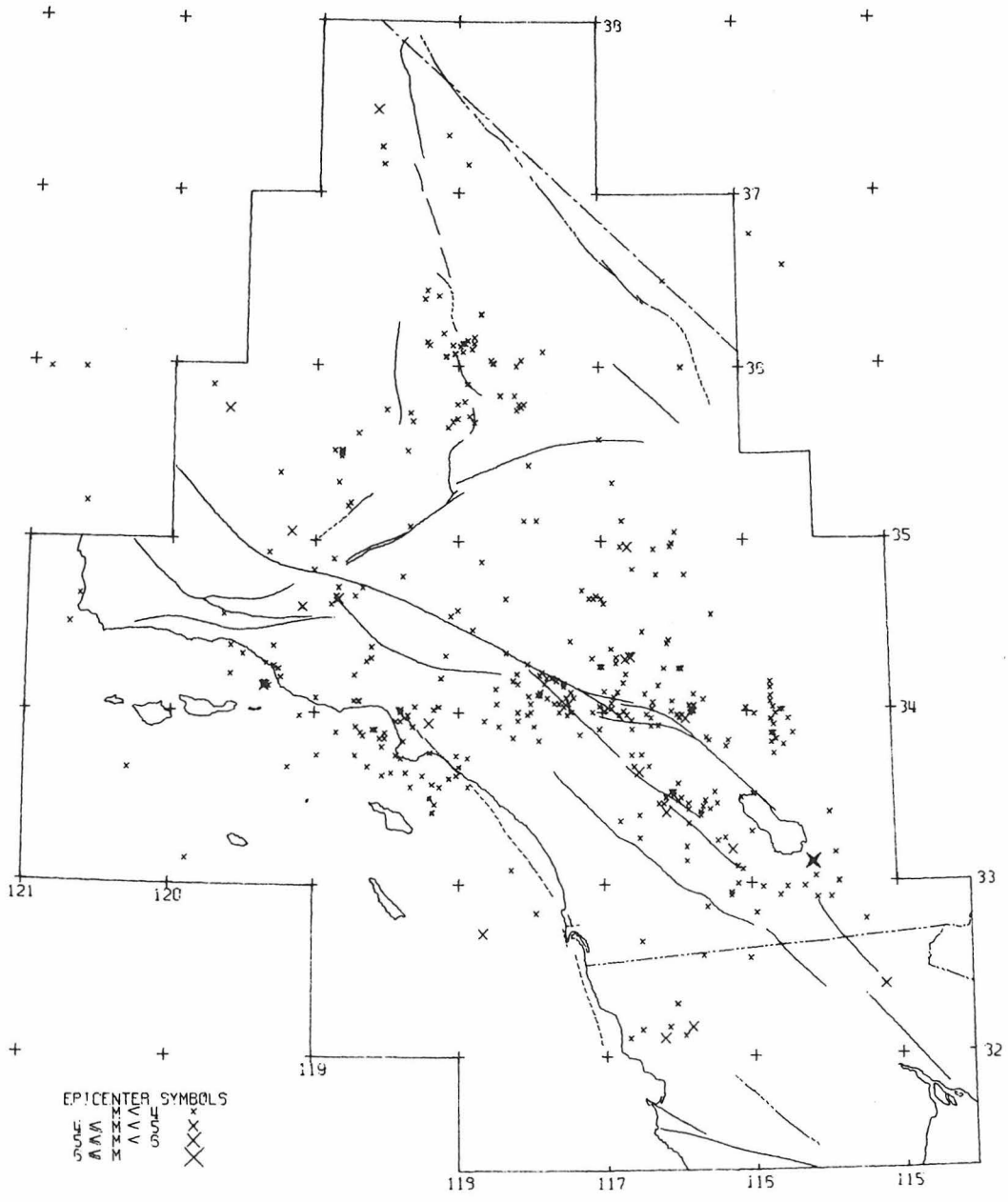

1950 ALL EVENTS

Figure I-20.

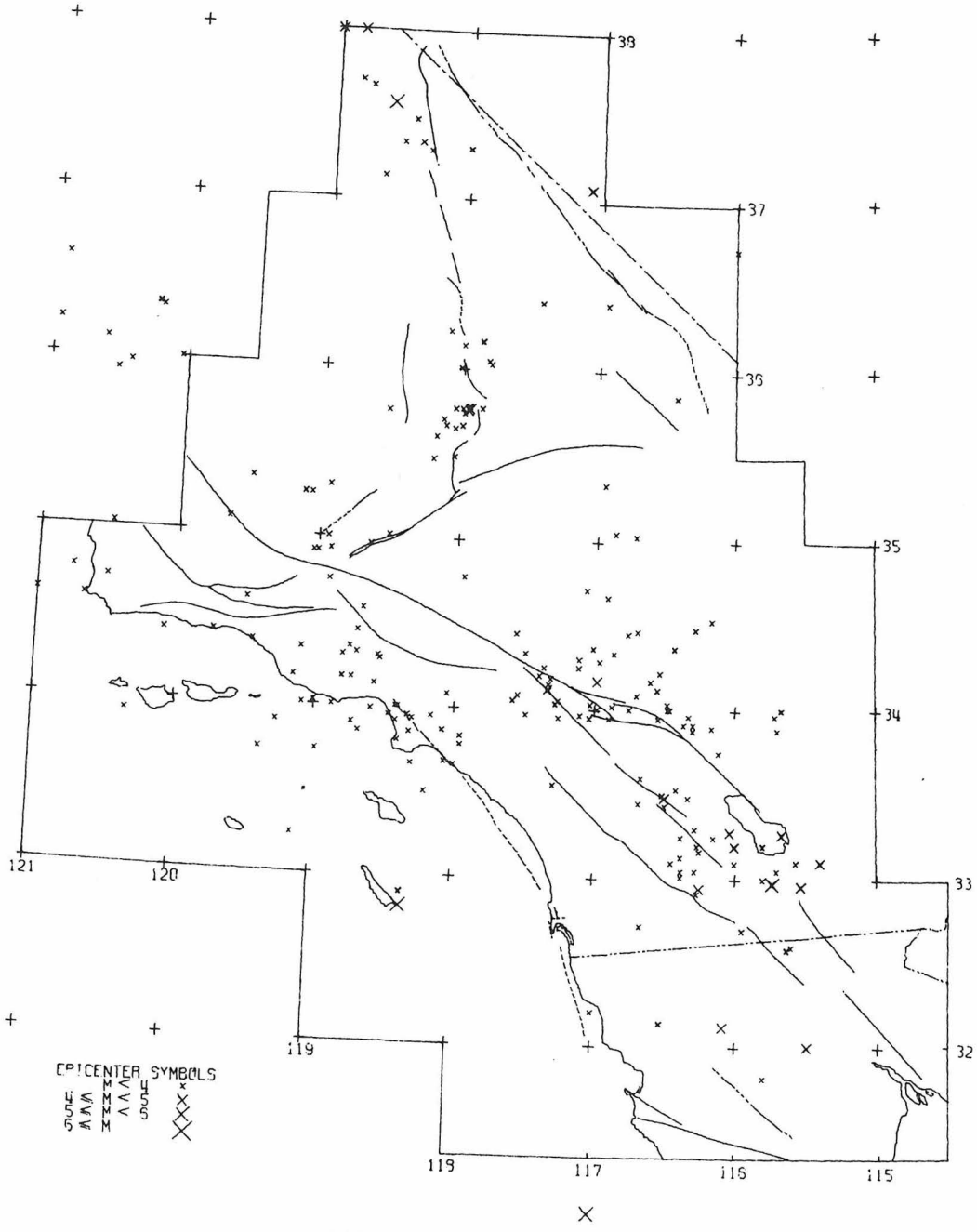

1951 ALL EVENTS

Figure I-21.

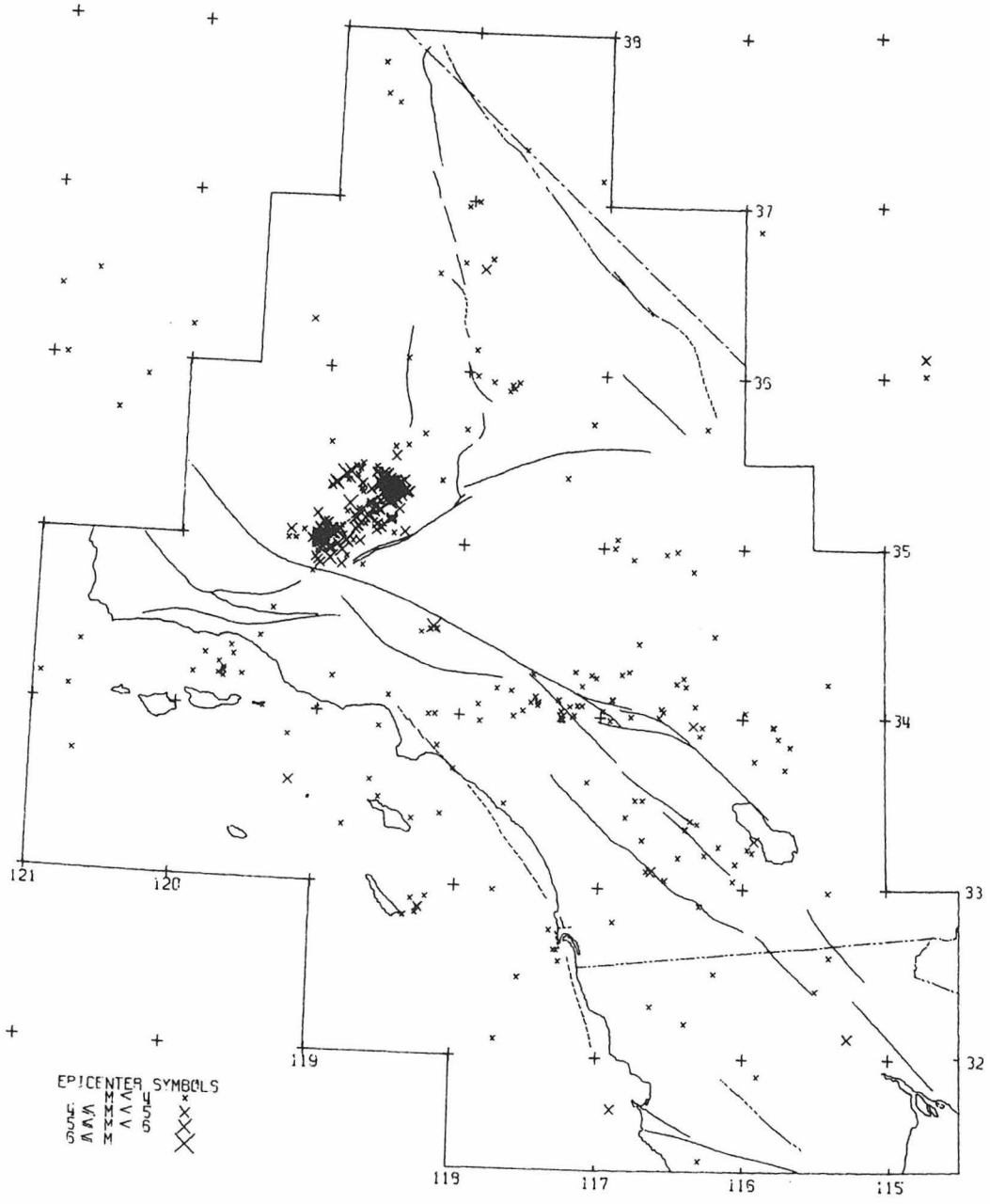

1952 ALL EVENTS

Figure I-22.

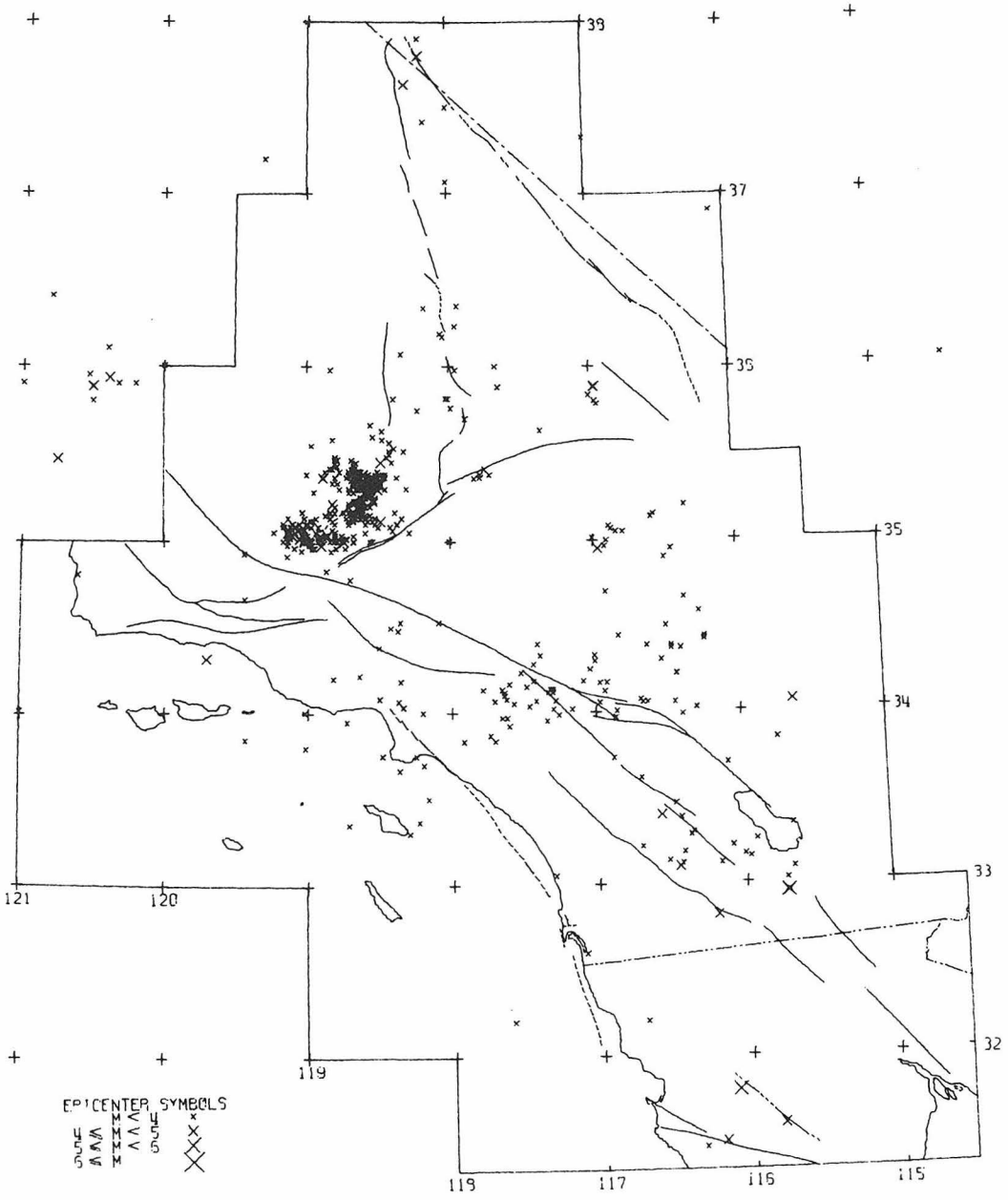

1953 ALL EVENTS

Figure I-23.

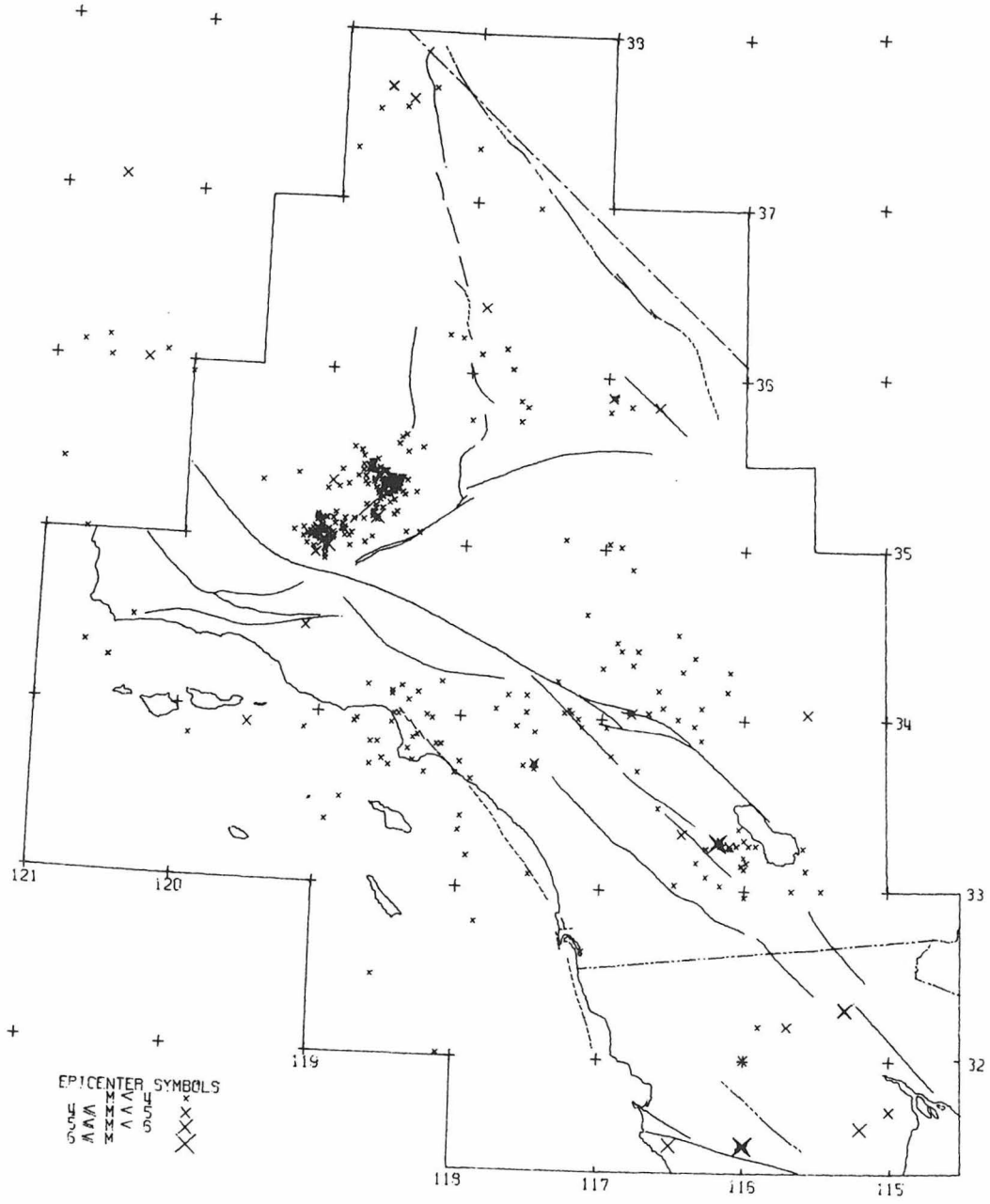

1954 ALL EVENTS

Figure I-24.

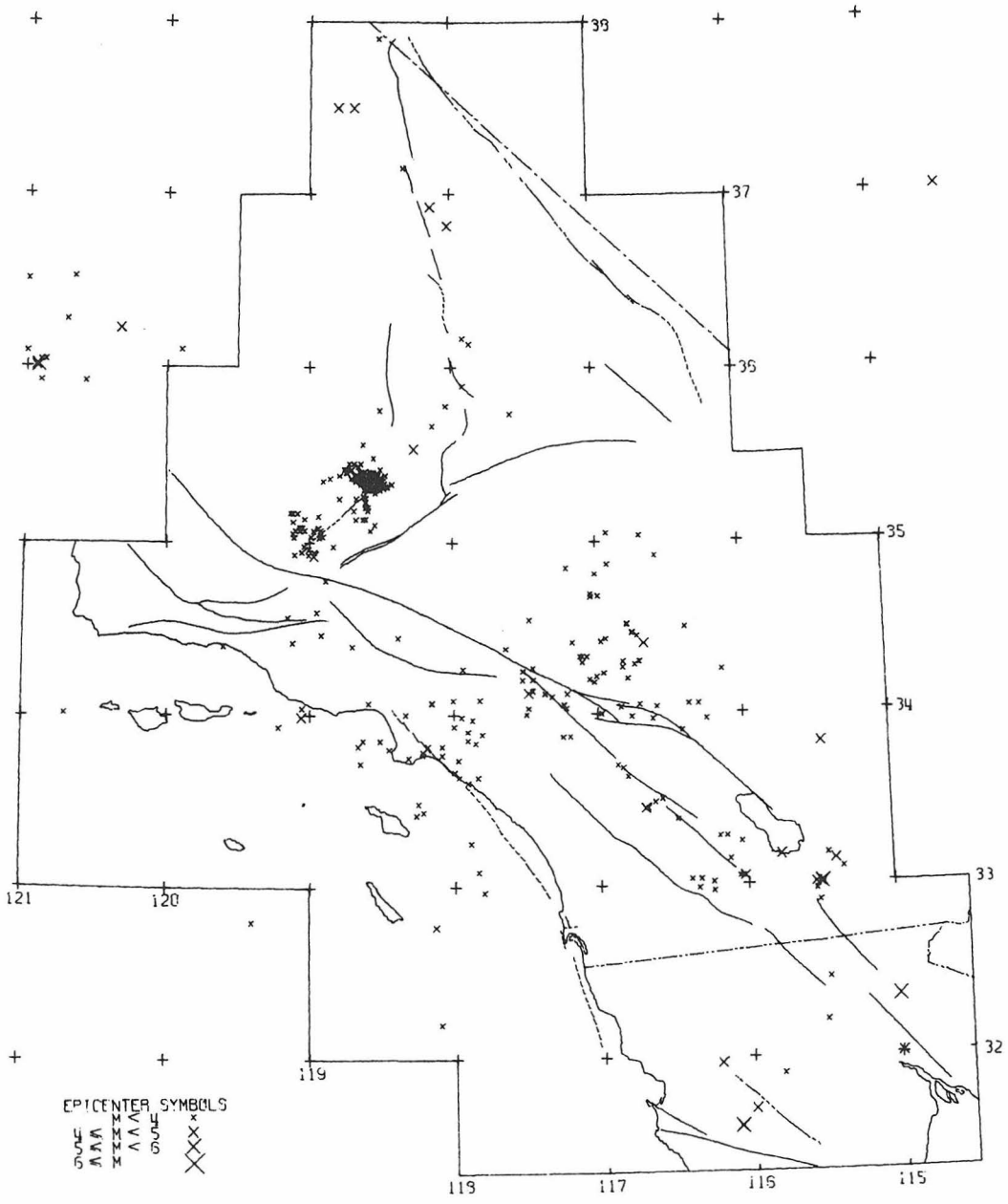

1955 ALL EVENTS

Figure I-25.

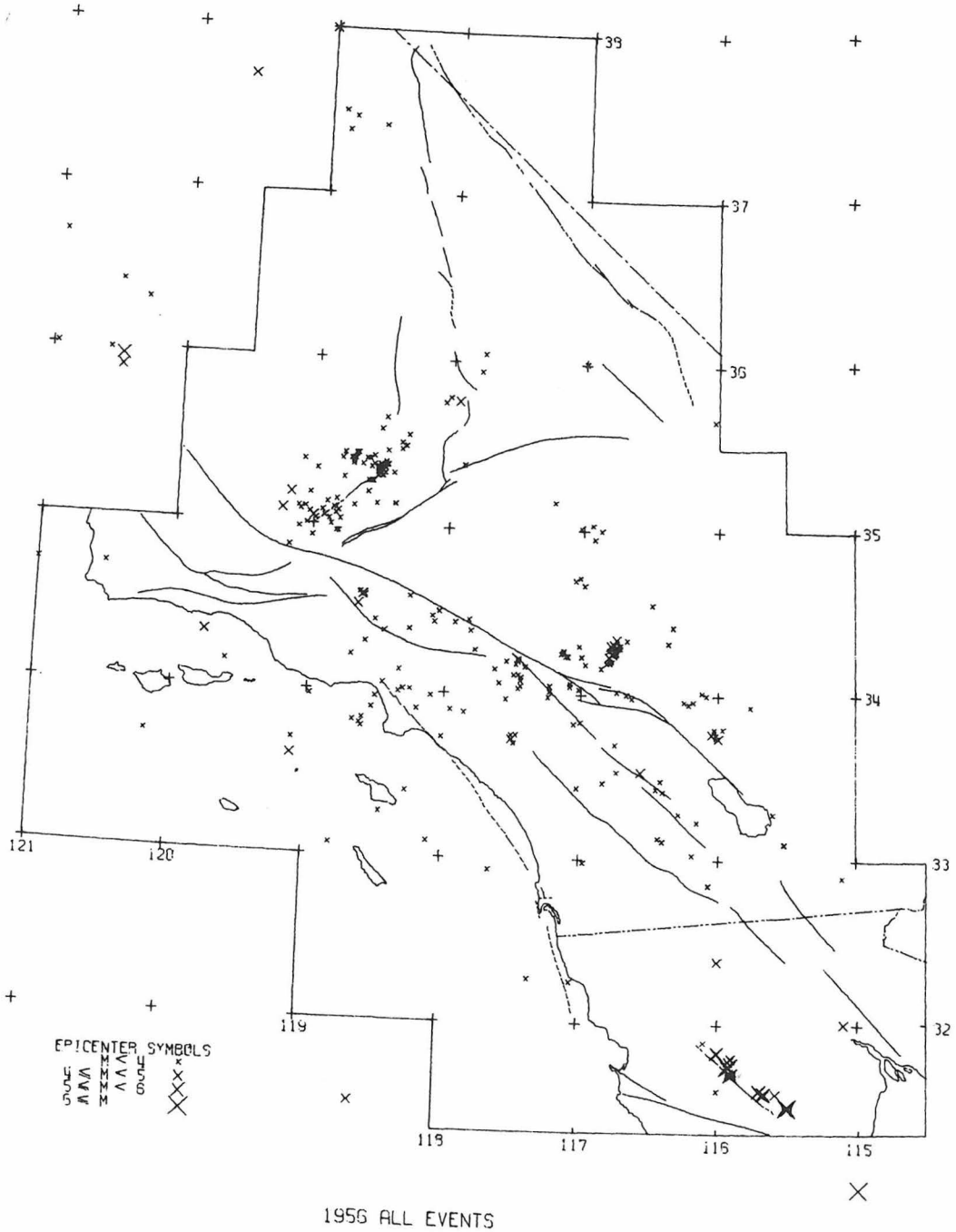

1956 ALL EVENTS

Figure I-26.

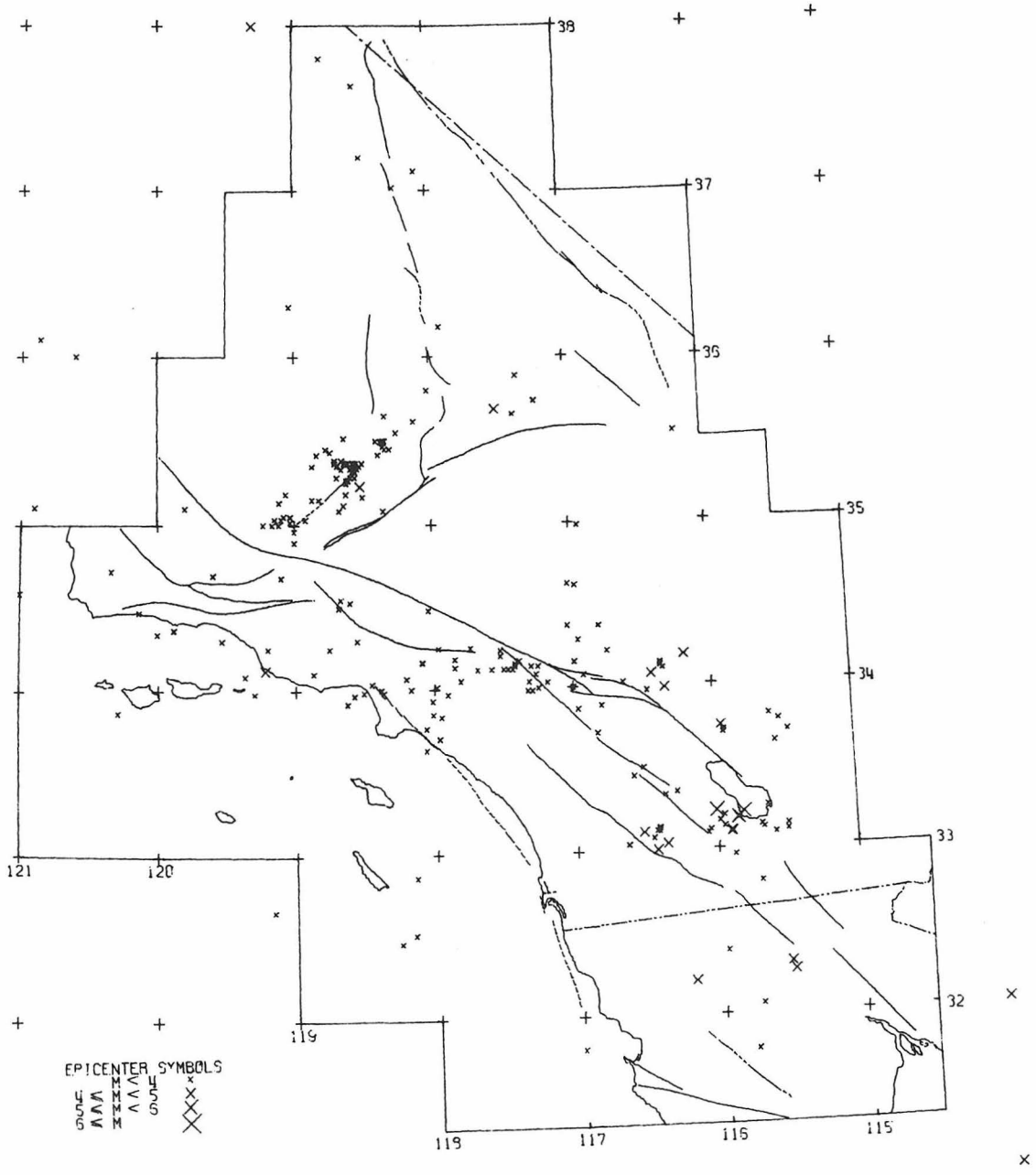

1957 ALL EVENTS

Figure I-27.

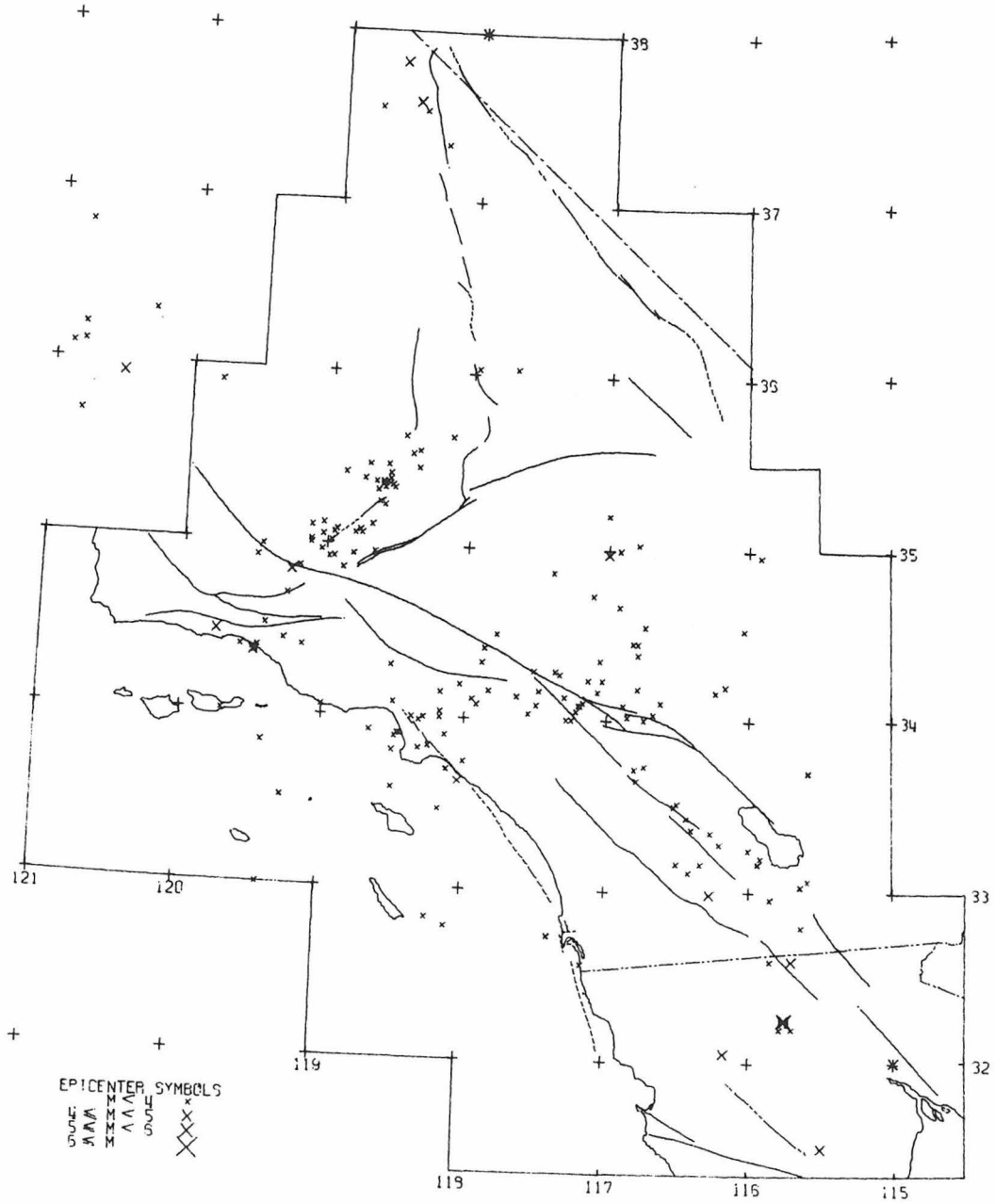

1958 ALL EVENTS

Figure I-28.

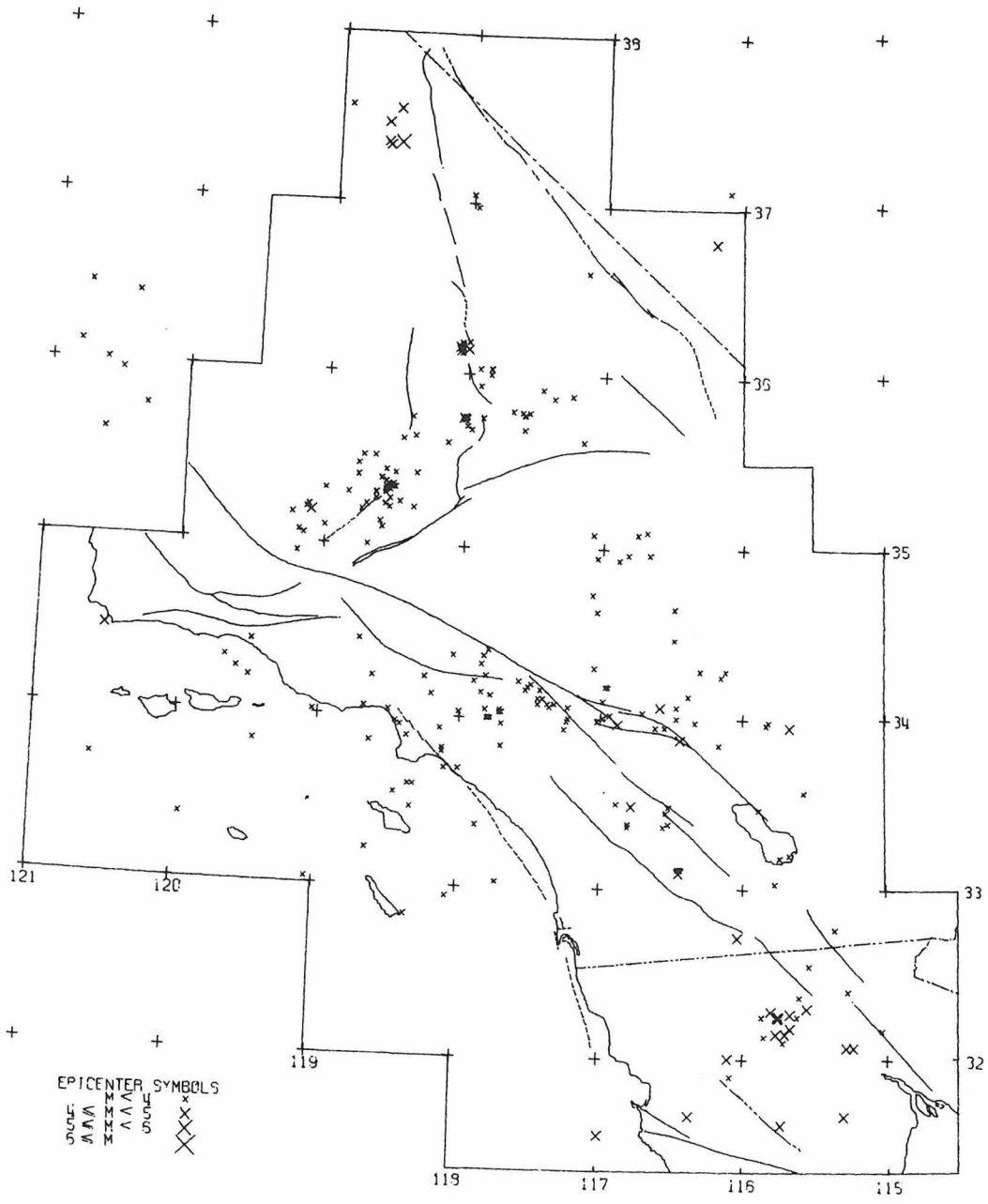

1959 ALL EVENTS

Figure I-29.

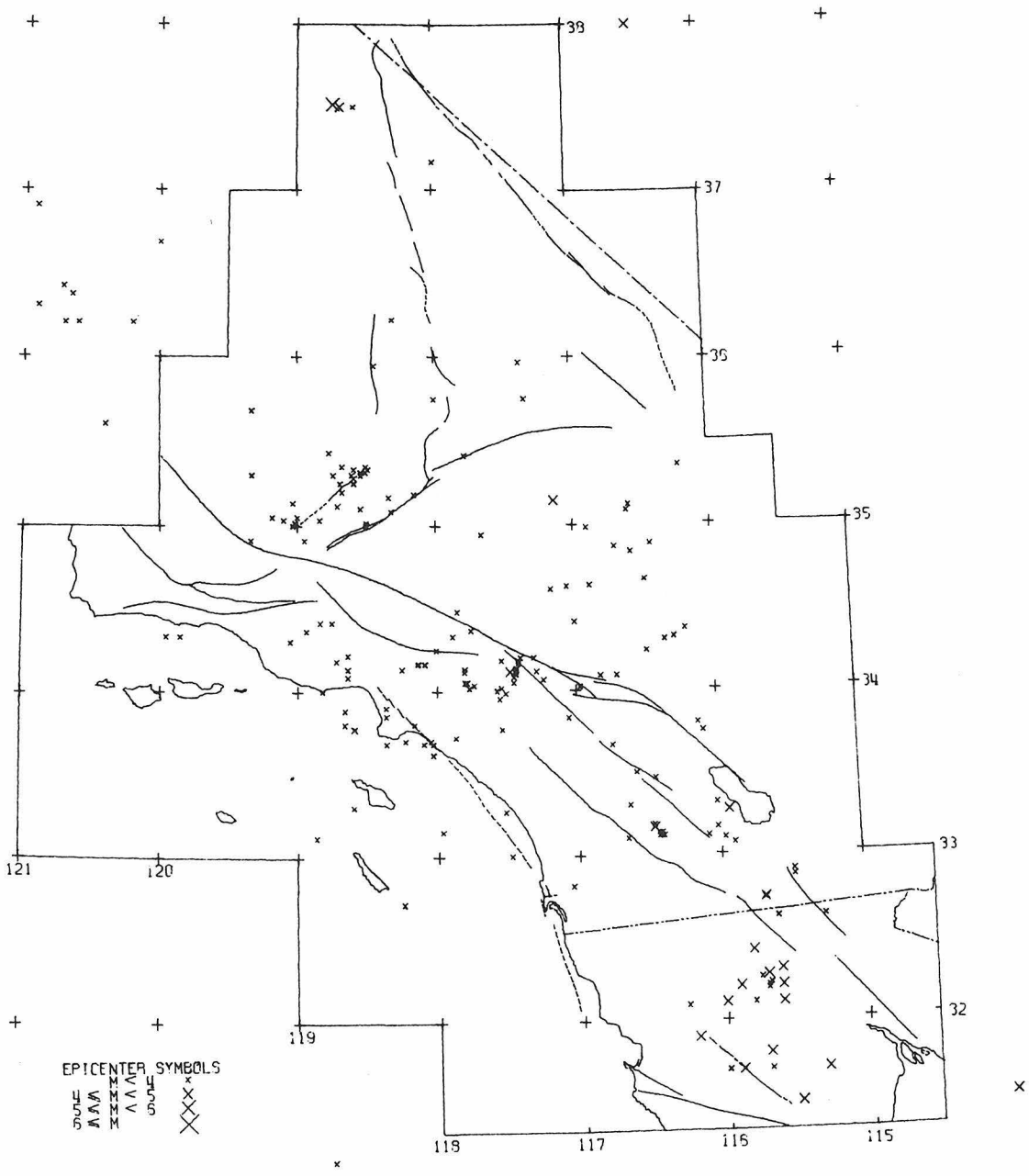

1960 ALL EVENTS

Figure I-30.

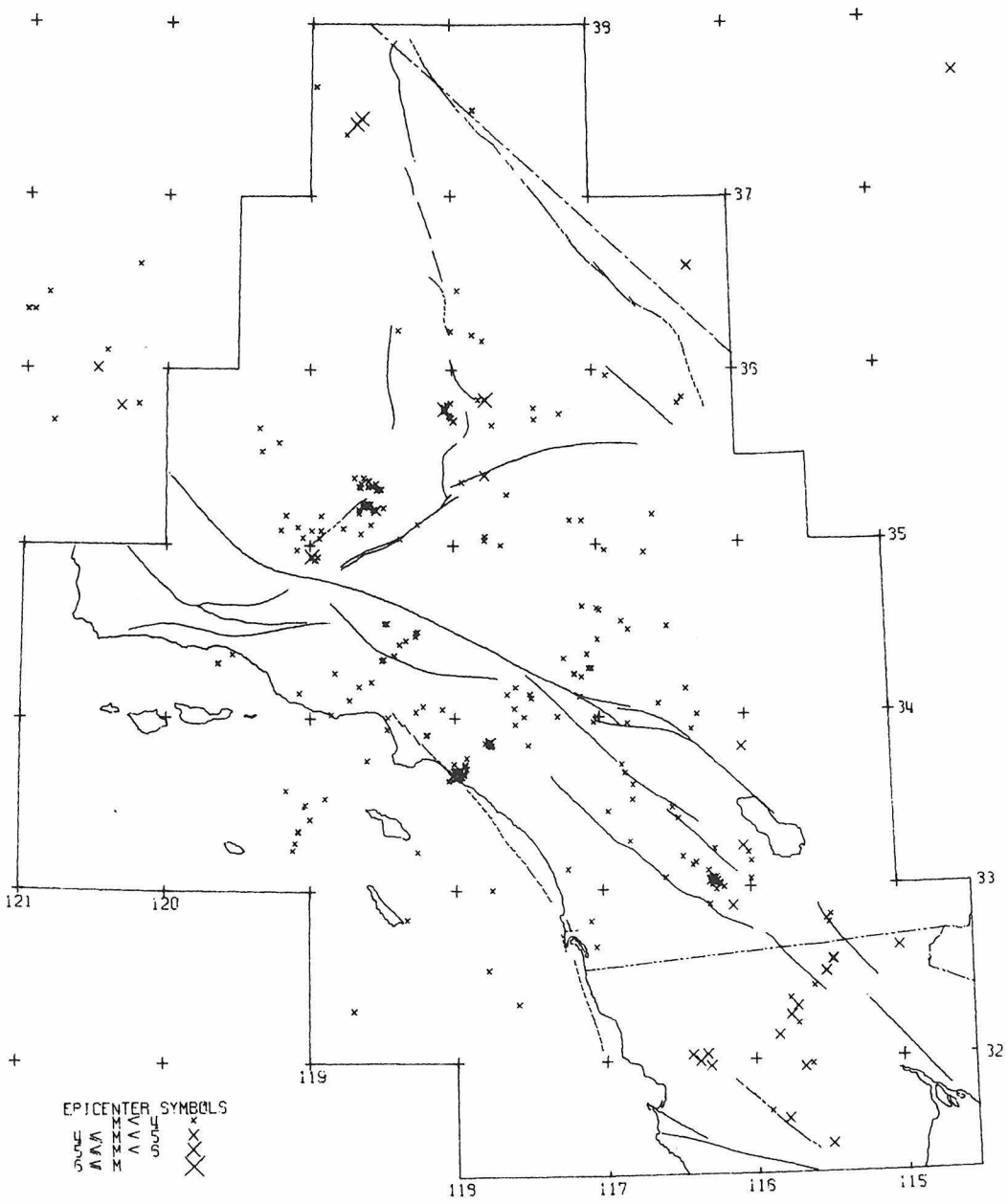

1961 ALL EVENTS

Figure I-31.

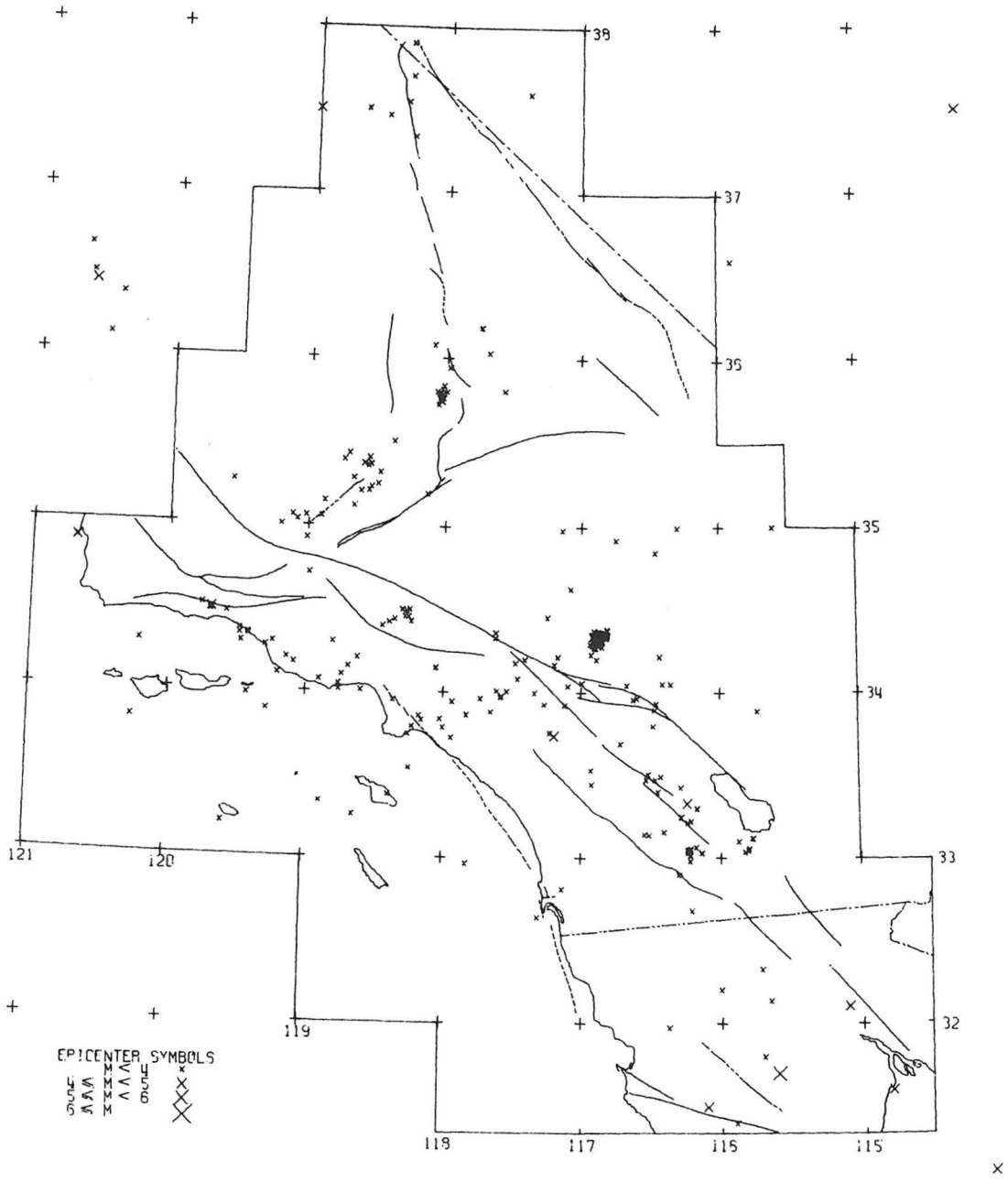

1962 ALL EVENTS

Figure I-32.

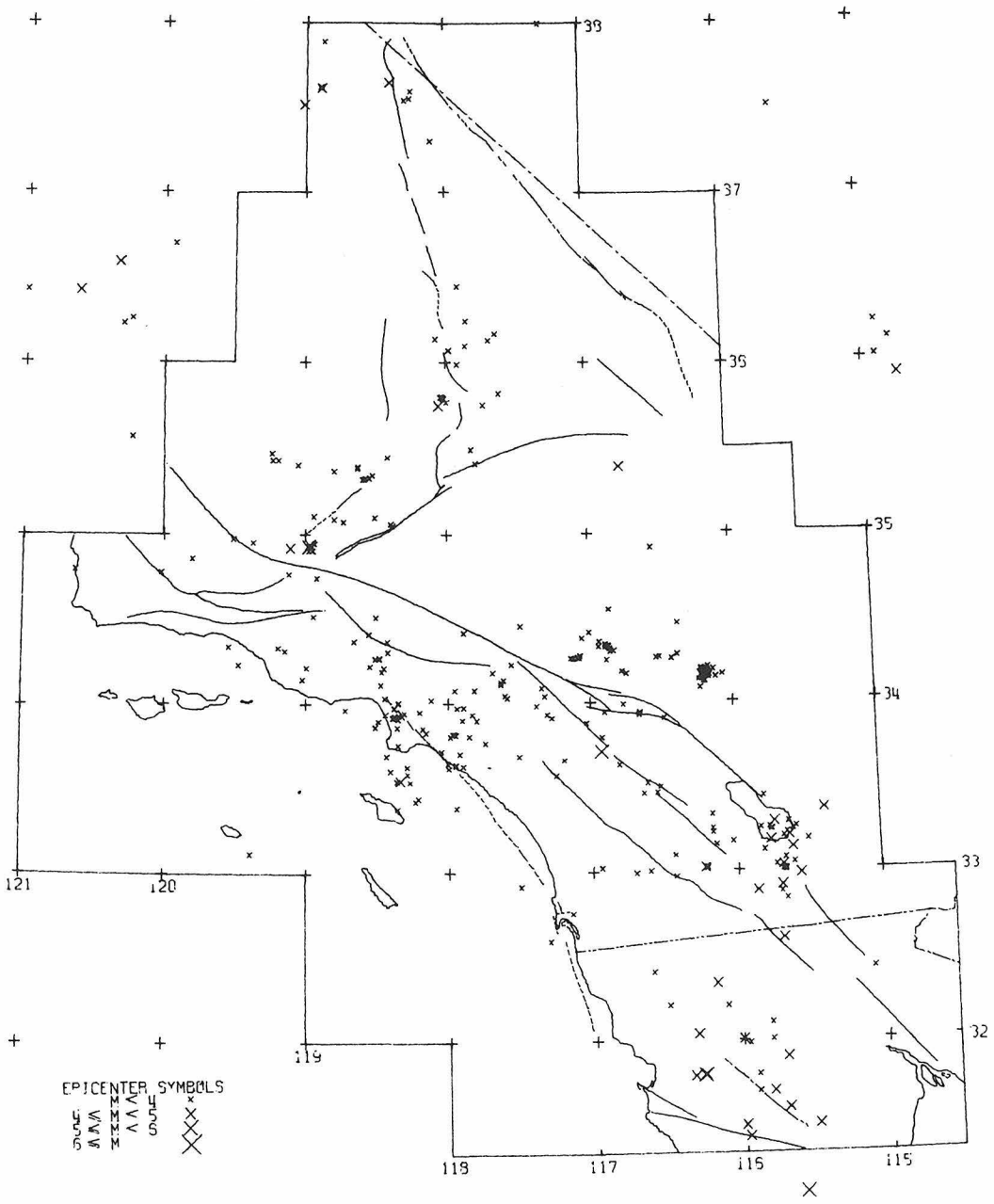

1963 ALL EVENTS

Figure I-33.

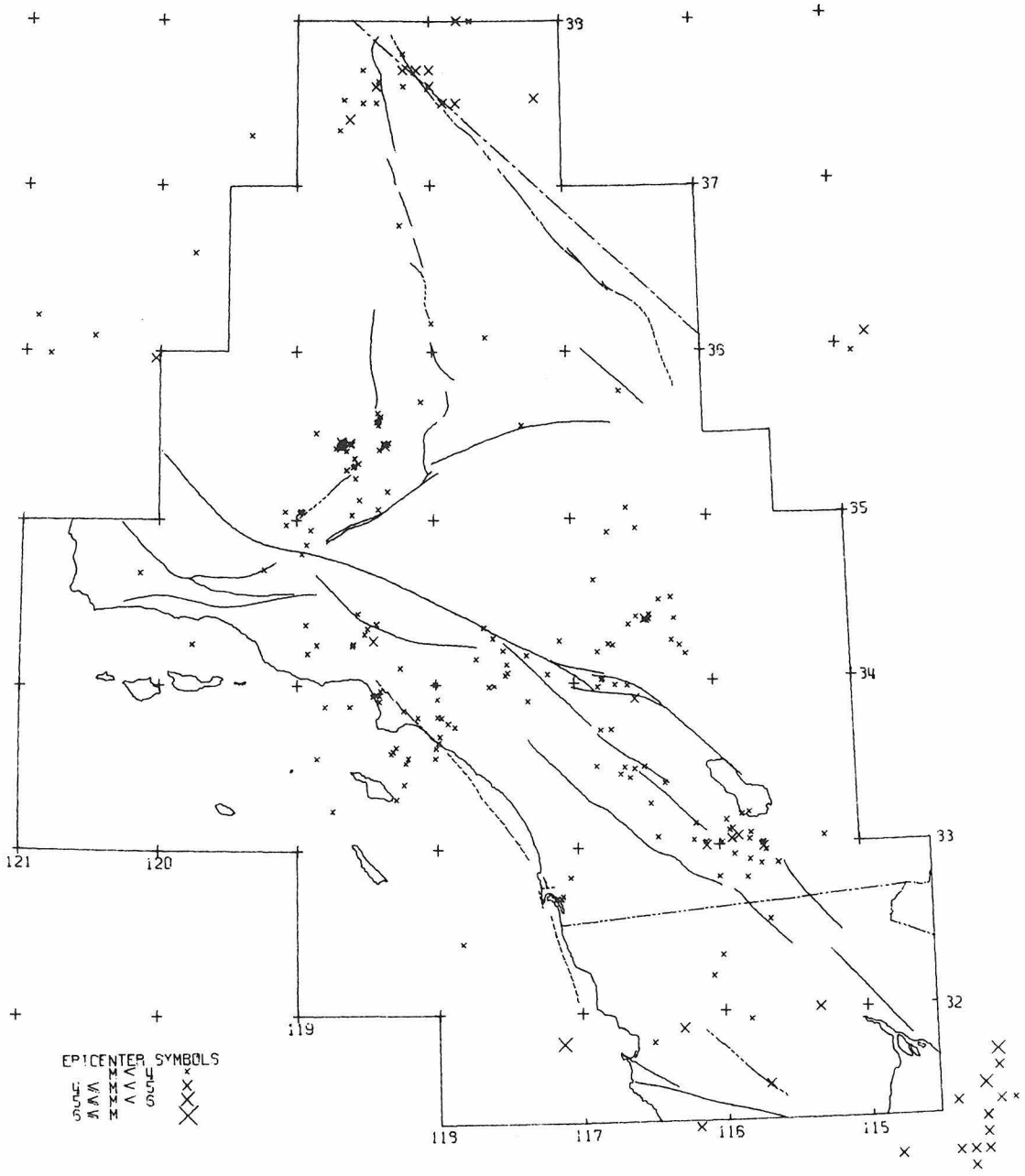

1964 ALL EVENTS

Figure I-34.

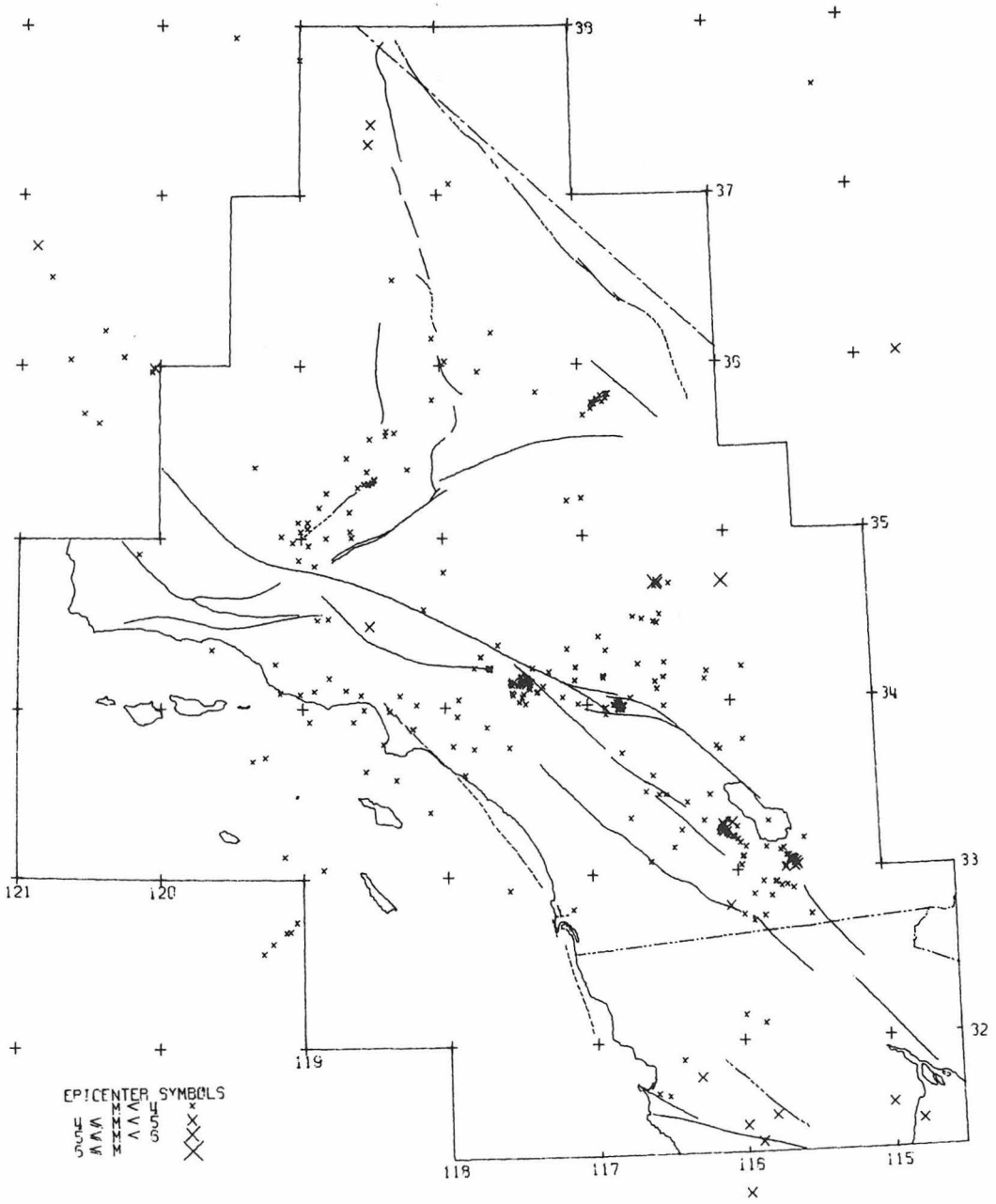

1965 ALL EVENTS

Figure I-35.

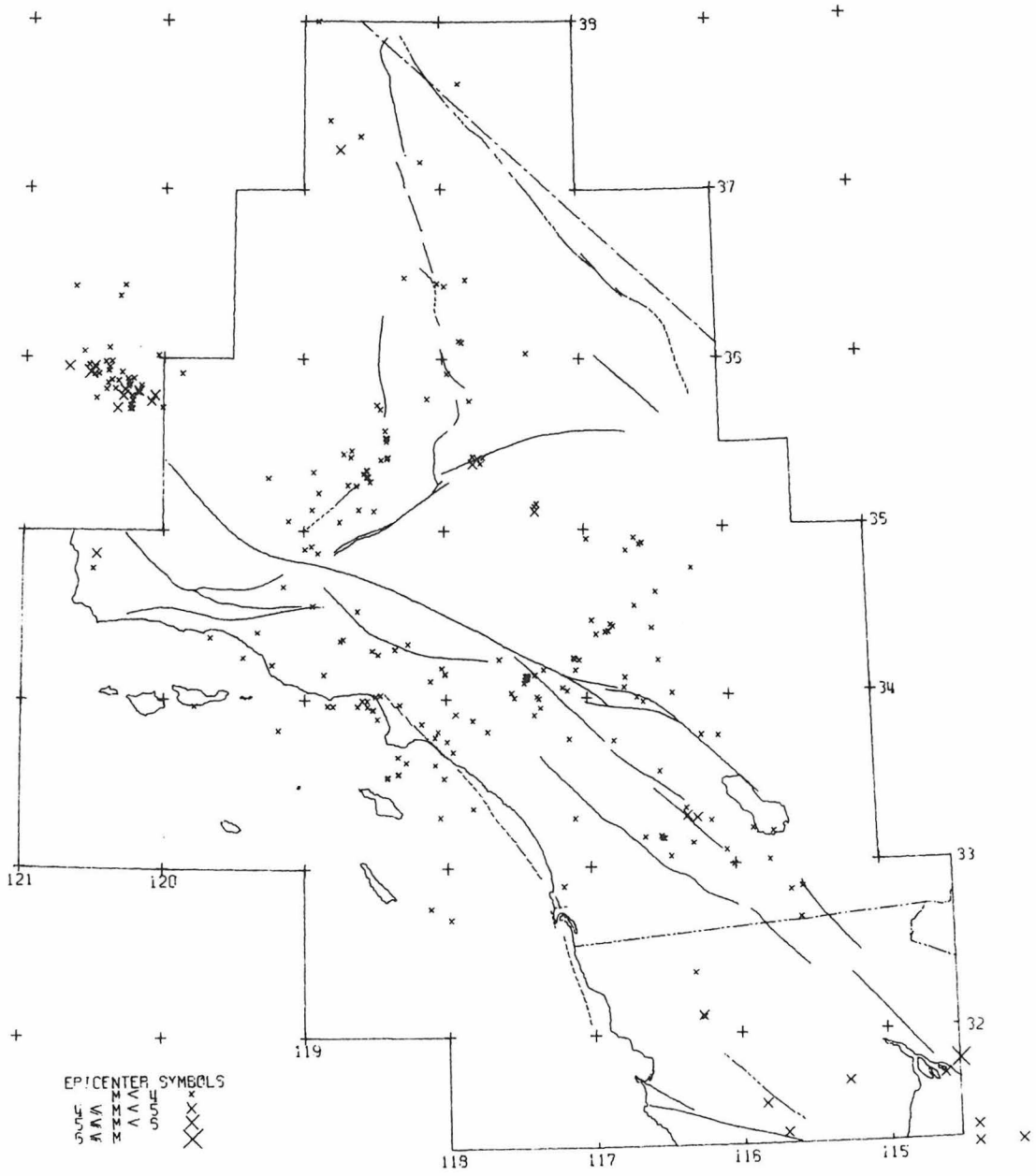

1966 ALL EVENTS

Figure I-36.

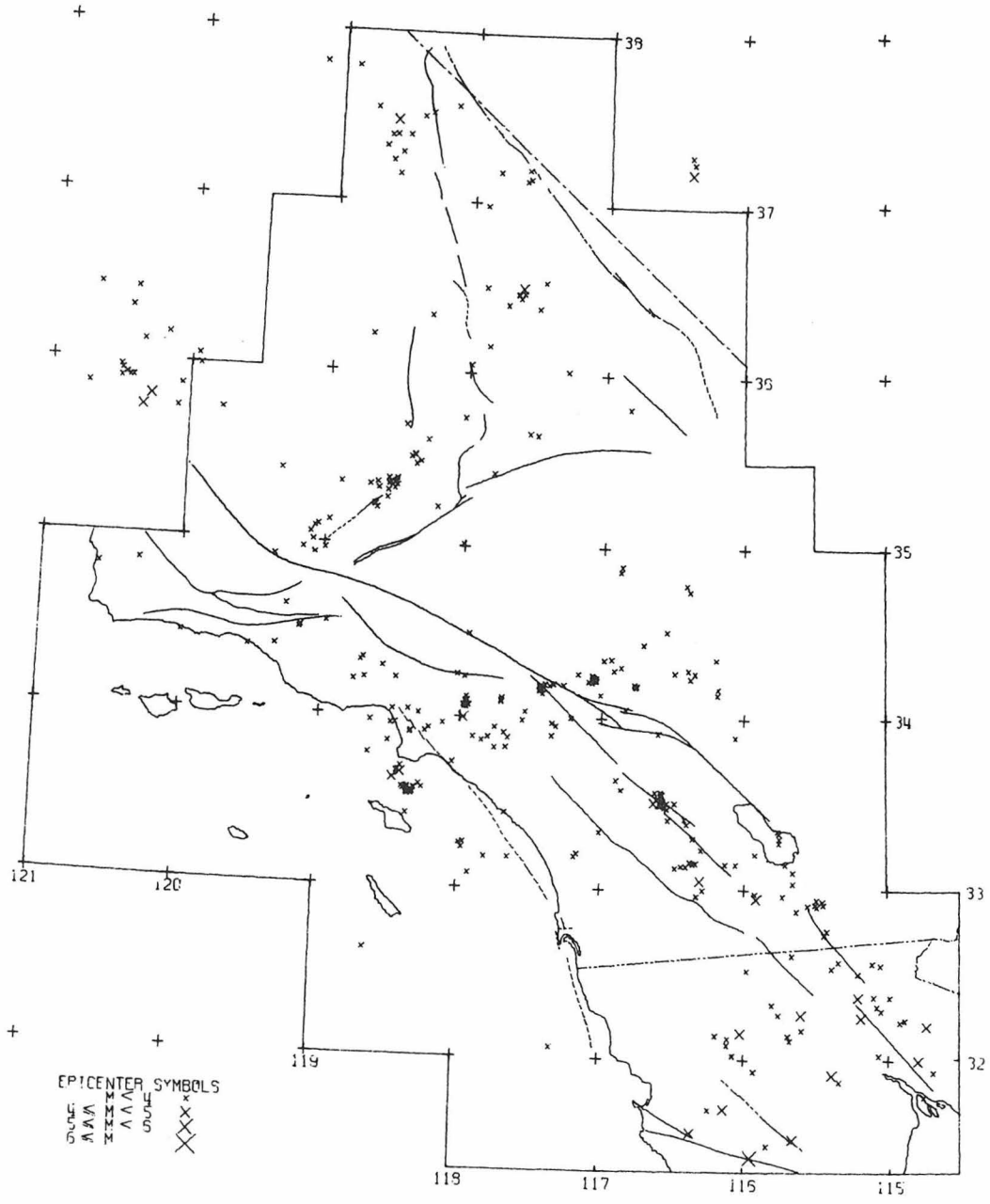

1967 ALL EVENTS

Figure I-37.

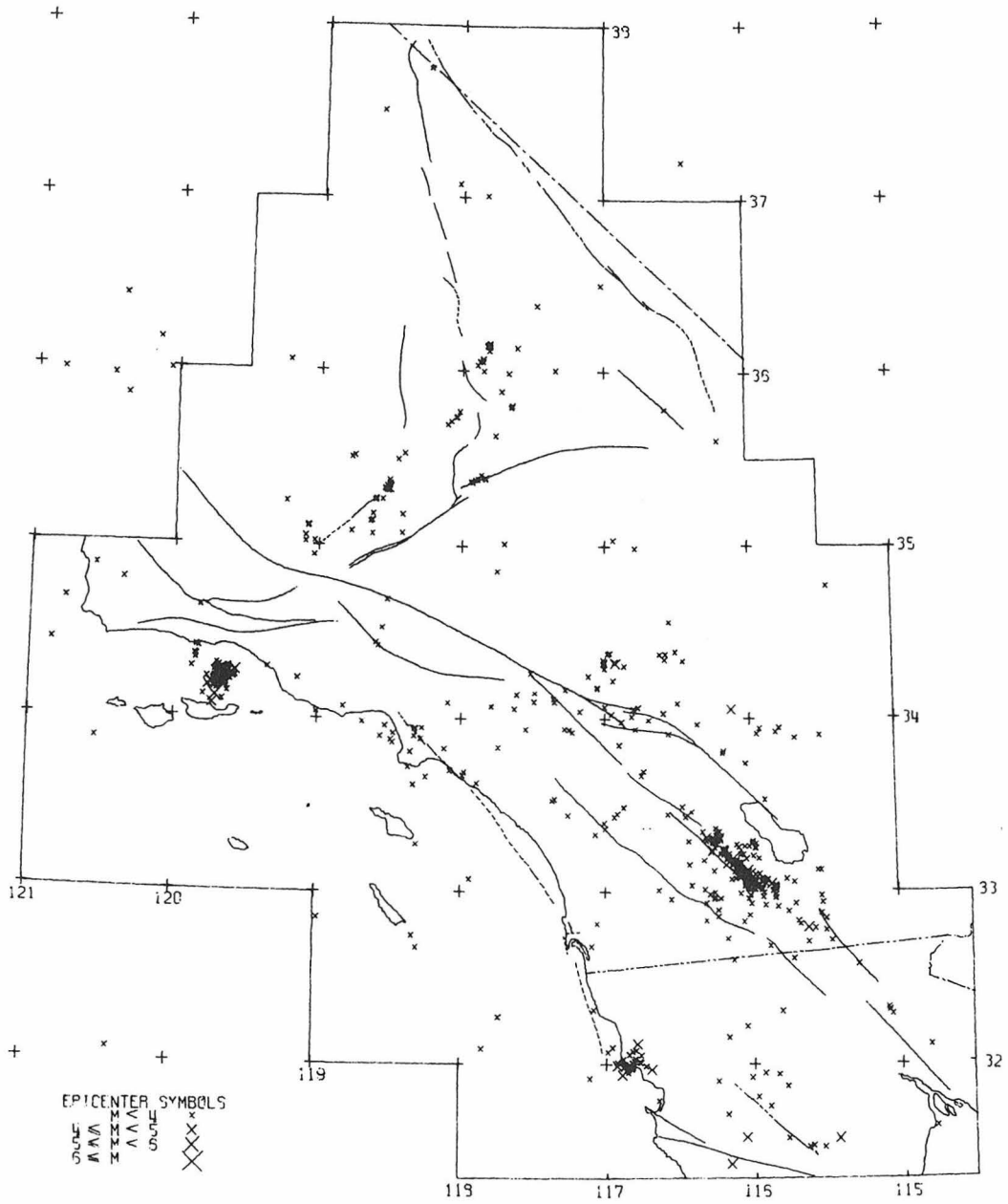

1968 ALL EVENTS

Figure I-38.

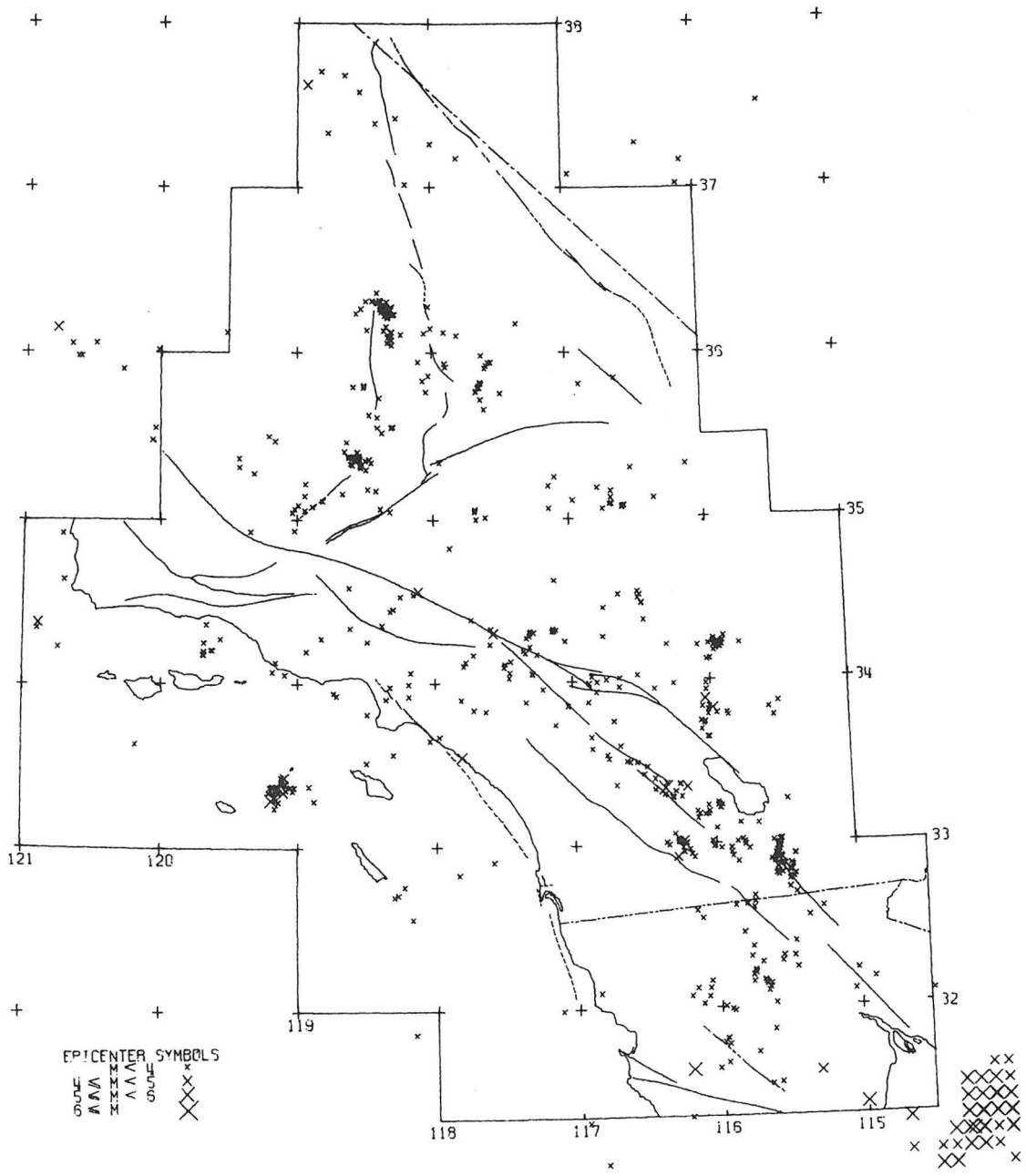

1969 ALL EVENTS

Figure I-39.

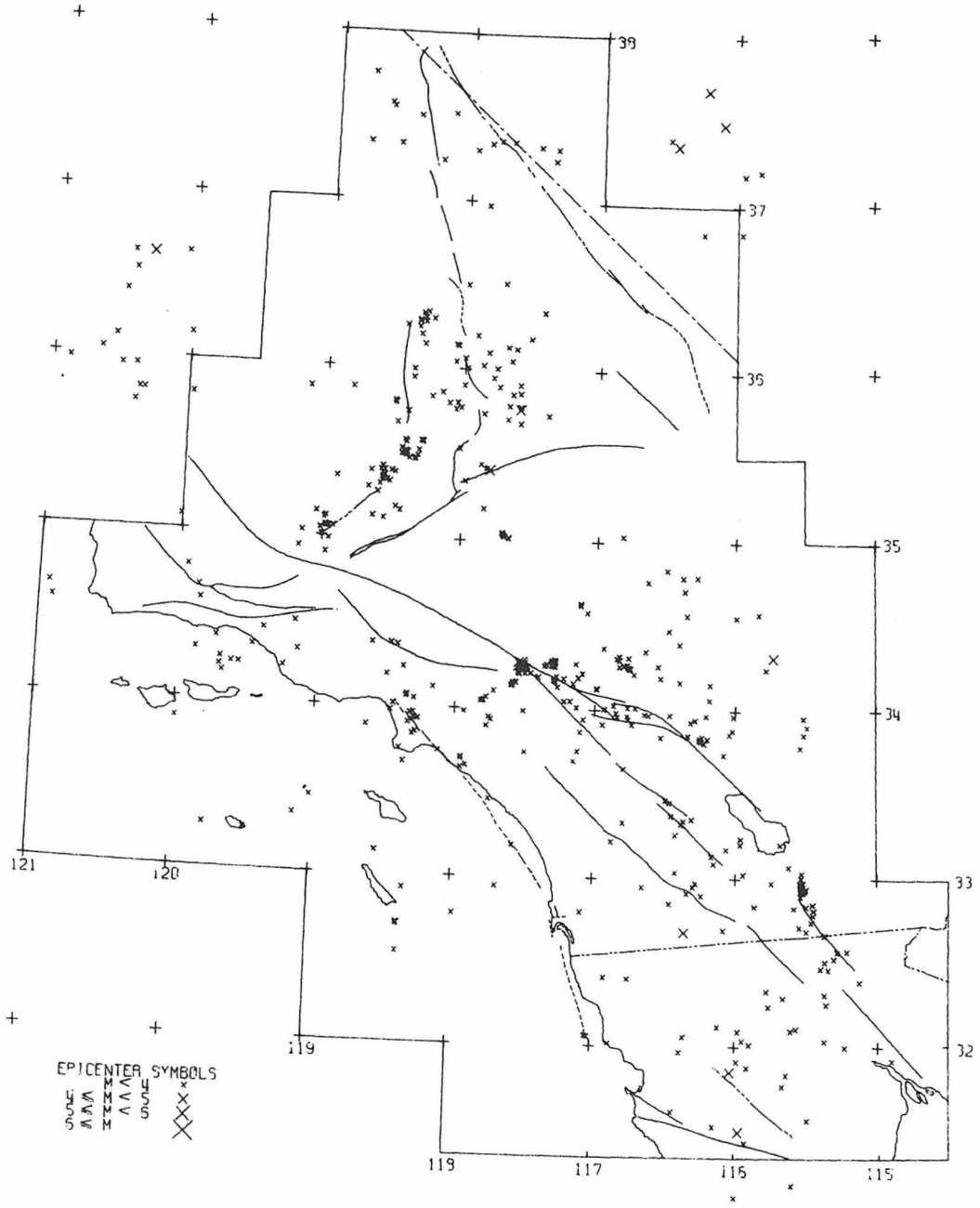

1970 ALL EVENTS

Figure I-40.

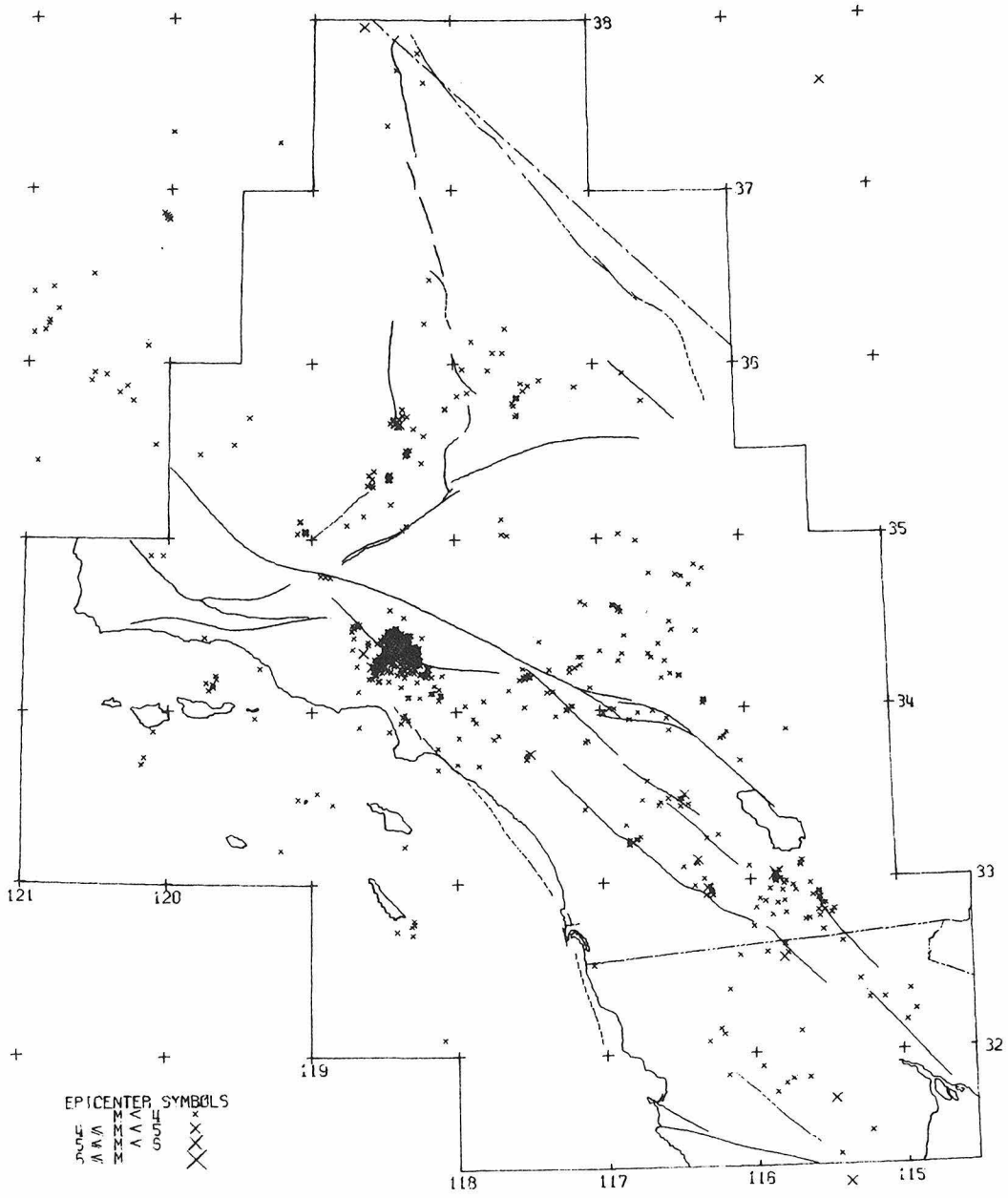

1971 ALL EVENTS

Figure I-41.

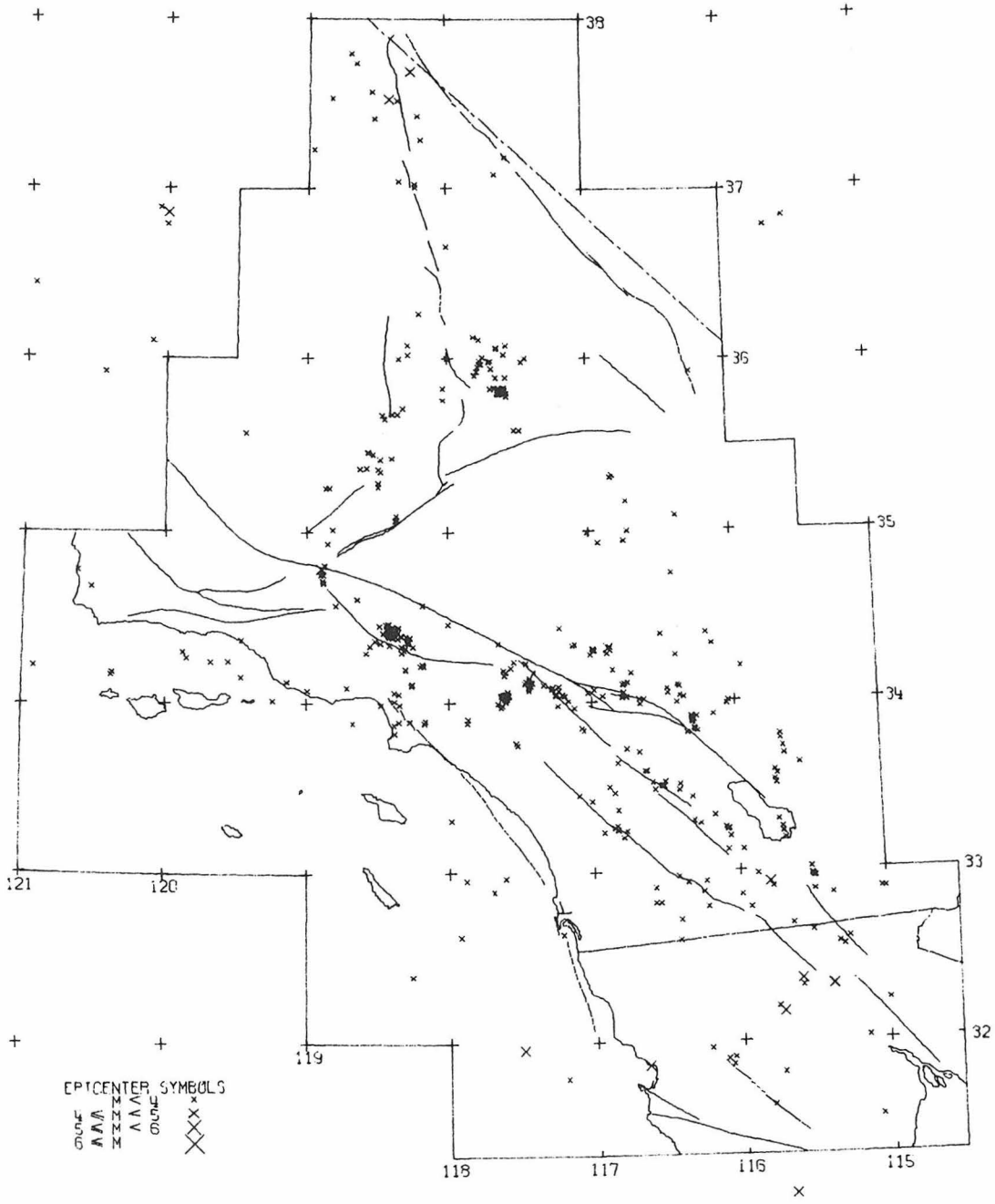

1972 ALL EVENTS

Figure I-42.

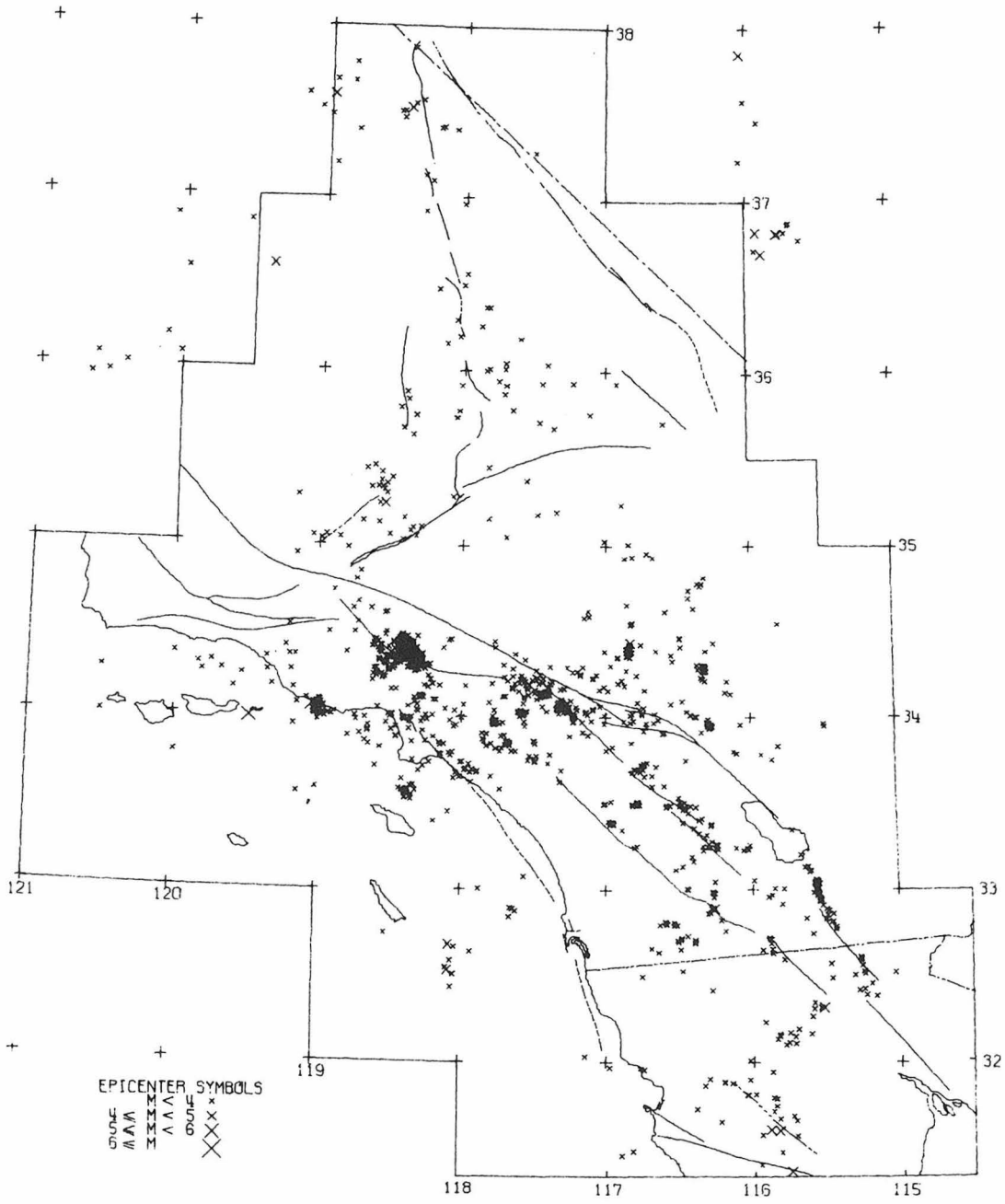

1973 ALL EVENTS

Figure I-43.

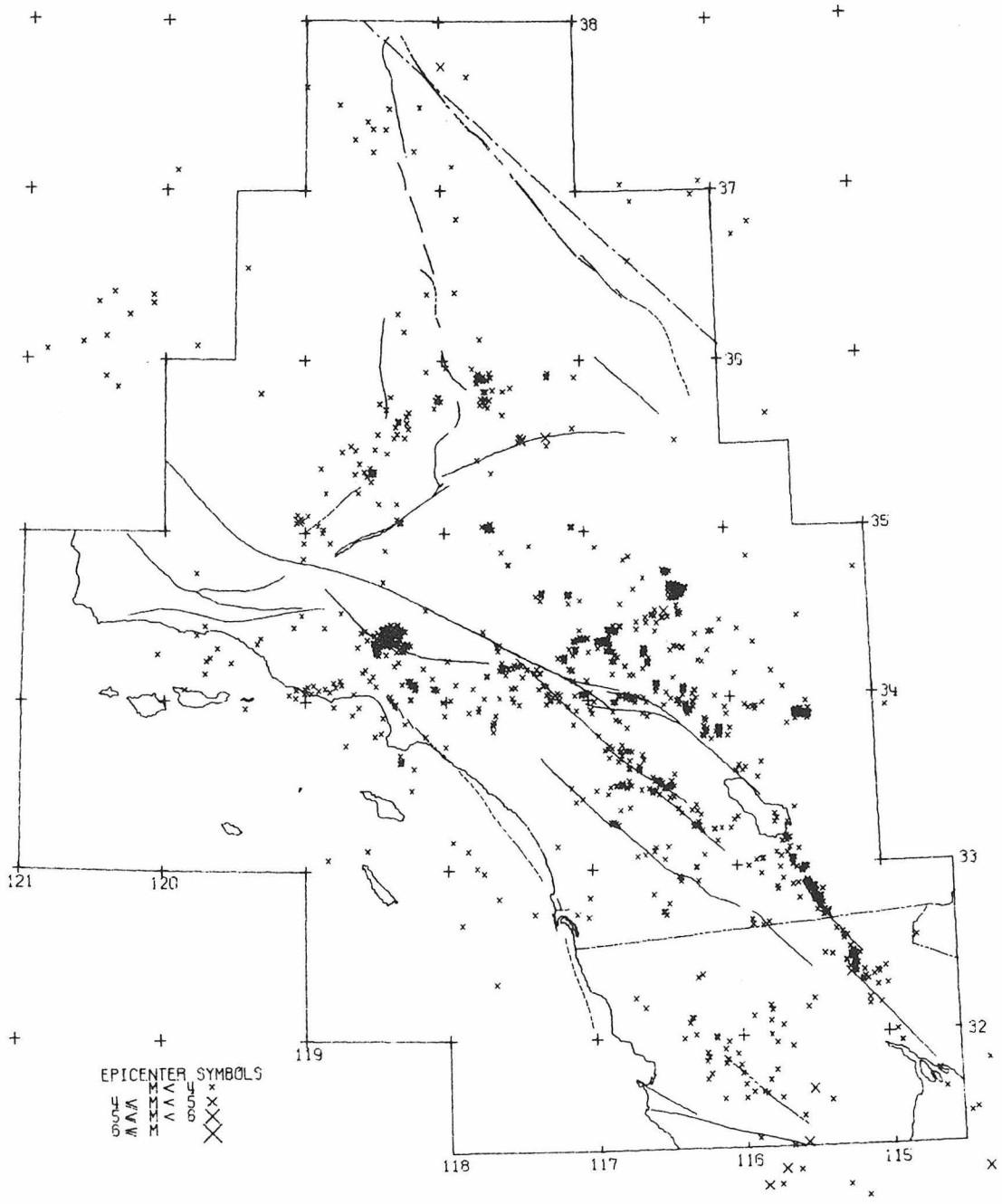

1974 ALL EVENTS

Figure I-44.

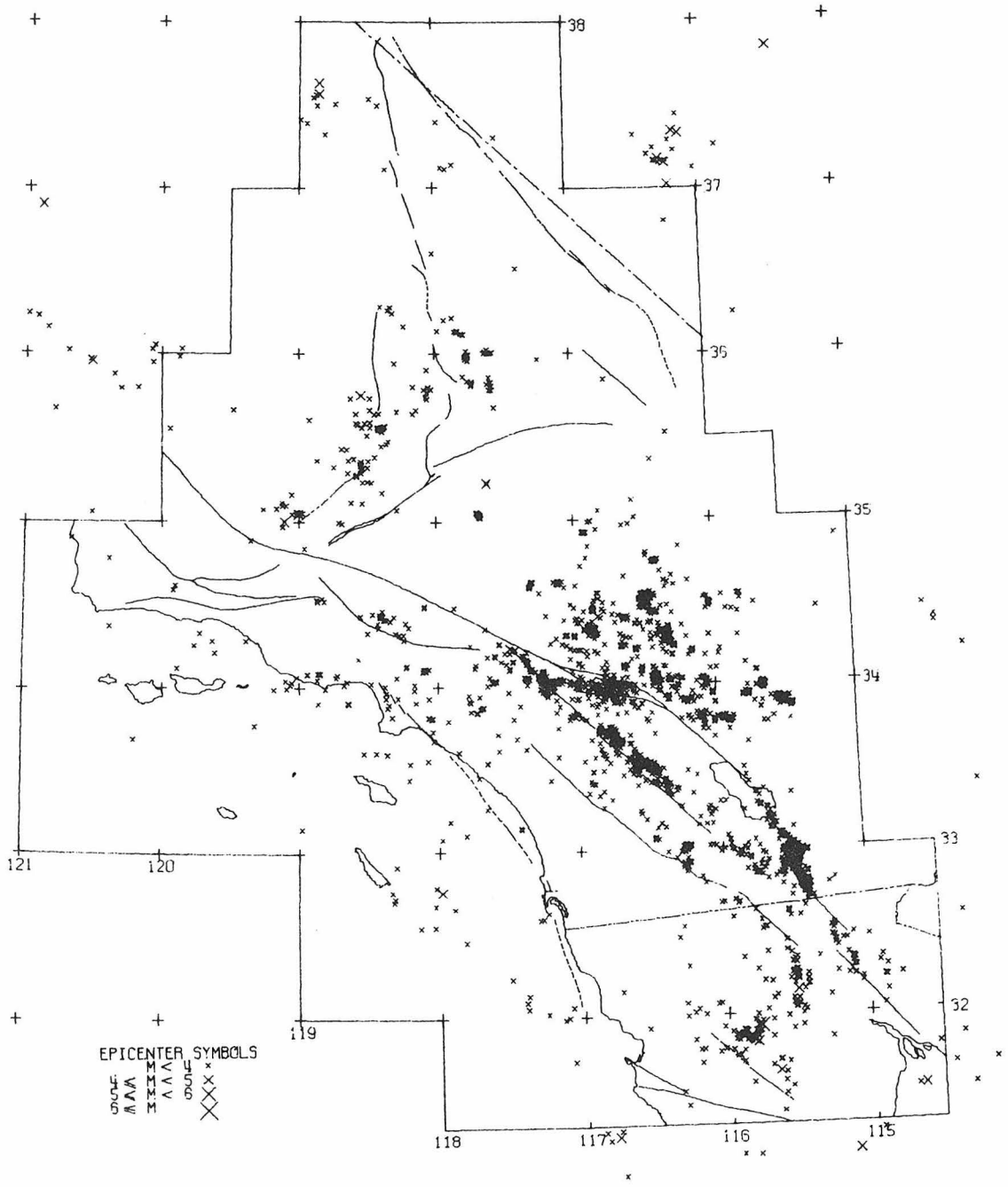

1975 ALL EVENTS

Figure I-45.

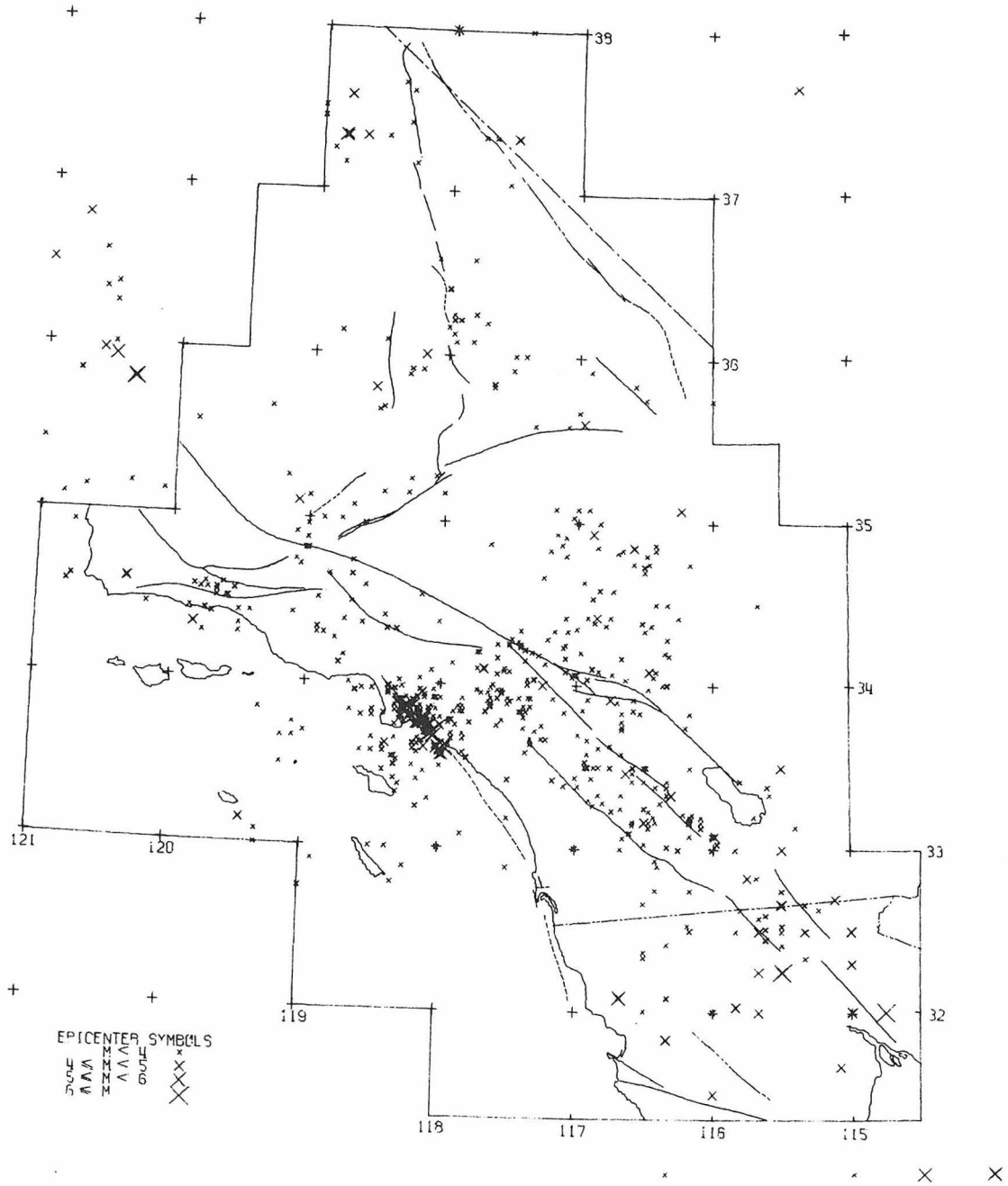

1932 THROUGH 1934, ALL EVENTS

Figure I-46.

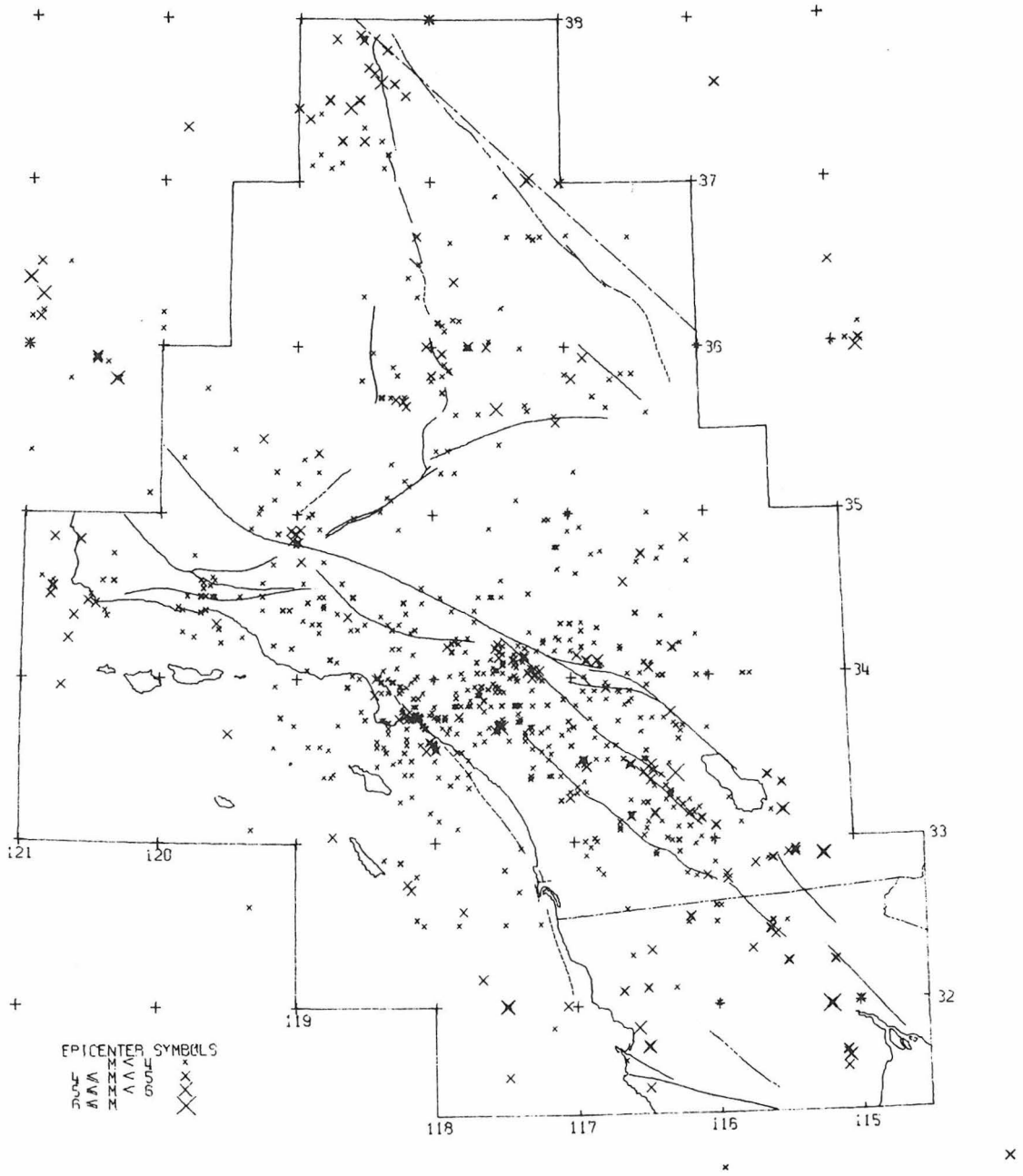

1935 THROUGH 1939, ALL EVENTS

Figure I-47.

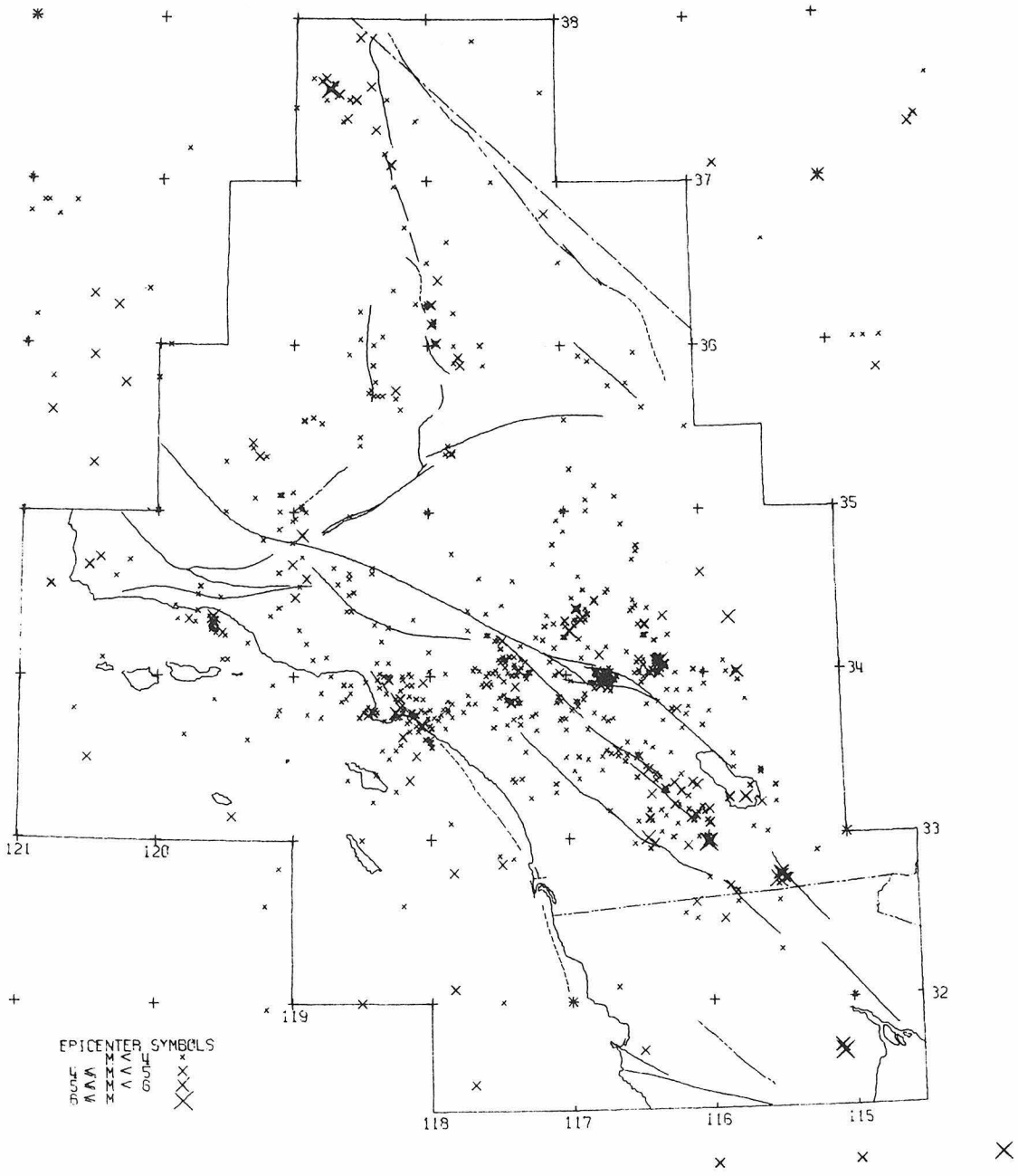

1940 THROUGH 1944, ALL EVENTS

Figure I-48.

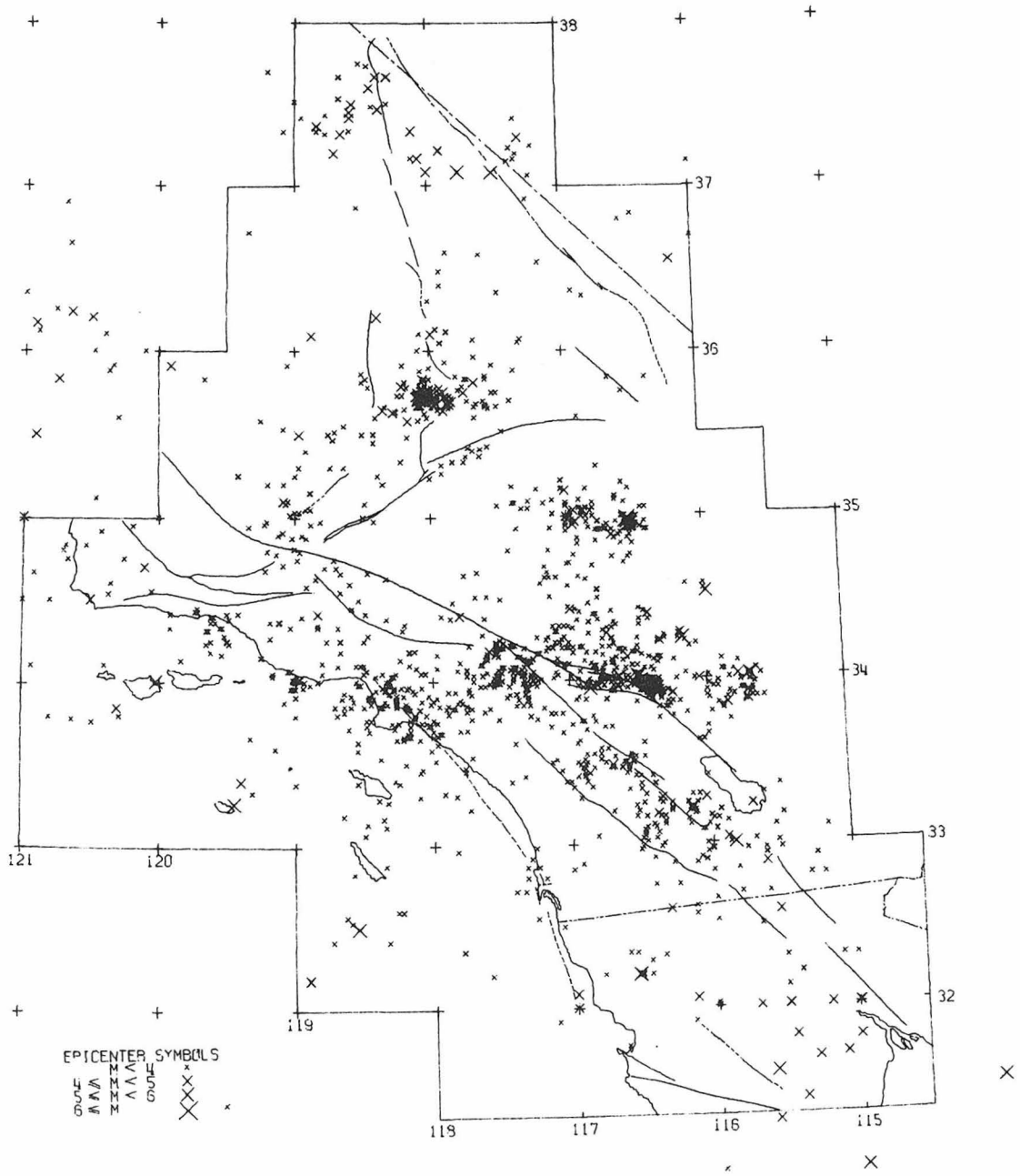

1945 THROUGH 1949, ALL EVENTS

Figure I-49.

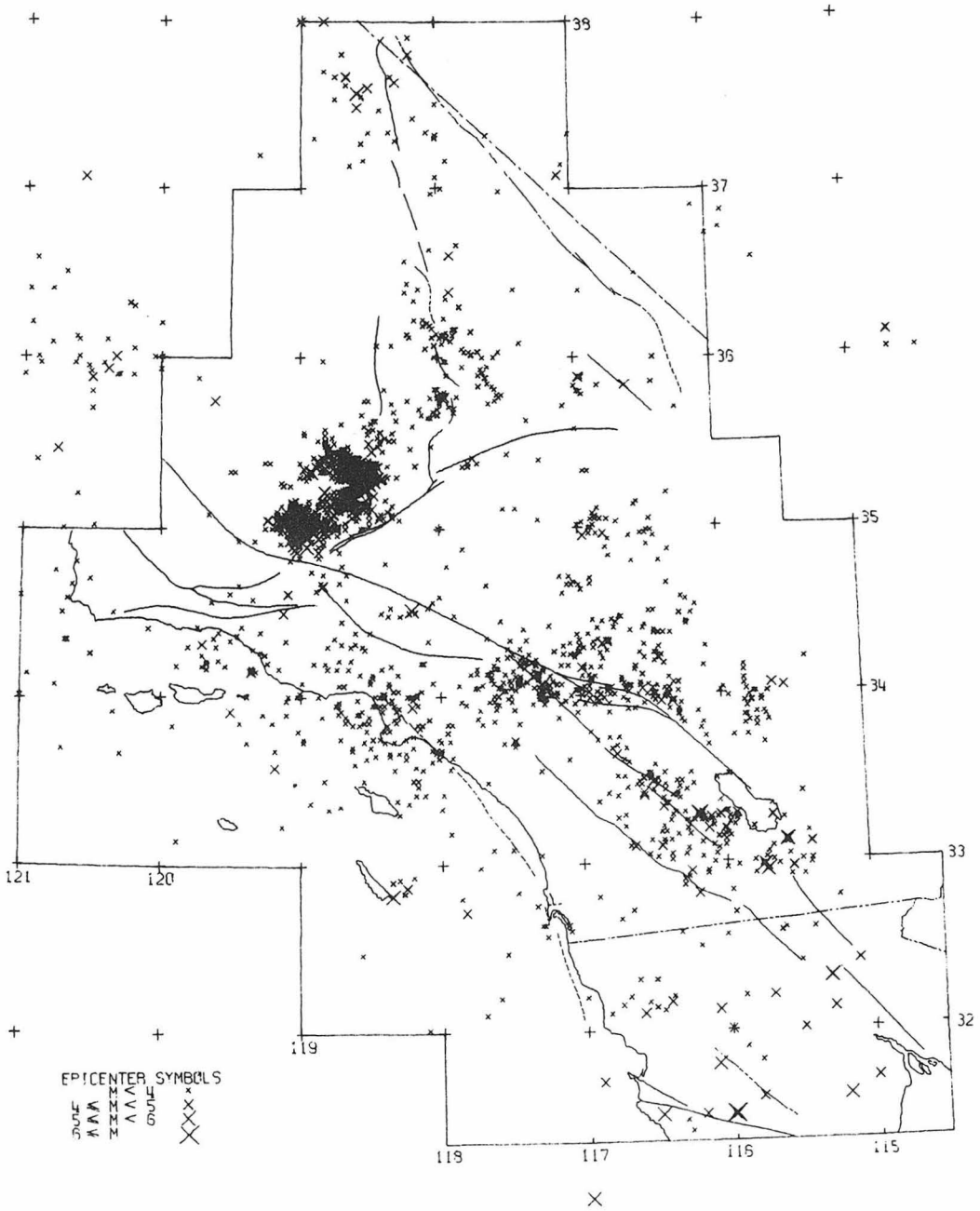
39
37
36
35
34
33
32
121
120
119
119
117
116
115
EPICENTER SYMBOLS
5
5+
6
1950 THROUGH 1954, ALL EVENTS

Figure I-50.

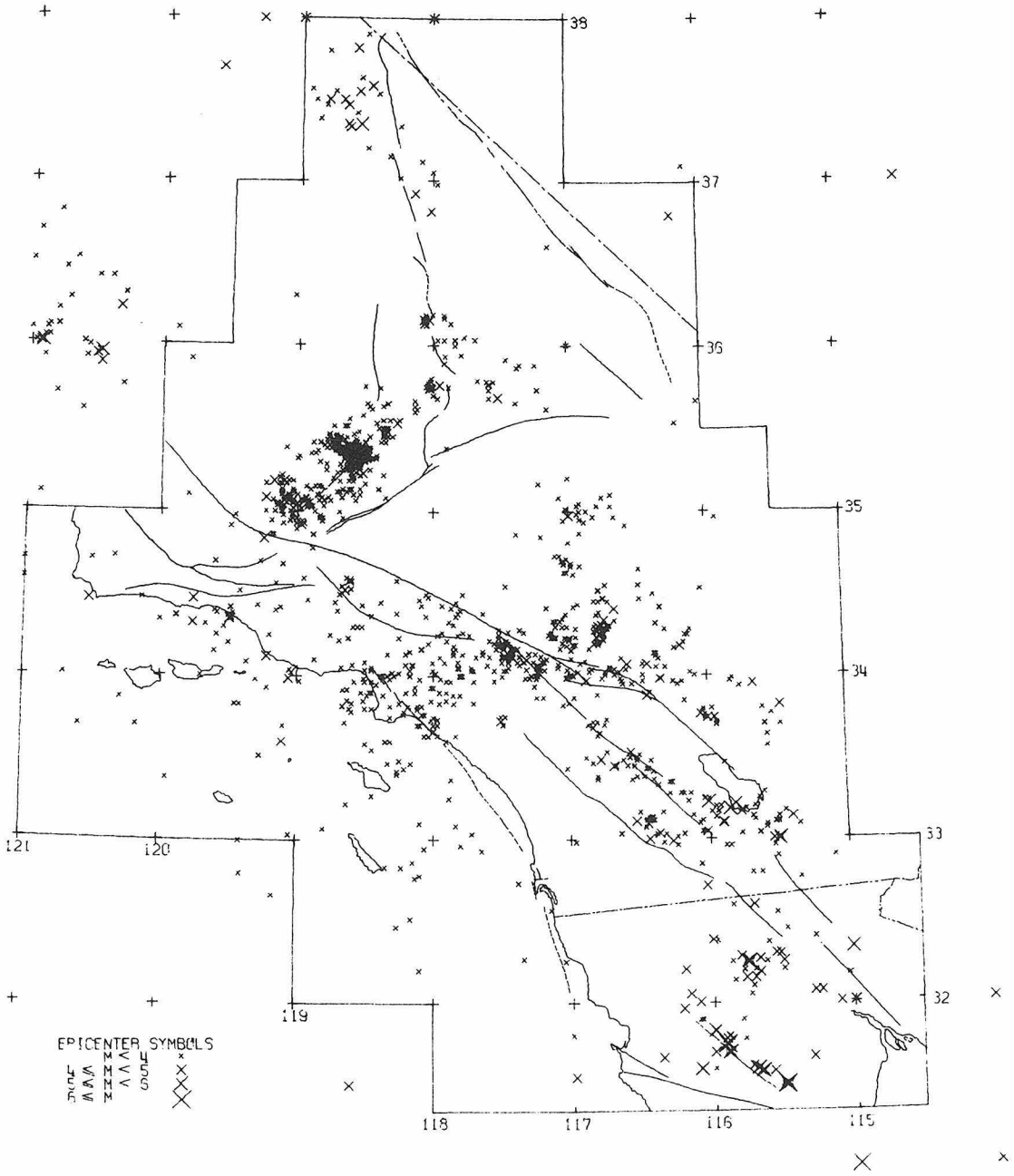

1955 THROUGH 1959. ALL EVENTS

Figure I-51.

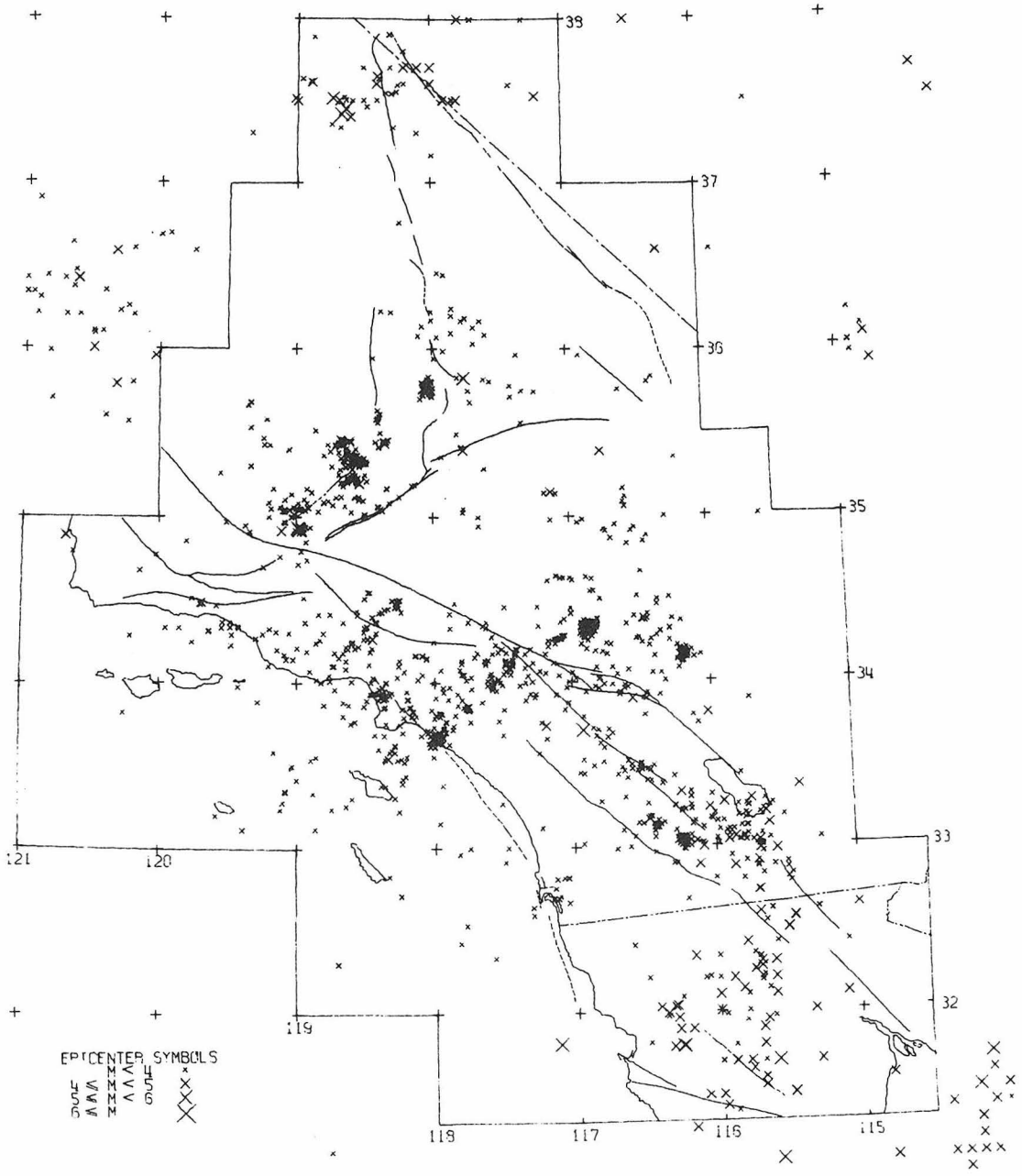

1960 THROUGH 1964, ALL EVENTS

Figure I-52.

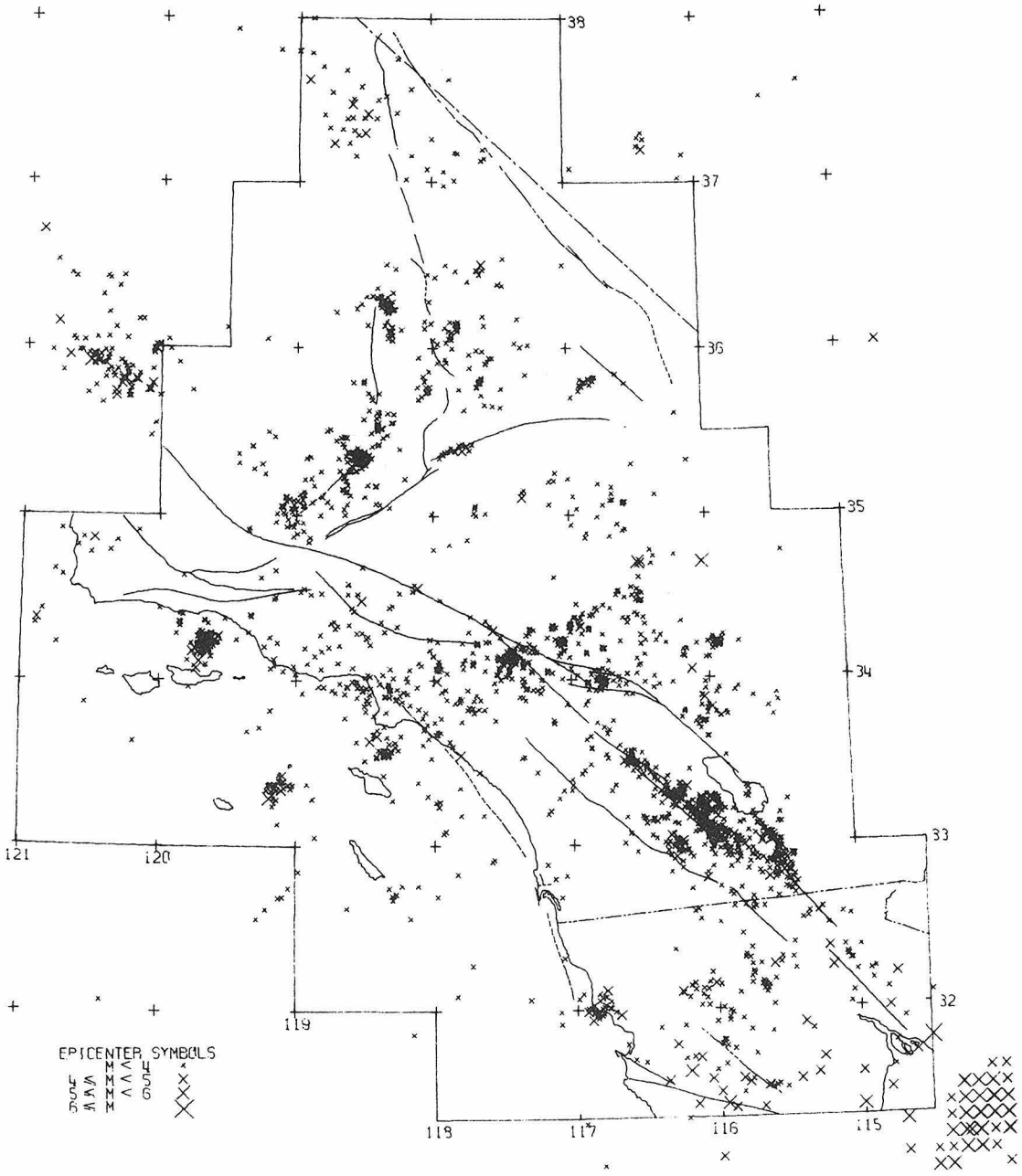

1965 THROUGH 1969, ALL EVENTS

Figure I-53.

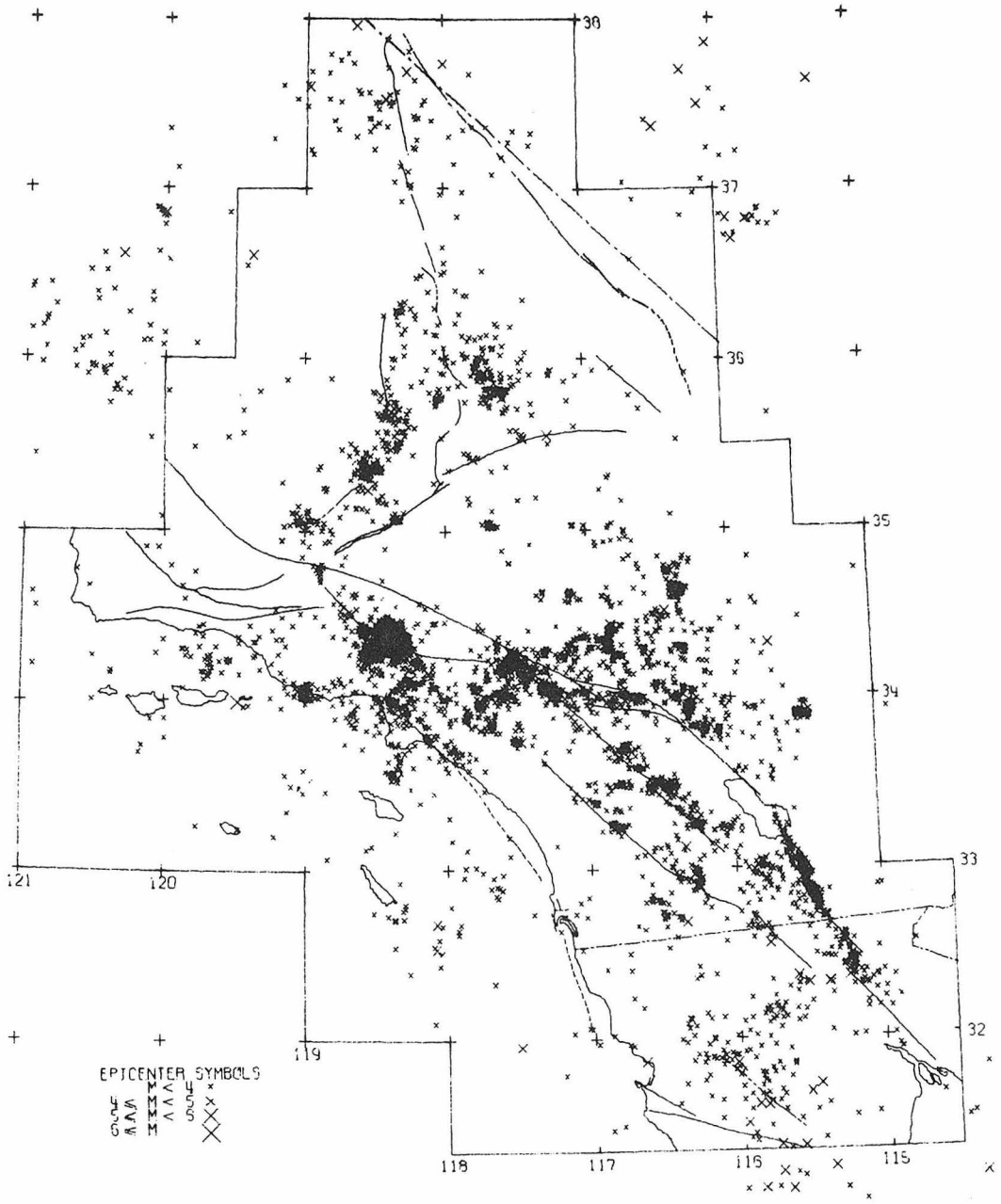

1970 THROUGH 1974 ALL EVENTS

Figure I-54.

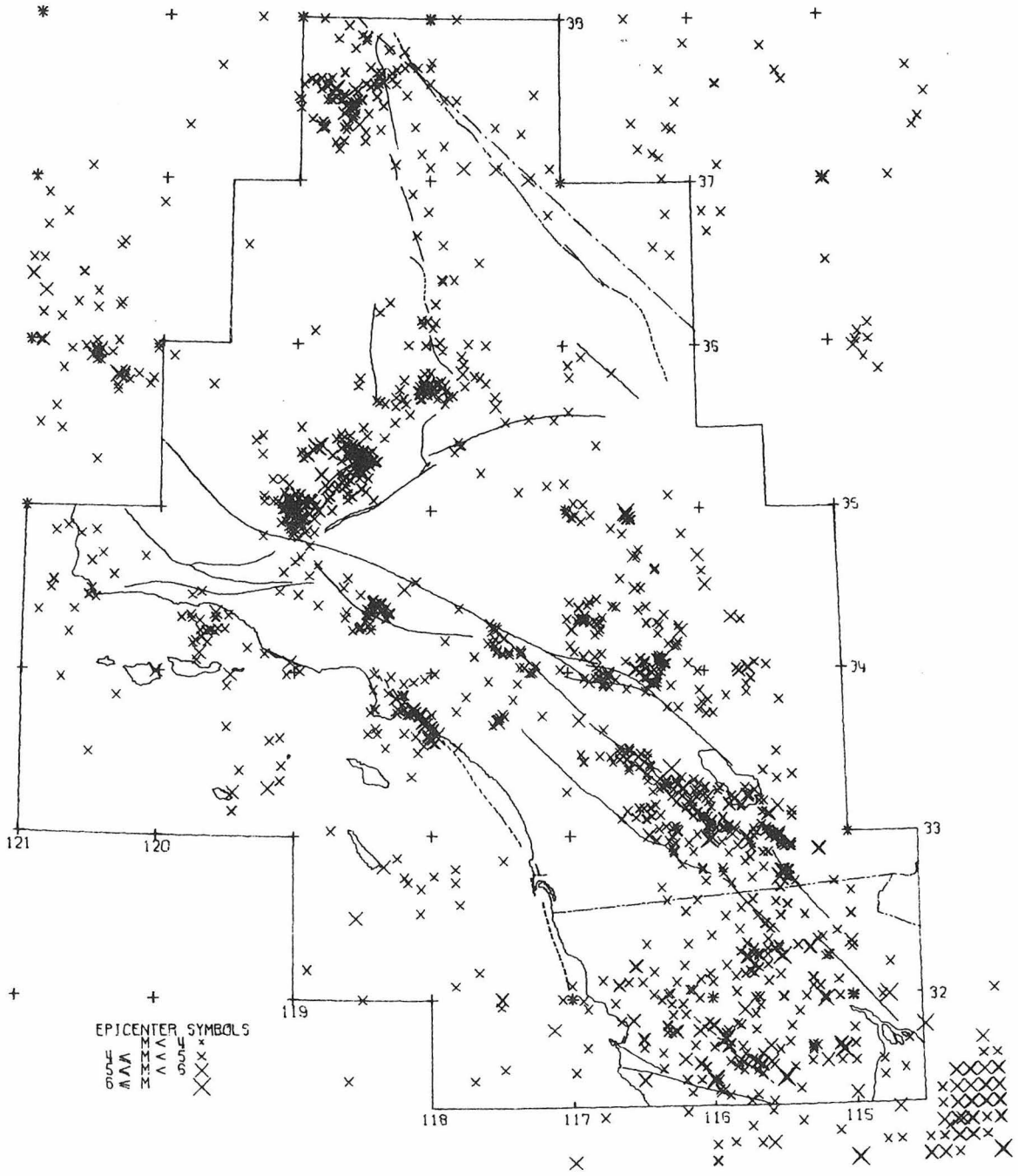

1932 THROUGH 1975, EVENTS EQUAL OR GREATER THAN MAGNITUDE 4

Figure I-55.

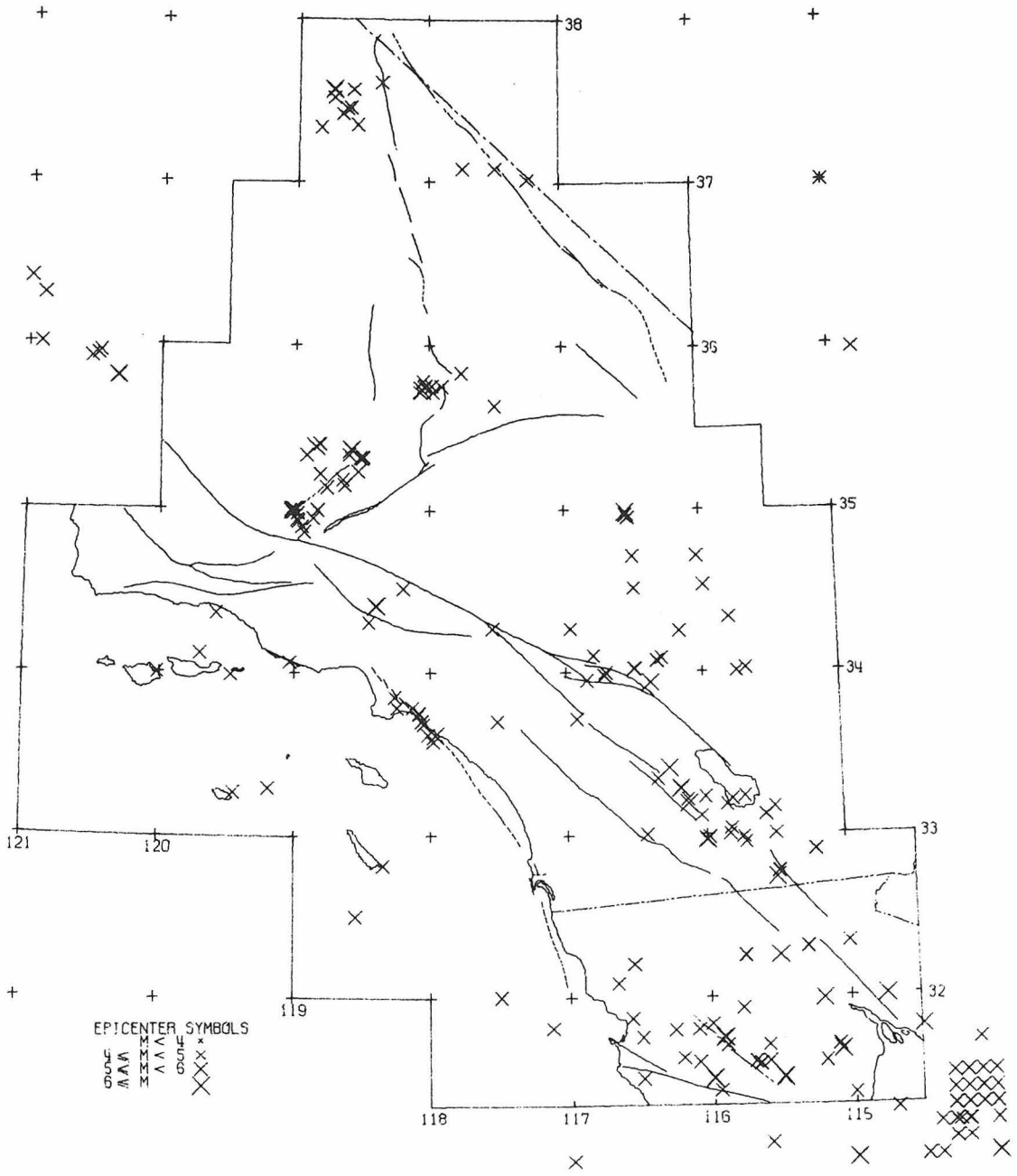

1932 THROUGH 1975, EVENTS EQUAL OR GREATER THAN MAGNITUDE 5

Figure I-56.

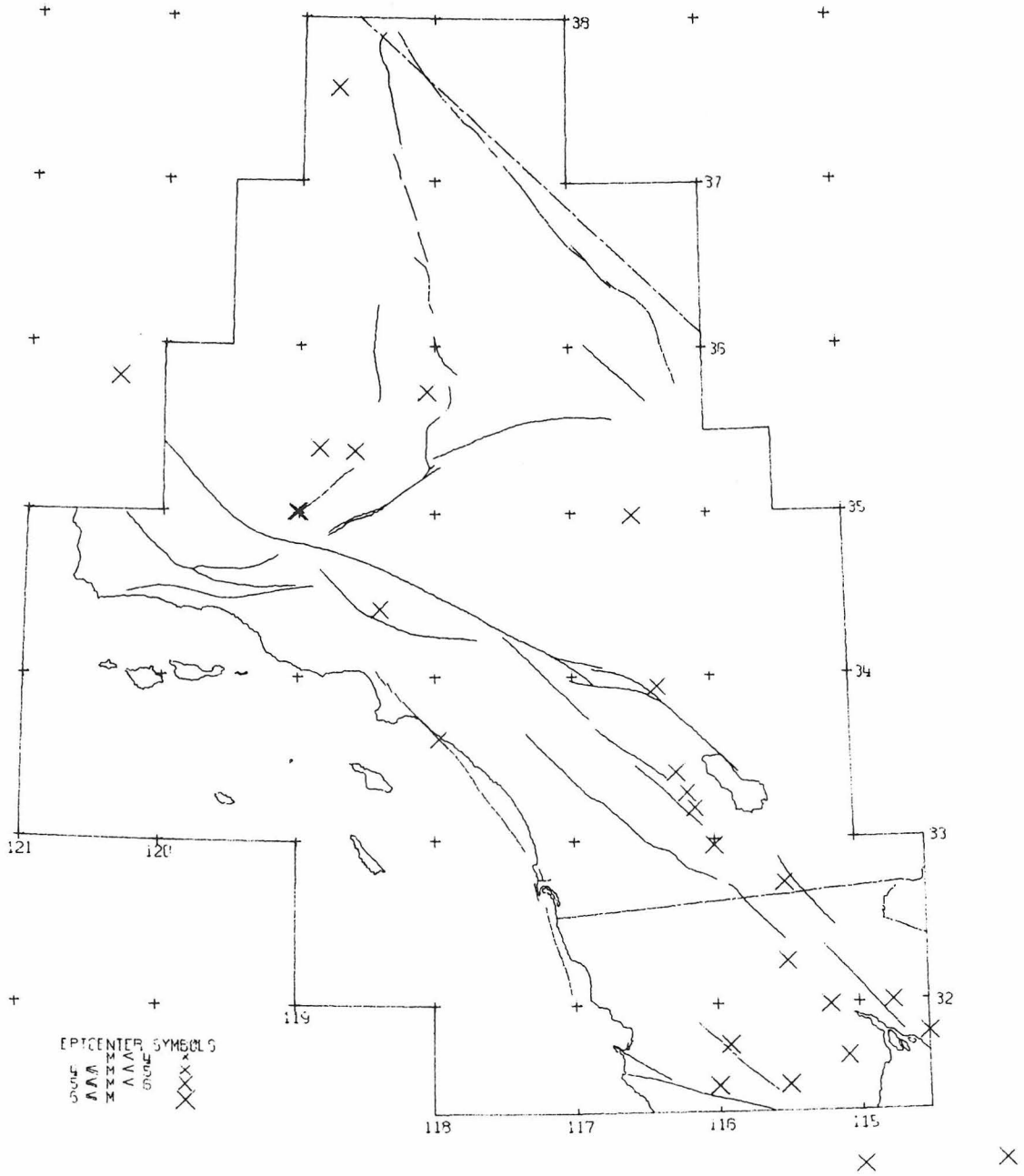

1932 THROUGH 1975, EVENTS EQUAL OR GREATER THAN MAGNITUDE-6

Figure I-57.

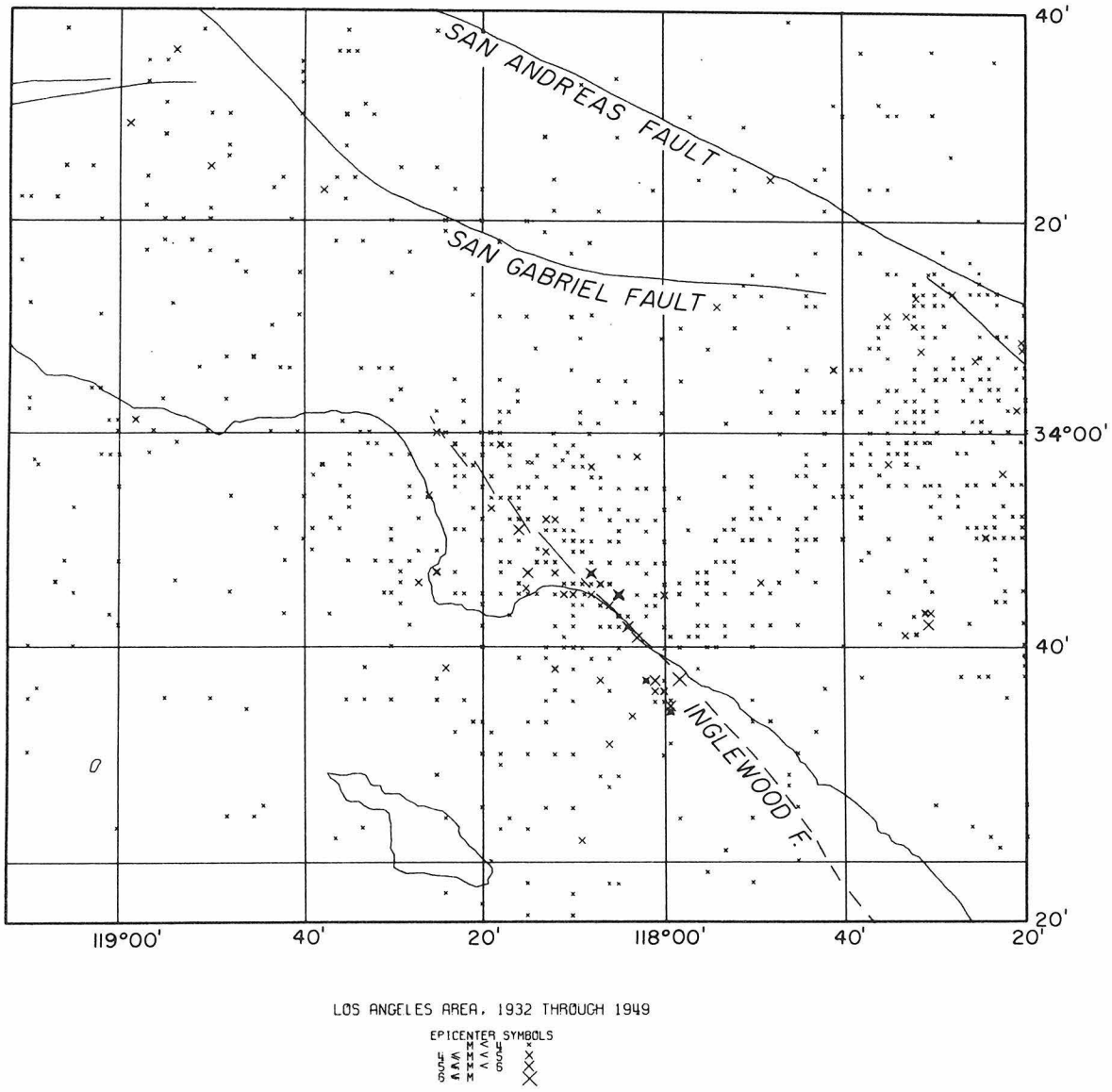

Figure I-58. Seismicity of the Los Angeles area, 1932 through 1949. The northerly and easterly alignments result from reporting epicenters to the nearest minute.

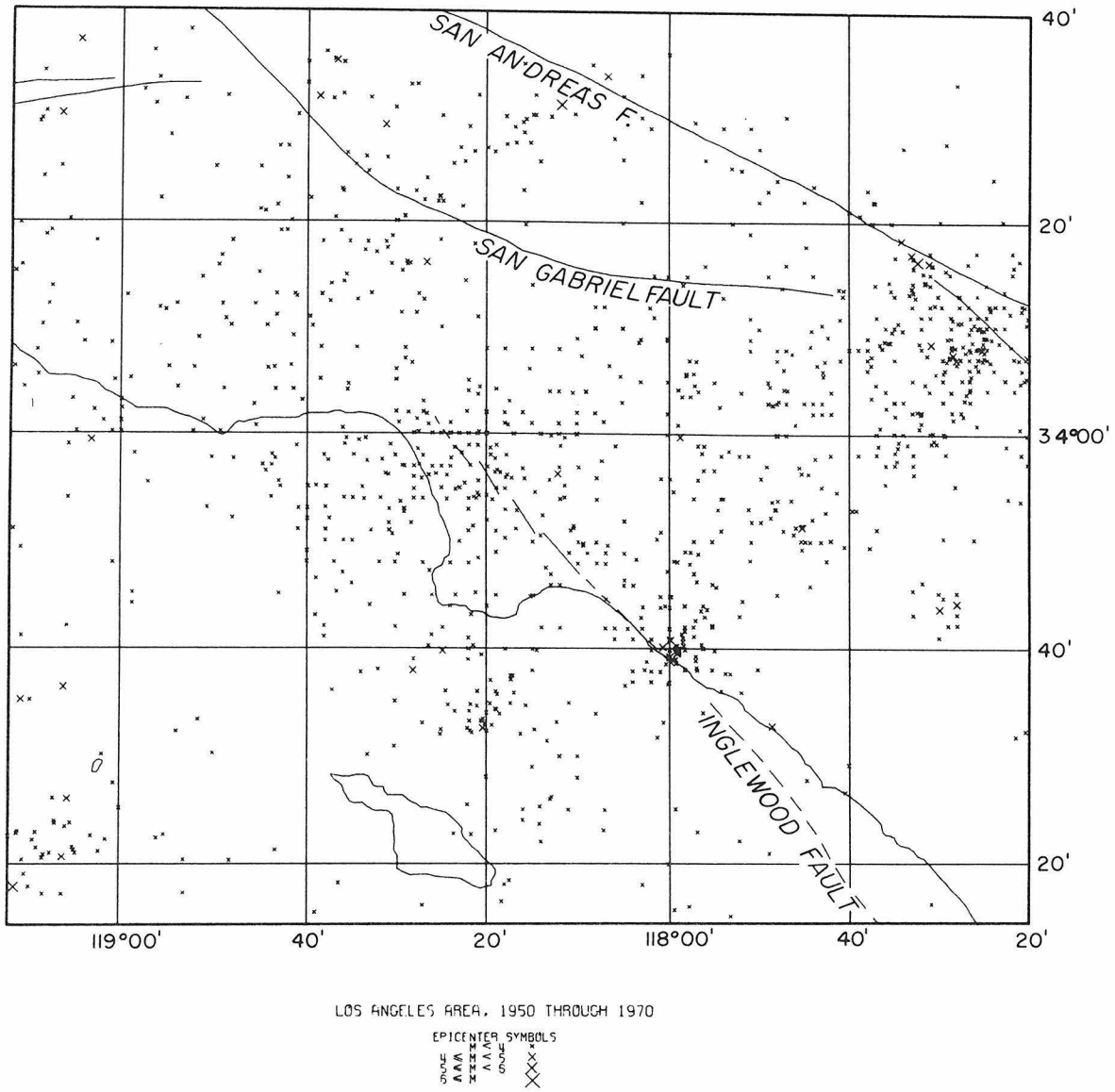

Figure I-59. Seismicity of the Los Angeles area, 1950 through 1970.

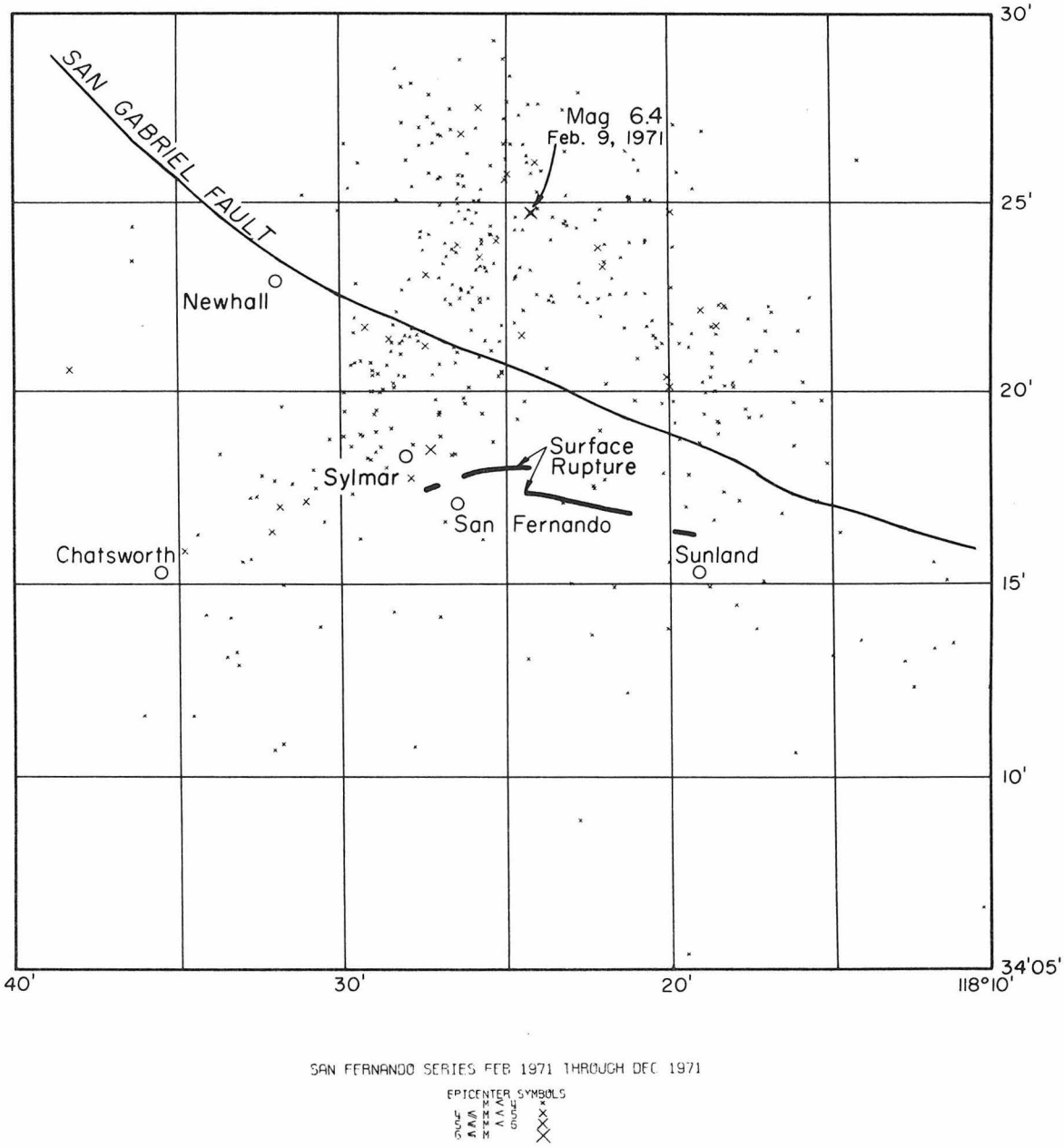

Figure I-60. The 1971 San Fernando earthquake and its aftershocks during 1971.

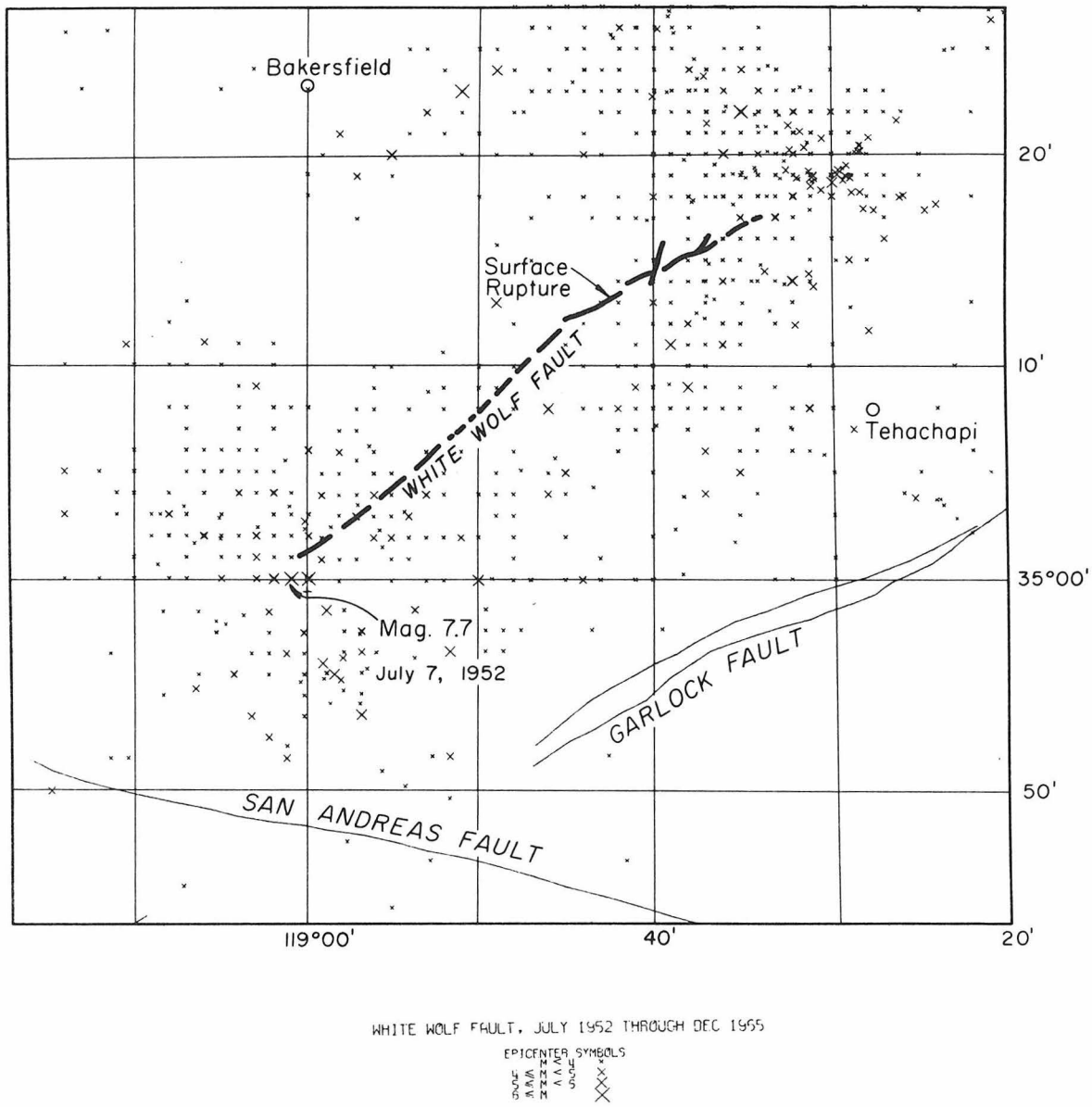

Figure I-61. The 1952 Kern County earthquake and its aftershocks through 1965. The northerly and easterly alignments result from reporting most epicenters to the nearest minute prior to 1961. Other shocks occurring in the area are shown also.

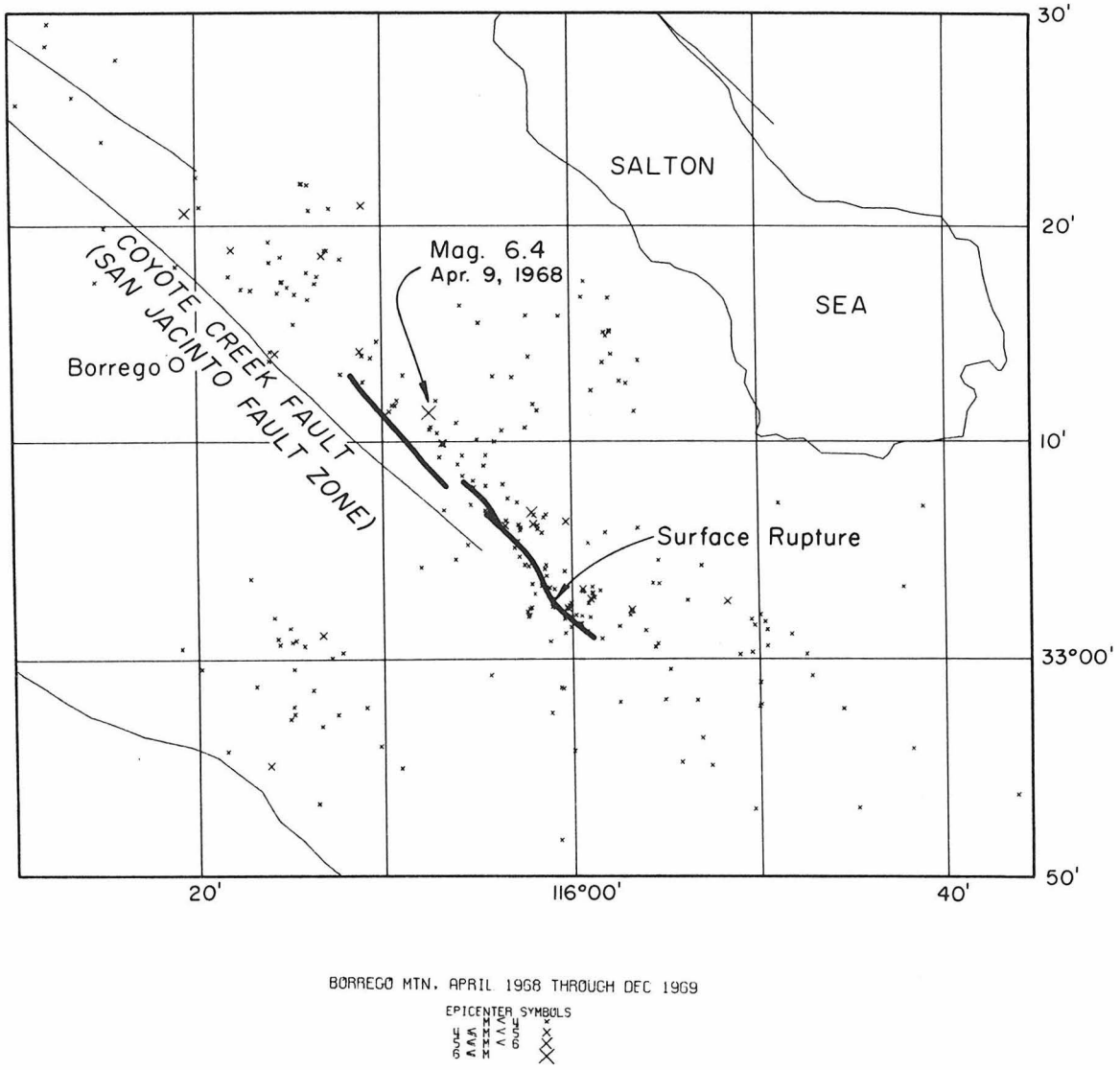

Figure I-62. The 1968 Borrego Mountain earthquake and its aftershocks through 1969. Other shocks occurring in the area are also shown.

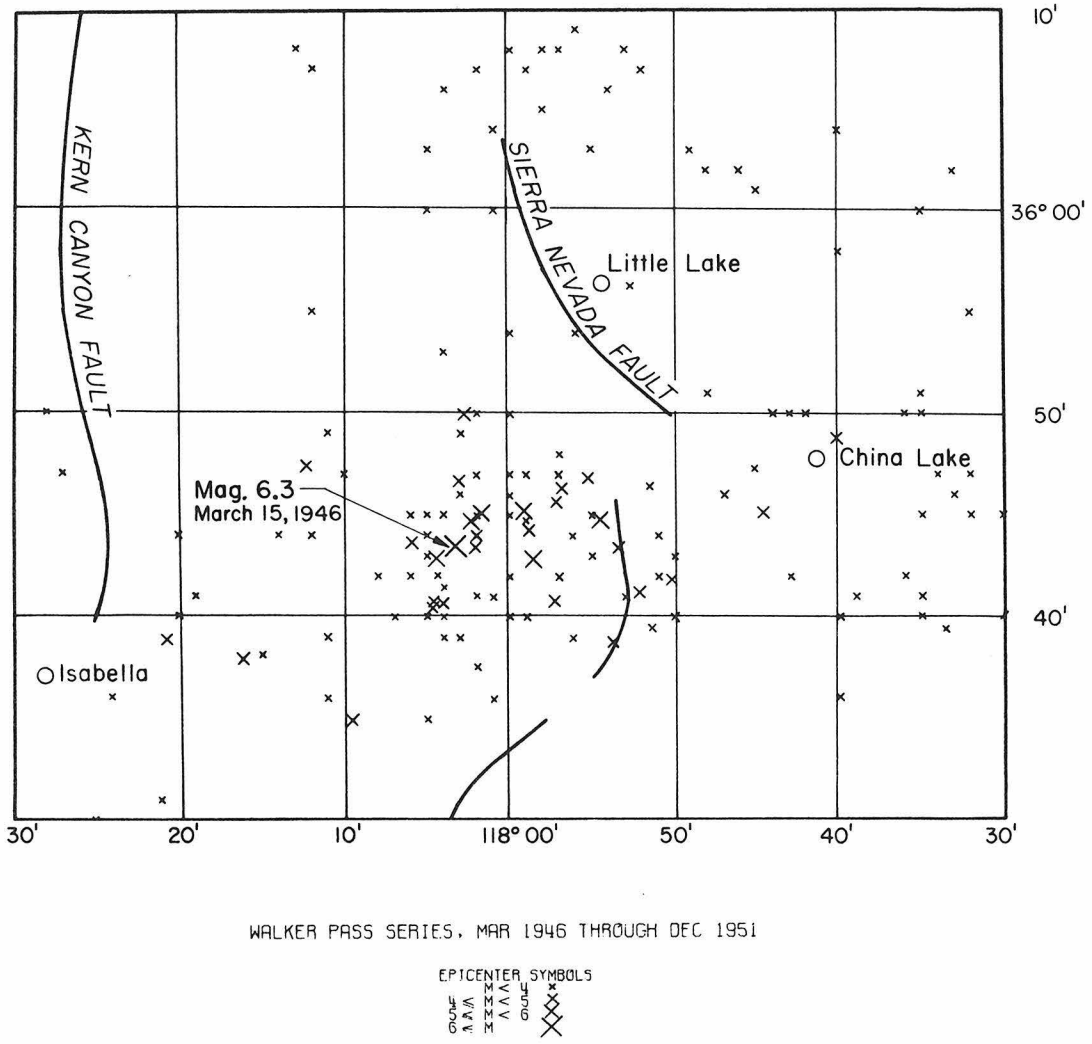

Figure I-63. The 1946 Walker Pass earthquake and its aftershocks through 1951. Other shocks occurring in the area are also shown.

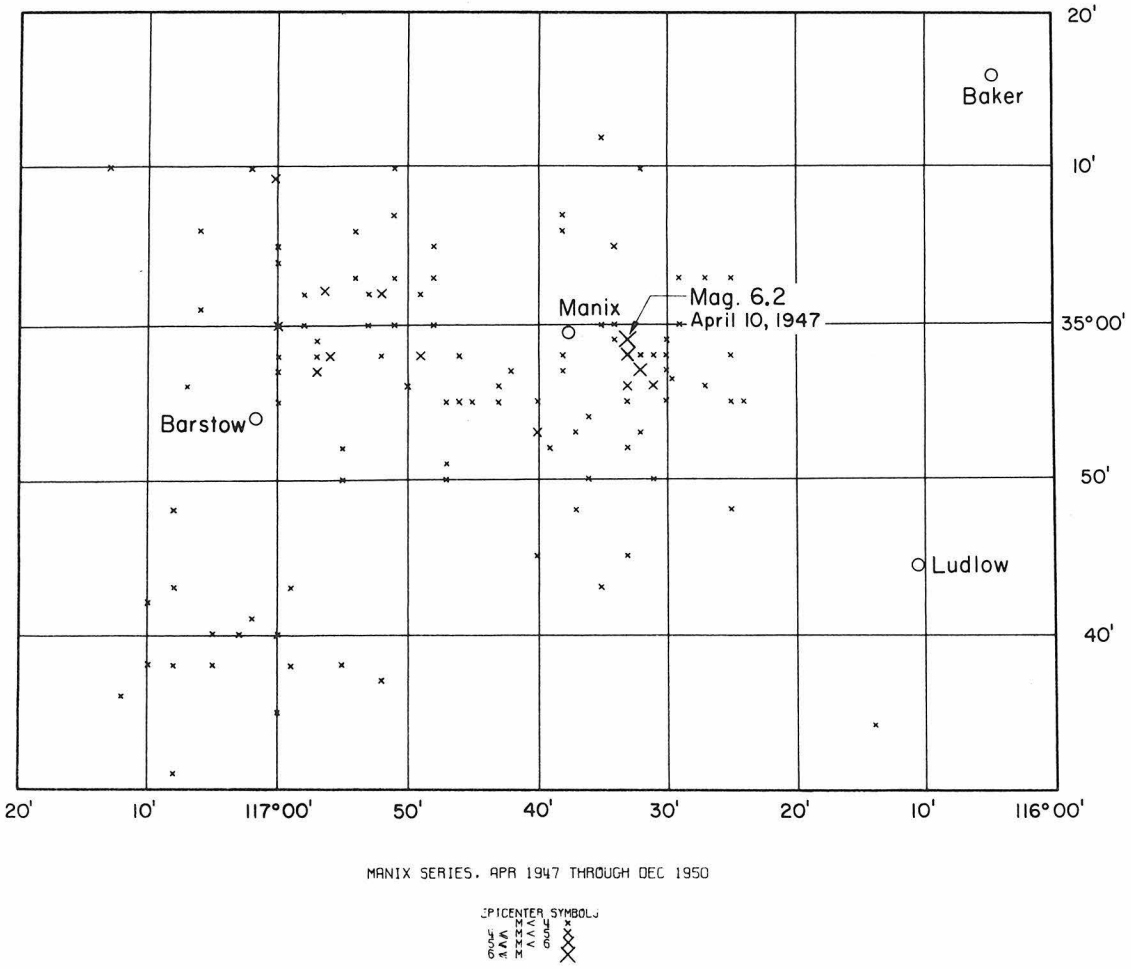

Figure I-64. The 1947 Manix earthquake and its aftershocks through 1950. Other shocks occurring in the area are also shown.

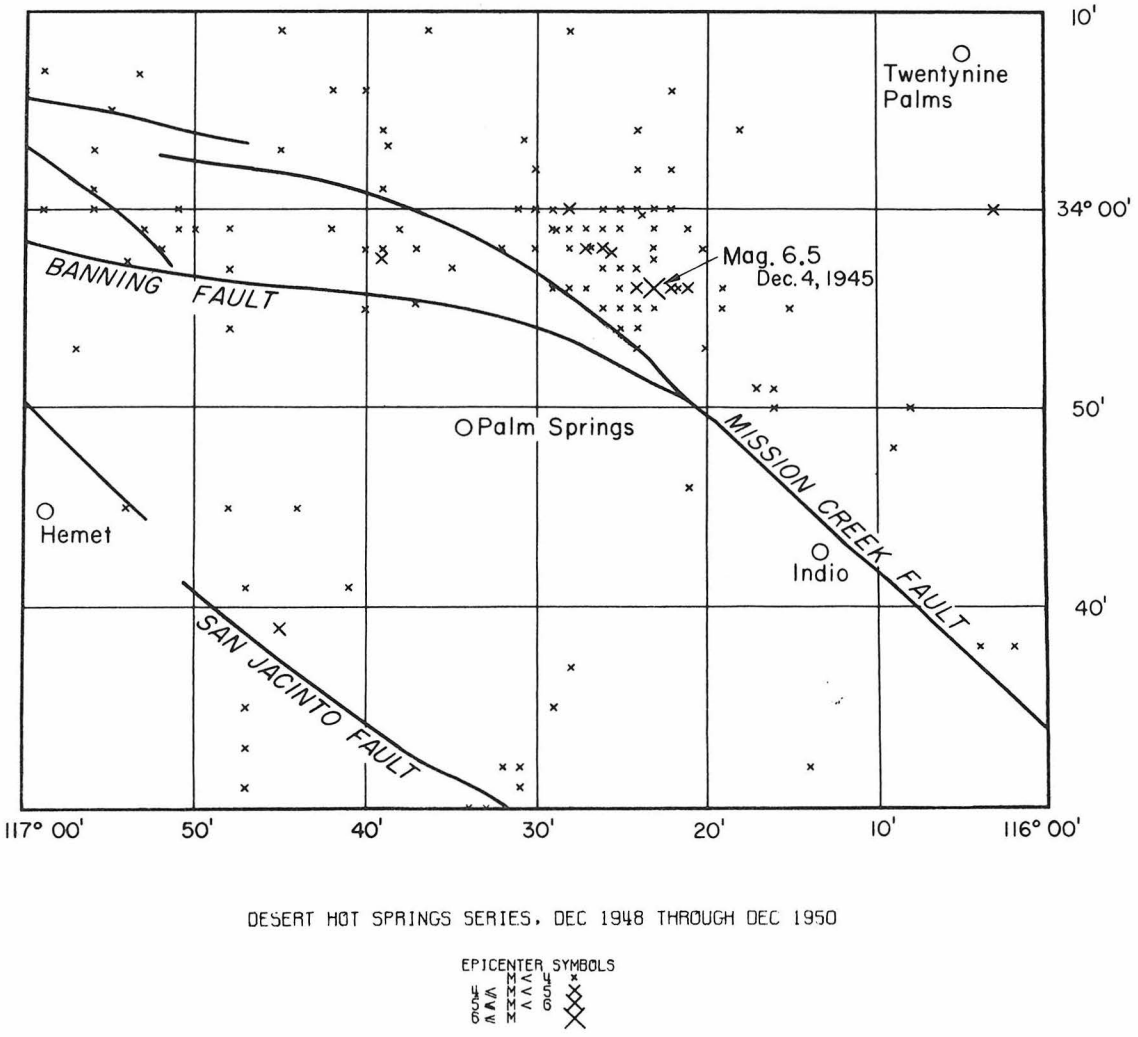

Figure I-65. The 1948 Desert Hot Springs earthquake and its aftershocks through 1950. The northerly and easterly alignments result from reporting epicenters to the nearest minute. Other shocks occurring in the area are also shown.

TABLE I-2

EARTHQUAKES IN SOUTHERN CALIFORNIA REGION OF MAGNITUDE-6.0 OR GREATER
1932 - 1976

YEAR	MO	DA	H	M	S	LAT-N	LONG-W	Q	MAG	DEPTH	NAME
1933	3	11	1	54	7.8	33 37.0	117 58.0	A	6.3	0.0	LONG BEACH
1934	6	8	4	47	0.0	35 48.0	120 20.0	B	6.0	0.0	PARKFIELD
1934	12	30	13	52	0.0	32 15.0	115 30.0	D	6.5	0.0	
1934	12	31	19	45	0.0	32 0.0	114 45.0	D	7.1	0.0	
1935	2	24	1	45	0.0	31 59.0	115 12.0	C	6.0	0.0	
1937	3	25	16	49	1.8	33 24.5	116 15.7	C	6.0	10.0	TERWILLIGER VALLEY
1940	5	19	4	36	40.9	32 44.0	115 30.0	A	6.7	0.0	IMPERIAL VALLEY
1940	12	7	22	16	27.0	31 40.0	115 5.0	C	6.0	0.0	
1941	4	9	17	8	30.0	31 0.0	114 0.0	D	6.0	0.0	
1941	9	14	18	39	11.9	37 34.0	118 44.0	A	6.0	0.0	LONG VALLEY
1942	10	21	16	22	13.0	32 58.0	116 0.0	B	6.5	0.0	
1946	3	15	13	49	35.9	35 43.5	118 3.3	A	6.3	22.0	WALKER PASS
1947	4	10	15	58	6.0	34 59.0	116 33.0	A	6.2	0.0	MANIX
1948	12	4	23	43	17.0	33 56.0	116 23.0	A	6.5	0.0	DESERT HOT SPRINGS
1952	7	21	11	52	14.0	35 0.0	119 1.0	A	7.7	0.0	KERN COUNTY
1952	7	21	12	5	31.0	35 0.0	119 0.0	D	6.4	0.0	KERN COUNTY
1952	7	23	0	38	32.0	35 22.0	118 35.0	A	6.1	0.0	KERN COUNTY
1952	7	29	7	3	47.0	35 23.0	118 51.0	A	6.1	0.0	KERN COUNTY
1954	3	19	9	54	29.0	33 17.0	116 11.0	C	6.2	0.0	BORREGO VALLEY
1954	10	24	9	44	8.0	31 30.0	116 0.0	D	6.0	0.0	
1954	11	12	12	26	47.0	31 30.0	116 0.0		6.3	0.0	
1956	2	9	14	32	38.0	31 45.0	115 55.0	C	6.8	0.0	
1956	2	9	15	24	26.0	31 45.0	115 55.0	C	6.1	0.0	
1956	2	14	18	33	34.0	31 30.0	115 30.0	C	6.3	0.0	
1956	2	15	1	20	38.0	31 30.0	115 30.0	C	6.4	0.0	
1956	12	13	13	15	37.0	31 0.0	115 0.0	D	6.0	0.0	
1966	8	7	17	36	26.7	31 48.0	114 30.0	D	6.3	0.0	
1968	4	9	2	28	59.1	33 11.4	116 7.7	B	6.4	11.1	BORREGO MOUNTAIN
1971	2	9	14	0	41.8	34 24.7	118 24.0	B	6.4	8.4	SAN FERNANDO

Chapter 2

SEISMICITY STATISTICS

Introduction

Recurrence curves are one of the fundamental statistical measures of seismic activity. The usual recurrence relation, $\log N = a - bM$, where N is the number of earthquakes in an interval $(M - \Delta M/2)$ to $(M + \Delta M/2)$, was first given by Gutenberg and Richter (1944) comparing the seismicity of California with that of the entire earth. A similar form, $NA^b = a$, for recurrence of measured amplitudes, was used by Ishimoto and Iida in 1939. On the basis of 8 1/3 years of instrumental data, Gutenberg and Richter found $b = 0.88 \pm 0.02$ for the slope of the recurrence curve for Southern California. Allen et al. (1965) measured $b = 0.86$ for a 29-year period. A value of $b = 1.00 \pm 0.02$ is reported here on the basis of 40 years of data, indicating that the shorter time periods originally used were deficient in smaller shocks. Additionally, recurrence curves for various smaller areas within the Southern California region display a range of b-values from 0.76 to 1.00. The b-values are observed to vary in both space and time. The stability of California b-values as a function of time and as a possible earthquake predictor is examined below for several areas.

The above definition may be termed the "interval" recurrence curve. A "cumulative" recurrence curve is frequently given using the same expression by letting N be the total number of earthquakes having magnitudes equal to or greater than M. Although the b-value for the seismicity of a particular area is the same for both interval and

cumulative recurrence curves, the a-values differ. The a-values, normalized to unit area, are affected by the geographic boundaries used to define the area unless the seismicity is uniformly distributed spatially. Spatial or temporal characteristics of the a-values are not considered here explicitly.

Recurrence Curves for Southern California Areas

The various areas in the Southern California region for which recurrence curves have been drawn are shown in Figure I-66. The heavily outlined area is here termed the "Southern California area". The stair-step boundaries are the same as those for the seismicity maps of Chapter 1. The stair-step nature of the outline is not significant here because only the b-values of the recurrence relationship are considered. The smaller areas were chosen because of their tectonic character, particular earthquake sequences or population density. Table I-3 lists the constants for the recurrence curves shown in Figure I-67. Allen et al. (1965) also have reported b-values for a number of selected areas of Southern California.

The slopes of the recurrence curves were obtained by first fitting a straight line visually to determine which portion of the data points to use in a least squares fit. The appropriate expressions are taken from Dixon and Massey (1957, p. 191) and then written in terms of the recurrence data. The slope b is given by

$$b = \frac{N\sum(M \cdot \log N) - \sum M \cdot \sum \log N}{N\sum M^2 - (\sum M)^2} , \qquad (I\text{-}1)$$

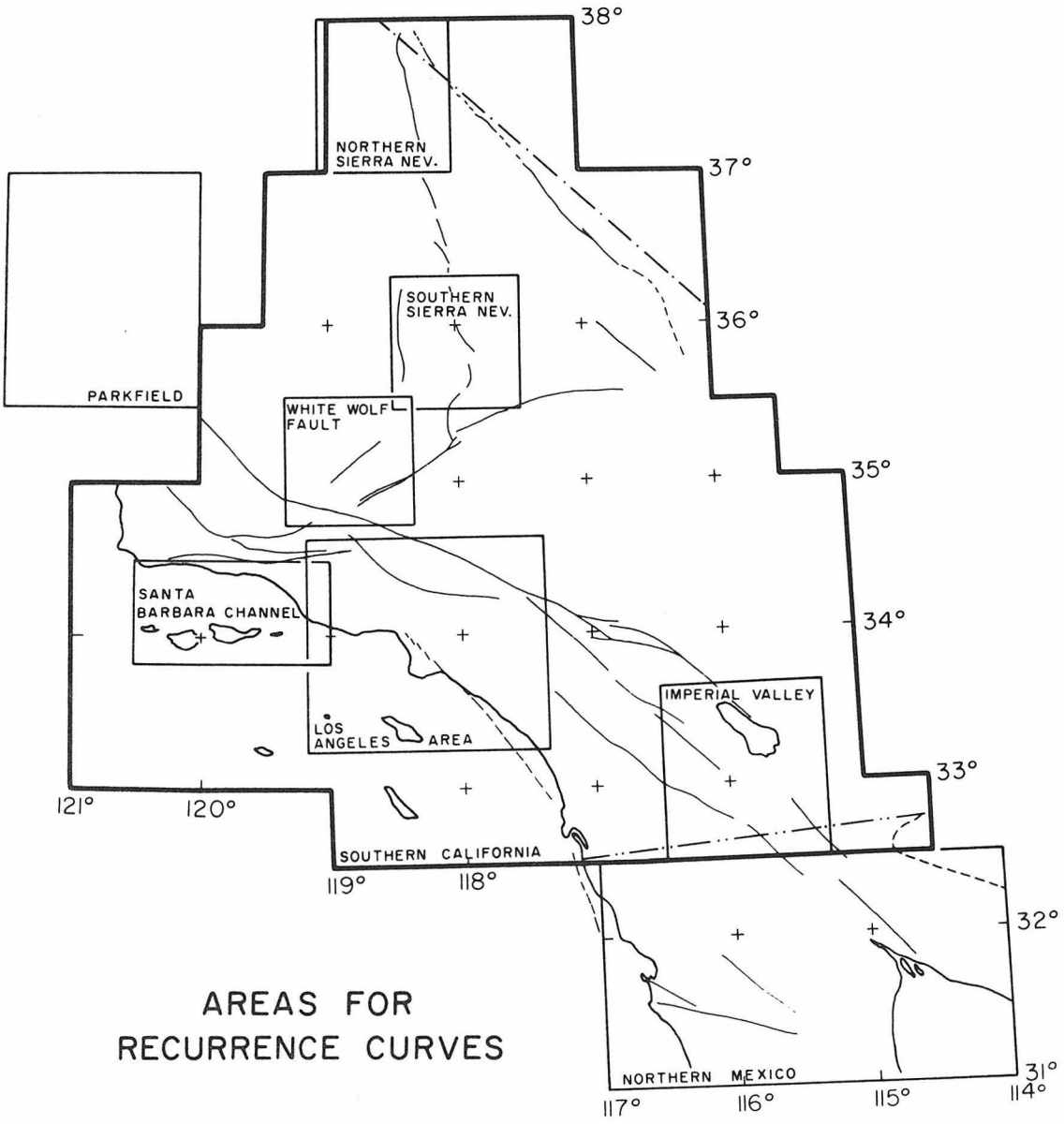

Figure I-66. Outlines of the various areas for which recurrence curves are given in Figure I-67. Note the heavy outline for the entire southern California area of coverage, excluding northern Mexico.

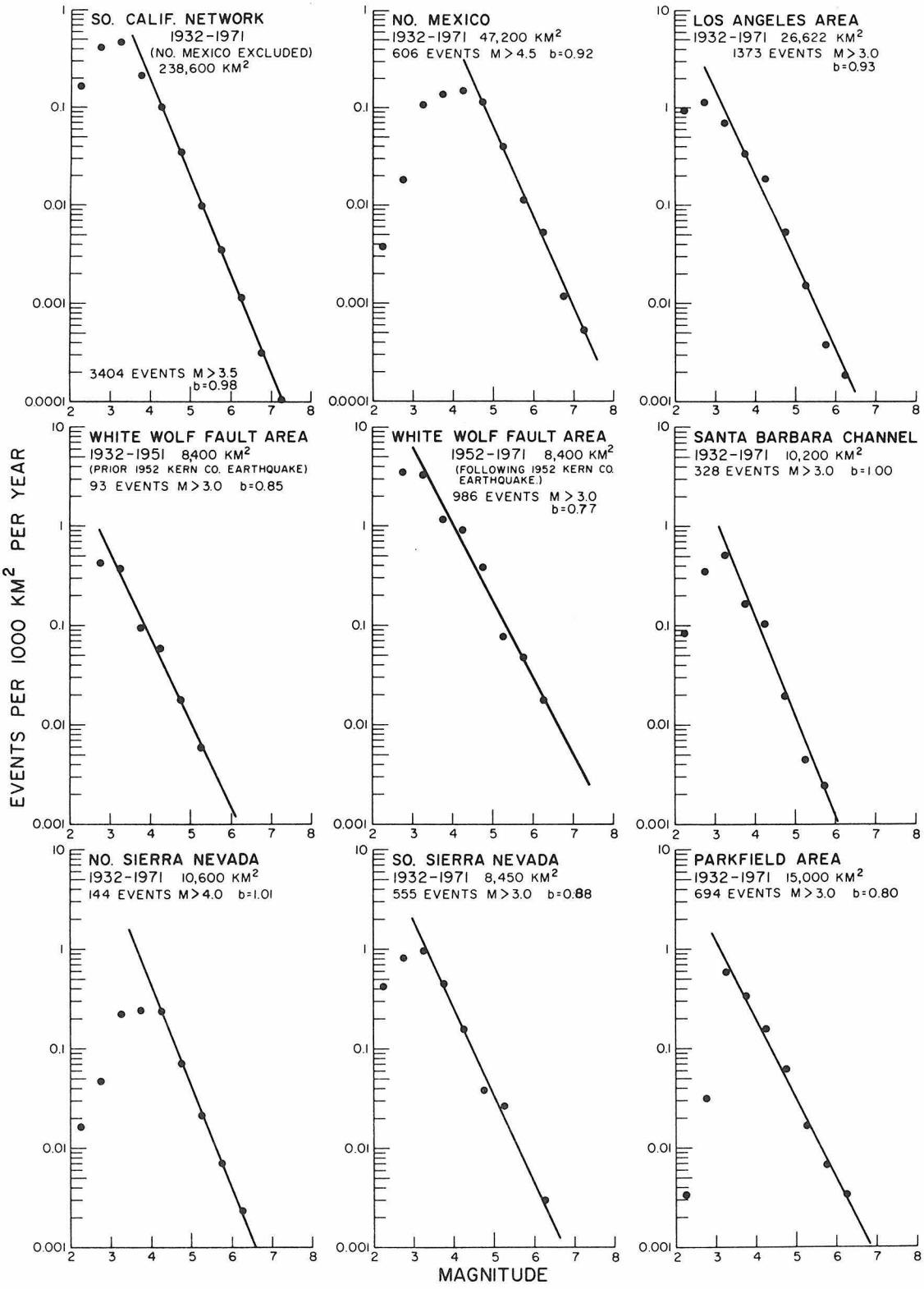

Figure I-67. Interval recurrence curves for each of the areas shown in Figure I-66. Note that the ordinate scales are identical for all curves except the curves for the southern California network and northern Mexico areas.

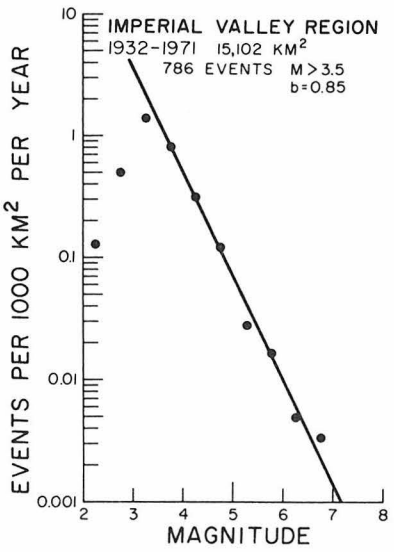

Figure I-67, continued.

Table I-3

Recurrence Curve Parameters

Name	Area	Threshold Magnitude	Events above Threshold	b initial	b least squares*
Southern California	238,600	4.0	1417	0.98	1.00 ± 0.02
Northern Mexico	47,200	4.5	606	0.92	0.95 ± 0.10
Los Angeles	26,600	3.0	1373	0.93	0.91 ± 0.10
White Wolf Fault 1932-1951	8,400	3.0	93	0.85	0.87 ± 0.15
White Wolf Fault 1952-1971	8,400	3.0	986	0.77	0.76 ± 0.10
Santa Barbara Channel	10,200	3.0	328	1.00	0.94 ± 0.14
Northern Sierra Nevada	10,600	4.0	144	1.01	1.00 ± 0.04
Southern Sierra Nevada	8,500	3.0	555	0.88	0.84 ± 0.09
Parkfield	15,000	3.0	694	0.80	0.79 ± 0.07
Imperial Valley	15,100	3.5	786	0.85	0.83 ± 0.07

* Errors are for 90% confidence intervals

in which the summations are taken over the N data points used. If s_x is the standard deviation of the M's and s_y the standard deviation of the log N's, then the error at a confidence level of 100(1-α) percent is

$$\varepsilon = \pm t_{1-\frac{\alpha}{2}} \frac{(N-1)\ (s_y^2 - b^2 s_x^2)}{(N-2)\ s_x\ (N-1)^{\frac{1}{2}}} \quad , \qquad \text{(I-2)}$$

where $t_{1-\frac{\alpha}{2}}$ is the value of a t-distribution for (N-2) degrees of freedom at $1 - \frac{\alpha}{2}$. For 90% confidence limits, $\alpha = 0.10$ and $t_{.95}$ is used. The error expression is based on the assumptions that log N for a given M is normally distributed and that the variance $s_{y\cdot x}^2 = (N-1)(s_y^2 - b^2 s_x^2)/(N-2)$ is not dependent on magnitude. Therefore the results here are only estimates, since the assumptions are not strictly true. We would expect N to be a normally distributed random variable, but the distribution of log N will be somewhat distorted. However, the expression is adequate to indicate the relative qualities of various estimates of b.

In Table I-3, all time periods are for the years 1932 through 1971 unless otherwise noted. The magnitude threshold for each area is taken to be that magnitude below which the data points depart from the linear relation shown in the figure. Of course, this threshold level is somewhat subjective because the straight line is chosen as a best fit to the linear portion of the data points. Interval recurrence curves are superior to cumulative recurrence curves for this purpose because each of the data points is independent and does not depend on data for higher magnitudes. The departure from linearity

in this data is taken to represent incomplete recording of earthquakes at the lower end of the data range.

Southern California Area. The b-value of 1.00 ± 0.02 reported here differs significantly from that of Gutenberg and Richter (1944), 0.88 ± 0.02, and from that of Allen, et al. (1965), 0.86. The data points of Figure I-67 clearly do not permit such uncertainty in the b-value. Both of the earlier measurements were derived from the complete catalog, up to the appropriate dates, for the Southern California region. The value given here does not include the data for Northern Mexico. The measured value for Northern Mexico is 0.95 ± 0.10 with only about 18% as many events as the rest of the region, so the value for the combined areas would still differ from the earlier estimates. Such differences indicate fewer earthquakes of small magnitudes in the data sets of the earlier estimates. These differences probably indicate genuine changes in seismicity because the previous authors considered the completeness of their data sets. Temporal variation of b is seen in the curves presented in a separate section below. The 1.00 value is higher than that for any of the individual areas treated separately below, so there must be other areas not considered here with higher values. Ryall, et al. (1966) measured b = 0.76 for portions of the Southern California area and the same value for the Ventura-Winnemucca seismic zone for the period 1932-1961. However, their boundaries were very irregular and omitted areas of low-level seismicity.

Northern Mexico Area. This area is treated separately because it is on the periphery of the coverage of the Southern California seismographic network. A b-value of 0.95 ± 0.10 is found, and a threshold of about M = 4.5 for complete registration of shocks is evident from the rolloff of the recurrence data points. Much of the Northern Mexico seismicity is a continuation of the type of activity seen in the Imperial Valley area. However, there is perhaps an equal contribution from the Peninsular Ranges province (see Figure I-55) with its major faults such as the San Miguel Fault and the more westerly trending Aqua Blanca Fault.

Los Angeles Area. This area was chosen because of its population density and because a large number of rather small shocks are reported felt. The b-value of 0.91 ± 0.10 shows that the ratio of small shocks to large shocks in the Los Angeles area is not significantly different from that for the rest of the region. Allen et al. (1965), using a more restricted area, obtained b = 1.02, which was higher than that for the other areas which they measured, 0.80 - 0.90. Within the bounds used for this area are several different tectonic regimes contributing to the seismicity: portions of the San Andreas Fault zone, the Transverse Ranges, Los Angeles Basin, and the Continental Borderlands.

White Wolf Fault Area. The White Wolf Fault was the source of the 1952 Kern County earthquake. The bounds of this zone have been taken

to enclose the aftershock zone of that earthquake. Two time periods were examined, 1932-1951 and 1952-1971, to determine any possible changes in the recurrence rates before and after this major shock. The values of 0.87 ± 0.15 and 0.76 ± 0.10 have large uncertainties at the 90% confidence level and thus are not appreciably different.

The data for the period 1952-1971 are not homogeneous because many small shocks were not analyzed during the early portions of the 1952 aftershock sequence. Richter (1955) states that only the "clearly distinguishable" shocks were read and that some events as large as 4.5 or 5 may have been missed during the first few hours. The magnitude threshold is estimated to have been about 4.0 initially and then lowered to about 3.5 after a few weeks (Richter, personal communication, 1977). If the 1952 data are omitted and b is estimated for 1953-1971, then $b = 1.05 \pm .06$ is obtained. This value is consistent with the curves given below in the section on temporal variation of b. This value also suggests a long-term increase in b after the 1952 earthquake. However, this evidence for such a change is not strong because the 1932-1951 time period comprises only 93 events, and the uncertainty of the estimated b is large.

Allen et al. (1965) measured $b = 0.80$ for the period 1934-1963. Their area also included the aftershock zone of the 1946 Walker Pass earthquake. Wesson and Ellsworth (1973) have reported a slight increase in the level of seismicity in the vicinity of the White Wolf fault prior to the 1952 shock, but they did not examine the recurrence curves. The detailed time history of the b-value using maximum

likelihood estimates is considered below in the section on temporal variation of b.

Santa Barbara Channel Area. This area was chosen because it contains only tectonic trends representative of the Transverse Ranges Province and because it has experienced several moderately strong shocks historically. An estimate of $b = 0.94 \pm 0.14$ is obtained. This estimate may be influenced by the 1968 Santa Barbara channel earthquake swarm which contained 58 shocks of magnitude 3.0 or greater, the threshold appropriate for this data set. There were only 328 shocks with magnitudes equal to or greater than 3.0 in the full data set. Other lesser swarm sequences have occured also in the Santa Barbara channel area and in this respect the area differs from the rest of the Transverse Ranges Province.

Northern Sierra Nevada Area. This area is taken to include the extent of the seismicity in the vicinity of the 1941 Long Valley earthquake. Although named here Northern Sierra Nevada, the area includes portions of the Sierra Nevada and the White Mountains, and the graben separating these two mountain ranges. There are only 144 events above the magnitude threshold, but the data points align linearly quite well to give $b = 1.00 \pm 0.04$. The high threshold for this area results from its location on the periphery of the Southern California Seismographic Network. The seismicity maps in Chapter 1 show that this area has low-level, but continuous, seismicity such

that the result is not dominated by the 1941 sequence.

Southern Sierra Nevada Area. The 1946 Walker Pass earthquake and its aftershock zone form the basis for this area. A b-value of 0.88 ± 0.09 is obtained here, somewhat lower than that for the entire Southern California area. However, the difference may not be significant since the ranges of the two estimates (90% confidence) are not clearly separated. Walker Pass is at the junction of the southern end of the Sierra Nevada Mountains with the northeastern end of the Tehachapi Mountains. The seismicity there has been ascribed by Ryall et al. (1966) to the Ventura-Winnemucca seismic zone, but Richter (1969) doubted the continuity. The geologic setting of the area is unique, and its teconics have yet to be adequately studied.

Parkfield Area. This area is somewhat outside the coverage of the local network, but numerous shocks originating there are registered. Also the data are supplemented by reports of the Berkeley seismographic network. A clear departure of the recurrence points from the linear portion of the data indicates a threshold of about magnitude 3, and $b = 0.79 \pm 0.07$ is obtained. Eaton et al. (1970) found $b = 0.85$ for the aftershock sequence of the 1966 Parkfield earthquake. This is the only area in the Southern California region where the San Andreas Fault Zone is clearly defined (not a broad zone of parallel faults), separated from other active structures, and which shows moderately active seismicity. It should be noted however that the epicenters

in the Caltech catalog (see Figure I-55 and I-56) do not delineate the fault clearly except for magnitudes greater than 5.

Imperial Valley Area. This area contains the San Andreas Fault Zone as a broad zone of parallel faults and represents a rather diffuse boundary between the plates. In addition, the region is characterized by recent vulcanism, closed tectonic depressions (Johnson and Hadley, 1976) and suggestions of small spreading centers (Lomnitz, et al., 1970). The measured b-value is 0.83 ± 0.07 and is comparable to that of Allen et al. (1965), 0.82. The active tectonics here are characterized by right-lateral faults of the San Andreas Fault system. Earthquake swarms have occurred many times in the Imperial Valley area.

Comparison of Regional Values. For some of the areas, the b-values are not significantly different from the regional value of 1.00 ± 0.02 — Northern Mexico (.95 ± .10), Santa Barbara Channel (.94 ± .14), Northern Sierra Nevada (1.00 ± .04), and White Wolf Fault 1953-1971 (1.05 ± .06). Several other areas seem to differ from the regional value, but their b-value estimates are not clearly different because their ranges come near, or overlap, the range for the regional estimate - Los Angeles (.91 ± .10), White Wolf Fault 1932-1951 (.87 ± .15), and Southern Sierra Nevada (.88 ± .09). Only two areas have b-values which are significantly different from the regional value — Parkfield (.79 ± .07) and Imperial Valley (.83 ± .07).

With a large data base representing all of the Southern California

area and 40 years of recording, b is reasonably well constrained to $b = 1.00 \pm 0.02$. This value supports the theoretical estimate of Kanamori and Anderson (1975), who derived $b \sim 1$ from geometrical considerations. The regional value represents several tectonic provinces which individually may have different b-values characterizing their seismicity. Miyamura (1962) has discussed variation in b-values as a function of tectonic regime. Scholz (1968) and Wyss (1973) suggested that low b-values correlate with high stress-drop. It is natural then to try to correlate the results obtained here with physical characteristics of the respective areas. The Imperial Valley (0.83) and Parkfield (0.79) are the only areas tested having predominantly strike-slip faulting and they have low b-values. Other areas with strike-slip faulting also contain other tectonic styles. The highest b-values are for the Northern Sierra, an area of normal faulting (presumably low stress-drop), and for the White Wolf Fault 1953-1971. It is not clear that the aftershocks of a thrust-type earthquake should necessarily be of low stress-drop. The observed increase in b for the White Wolf Fault area is consistent with changes reported by Suyehiro (1966) for a Japanese shock and for the 1960 Chilean earthquake. The remaining Southern California areas have intermediate b-values with large uncertainties and have mixed geological characteristics.

Conversion of Interval Curve Data to Cumulative Curve Data

If N_I is the number of earthquakes in the interval M to $M + \Delta M$ and N_c is the number of earthquakes with magnitudes equal to or greater

than M, then

$$\log N_I = a - bM$$
$$\log N_c = A - BM \ . \qquad \text{(I-3)}$$

As stated earlier, b = B which can be shown by evaluating

$$N_c = 10^a \int_M^\infty 10^{-bm} dm = \frac{10^a}{b \ \ln 10} \ 10^{-bM} \ . \qquad \text{(I-4)}$$

Rewriting the result as

$$\log N_c = a - \log b - \log (\ln 10) - bM \qquad \text{(I-5)}$$

shows that B = b and A = a - log b - 0.362. The number of shocks equal to or greater than a given magnitude can be found directly from the interval recurrence curve as follows.

$$N_{\geqslant M} = N_M + N_{M+\Delta M} + N_{M+2\Delta M} + N_{M+3\Delta M} + \ldots \qquad \text{(I-6)}$$

Since the recurrence relation is linear, values for successive intervals have a fixed ratio and form a geometric progression.

$$N_{\geqslant M} = N_M + N_M(r) + N_M(r)^2 + N_M(r)^3 + \ldots \qquad \text{(I-7)}$$

or $N_{\geqslant M} = \frac{N_m}{1-r}$ for an infinite number of terms. The constant ratio is

$$r = \frac{N_{M+\Delta M}}{N_M} = \frac{10^a \ 10^{-b(M+\Delta M)}}{10^a \ 10^{-bM}} = 10^{-b(\Delta M)} \ . \qquad \text{(I-8)}$$

The final relation then is

$$N_{\geq M} = \frac{N_M}{1 - 10^{-b(\Delta M)}} \quad . \tag{I-9}$$

This expression is approximate in that it assumes no maximum earthquake, but the % error is small except for high magnitudes. If b = 0.85 and the interval curve has 800 shocks at M = 3.75, then the error is about 1 shock at M = 3.75 and ½ shock at M = 7.25. Alternatively, if there are n intervals ΔM up to a known maximum shock, then the exact result is

$$N_{\geq M} = N_M \left(\frac{r^n - 1}{r - 1} \right) = N_M \left(\frac{10^{-nb\Delta M} - 1}{10^{-b\Delta M} - 1} \right) \quad . \tag{I-10}$$

It should be remembered that interval data are usually plotted at the midpoint of each magnitude range.

Temporal Variation of b

Although the observed b-values for Southern California areas are approximately equal to 1, which is the theoretical value predicted by Kanamori and Anderson (1975), there are suggestions of both spatial and temporal variations as described above. In particular, the area around the White Wolf Fault exhibited low-level seismicity with b = 0.87 before 1952, and high-level seismicity of an aftershock sequence with b = 1.05 after 1952. Both of these estimates were for a number of years. The short-term variation for this area is discussed below, as well as the variation for other areas.

Temporal variation in b has been reported for several areas previously (e.g., Suyehiro (1966, 1969), Ikegami (1967), Healy, et al., (1968)). For several shocks in the Central California area, Wyss and Lee (1973) found that b increased relative to the long-term value before and after the shocks.

The value of b is a statistic of any particular set of earthquakes chosen for study. If the set does not contain a large number of shocks, its statistics may be subject to considerable uncertainty. The difficulty becomes apparent quickly if b-values are to be estimated by measuring the slopes of recurrence curves for restricted data sets. This problem is illustrated in Figure I-68 which shows recurrence data for the Southern California area for the individual years 1952 through 1955. Curves are shown for sliding time windows of 1, 2, and 3 years respectively. For some years, such as 1953, the individual year's data are relatively easy to interpret for the value of the slope. For other years, such as 1954, a single year's data are somewhat ambiguous and smoothing over 2 or 3 years' data helps. In other cases, such as 1952, even greater smoothing would be required, but this would be at the expense of time-resolution of any variations. 1952 is the year of the Kern County earthquake and is represented by a very inhomogeneous set of data. A solution to this problem is to use the maximum likelihood determination of the b-values, which provides an estimate of the most reasonable b-value and of its uncertainty.

Utsu (1965) showed that b can be estimated from an ensemble of

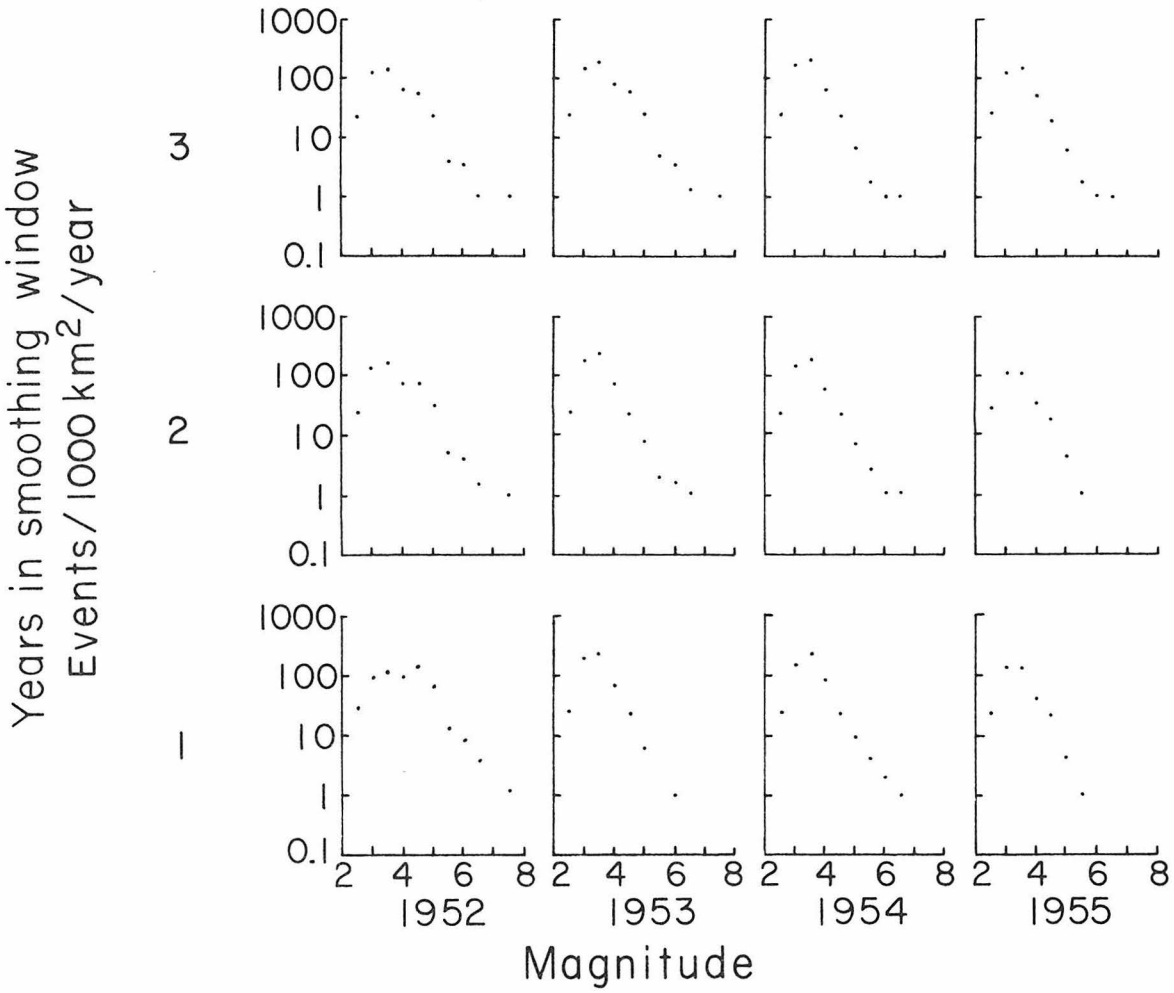

Figure I-68. Southern California area recurrence data for selected years. Data are shown for time windows of 1, 2 and 3 years. The data illustrate the potential difficulties in choosing a linear relation when the data are few or incomplete.

earthquakes using the expression

$$b = \frac{s \log e}{\Sigma M_i - s M_s} \qquad \text{(I-11)}$$

where the M_i are the magnitudes of the s individual earthquakes greater than or equal to M_s, which is the smallest magnitude for which the set is complete. An equivalent form usually used is

$$b = \frac{\log e}{\overline{M} - M_o} \qquad \text{(I-12)}$$

where $\overline{M}$ is the average magnitude of shocks and M_o is the threshold magnitude. Aki (1965) showed that the above expression is the maximum likelihood estimate of the b-value, and he provided a table of values for the associated uncertainty in terms of the confidence limits and the size of the earthquake set. Because earthquake magnitude itself is not a very precise quantity, magnitudes are usually quantified at intervals of 0.1 unit. Furthermore, recurrence data are sometimes lumped together in intervals of ¼ or ½ unit. The earthquake distribution is logarithmic with magnitude and not uniform across the intervals, so an error is introduced when computing the average magnitude of a set of earthquakes. Utsu (1967) derived an expression for this error and tabulated correction factors in terms of the quantity $b\Delta M$.

There still remains the difficulty of correctly identifying the appropriate M_o for a particular data set. If the threshold M_o is taken too low, the set appears deficient in small events, and a low estimate of b is obtained. If the threshold is too high, the number of events used may be too few to provide reasonable statistics, and

the uncertainty may be unacceptably high. Because of these considerations, curves for the time variation of b were computed for several threshold levels, M_o = 2.5, 3.0, 3.5, 4.0, as well as for time windows from 1 year through 5 years.

Southern California Area. The temporal variation of b-value estimates for the Southern California area are shown in Figure I-69. The curves (a) through (d) show the results for each of the threshold levels when using one year's earthquakes for each estimate. Similarly, curves (e) through (h) are for three years of data in each estimate, using a sliding window and plotting the estimate at the central year of the window. Adjacent points are independent in curves (a) through (d) but not independent in curves (e) through (h). On the basis of the recurrence curve of Figure I-67, a threshold value of M_o = 3.5 was estimated for the full 40-year time period. Curves (d) and (h) show quite low values for the b estimates because of the low threshold of M_o = 2.5. Conversely, curves (a) and (e) show the instability of the estimate for high thresholds and their correspondingly reduced data sets. Curve (c) for a threshold of M_o = 3.0 shows the best agreement with the long-term estimate of b = 1.00. Similarly, curve (g) of the 3-year smoothed curves shows the best agreement.

Curves (c) and (g) reflect the time variation in b that was noted from the earlier results. The time period up to about 1953 shows b fluctuating at values less than 1, while after 1953 the values tend to be greater than 1. Thus the measurement of Allen et al. (1965) of

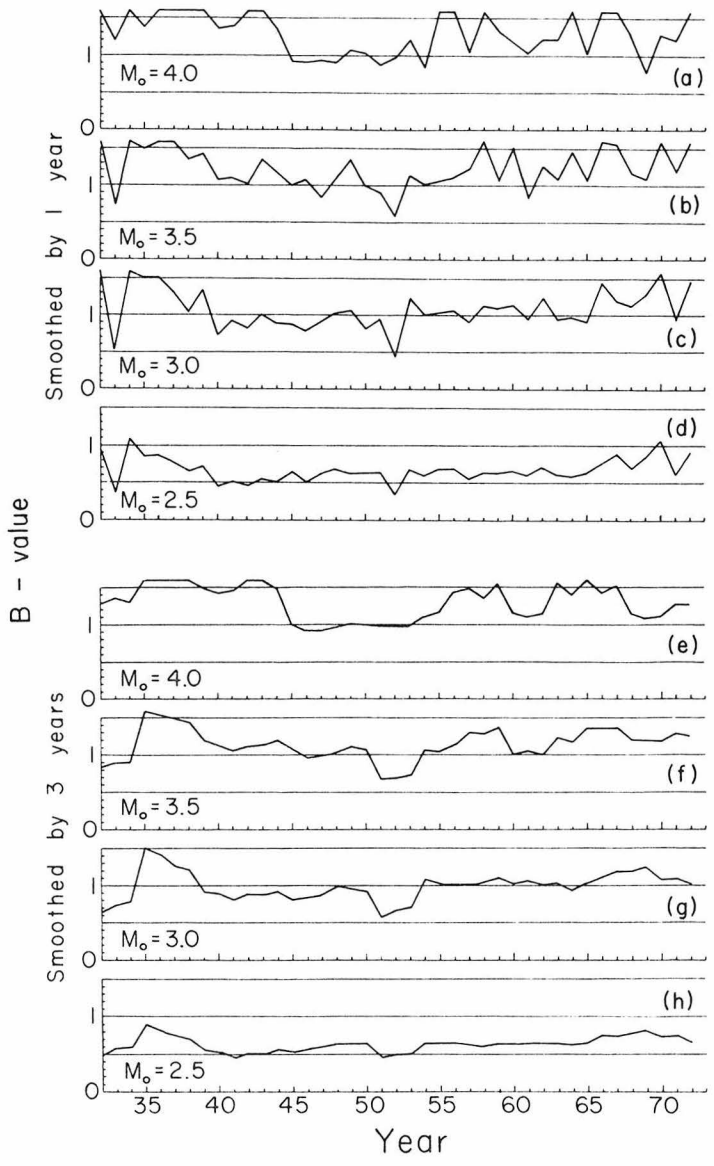

Figure I-69. Estimates of the temporal variation of b in the Southern California region using several threshold magnitudes (M_o in the maximum likelihood estimator) and sliding time windows of 1 year and 3 years.

b = 0.86 for the period 1934 through 1962 and the estimate of b = 1.00 presented here are not unreasonable. The result of Gutenberg and Richter (1944) of b = 0.88 for the early years, 1934-1943, are not reflected in these curves, but their data set was for the entire Southern California region.

Several features of these curves are noteworthy. First is an anomalously low value of b = 0.5 for the year 1952 corresponding to the Kern County earthquake and its initial aftershocks. This same feature appears in the curves derived from data restricted to the aftershock region of this earthquake. As described earlier, the data for 1952 are certainly incomplete for magnitudes less than 4.0 and may be incomplete for magnitudes as high as 4.5 (Richter, personal comm., 1977). It is most likely that the anomalously low b-value for 1952 is caused by the omission of these smaller events from the record. Notice that curve (a) for a magnitude threshold of 4.0 does not have a sharp drop for 1952. Because of the data shortcomings, a good estimate of b for the early portion of the Kern County aftershock sequence is not available. The entire Southern California area had b-values of about 0.85 for the 12 years preceding the 1952 shock. For 13 years following the shock, the b-values were a little greater than 1, and then they rose slightly higher to about 1.1 - 1.2. It would not be correct to label these pre-1952 values of b as a long-term precursor to the 1952 shock, because there are not enough previous data to establish an adequate baseline. Assuming that the observed change in average b-values is related to the 1952 earthquake and that the

b-value is related to state of stress (Scholtz, 1968; Wyss, 1973), then the change may reflect simply a relaxation of regional stresses at the time of the earthquake. There is also an anomalously low b-value for 1933, the year of the Long Beach earthquake. This shock was much smaller than that of 1952 and was comparable to other moderate shocks not particularly reflected in these curves. According to Richter (personal comm., 1977) the data for the Long Beach earthquake have the same shortcoming with respect to magnitude threshold as the 1952 data. The seismicity map for 1933 (Figure I-3) suggests that small-magnitude shocks throughout the region are missing from the record.

White Wolf Fault Area. Curves (a) through (h) of Figure I-70 are similar representations to those of Figure I-69 but constructed only for the area of the aftershock zone of the 1952 Kern County earthquake. In the years prior to the earthquake, 1932-1951, the level of seismicity was so low that there are no good estimates of the b-values. The curves are clipped at b = 1.6 by the computer routine and at b = 0 by lack of data above the threshold. Figure I-70 also shows a time histogram of the largest event each year within the bounds of this area. The curves here show the low value for 1952 consistently. The lack of agreement with the long-term averages shows that the results here are very sensitive to the level of M_o. Curves (c) and (d) suggest that the correct level is between 2.5 and 3.0 since they bracket the long-term estimate. From Figure I-69 for the Southern California area, it is apparent that a threshold too low leads to underestimating the

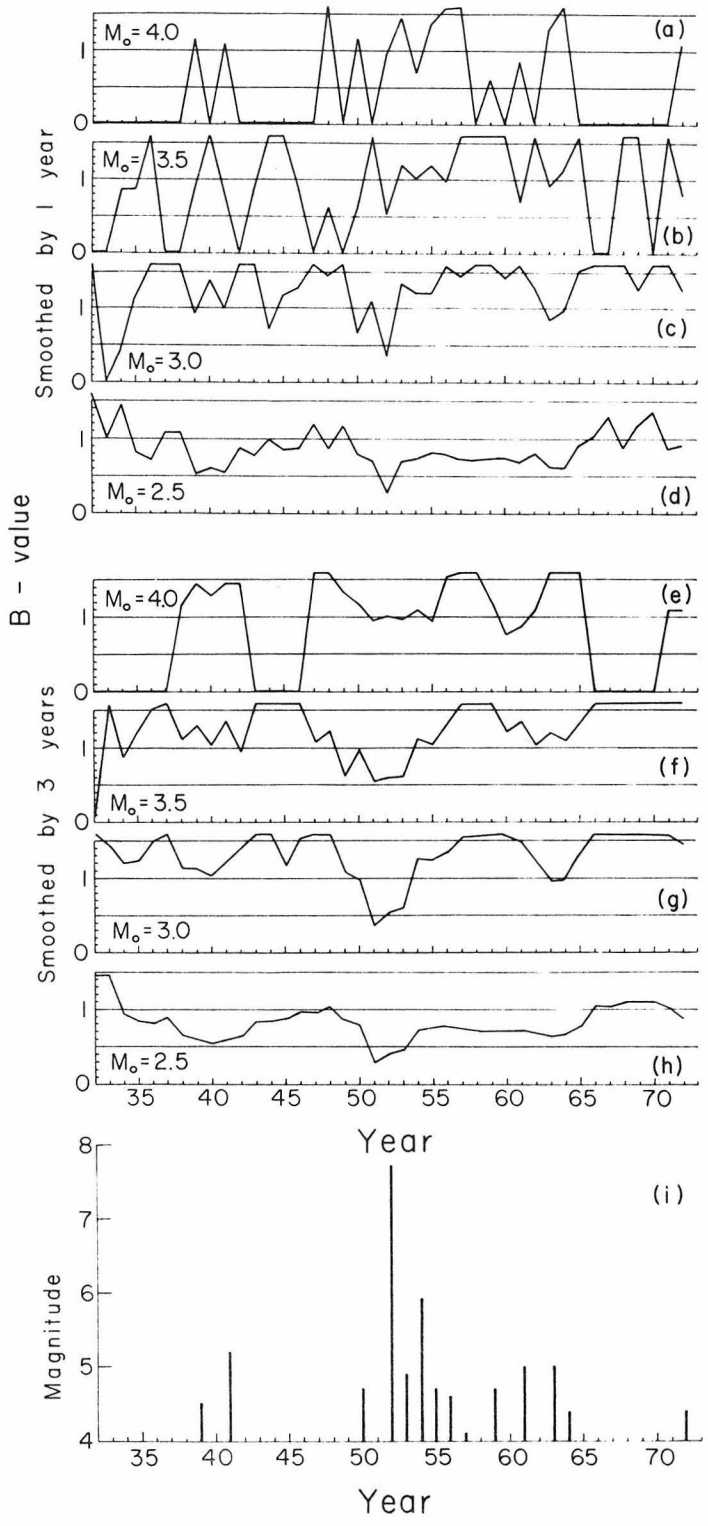

Figure I-70. Estimates of the temporal variation of b in the area of the 1952 Kern County earthquakes. The curves are similar to those in Figure I-69, except curve (i) is added to show the largest earthquake in the area during each year.

b-values, but does preserve the general shape of the time variation of the curve. Thus, the shape of curve (h) can serve as an estimate of the time variation. On this basis, the general changes in b seen in the regional data are not seen for this local data within the immediate area of the aftershock zone. These data do show the same relatively higher values of b for the late 1960's as was evident for the entire Southern California area.

Imperial Valley Area. The long-term estimate for the Imperial Valley area is b = 0.85 with a threshold of about M_o = 3.5. The curves (b) and (f) of Figure I-71 show very erratic temporal changes in the b-value if a threshold of 3.5 is taken, as well as indicating a higher long-term average. These erratic changes show that for larger earthquakes, magnitude 3.5 and above, 1 year is not an adequate statistical sample. The M_o = 3.0 data, curves (c) and (g), are more representative of the long-term results. Figure I-71 also shows a time histogram of the largest Imperial Valley events each year. There are relatively low b-values for the years of the 1940 and 1942 earthquakes, but no similar results for large earthquakes in the years 1937, 1954, and 1968. Again, this effect is probably caused by incomplete analysis of smaller magnitude events. Because the area is so active, there may well be too much interference between the b-value effects of the various shocks to allow any individual effects to be identified. In more general terms, especially with the smoothed data of curve (g), the Imperial Valley shows relatively higher b-values in the late 1930's

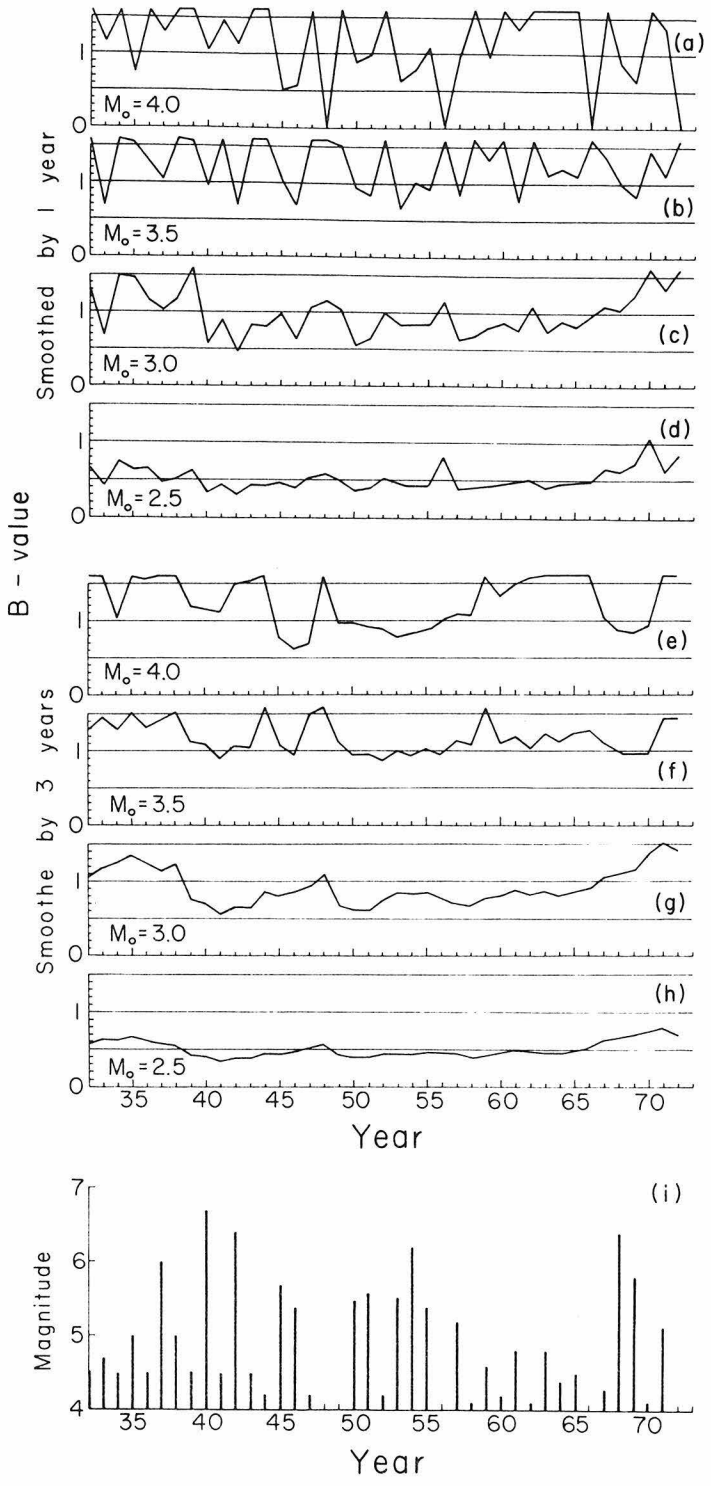

Figure I-71. Estimates of the temporal variation of b in the Imperial Valley area. The curves are similar to those in Figure I-69, except curve (i) is added to show the largest earthquake in the area during each year.

and late 1960's, similar to the variation for the entire Southern California area. Separating these two times is a period with generally lower b-values except for a peak about 1948. The seismicity map for 1948 (Figure I-18) shows the lack of larger events clearly.

San Fernando Area. The San Fernando area was also examined for temporal variation of b-values because of the 1971 earthquake and the report by Whitcomb, et al. (1973b) of precursory changes in the V_p/V_s ratio for this area. The results are shown in Figure I-72, and a histogram of the largest event annually is also given.

Within the bounds used for this area, there was only rather low seismicity prior to 1971 and the b-value estimates are correspondingly erratic. Curve (d) does not show any precursory changes in b-values for the 1971 shock. The value for 1970 is low because of the 3-year smoothing.

Temporal variations of b-values for the various areas of Southern California studied do not show any strong correlation with the occurrence of large earthquakes. A slight increase of the regional b-value following the 1952 Kern County earthquake is suggested, but this same change is not seen in the data for the aftershock zone itself. The data prior to 1952 for the aftershock zone are few and do not give good b-value estimates. Because the Imperial Valley is so active, the individual effects of large shocks are not very evident in the b-value curves. For some years having large earthquakes, such as 1940 and 1942, the b-values for the Imperial Valley are low. Other years, such

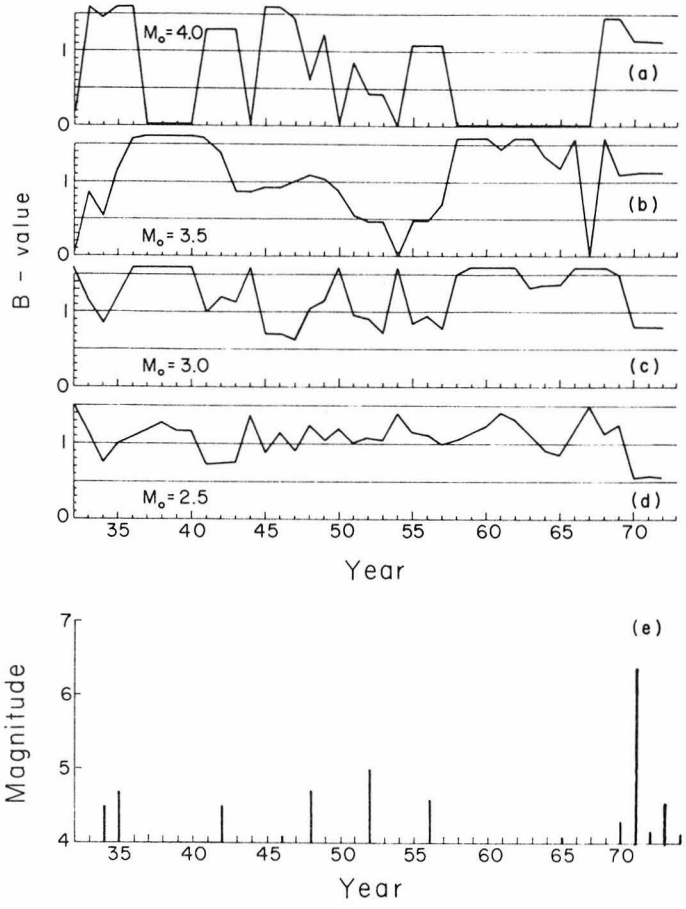

Figure I-72. Estimates of the temporal variation of b in the area of the 1971 San Fernando earthquake sequence. The curves are similar to those in Figure I-69, except curve (e) is added to show the largest earthquake in the area during each year. All curves are for a 3-year sliding window since many years have only a few events.

as 1968, do not show the effect. The b-values are known to be anomalously low for 1952 and 1933 because smaller earthquakes during the early parts of aftershock sequences were not analyzed. Some of the Imperial Valley data probably have the same deficiency.

Chapter 3

IMPERIAL VALLEY SEISMICITY

Introduction

The Imperial Valley is unique among well-instrumented seismic areas in that it has a broad zone of strike-slip faulting as well as possible elements of crustal spreading (Elders et al., 1972). This area is characterized by the boundary interactions of the Pacific plate with the North American plate. It also contains part of the transition from spreading tectonics of the East Pacific Rise to the transcurrent tectonics of the San Andreas Fault system. It is currently one of the most seismically active areas in the Southern California region. Structurally, the valley is a trough containing and bounded by large right-lateral strike-slip faults of the San Andreas fault system. The trough is a structural continuation of the Gulf of California, but it has been dammed by an immense volume of sediments from the Colorado River.

The data given in this chapter show that the tectonic environment of the Imperial Valley can be thought of as that of a set of approximately parallel faults that are loosely coupled. Slip on one fault sometimes induces slip on other faults of the set. In a sense, individual members of all fault systems are coupled because strain release on one fault modifies the surrounding strain field, changing the stresses on adjacent faults. However, in the Imperial Valley, this coupling is particularly evident.

Allen and Nordquist (1972) reported slip on the Imperial Fault and on the San Andreas fault at about the same time as the 1968 Borrego Mountain earthquake occurred on the San Jacinto Fault zone. A 1963 Imperial Valley earthquake swarm, described below, had a rapid succession of shocks widely distributed across the valley.

An earthquake swarm with many shocks on a single fault zone implies fault surface conditions favorable for coupled movements. Each of the many shocks represents a region of the fault surface which must have been stressed previously close to the maximum stress which it could support. Such a fault, with many areas stressed close to failure, is susceptible to triggering. Many shocks of a 1975 swarm were associated with the Brawley Fault (Johnson and Hadley, 1976). A survey of the swarm activity in the Imperial Valley is given to show the widespread and frequent occurrence of swarms.

Some Imperial Valley aftershock sequences are unusual because the activity has been periodic. Periodicity within a sequence is taken to indicate faults which are sensitive to small changes in the stress field. Two of these periodic sequences are described here. One of them seems to involve two spatially separated clusters of activity.

Periodicity of Some Imperial Valley Aftershock Sequences

In this section, the periodic nature of some aftershock sequences is described in support of the concept of coupling of fault motions in the Imperial Valley. For many areas in the valley, the epicenters within aftershock sequences are widely distributed and represent

motions on different fault surfaces. These fault sets respond to the mainshock and are therefore coupled to some extent, but not to the degree proposed for some other faults. Periodicity in the Imperial Valley is significant because it implies that certain faults, or perhaps certain portions of a single fault, are in a highly stressed state, easily influenced by slight additional forces, and thus responsive to slight changes in the stress field.

Periodicity in some aftershock sequences was noticed during a survey of the aftershock sequences. The survey included all Southern California earthquakes of magnitude 6 and larger since 1932. For the most part, these sequences follow the expected behavior of generally decreasing magnitude and frequency as a function of time. Lomnitz and Hax (1966) also examined the 1952 Kern County sequence, as well as the 1957 San Francisco and 1964 Alaska sequences, and found no periodicity or clustering of events. However, for a few sequences which were located in the Imperial Valley and Northern Mexico region, the time histories show definite periods when the activity is absent or very low. In some instances, these gaps in activity seem to occur periodically. Two periodic sequences are presented here: a 1954 sequence in the Borrego Valley and a 1942 sequence in the area of the Fish Creek Mountains. For comparison, the aftershock activity of the 1968 Borrego Mountain earthquake and the 1948 Desert Hot Springs earthquake are also shown. Although both of the periodic aftershock series are near the San Jacinto fault, other examples are also available farther south in northern Mexico. These other examples

are less distinct in their periodicity, and the epicenters have greater uncertainties.

Figure I-73 shows a comparison of two normal aftershock sequences, those of the Desert Hot Springs earthquake and the Borrego Mountain earthquake, with one of the periodic sequences. The 1954 earthquake will be called herein the Borrego Valley earthquake. In the figure, the magnitude of each earthquake is plotted at its time of occurrence after the mainshock. About 12 days of activity are shown for each event. The magnitude axis is cut off at a lower magnitude of 2 because events smaller than 2 are not in the catalog for these sequences. The Borrego Mountain and Desert Hot Springs earthquakes are typical of the majority of aftershock sequences in their time behavior. The aftershocks generally decay in both amplitude and frequency, although parameters characterizing this decay have not been computed. However, the Borrego Valley earthquake does show distinct gaps in the aftershock occurrences, and these gaps appear to be rather uniformly spaced in time.

An initial question is whether the gaps are real or possibly only reflect some vagaries in the threshold of events located and recorded in the catalog. The original seismograms for the 1954 sequence and a 1942 sequence described below were examined, and they do in fact display the changes in seismic activity shown in the figures. Only those shocks with magnitudes greater than about 2.5 were recorded in the catalog, and thus are shown in the figures. Many smaller shocks are recorded on the seismograms. These smaller shocks are less

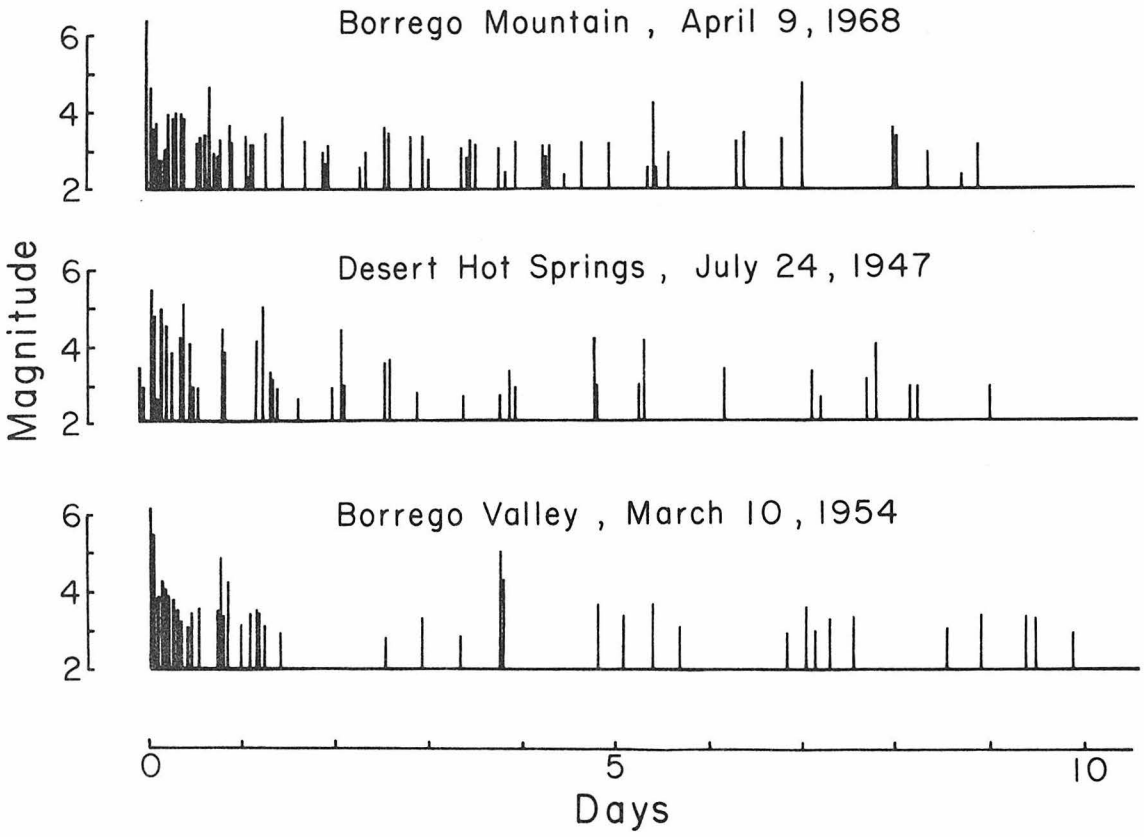

Figure I-73. Time series representation of three earthquake sequences in the Imperial Valley. The Borrego Valley sequence has periodic activity. The Borrego Mountain and Desert Hot Springs sequences are shown for comparison.

numerous by one third to one half during the gaps in seismic activity shown in the figures.

The way in which these data were handled is shown in Figure I-74. Each aftershock sequence was considered as a time series. A power spectrum was computed from the Fourier transform of the autocorrelation function for each series. In Figure I-74(a), each event is plotted at its actual time of occurrence after the mainshock and each event appears as a spike with height equal magnitude. Figure I-74(b) is a time series representing the largest earthquake during each one-hour time period. The number of events within an hour is disregarded in favor of the largest event, because the largest event usually dominates the sum of the remaining events in terms of moment, energy, or strain release. In Figure I-74(c) each pulse represents a three-hour sliding window. This smoothing of the time series has the effect of smoothing the power spectrum and suppressing spurious peaks. During analysis, spectra were computed using time series with smoothing windows of 1,3 and 5 hours respectively. The spectral peaks here identified with periodicity in the aftershock activity were persistent in each spectrum. The spectra in subsequent figures were all computed using the 3-hour window.

The time series and resulting power spectrum for the 1942 earthquake near the Fish Creek Mountains are shown in Figure I-75, where power has been plotted as a function of period in hours. Because the level of power in the time series is arbitrary, the results have been normalized to a DC value of unity. For the Fish Creek Mountains

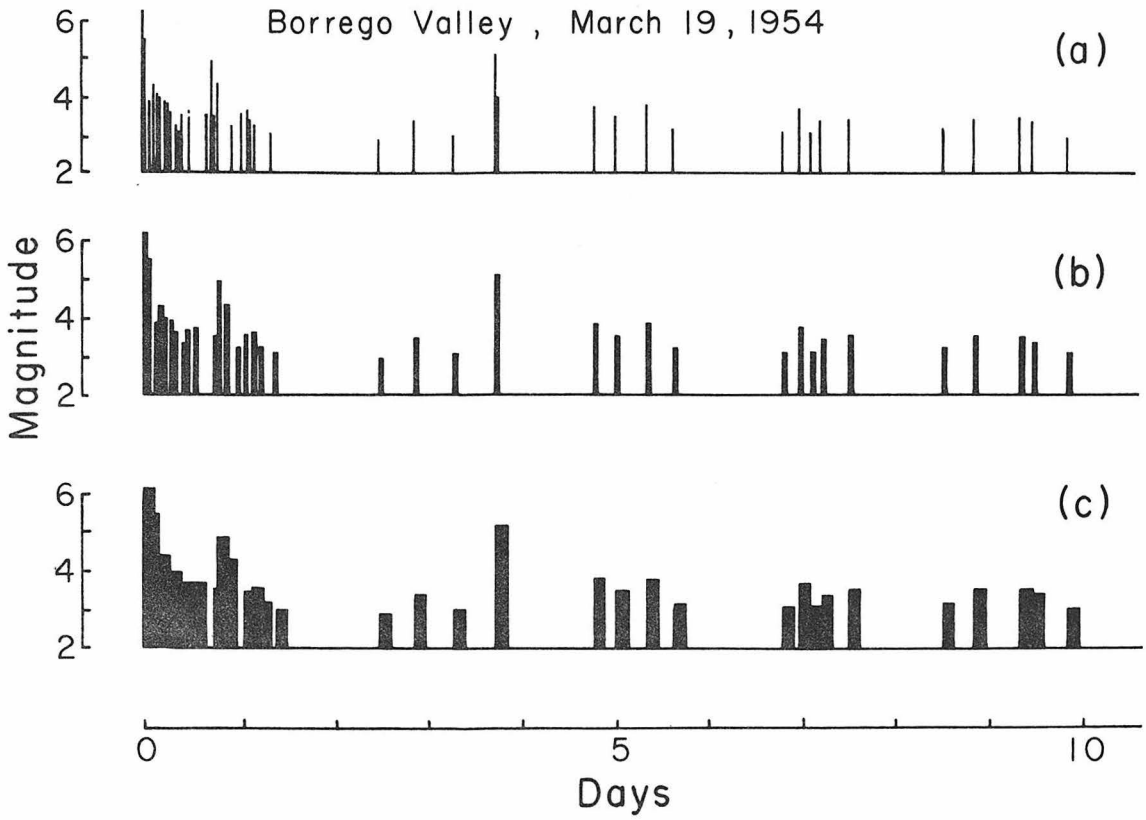

Figure I-74. Smoothing of the time series prior to spectral analysis. Curve (a) is the time series. Curve (b) is the largest event during each hour. Curve (c) is the largest event in each three-hour period.

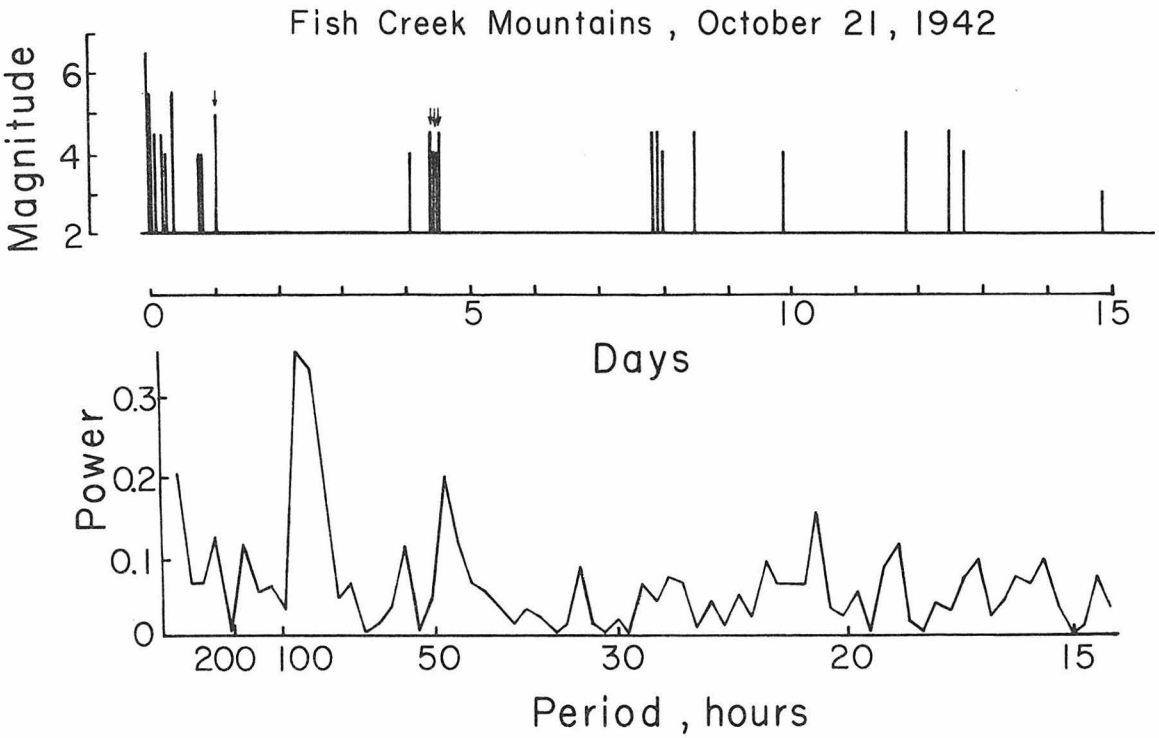

Figure I-75. Time series and power spectrum for a 1942 aftershock sequence near the Fish Creek Mountains, Imperial Valley. Arrows indicate those shocks which were spatially separated from the main area of aftershock activity.

aftershock sequence, there is a peak in the power spectrum at about 96 hours. Visually, the periodicity is apparent in the time series. The smaller peak in the spectrum at a little less than 50 hours period may be due to single events centered in the third and possibly fourth cycles of low activity.

It is important to note that there are four bursts of activity evident in the time series, separated by intervals of relative quiescence. A minimum of three bursts is necessary to even claim any periodicity. If there were but two periods of earthquake activity, the Fourier analysis would easily show peaks associated with the separation, but there would not necessarily be a periodic phenomenon.

The geographic distribution of these events is interesting even though only a few of the aftershocks have been located individually. The nearest reporting stations were Pasadena, Mount Wilson, Riverside, and La Jolla, giving a very poor azimuthal distribution. The mainshock and most of the aftershocks were assigned a location on trend with the Coyote Creek fault as shown on the seismicity map for 1942 (Figure I-12). However, five of the aftershocks were located about 40 km to the northeast, near the center of the southern end of the Salton Sea. These particular aftershocks were felt at the town of Niland, which is east of the Salton Sea. Four of these events are labelled with short arrows in Figure I-75. The fifth occurred 23 days after the main shock. Although these events are rather distant from the main shock, they are treated as aftershocks because of their intimate temporal association with the rest of the aftershocks. These

shocks fit the periodic pattern described here, but they are not necessary to define the pattern. Additional small-magnitude shocks which were not located presumably occurred in the same area.

This separation of the aftershocks probably represents triggering of shocks on a parallel fault. No shocks were located in the intervening area, and the known geology (Sharp, 1972) is dominated by northwestward trending faults.

The mechanism of the periodicity is yet to be learned. It is interesting to speculate that the period between bursts of activity represents the propagation of significant stress changes between the mainshock area of activity and the Salton Sea area of activity. Various periods have been observed for the aftershock sequences: about 96 hours for this Fish Creek Mountains sequence; about 50 hours for the Borrego Valley sequence described below; and other sequences which weakly suggest periods from 1 to 15 days. Variation in the observed periods indicates some condition peculiar to each series rather than a common outside driving force such as earth-tides. Stress propagation is not clearly demonstrated for the 1942 Fish Creek Mountains sequence. Events from both the mainshock area and the Salton Sea area occur together in the initial burst of activity and also in the second burst as shown in Figure I-75. Whatever the mechanism, the activity of these two areas during the 1942 sequence seems strongly related, i.e. coupled.

It should be noted here that periodicity has been reported for Imperial Valley earthquake swarms by Klein (1976). He found that shocks within swarms tend to cluster at times when the solid-earth

tide is rising and the tidal stress is oriented to enhance the regional tectonic stress. Mainshocks and aftershocks were found to be uncorrelated with the tides.

Another Imperial Valley aftershock sequence which showed periodicity followed the Borrego Valley earthquake of March, 1954. The time series and power spectrum for the Borrego Valley aftershock sequence are shown in Figure I-76. For this sequence, there is a strong peak at about 50-55 hours. This corresponds well to a visual estimate of the interval between the beginning times of each burst of seismicity. Periodicity is clearly exhibited, as for the Fish Creek Mountains sequence, but widely separated faults are not indicated here.

For the Borrego Valley sequence, the aftershocks were not located individually in the seismicity catalog; all were assigned coordinates of the mainshock. The Caltech Seismological Laboratory phase-data card file showed very consistent S-P times at the Barrett station, 9.9 ± 0.6 seconds, with a range of 8.6 - 11.6 seconds for 54 shocks. The standard deviation of 0.6 seconds corresponds to about 5 km. Only two shocks were beyond 12 km from the mean. At the Riverside station, S-P times were 16.9 ± 1.1 seconds with a range of 14.5 - 18.8 seconds. The standard deviation here corresponds to about 10 km. The Riverside station is northwest of the epicentral area, and the Barrett station is southwest. Thus the S-P data are consistent with an aftershock zone about 10 km by 20 km elongated in a northwesterly trend.

A final point concerns the significance of the power spectra peaks which have been identified with periodicity. This is considered

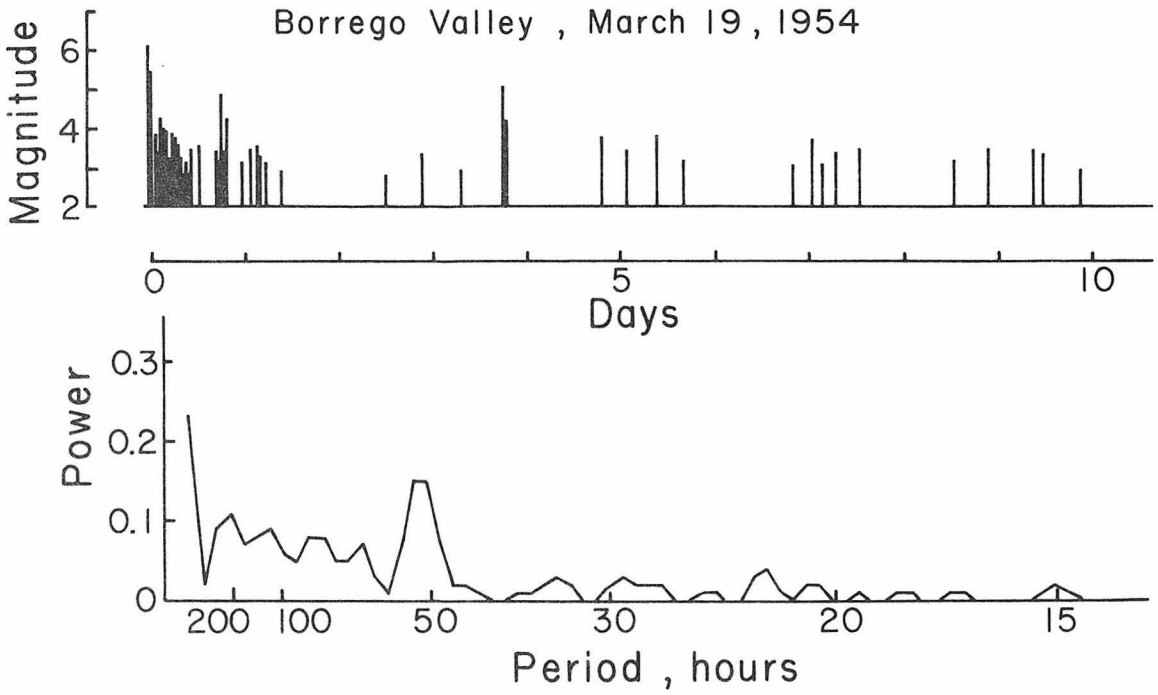

Figure I-76. Time series and power spectrum for a 1954 aftershock sequence in the Borrego Valley area.

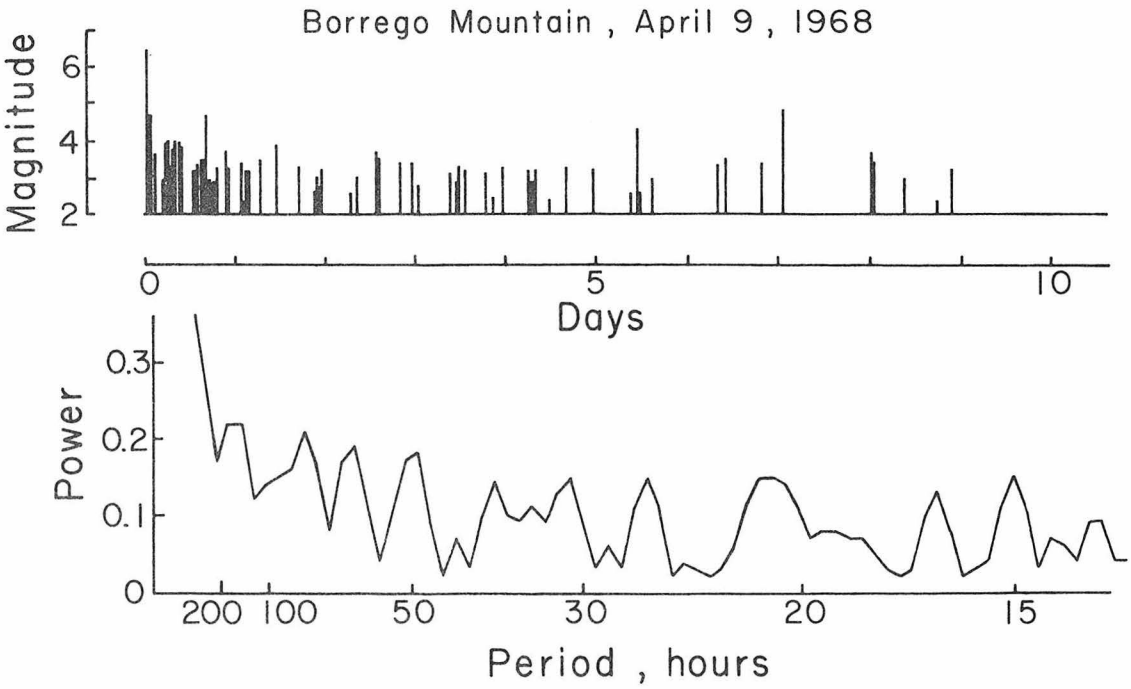

Figure I-77. Time series and power spectrum for the 1968 Borrego Mountain sequence. This series is not considered periodic; all the spectral peaks have similar amplitudes.

qualitatively by comparing the spectra of the periodic sequences with the spectra of other aftershock sequences which seem aperiodic. The spectrum of the 1968 Borrego Mountain earthquake sequence is shown in Figure I-77 along with the time series of the sequence. The data here were handled in a manner identical to that already described to give the power spectrum shown. There are many peaks in this spectrum, but the general levels of the peaks are all about the same and none is significantly stronger. Conversely, the spectral peaks identified in Figures I-75 and I-76 are twice the amplitude of the average peaks of those spectra and are considered significant peaks.

These data for the 1942 and 1954 earthquake sequences demonstrate periodicity for some Imperial Valley aftershocks. The data do not shed much light on possible mechanisms causing the periodicity. But the periodicity itself suggests that motions on the faults involved are easily triggered. If fault slip can be easily triggered, then motions on a fault can be coupled to the motions of other neighboring faults.

Earthquake Swarms

Swarm-type earthquake activity has occurred often in the Imperial Valley region. The prevalence of swarms is taken here to indicate fault environments which are suitable for coupling of fault motions, i.e., movement is easily triggered by movement on neighboring faults. Some faults may respond to stress by moving with aseismic creep. These fault zones must be relatively free of conditions which could lock the

fault. Other faults are locked so tightly that they support high total stresses, and their eventual rupture extends over a major portion of the fault. An earthquake swarm which has many of its shocks along one fault zone, such as the 1975 Brawley swarm (Johnson and Hadley, 1976), is presumed to represent conditions between these two extremes. Total stress supported by the fault is not high, the shocks are easily triggered, and individual ruptures are not extensive. Swarms which clearly involve many different faults, such as a 1963 Imperial Valley swarm described below, directly demonstrate coupling of fault movements.

As used here, an earthquake swarm is taken to be an earthquake sequence of four or more events in which the largest event is within one-half unit of magnitude of the next largest event and does not occur near the beginning of the sequence. The shocks are also close enough together in time and space to appear related. However, an earthquake swarm cannot be precisely defined in general usage because observed seismicity presents too many borderline cases in terms of number of shocks and relative magnitudes. In the Imperial Valley, for example, there are many pairs, triplets, etc. of earthquakes with comparable magnitudes. Choosing four shocks as a threshold is purely arbitrary. Also there are otherwise normal mainshock-aftershock sequences which have one or two unusually large "aftershocks". The value of b in the usual recurrence relationship, $\log N = a - bM$, is not a good criterion to define a swarm, although the values can be rather low. The 1975 Brawley swarm had $b = 0.51$, but the 1968 Santa

Barbara swarm had b = 0.86, both maximum likelihood estimates. Normal earthquake sequences have b usually in the range 0.8 - 1.2, but more extreme values are sometimes reported (Wyss and Lee, 1973).

Earthquake swarms have occurred often in the Imperial Valley. Those which have been registered since instrumental observations began in 1932 are shown in Figure I-78. They are distributed widely in the California portions of the Imperial Valley, but the most extensive swarms seem clustered along a northwest trend just east of Brawley. It is likely that similar swarm activity continues on into Mexico, but has not been registered, except for swarms with shocks greater than magnitude 4, because of the effective detection threshold for northern Mexico. The 1975 Brawley swarm has been described by Johnson and Hadley (1976), and their results imply that the time-space sequence approximated an extremely slow bi-lateral rupture on a fault surface. None of the Imperial Valley swarms has produced shocks larger than magnitude 5.5, but normal earthquakes up to magnitude 7 (in 1934, 1940) have shaken the region.

This distribution of swarm activity suggests that there are a number of faults in the Imperial Valley whose slip characteristics are intermediate between creep and normal earthquakes, at least at some times. At other times, these same faults may lock and subsequently produce large earthquakes. With many parallel faults in the system, some can be expected to be locked by large irregularities and capable of creating large earthquakes. Others may be free to creep or are held only by small asperities and conform to the coupling model.

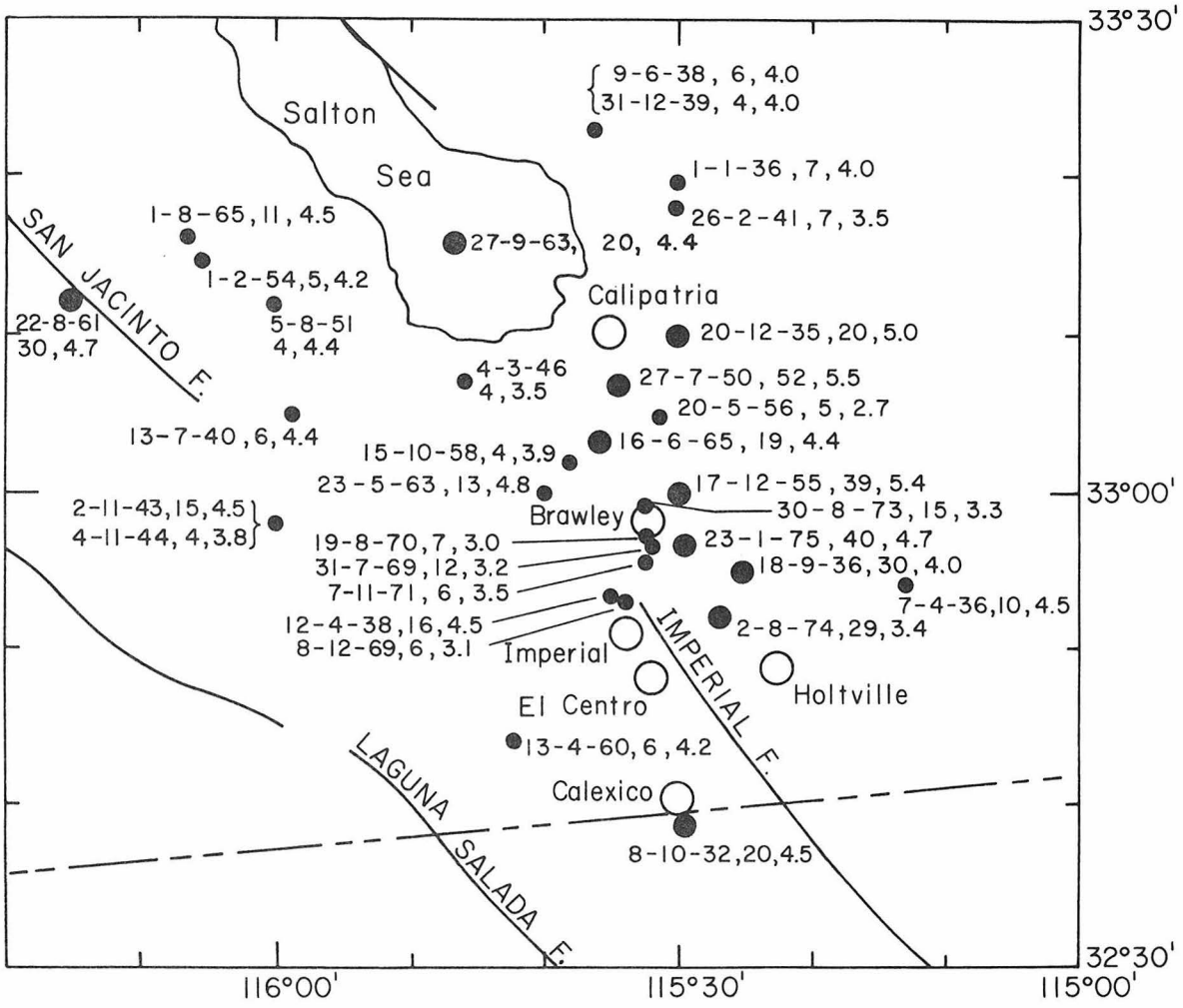

Figure I-78. Earthquake swarms in the Imperial Valley area, 1932-1975. The notation for each swarm gives the initial date, the number of shocks, and the magnitude of the largest shock. Swarms with more than 20 shocks have the larger symbols.

As relative motions proceed, a particular fault may be in one mode at a given time and in another mode at a later time.

One particular swarm in the Imperial Valley offers further direct evidence of coupling between faults in the valley. This swarm of 19 shocks took place during a 28-hour period beginning September 27, 1963, at 1450. Epicenters for the sequence are shown in Figure I-79. The initial shock and a total of 12 of the 19 occurred in the south end of the Salton Sea. But the remaining 7 earthquakes were rather widely distributed, as the figure shows. The initial 4 shocks of the sequence covered the full width of the distribution, about 60 km, during the first 8 minutes of the sequence. All of the locations here are of C quality and have estimated uncertainties on the order of 15 km, so the wide distribution is considered real.

Earthquake swarms seem to be a regular feature of the Imperial Valley seismicity, but swarms have also occurred from time to time at other places in Southern California. These are mentioned here to place the level of swarm activity in the Imperial Valley in its proper perspective. Many faults can temporarily exhibit the activity which is currently common in the Imperial Valley. The 1968 Santa Barbara Channel earthquake swarm was the most notable of these swarms recently (Sylvester, et al. 1970). This swarm contained 63 shocks with magnitudes greater than 2.8 and lasted a little longer than one month. In contrast to the 1975 Brawley swarm, the Santa Barbara Channel swarm epicenters were more widely distributed in a 10-km circular pattern. Several lesser swarms are also known to have occurred

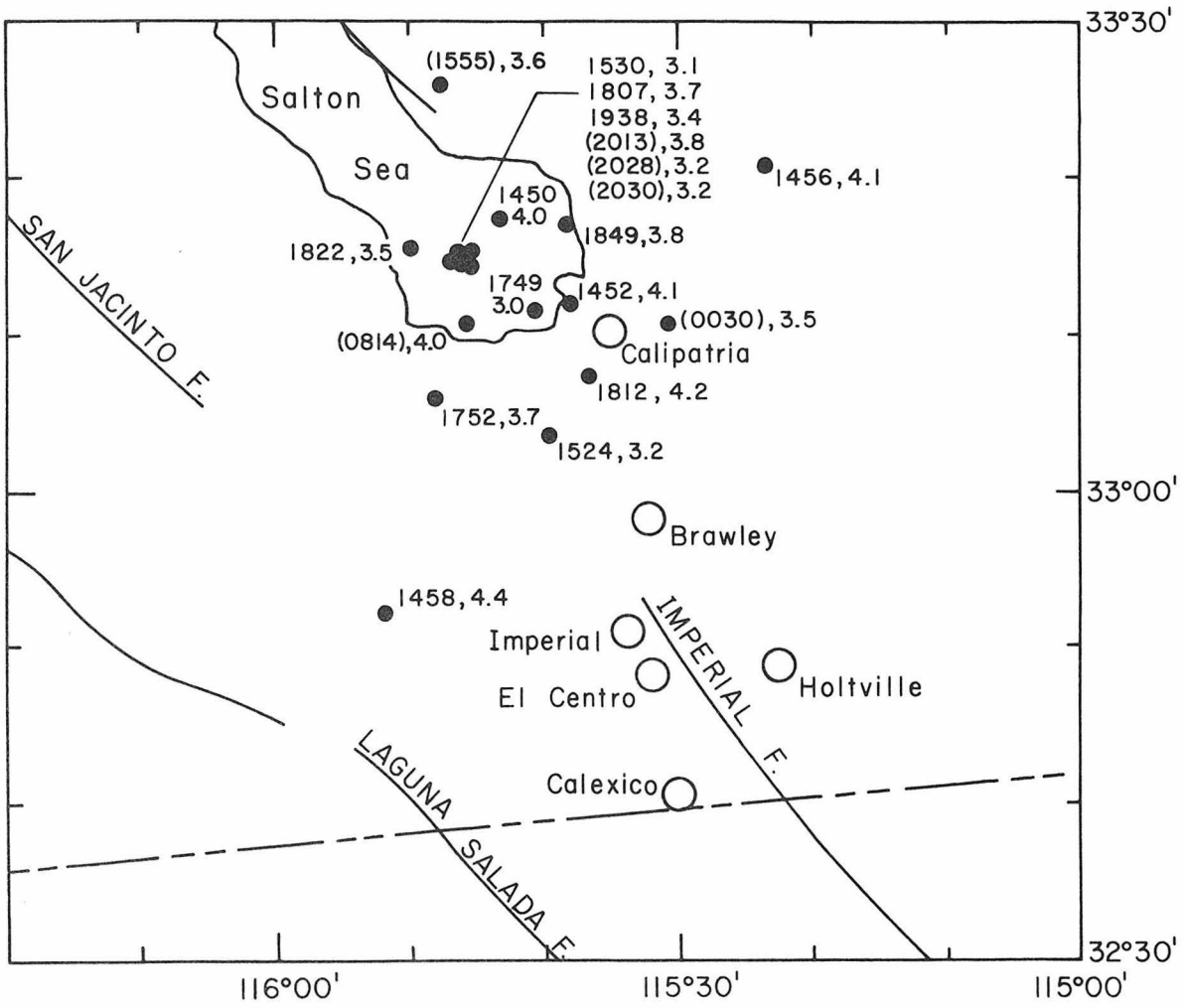

Figure I-79. A widely distributed Imperial Valley swarm in September, 1963. The notation on each shock indicates the time of occurrence and the magnitude. Times in parentheses are on the second day.

in the Santa Barbara Channel. The tectonic implications of the 1968 swarm are not clear since focal mechanism solutions were at variance with local geologic trends. Although swarm activity has occurred widely throughout the Southern California region, nowhere has the frequency been equal to that in the Imperial Valley. The next most swarm-active area is in the vicinity of the Little San Bernardino Mountains and includes an area about 30 miles in diameter in which there have been 6 swarms since 1932. Only 3 of the six swarms had 10 or more shocks. A list of regional swarms of 5 or more shocks, exclusive of the Imperial Valley, is given in Table I-4. Such a list is at best a guide because of the difficulty in defining a swarm.

The historical record (Townley and Allen, 1939) also contains descriptions of earthquake swarms, but they are often difficult to identify with certainty. Two examples are: June 24-Aug 3, 1917, in the Los Angeles area, with 19 shocks having maximum intensities from III to IV; July 21-Aug 14, 1920, in the Los Angeles area, with 20 shocks having maximum intensities from II to VI. An intriguing series occurred July 27-Aug 16, 1902 at Los Alamos. There were about 75 shocks. Since the largest shocks were on the first and fifth days, this may not be a swarm. However the magnitude and frequency of shocks does not seem to have diminished as in a normal sequence. The report indicates that residents were in a sustained state of panic and evacuated the area on a special train to San Luis Obispo after the fifth day (Townley and Allen, 1939).

Table I-4

EARTHQUAKE SWARMS IN SOUTHERN CALIFORNIA REGION EXCLUSIVE OF THE IMPERIAL VALLEY

Date	Duration	Lat	Long	Area	Number	Magnitude Range
350510	20 days	35°-42′	118°-20′	E. of Isabella	41	2.0 - 3.0
350628	29 hr	33-35	117-00	Murrieta Hot Spr.	6	2.0 - 2.5
350904	4 days	33-09	116-35	Julian	7	2.5 - 3.5
360823	4 days	34-30	118-35	Castaic	8	2.0 - 3.0
360908	7 hr	33-34	117-59	Santa Ana	8	2.0 - 3.5
400518	37 days	34-03	116-17	Joshua Tree	52	4.0 - 5.4
410914	5 hr	37-34	118-44	Lake Crowley	6	4.0 - 6.0
	(5.8, 4.5, 5.5, 6.0, 4.0, 5.0 in 5 hr, then a normal aftershock sequence)					
420121	20 days	34-24	116-55	San Bernardino Mts	19	2.5 - 4.5
430915	8 days	36-01	117-56	Haiwee	9	2.5 - 4.5
440120	12 days	35-33	118-55	NE of Bakersfield	11	2.3 - 3.5
480803	5 hr	34-11	118-10	Pasadena	6	1.8 - 2.1
520721	22 min	33-59	117-16	E. of Riverside	5	2.0 - 2.9
	(5½ hr after Kern Co mainshock)					
571225	7 days	34-10	118-05	Pasadena	5	1.5 - 3.2
590729	9 days	34-00	117-48	Pomona	24	2.2 - 3.5
600524	6 days	34-10	118-08	La Canada	8	1.1 - 1.5
611020	22 hr	33-40	117-58	Santa Ana	14	2.6 - 4.3
630503	26 hr	37-37	118-54	Lake Crowley	7	3.2 - 4.2
630705	57 days	34-10	116-10	Twentynine Palms	24	2.6 - 4.7
640203	24 hr	31-10	114-15	Gulf of Calif.	5	4.5
661214	33 days	33-35	118-20	S. of San Pedro	23	2.3 - 4.0
680205	5 days	36-08	117-48	Haiwee	8	2.1 - 2.6
680626	39 days	34-15	119-40	Santa Barbara Ch.	63	2.9 - 5.2
690318	11 days	31-20	114-05	Gulf of Calif.	>200	- 5.8
720111	5 hr	33-50	116-18	Thousand Palms	7	2.5 - 3.7
720405	3 days	33-35	115-42	Hayfield	7	2.7 - 3.2
720626	9 days	35-50	117-35	Searles Lake	7	2.8 - 3.4
721112	32 days	34-00	117-35	Ontario	20	2.1 - 3.5
731117	11 days	33-58	116-18	Thousand Palms	15	2.0 - 2.9
740108	23 hr	33-56	116-18	Thousand Palms	6	2.3 - 2.8
740506	20 hr	34-04	116-31	Morongo Valley	5	2.2 - 3.0
740519	22 hr	35-54	117-44	Little Lake	12	2.0 - 3.1
740712	37 days	34-38	116-20	Pisgah Crater	47	2.4 - 4.4

Note: Dates are YYMMDD.

Chapter 4

TRANSVERSE SEISMICITY

Introduction

The distribution of instrumentally determined epicenters in Southern California shows several areas in which epicenters are closely aligned along known active fault zones. A causal relationship between active faulting and nearly all earthquakes is now widely accepted. Such distributions occur along the San Jacinto fault zone, particularly for earthquakes greater than magnitude 6 (Figure I-57), the northern end of the Newport-Inglewood fault zone (Figure I-55), and the White Wolf fault (Figure I-55). Epicenter estimates in the Imperial Valley have recently been improved because of the dense network of seismographic stations installed by the U. S. Geological Survey in 1973. These epicenters with improved accuracy show clear alignment (Figure I-54) along the Imperial and Brawley faults (Hill et al., 1975; Friedman et al., 1976). Imperial Valley epicenters prior to 1973 did not show these trends so clearly.

Much of the Southern California seismicity, however, is more widespread and does not clearly delineate particular active faults. This distribution can be attributed both to low-level activity on many different faults and to errors in epicenter solutions. In an ideal sense, long-term recording with a dense network of seismographs might be expected to overcome these problems. Realization of this ideal is unlikely because seismic activity is not necessarily a time-stationary process. Allen (1974) has pointed out examples from China, Turkey and

Korea where extensive historical records are available and for which levels of seismic activity have varied on time scales up to 800 years. Richter (1971) suggested that certain areas of central Asia, New Zealand, and Japan were characterized by sporadic seismicity.

Transverse Seismicity Trends

Some trends in the distribution of Southern California seismicity are not clearly associated with recognized faulting or structural features. These trends seem to cut across the general tectonic fabric of the region. A transverse trend of seismicity in California was first suggested by Ryall et al. (1966) when they defined the "Ventura-Winnemucca" zone. This zone extends from the Ventura and Santa Barbara area northeastward to the eastern Sierra Nevada front and then northward into central Nevada. It includes the epicentral areas of the 1952 Kern County earthquake, the 1946 Walker Pass earthquake, the 1872 Owens Valley earthquake and all of Nevada's large historic earthquakes. Richter (1969) felt that this zone was not continuous southward beyond the area of the Owens Valley earthquake. He pointed out major transverse trends in other seismically active regions of the world as well as several minor localized transverse alignments in Southern California.

The detailed seismicity maps presented herein show the transverse alignment in the vicinity of Ventura and Santa Barbara (part of the "Ventura-Winnemucca" zone) as well as certain other parallel trends which are more regional in character than those pointed out by Richter.

The transversly aligned trends of seismicity proposed herein are not so clearly developed as those trends defined by joining the epicenters of large earthquakes. These proposed trends are seen most clearly on various maps of annual seismicity. Cumulative seismicity maps show these trends less clearly, and sometimes only when viewed with the benefit of a liberal imagination. Selected examples of seismicity maps showing the transverse trends are shown in Figure I-80 in which lines and shading show the trends as they have been interpreted. Other annual maps which also shown these trends, though sometimes less clearly, are those for 1938, 1942, 1943, 1944, 1946, 1950, 1952, 1954, 1958, 1961, 1964, 1971, 1973 (found in Figures I-8 through I-43).

Do these trends in fact exist or are they merely fortuitons alignments of seismic activity? The presence of such trends was first suggested by seismicity maps such as Figure I-80(c) for 1967. Here a rather sharp boundary trends east-northeast, separating a higher level of seismicity in the Los Angeles region from that in the region to the north of the boundary. The most significant aspect of the boundary is that it extends beyond the San Andreas fault for a considerable distance into the Mojave Desert. This same general boundary separating high and low levels of seismicity is present in many of the seismicity maps listed above. On maps such as Figures I-80(a) for 1955 and I-80(b) for 1959, the boundary and its extension across the San Andreas fault are less clear, but the lines shown do separate two areas of high and low seismicity, respectively. Figures I-80(e) for 1940-1944 and I-80(f) for 1965-1969 are five-year seismicity maps

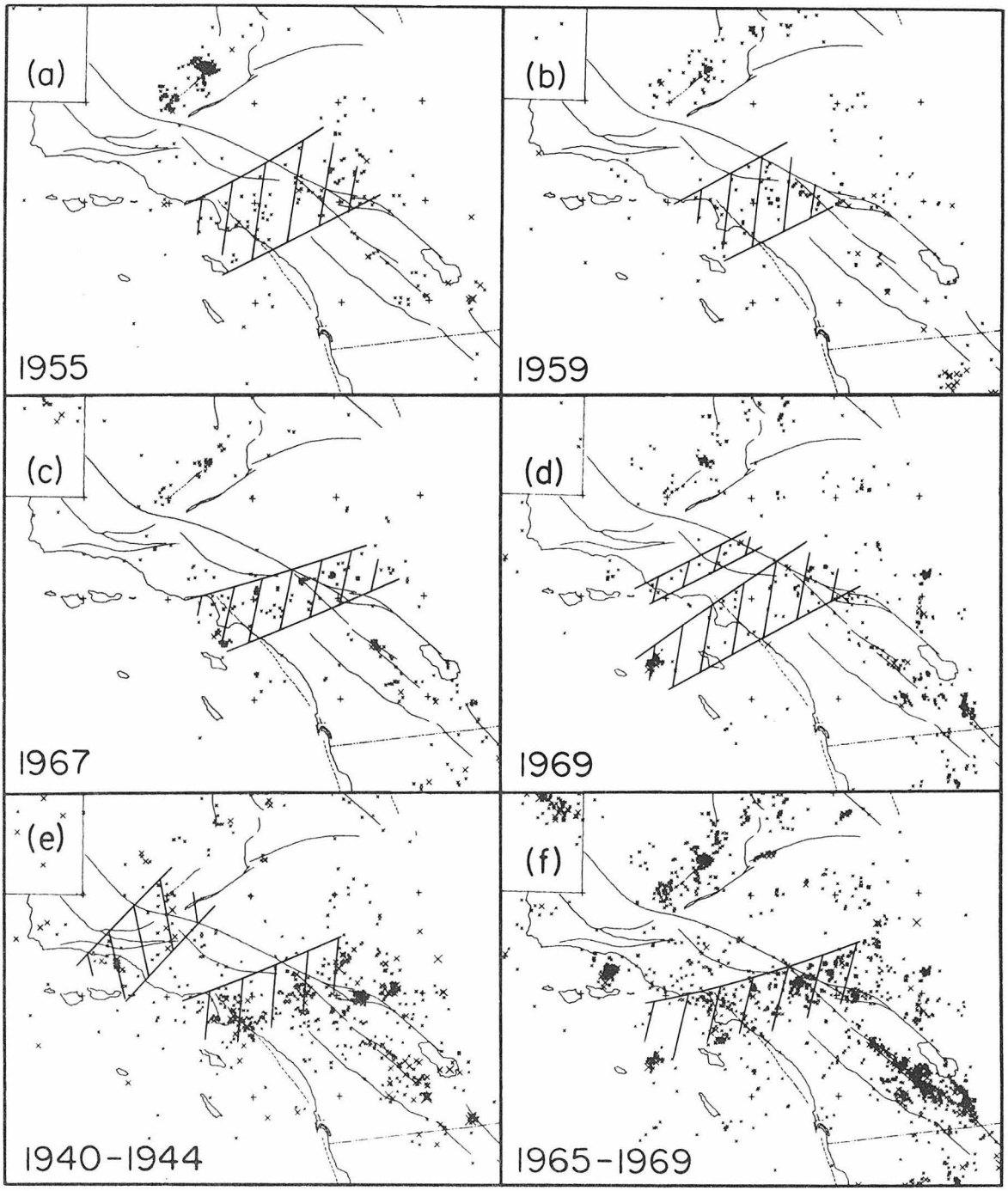

Figure I-80. Selected seismicity maps showing transversly aligned seismicity trends.

which also show the boundary. Although more epicenters are now evident in the area north of the boundary, there is still a distinct difference in the levels of seismicity, and this difference extends across the San Andreas fault zone.

If this boundary were to stop near the San Andreas fault zone, it might be explained quite simply as the northern edge of the Los Angeles basin and its extensions. The southern frontal fault system along the San Gabriel mountains (Ellsworth et al., 1973) coincides with much of this boundary. However, the boundary does extend transversely across the San Andreas fault zone, a major regional tectonic feature. The Transverse Ranges themselves also extend across the San Andreas Fault zone, but the ranges trend nearly east while the seismicity boundary trends about N 70^{o} E, oblique to the range.

Assuming that the observed boundary is real, other similarly trending features were sought. A southern boundary to this zone of higher seismicity can be drawn as shown in Figures I-80(a), (b), (c) passing south of Catalina Island. Separation of areas with different seismicity levels is less clear here because of a high level of seismicity trending northwest along the San Jacinto Fault zone. Low seismicity characterizes the Peninsular Ranges within Southern California, and this contrasts with the higher level of seismicity in the Los Angeles area.

The so called Ventura-Winnemucca zone seems to be best defined by moderate to large earthquakes. Definition of the zone using large earthquakes, magnitude 6 and greater, has already been noted by Ryall

et al. (1966). Small earthquakes, of magnitudes less than 4, do not seem to define this zone in the Transverse Ranges region except as aftershocks to the larger earthquakes. There do seem to be occasional concentrations of moderate shocks, of magnitudes 4-5, that coincide with this zone. In Figure I-80(e) for 1940-1944, epicenters of shocks with magnitudes in the 4's and 5's are localized along this zone. Similar distributions can be found in Figures I-50 for 1950-1954 and I-51 for 1955-1959, but these maps display many aftershocks of the 1952 Kern County earthquake.

A smaller transverse alignment of epicenters is shown in Figure I-80(d) for 1969, trending northeast and passing through the subsequent epicentral area of the 1971 San Fernando earthquake. This alignment and a similar one in 1961-1962 (Figures I-31 and I-32) were noted by Whitcomb et al. (1973a). At its southwest end, this trend also includes the 1973 Point Mugu earthquake. At its northeast end, it coincides with the largest instrumentally recorded events of the low-level seismicity along this portion of the San Andreas Fault zone.

An interpretation of transverse seismicity zones in the Southern California region is shown in Figure I-81. It must be emphasized that the zones shown are inferred from the full ensemble of seismicity maps rather than just the epicenters shown in Figure I-81. Zone A which traverses the Los Angeles basin is defined primarily by a sharp contrast in seismicity along its northern limit; the southern limit is drawn approximately parallel but is much less clear. Zone B joins the epicentral areas of the 1973 Point Mugu earthquake, the 1971 San

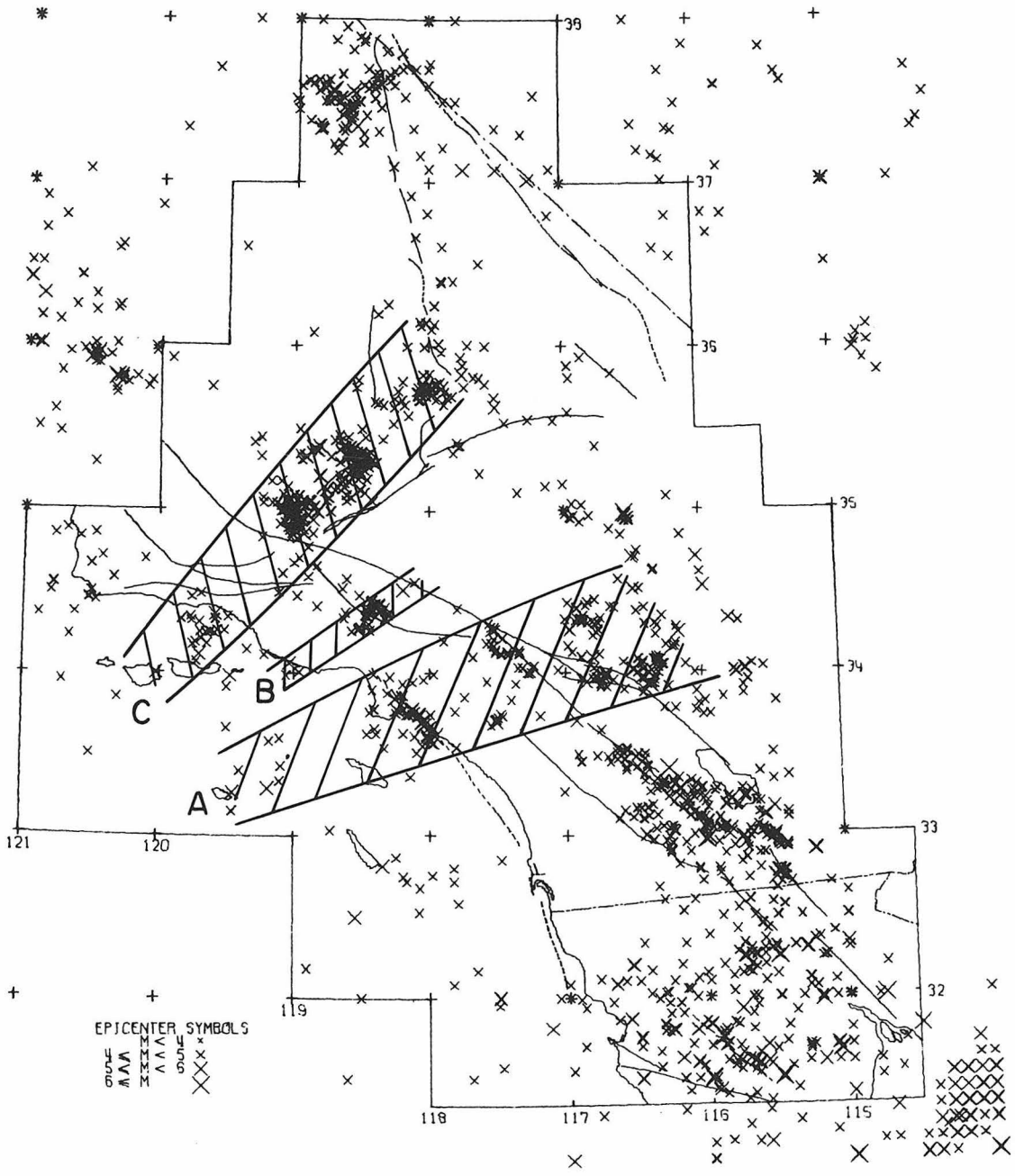

1932 THROUGH 1975, EVENTS EQUAL OR GREATER THAN MAGNITUDE 4

Figure I-81. Composite interpretation of transversly aligned seismicity trends based on all of the seismicity maps.

Fernando earthquake and smaller shocks near Palmdale; it has been marked by linear alignments of epicenters in 1961-1962 and 1969. Zone C is the southernmost portion of the Ventura-Winnemucca seismic zone and is marked by alignment of moderate to large earthquakes in the instrumental record. Zone C contains the 1952 Kern County earthquake, the 1946 Walker Pass earthquake, the 1925 and 1941 Santa Barbara earthquakes. It may also include the 1812 Santa Barbara earthquake and the 1852 shock thought to be on the Big Pine Fault (Jennings, 1973).

Interpretation of the Transverse Seismicity Zones

Two characteristics of these transverse zones are basic to their interpretation. First, they are not well defined and do not neatly categorize the observed seismicity. Second, they are transverse to the major structural trends in Southern California, including the Transverse Ranges, and they extend across the boundaries of tectonic provinces.

Richter (1969) suggested that transversely aligned seismicity could be explained by some elaboration of complementary fault trends, approximately N 30^{o} W and N 60^{o} E, in response to roughly north-south regional compression. The trend of the San Andreas system is more likely determined by the relative motions of the Pacific Plate and the North American Plate, but complementary faulting is not ruled out. The recognized Quaternary faults (Jennings, 1973) with complementary trends are less extensive than the seismicity in each of the transverse zones. Also, these faults do not cross the boundaries of tectonic

provinces. Complementary faulting on a local scale may be present. Davis and Burchfiel (1973) interpret the Garlock fault as resulting from the extensional origin of the Basin and Range Province and not as a feature conjugate to the San Andreas trends.

Much of the seismicity which occurs in the transverse zones can be associated with faults which are part of the northwest-trending regional structural fabric or with the east-trending Transverse Ranges. It may be significant that zones A and C, the two prominent zones, intersect the San Andreas Fault system just at the points of its "big bend". The fact that the zones are diffuse rather than clearly defined suggests that they may be related to some process which serves to modulate or localize the existing seismicity. For example, the observed lateral motion across the San Andreas Fault zone certainly explains the fault's seismicity. However, the distribution of small shocks along the fault zone and the epicenters of great earthquakes may be influenced by additional factors. A portion of the San Andreas Fault in central California, from Hollister to Parkfield, has seismic behavior different historically from that on either of the adjacent sections (Allen, 1968). This zone exhibits aseismic creep and its seismicity is limited to only moderately sized earthquakes (Magnitude 6). Wesson et al. (1973) equate this expression of seismicity to the local physical properties and configuration of the fault surface. The seismicity of faults crossing these transverse zones may be localized in a similar way. The appropriate conditions are unknown, but transverse zones of anomalous temperatures are one

plausible example. Because the transverse zones are extensive and seemingly not related to the known near-surface geology, their cause may be below the shallow portions of the crust.

Although the seismic zones proposed here are transverse to contemporary geologic trends, some ancient geologic trends are similar. Upper Precambrian and lower Paleozoic rocks in Nevada, California, and Arizona show northeast trending isopacks (Stewart, 1970) which are shown in Figure I-82. These rocks are interpreted as indicating a northeast-trending continental margin in late Precambrian and early Paleozoic time. Burchfiel and Davis (1972) show a sketch map (Figure I-83) generalizing the tectonics during late Mesozoic time, when northwest trends were superimposed by a subduction zone and a plutonic-volcanic arc. The earlier northeast trends are considered to have been still present to some degree in Southern California, but their extent to the southwest is undetermined. In late Cenozoic time (Atwater, 1970), the subduction zone was replaced by right-lateral strike-slip motion evident today. Whether any of these very early tectonic trends related to the continental craton could still be represented at depth in Southern California is highly conjectural. These trends would exist primarily in the North American plate. A single trend could not still be continuous across the plate boundary. However, the position of the plate boundary, past and present, may not be a simple issue.

Hadley and Kanamori (1977) have proposed that the current position of the San Andreas fault at depth is considerably eastward of the

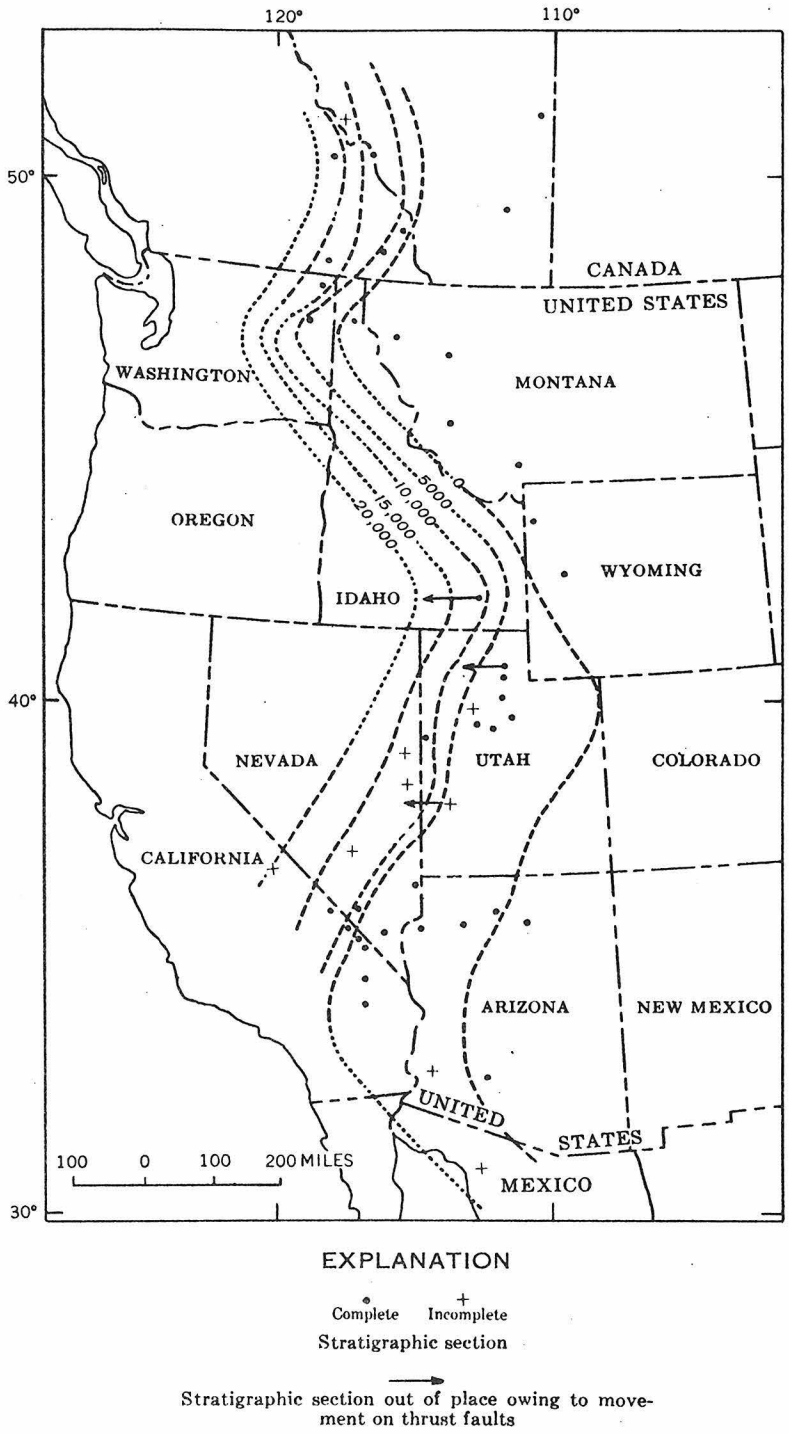

Figure I-82. Late Precambrian and early Paleozoic stratigraphic trends indicating the early continental craton. Figure from Stewart (1970).

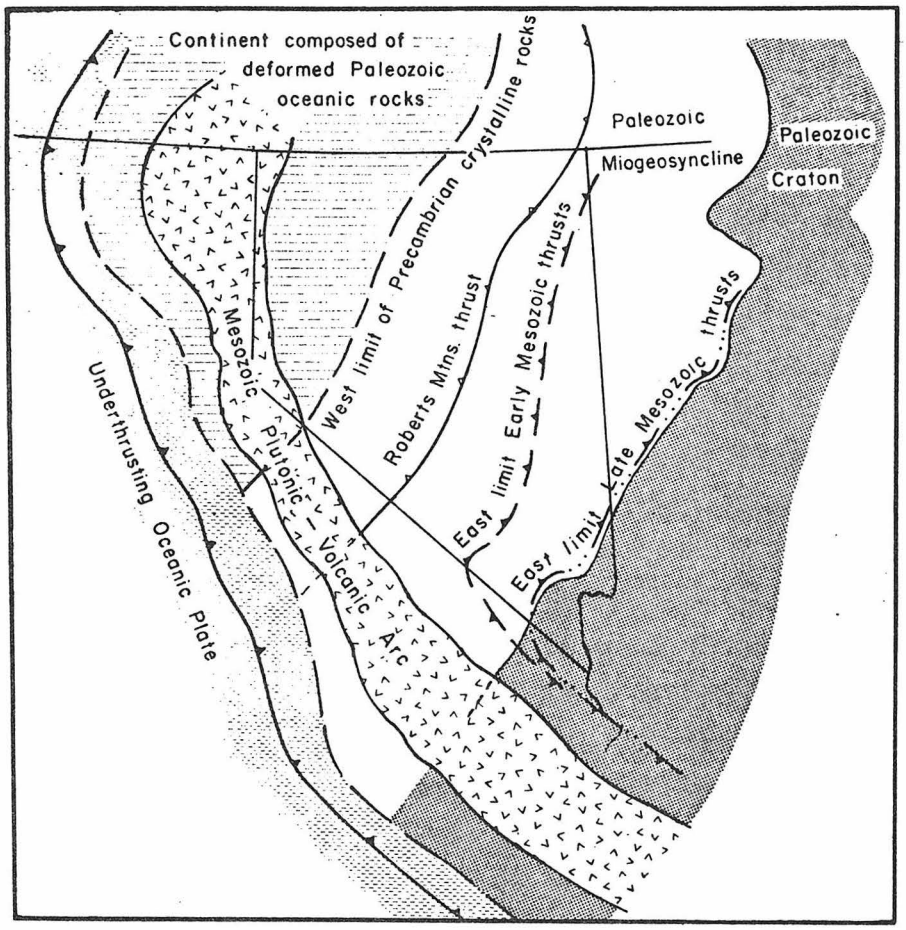

Figure I-83. Generalized map of the late Mesozoic tectonic trends. Figure from Burchfiel and Davis (1972).

surface trace. They have interpreted regional seismic velocity measurements and P-wave delays for vertically incident teleseismic waves as indicating a broad northeast-trending anomaly of high velocity in the upper mantle (Figure I-84). The truncation of the anomaly on the northeast in the Mojave Desert is taken as the subcrustal position of the boundary between the North American Plate and the Pacific Plate. The San Andreas fault zone is the recognized interplate boundary. This interpretation precludes the current existence of the ancient tectonic trends under the transverse seismic zones, because materials of the Pacific Plate are present at depth and extend beyond the surficial San Andreas fault zone. Hadley and Kanamori propose that the velocity anomaly results from subduction of some thermal or compositional anomaly while the interplate boundary was convergent.

Some of the transverse seismic zones proposed here have trends similar to that of the high-velocity anomaly. The northern boundary of Zone A follows the crest of the anomaly quite closely. Zone B is somewhat skewed, and Zone C is both skewed and outside the contoured area. It should be noted that Zone B is very narrow—15-20 km—relative to the 40-50 km depth of the velocity anomaly.

If the transverse seismic zones described here are in fact manifestations of some conditions which tend to modulate the surficial tectonic environment, we might expect future seismicity to occur similarly. Small to moderate shocks should continue to show slightly higher concentrations along the trends of the zones. Large earthquakes on through-going faults would be more likely to have their epicenters

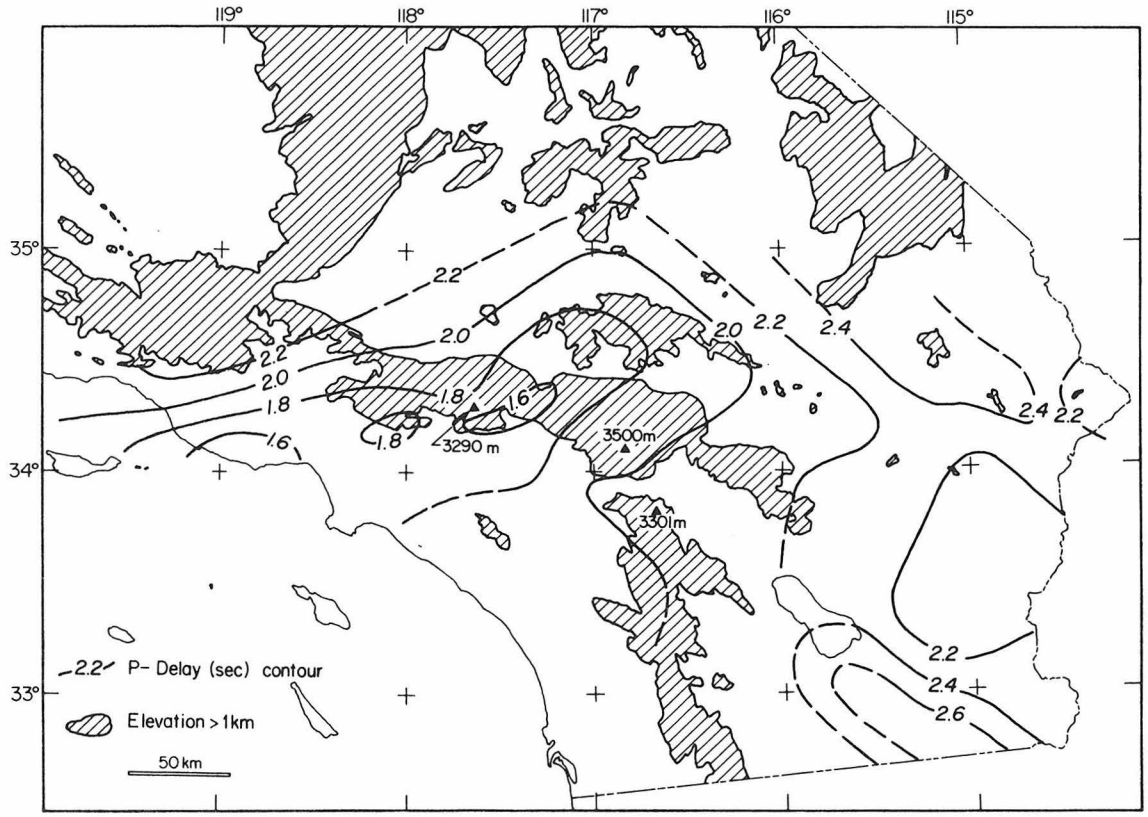

Figure I-84. Contours of observed delays in teleseismic P-waves, southern California. Figure from Hadley and Kanamori (1977).

within the transverse seismic zones. A major rupture affecting the big bend of the San Andreas Fault would be expected to have its epicenter (i.e., point of initial rupture) near Cajon Pass, Palmdale, or Tejon Pass.

PART II.

INVERSION OF PHASE TIMES FOR HYPOCENTERS AND SHALLOW CRUSTAL VELOCITIES

INTRODUCTION TO PART II

A recurring problem in many studies utilizing seismicity data is the accuracy of the earthquake hypocenter locations. As discussed in Chapter 1, the accuracy of a hypocenter determination depends on many factors such as number and spatial distribution of the seismographic stations recording the event, accuracy with which the onset of individual phase arrivals can be identified, and the velocity properties of the paths traversed by the phases. Many of these difficulties have been reduced over the years primarily by improved instrument design, more extensive arrays with closely-spaced seismographic stations, and some detailed velocity studies. The results of these efforts have been to greatly increase the accuracy of epicenters so that errors may be less than a kilometer under favorable conditions. Still, the accurate determination of depths of shallow earthquakes, less than 20 km, depends critically on the accuracy of the velocity model which is used.

This sensitivity to the velocity model comes about because the seismic wave travel times generally are much less affected by small changes in depth than they are by small changes in horizontal coordinates. These depth effects are shown explicitly in several of the figures given later.

The time-depth relationship can be seen heuristically by considering the seismographic array as a planar array and the earthquake source as being slightly out of the plane of the array. For changes in the horizontal location of the source, the array has the source

surrounded, and changes in arrival times easily indicate corrections for the source position. For changes in depth, the travel times are much less affected because the travel-time function is essentially stationary when the depth is much less than the distance. In such a case, the depth is poorly constrained. If the velocity model is simply a halfspace and only P-arrivals are used, the constraints are so weak that there may be no solution with real data (i.e. having uncertainties). The use also of S-arrivals or a layered velocity model, or both, constrains the depth variations so that a solution can be obtained. However, the solution generally can be adjusted to minimize the residuals for any reasonable velocity model, and the depth uncertainty due to velocity inaccuracy remains. Further constraints can be included if an ensemble of sources are used and the velocity model is allowed to vary also. In this way, we hope to improve the locations, particularly the hypocentral depths, by adjusting the velocity model simultaneously with the locations to fit the travel-time data better. Alternatively, the adjusted velocities may be considered the prime desired result rather than the hypocenters.

We can also consider that the arrival-time data can provide more information than just earthquake locations. Conventionally, phase times are used to determine only four parameters for each earthquake — latitude, longitude, depth, origin time. However, for well-recorded local shocks, ten to twenty or more independent arrival times are available. Such data redundancy normally helps the least-squares solution for location, but can also be used toward determining

additional parameters of the problem such as seismic velocities. For velocity determinations, many earthquakes in different locations are necessary so that their raypaths to the seismographic stations adequately sample each of the various velocity layers. The form of the problem then becomes that of the inversion of arrival times from many earthquakes to obtain simultaneously their locations and the velocity structure in a least-squares sense. The formal theory of such inversion is well known, and some problems have been studied for crustal velocity estimates. Peters (1973) and Crosson (1976a, 1976b) derived a crustal model for the Puget Sound region. Aki and Lee (1976) studied velocities near the San Andreas Fault in Central California.

In Southern California, the varied tectonic provinces lead one to expect that the shallow crustal velocity structure might well be different for each province. Perhaps spatial variations are present even within a province. The problem set forth here considers shallow crustal velocities and limited areal extent. When applied to a sequence of aftershocks or some other area of concentrated seismic activity, the technique provides improved hypocenter locations, particularly depths, and thus aids geologic interpretation of the activity.

In practice, the method here consists of first locating each earthquake of an ensemble using an average Southern California velocity model. These initial locations and the average velocity model then become the first trial model for the inversion routine which jointly considers the locations and velocities.

Velocity models appropriate to Southern California were first obtained by fitting travel-time curves to the arrival times of a large number of earthquakes. Systematic differences between observed and calculated times were used to locate shocks more accurately. The improved locations in turn provided better accuracy for the computed travel times and the improvement of both locations and an average velocity model was an iterative process (Gutenberg, 1932, 1943, 1944a, 1944b, 1951a, 1951b, 1951c). The least squares inversion techniques used here are simply formalized procedures for accomplishing this iterative process. In both instances, the underlying idea is that a systematic distribution of residuals implies corrections to the hypocenter locations and to the velocity model.

Chapter 5

FORMULATION OF THE INVERSION PROBLEM

Introduction

A general development of inversion theory has been given in a series of papers by Backus and Gilbert (1967, 1968, 1970). Their formalism has been modified and applied to crustal velocity estimation by Peters (1973), Crosson (1976b), Aki and Lee (1976) and others. The particular form used here is similar to that of Minster et al. (1974) and Minster et al. (1977) and is modified for the determination of shallow crustal velocities and hypocenter locations simultaneously. In the following, the problem is set up initially for the location of a single earthquake. The results are then easily generalized to the full problem of many locations and the velocity parameters.

Single Earthquake Location Problem

The given quantities are: an initial estimate of the hypocenter location $\vec{m}^* = (x^*, y^*, z^*, t^*)$, the locations of the seismographic stations, and the observed arrival times T_i^o, $i = 1, N$. The epicentral distances Δ_i^* and the predicted arrival times T_i^* are then computed using a velocity function appropriate for the area. Later, in the full problem, this velocity function will be considered as a trial velocity function. This portion of the technique is known as the "forward problem" and requires that the functional relationship between epicentral distance, source depth, and travel time be known.

The initial trial location will include some errors which in turn lead to errors in the calculated arrival times. Residual times δT_i are defined such that $\delta T_i = T_i^o - T_i^*$ (observed-minus-computed) and $\delta\vec{T}$ is the vector of all residuals. It is desired to obtain the corrections $\delta\vec{m} = (\delta x, \delta y, \delta z, \delta t)$ to the trial location so that the corrected location, $\vec{m}^* + \delta\vec{m}$, will have the new residuals minimized.

The linearized relationship between the residuals and the desired corrections is $A\delta\vec{m} = \delta\vec{T}$, or

$$\begin{bmatrix} \frac{\partial T_1}{\partial x} & \frac{\partial T_1}{\partial y} & \frac{\partial T_1}{\partial z} & \frac{\partial T_1}{\partial t} \\ & \vdots & & \\ \frac{\partial T_N}{\partial x} & \frac{\partial T_N}{\partial y} & \frac{\partial T_N}{\partial z} & \frac{\partial T_N}{\partial t} \end{bmatrix} \begin{Bmatrix} \delta_x \\ \delta_y \\ \delta_z \\ \delta_t \end{Bmatrix} = \begin{Bmatrix} \delta T_1 \\ \vdots \\ \delta T_N \end{Bmatrix} . \qquad \text{(II-1)}$$

A solution for $\delta\vec{m}$ in the presence of uncertainties in the observed quantities T_i^o and the linearization of the problem that justifies equations (II-1) is obtained following Minster et al. (1974). Let $\delta T_i = T_i^o - T_i(\vec{m})$ be the ultimate residuals obtained from the final best location $\vec{m}$. Assume that the δT_i have independent gaussian distributions with variences σ_i^2. Then from Mathews and Walker (1970, p. 391), the likelihood function is

$$L(x,y,z,t) = L(\vec{m}) = \frac{1}{(2\pi)^{N/2} \prod_{i=1}^{N} \sigma_i} \exp\left[-\sum \frac{\left[T_i^o - T_i(\vec{m})\right]^2}{2\sigma_i^2} \right] . \qquad \text{(II-2)}$$

The likelihood $L(\vec{m})$ will be maximized when the exponential term in (II-2) is minimized. Define

$$F = \sum_{i=1}^{N} \frac{\left[T_i^o - T_i(\vec{m})\right]^2}{2\sigma_i^2} \quad . \tag{II-3}$$

The minimization of F requires

$$\frac{\partial F}{\partial x} = 0, \quad \frac{\partial F}{\partial y} = 0, \quad \frac{\partial F}{\partial z} = 0, \quad \frac{\partial F}{\partial t} = 0 \quad .$$

Thus

$$\frac{\partial F}{\partial m_j} = \sum_{i=1}^{N} \frac{T_i^o - T_i(\vec{m})}{\sigma_i^2} \cdot \frac{\partial T_i(\vec{m})}{\partial m_j} = 0, \; j=1,4$$

or

$$\sum_{i=1}^{N} \frac{T_i^o}{\sigma_i^2} \cdot \frac{\partial T_i(\vec{m})}{\partial m_j} = \sum_{i=1}^{N} \frac{T_i(\vec{m})}{\sigma_i^2} \cdot \frac{\partial T_i(\vec{m})}{\partial m_j}, \quad j=1,4 \; . \tag{II-4}$$

Equations (II-4) relate the observed arrival times T_i^o with the calculated times $T_i(\vec{m})$ for the best solution. Now introduce $\vec{m}^*$ for the current trial model. Assume that the current calculated arrival times $T_i(\vec{m}^*)$ vary smoothly with small changes in the model $\vec{m}^*$ and that the current model $\vec{m}^*$ is close enough to the correct model such that

$$\frac{\partial T_i(\vec{m})}{\partial m_j} \sim \frac{\partial T_i(\vec{m}^*)}{\partial m_j} \quad . \tag{II-5}$$

Subtracting $\sum_{i=1}^{N} \frac{T_i(\vec{m}^*)}{\sigma_i^2} \cdot \frac{\partial T_i(\vec{m}^*)}{\partial m_j}$ from both sides of (II-4) and

using the approximation (II-5) gives

$$\sum_{i=1}^{N} \frac{1}{\sigma_i^2} \left[T_i(\vec{m}) - T_i(\vec{m}^*)\right] \frac{\partial T_i(\vec{m}^*)}{\partial m_j}$$

$$= \sum_{i=1}^{N} \frac{1}{\sigma_i^2} \left[T_i^o - Ti(\vec{m}^*)\right] \frac{\partial T_i(\vec{m}^*)}{\partial m_j}, \quad j=1,4 . \qquad \text{(II-6)}$$

Using Taylor series expansion to first-order terms,

$$T_i(\vec{m}) - T_i(\vec{m}^*) = \sum_{k=1}^{4} (m_k - m_k^*) \frac{\partial T_i(\vec{m}^*)}{\partial m_k} = \delta T_i , \qquad \text{(II-7)}$$

which is substituted into the LHS of (II-6) to give

$$\sum_{i=1}^{N} \sum_{k=1}^{4} \frac{1}{\sigma_i^2} (m_k - m_k^*) \frac{\partial T_i(\vec{m}^*)}{\partial m_k} \cdot \frac{\partial T_i(\vec{m}^*)}{\partial m_j}$$

$$= \sum_{i=1}^{N} \frac{1}{\sigma_i^2} \left[T_i^o - T_i(\vec{m}^*)\right] \frac{\partial T_i(\vec{m}^*)}{\partial m_j}, \quad j=1,4. \qquad \text{(II-8)}$$

The assumptions leading to (II-5) above and discarding the higher-order terms of the Taylor series expansions are the steps which linearize the problem. These steps are similar to the usual linearization of the least-squares location problem (Flinn, 1960).

Now let $\delta\vec{m} = \vec{m} - \vec{m}^*$

$$\delta\vec{T}^* = \vec{T}^o - T(\vec{m})$$

$$A_{ik} = \frac{\partial T_i(\vec{m}^*)}{\partial m_k} \quad \text{and} \quad A^T_{ik} = A_{ki}$$

$$V_{ii} = \sigma_i^2 \quad \text{and} \quad V_{ij} = 0.$$

Direct substitution of these quantities into (II-8) gives

$$\sum_{i=1}^{N} \sum_{k=1}^{4} \frac{1}{V_{ii}} \delta m_k A_{ik} A_{ij} = \sum_{i=1}^{N} \frac{1}{V_{ii}} \delta T_i^* A_{ij}, \quad j=1,4 \qquad \text{(II-9)}$$

or

$$\sum_{i=1}^{N} \sum_{k=1}^{4} A^T_{ji} \frac{1}{V_{ii}} A_{ik} \delta m_k = \sum_{i=1}^{N} A^T_{ji} \frac{1}{V_{ii}} \delta T_i^*, \quad j=1,4\,. \qquad \text{(II-10)}$$

Written out as matrices, these equations become

$$\begin{bmatrix} A_{11} & & A_{N1} \\ A_{12} & \cdots & A_{N2} \\ A_{13} & & A_{N3} \\ A_{14} & & A_{N4} \end{bmatrix} \begin{bmatrix} \frac{1}{V_{11}} & & 0 \\ & \ddots & \\ 0 & & \frac{1}{V_{NN}} \end{bmatrix} \begin{bmatrix} A_{11} & A_{12} & A_{13} & A_{14} \\ & & \vdots & \\ A_{N1} & A_{N2} & A_{N3} & A_{N4} \end{bmatrix} \begin{Bmatrix} \delta m_1 \\ \delta m_2 \\ \delta m_3 \\ \delta m_4 \end{Bmatrix}$$

$$= \begin{bmatrix} A_{11} & & A_{N1} \\ A_{12} & \cdots & A_{N2} \\ A_{13} & & A_{N3} \\ A_{14} & & A_{N4} \end{bmatrix} \begin{bmatrix} \frac{1}{V_{11}} & & 0 \\ & \ddots & \\ 0 & & \frac{1}{V_{NN}} \end{bmatrix} \begin{Bmatrix} \delta T_1^* \\ \\ \\ \delta T_N^* \end{Bmatrix}. \qquad \text{(II-11)}$$

In matrix notation, (II-11) is

$$A^T V^{-1} A \ \delta M = A^T V^{-1} \delta T^*\,. \qquad \text{(II-12)}$$

The vector δM of desired corrections to the trial model then is

$$\delta M = \left[A^T V^{-1} A\right]^{-1} A^T V^{-1} \delta T^* \; . \qquad \text{(II-13)}$$

The usual least-squares solution for the location problem is $\delta M = \left[A^T A\right]^{-1} A^T \delta T^*$. The effect of the maximum likelihood formulation is to include the variances of the observed data into the solution and give a rationally-based, weighted least-squares solution. If all the variances in equation (II-12) are taken to be equal, the equation reduces to the normal equation associated with (II-1).

Simultaneous Hypocenters and Velocity Model Problem

Equation (II-13) is generally applicable to weighted least-squares problems. The RHS vector δT^* represents the set of residuals for a particular problem, the vector δM represents the set of adjustments to be made to the trial model, and the elements of the matrix A are the partial derivatives relating changes in observed quantities to changes in the model. The extension of the problem to several earthquakes and a velocity model consists of just enlarging the matrices appropriately. The vector of residuals has the form

$$T^* = (R_{11}, R_{12}, \cdots R_{1N}, \cdots R_{ij}, \cdots R_{k1}, R_{k2}, \cdots R_{kM})$$

where there are k earthquakes each with its own set of N, M, etc. observed arrival times, and R_{ij} is the jth arrival time of the ith

event. Variances σ_{ij} are associated with each observed arrival R_{ij}. The matrix A is enlarged to contain each of the proper partial derivatives. In the form of equation (II-1), a problem with three earthquakes and two velocity parameters can be written as shown in (II-15).

For the system shown in (II-15), the first earthquake has 5 arrivals, the second has 6, and the third has 5. The thicknesses of two velocity layers are fixed and only the magnitudes of the velocities are allowed to vary. The A matrix is sparse, having many zero terms, because all of the earthquakes are independent. There is no relation between the location of one earthquake and the arrival times of any other earthquake. In computing the solution $\delta\vec{M}$ of this system of equations, the matrix $A^T V^{-1} A^T$ is also sparse and is block diagonal with each block being 4-by-4 except the right-most block which has the same dimension as the unknowns in the velocity model. In the following applications, the problem is much larger. There is provision for up to 20 separate earthquakes with a total of 300 arrival times, and 20 parameters in the velocity model.

Singularity and Near-Singularity Considerations

Solution of the problem as indicated in equation (II-13) requires the inverse of the matrix $A^T V^{-1} A$. For the hypocenter location and velocity determination problem, this matrix per se can be singular and often is near-singular. Then the matrix cannot be successfully inverted by numerical methods without modification. The condition arises when there is a fundamental lack of information in the data

$$
\begin{bmatrix}
\begin{bmatrix} \frac{\partial T_1}{\partial x_1} & \frac{\partial T_1}{\partial y_1} & \frac{\partial T_1}{\partial z_1} & \frac{\partial T_1}{\partial t_1} \\ \vdots & & & \\ \frac{\partial T_5}{\partial x_1} & \frac{\partial T_5}{\partial y_1} & \frac{\partial T_5}{\partial z_1} & \frac{\partial T_5}{\partial t_1} \end{bmatrix} & \mathrm{O} & \mathrm{O} & \begin{bmatrix} \frac{\partial T_1}{\partial V_1} & \frac{\partial T_1}{\partial V_2} \\ \vdots & \\ \frac{\partial T_5}{\partial V_1} & \frac{\partial T_5}{\partial V_2} \end{bmatrix} \\
\mathrm{O} & \begin{bmatrix} \frac{\partial T_6}{\partial x_2} & \frac{\partial T_6}{\partial y_2} & \frac{\partial T_6}{\partial z_2} & \frac{\partial T_6}{\partial t_2} \\ \vdots & & & \\ \frac{\partial T_{11}}{\partial x_2} & \frac{\partial T_{11}}{\partial y_2} & \frac{\partial T_{11}}{\partial z_2} & \frac{\partial T_{11}}{\partial t_2} \end{bmatrix} & \mathrm{O} & \begin{bmatrix} \frac{\partial T_6}{\partial V_1} & \frac{\partial T_6}{\partial V_2} \\ \vdots & \\ \frac{\partial T_{11}}{\partial V_1} & \frac{\partial T_{11}}{\partial V_2} \end{bmatrix} \\
\mathrm{O} & \mathrm{O} & \begin{bmatrix} \frac{\partial T_{12}}{\partial x_3} & \frac{\partial T_{12}}{\partial y_3} & \frac{\partial T_{12}}{\partial z_3} & \frac{\partial T_{12}}{\partial t_3} \\ \vdots & & & \\ \frac{\partial T_{16}}{\partial x_3} & \frac{\partial T_{16}}{\partial y_3} & \frac{\partial T_{16}}{\partial z_3} & \frac{\partial T_{16}}{\partial t_3} \end{bmatrix} & \begin{bmatrix} \frac{\partial T_{12}}{\partial V_1} & \frac{\partial T_{12}}{\partial V_2} \\ \vdots & \\ \frac{\partial T_{16}}{\partial V_1} & \frac{\partial T_{16}}{\partial V_2} \end{bmatrix}
\end{bmatrix}
\begin{Bmatrix} \delta x_1 \\ \delta y_1 \\ \delta z_1 \\ \delta t_1 \\ \delta x_2 \\ \delta y_2 \\ \delta z_2 \\ \delta t_2 \\ \delta x_3 \\ \delta y_3 \\ \delta z_3 \\ \delta t_3 \\ \delta V_1 \\ \delta V_2 \end{Bmatrix}
=
\begin{Bmatrix} \delta T_1 \\ \cdot \\ \cdot \\ \cdot \\ \cdot \\ \cdot \\ \cdot \\ \cdot \\ \cdot \\ \cdot \\ \cdot \\ \cdot \\ \cdot \\ \delta T_{16} \end{Bmatrix}
$$

Equations (II-15)

concerning some of the model parameters.

The matrix will be singular, have a zero eigenvalue, if a model parameter is included which has no effect on the calculated travel times. For example, a layered velocity model might be used for which none of the computed rays traverse the deepest layer. Alternatively, the geometry of the sources and receivers could be such that two velocity layers are always sampled identically by all raypaths resulting in no independent information about one or the other of the layers. This would occur if the sources were all below the two layers and far enough distant that all arrivals were refractions from the same horizon. The occurence of any real singularities is avoided by attention to the distribution of the sources and to the raypaths as indicated by locating the events individually.

Near-singularity of the matrix can easily occur and must be provided for. If a small change in some model parameter has negligible effect on the calculated times, the matrix will be near-singular. As the depth of an earthquake becomes very shallow, the partial derivatives of the travel times with respect to depth will approach zero for that earthquake, and the matrix becomes near-singular. In principle, an inverse matrix exists, but numerical difficulties in matrix inversion algorithms prevent an accurate calculation of the inverse. These errors can cause large fluctuations in the solution vector $\delta\vec{m}$. Because the location-velocity problem is highly nonlinear, the problem and the partial derivatives can change with each iteration. The solution can move around considerably in solution space, and the problem

may become near-singular as iterations proceed. If the solution were changed too drastically, it might violate the condition that the current solution remain linearly close to the final solution. Then the calculated derivatives would not be appropriate.

There are several well-known techniques for stabilizing matrix inversion in the presence of near-singularities. The simplest is to add a constant to each diagonal term of the matrix to be inverted; this scheme in a more general form was given by Levenberg (1944). Wiggins (1972) chose to compute all of the eigenvectors and eliminate those having eigenvalues below some arbitrary threshold. The method used here is that of Minster et al. (1977) and is best thought of as controlling the distance in model space that the solution is allowed to move at each iteration. The exponential term of the likelihood function of equation (II-3) is modified to

$$F = \cos\theta \sum_{i=1}^{N} \frac{\left[T_i^o - T_i(\vec{m})\right]^2}{2\sigma_i^2} + \sin\theta \sum_{j=1}^{M} \frac{\left[m_j - m_j^o\right]^2}{2\omega_j^2} . \qquad \text{(II-16)}$$

The m_j are the elements of the current model, m_j^o are the elements of a preferred model, and ω_i^2 are the allowable variances of the model parameters. The summation in the first term is identical to that of equation (II-3) and represents a measure of the "distance" in data space between the observed data and the calculated data functionals. The summation in the second term represents a measure of the "distance" in model space between the current model $\vec{m}$ and a preferred model $\vec{m}^o$. By always choosing the preferred model $\vec{m}^o$ to be identical with the

current model, the problem is constrained to solutions not greatly different than the current model. The parameter θ allows a tradeoff in the degree to which the solution minimizes the residuals (first term) or the change in the model (second term). Varying θ from 0 to $\pi/2$ provides a full range of tradeoff between these two extremes. If $\theta \sim \pi/2$, only very small perturbations of the model are allowed and the iterative solution is strongly damped. If $\theta \sim 0$, there is practically no damping of the model changes and near-singularities can cause large fluctuations in the inverse.

The minimization of (II-16) is given by Minster et al. (1977) and follows the same steps as given above for (II-3). The result is

$$\delta\vec{M} = \left[\cos\theta\ A^T V^{-1} A + \sin\theta\ W^{-1}\right]^{-1} \left[\cos\theta\ A^T V^{-1}\ \delta\vec{T}^* + \sin\theta\ W^{-1}\delta\vec{m}^o\right] \tag{II-17}$$

where W is the matrix of model variances ω_i^2, just as V is the matrix of data variances σ_i^2. If the preferred model $\vec{m}^o$ is always taken to be the current trial model $\vec{m}$, then $\delta\vec{m}^o \equiv 0$ leaving

$$\delta\vec{M} = \left[\cos\theta\ A^T V^{-1} A + \sin\theta\ W^{-1}\right]^{-1}\ \cos\theta\ A^T V^{-1}\ \delta T^* \ . \tag{II-18}$$

This form reduces to addition of a constant along the diagonal of $A^T V^{-1} A$ if the model variances are taken as all equal to a constant. Minster et al. (1977) discuss criteria for choosing the value of θ. In the application here, a value of $\theta = \pi/36$ was choosen on the basis of the rates of convergence of several trial problems.

Constraints on the Station Corrections

Station corrections, times added to the observed arrival times at each station to accommodate local velocity irregularities, are an integral part of the velocity model. Only relative corrections are significant because a constant added to each of the station corrections can be offset by adding the same constant to the earthquake origin times. The problem is constrained to computing relative station corrections by holding one of the station corrections fixed. In the program, this is done by not including the station correction for the reference station in the velocity model parameters to be determined. A similar effect would result by making the appropriate model variance a very small number.

Experience in applying the inversion program showed the need for another type of constraint on the station corrections. These results will be discussed further in Chapter 5, but in essence it was found that there was a systematic geographic dependence in the station delays. The algorithm was able to tradeoff between a systematic change in station corrections and a systematic shift in epicenters. Corrections to the station delays can be thought of as defining a plane by means of a least-squares fit (see Figure II-6). The plane itself represents a function for the systematic portion of the delay corrections. Deviations from the plane are the desired corrections. The systematic effects of the station delays can be removed by constraining the delays so that they fit a horizontal plane in the least-squares sense.

A plane fitted to the station delay corrections has the form

$$ax + by + cz + d = \delta \qquad \text{(II-19)}$$

where x, y, z are the coordinates of a station relative to the reference station, δ is the station correction, and a, b, c, d are the constants of the plane. The constant d is identically zero because the reference station delay is fixed. Using all the stations gives the system of equations

$$[X]\vec{C} = \vec{D} \qquad \text{(II-20)}$$

where X is the matrix of station coordinates (x, y, z), $\vec{C}$ is the vector of plane constants (a, b, c), and $\vec{D}$ is the vector of station delay corrections (δ_i). The least-squares fit of a plane to the data gives

$$\vec{C} = [X^T X]^{-1} X^T \vec{D} \ . \qquad \text{(II-21)}$$

Setting a and b of $\vec{C}$ equal to zero in (II-21) provides two equations which are to be satisfied if the plane is to be horizontal. The least-squares fit fulfills the zero-mean requirement. Setting C to zero would tend to force the corrections onto the plane; all that is desired is that the mean be zero. In the program, coefficients from the first two rows of $X^T X$ are inserted as two additional rows in the A matrix of equation (II-18), and the $\delta\vec{T}^*$ vector is lengthened by adding two null elements. The matrix V of data variances is also enlarged by two terms whose magnitude control how strongly the program will

attempt to fulfill these constraints. The values used were found by trial choosing the largest variance for which the geographic dependence in station delay corrections was eliminated.

Chapter 6

INVERSION OF DATA FROM THE GALWAY LAKE EARTHQUAKES

Introduction

In principle, the inversion technique described in the previous chapter is applicable to any particular area. However, the travel-time calculations, subroutine TTIM, for the forward problem were written for flat layers over a halfspace. Areas known to have complex geology may not be described adequately by flat layers and are not suitable for application of this routine without modification of the travel-time calculations. Much of the Transverse Ranges Province was excluded from consideration on this basis because of the range-front thrust faults. The Imperial Valley has areas of relatively flat structure between some of the large right-lateral faults, but refraction data (Biehler et al., 1964) and hypocenter location experience (Johnson and Hadley, 1976) suggest lateral velocity changes. The data chosen for inversion come from the central portion of the Mojave block where the basement rocks are mostly granitic and the alluvial basins are not extensive.

A subset of earthquakes from the 1975 Galway Lake sequence was selected for inversion. A velocity model used by the U.S. Geological Survey was selected as the initial trial model for the first program runs. Rather erratic relocation results were obtained until a geographical dependence in the station delays was discovered and constrained. Then, the relocation results were uniform and the program modified the velocity model to have lower velocities. A velocity model of Hadley and Kanamori (1977)

for the Mojave region was also used as an initial trial model and again lower velocities were calculated. Finally, an arbitrary trial model with 1-km layers was used. The results of all these models show that the data do not strongly constrain the shallow velocities because of the shallow and limited range of hypocenter depths.

Data Selection

A series of earthquakes in the Mojave block occurred in 1975 with a mainshock of magnitude 5.2 near Galway Lake, 34^{o} 31.12' N, 116^{o} 29.56' W, at 0138 hours on June 1 (Fuis, 1976). The existing U.S. Geological Survey Mojave seismographic network was augmented by portable stations operated near the epicentral area of the aftershocks from June 5 through June 15. During that time interval, 94 aftershocks were recorded. The mainshock produced surface cracks for a distance of 6.8 km along a fault subsequently named the Galway Lake fault. Surface effects along this fault are described by Beeby and Hill (1975).

This series of shocks has been studied in detail by Fuis (1976) who graciously provided phase-arrival times and location results prior to publication. Fuis, using the U.S. Geological Survey location program HYPO71, located all of the shocks of the sequence and constructed many focal-plane solutions. He concluded that the fault was near vertical with predominantly right-lateral movement. Figure II-1 shows the distribution of epicenters for the period June 5 though June 15 when the portable stations were in operation. A few foreshocks and the initial aftershocks were in the immediate area of the mainshock. The aftershock

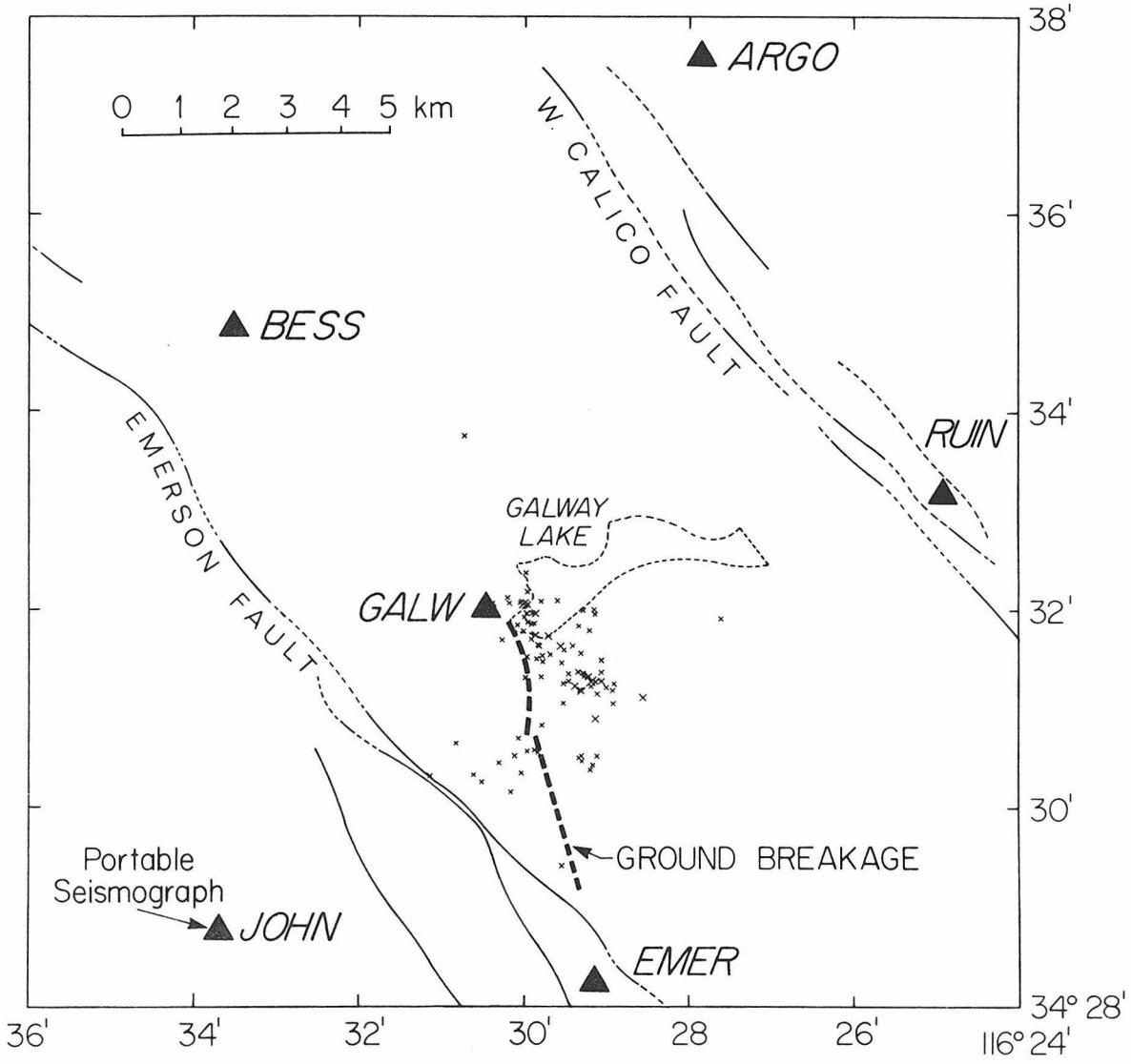

Figure II-1. Aftershocks of the Galway Lake earthquake from June 5 to June 15, 1975 while portable seismographs were operated. Triangles are the station locations.

area expanded bilaterally along the general fault trend and within 24 hours occupied the same area as the shocks shown in Figure II-1. The trend of the epicenters is in general agreement with that of the mapped surface ruptures. There is an unexplained displacement of the epicenters somewhat to the east of the fault trace, particularly for the southern half of the fault. Projection of the southern hypocenters onto a cross-section suggests a fault plane slightly displaced from the surface trace. The fault-plane solutions give planes which dip steeply westward rather than eastward as would be the case if the epicenters and surface rupture were consistent. These considerations suggest that the velocity structure for this area should be carefully studied.

In the vicinity of the Galway Lake fault, there are many scattered granitic outcrops. The desert playas are not large and presumably do not represent deep basins. There are large through-going faults: the Calico fault to the northeast of Galway Lake and the Camp Rock fault to the southwest. These faults are right-lateral strike-slip with total movement on the order of 10 miles horizontally and only a little vertically (Garfunkle, 1972). It is presumed here, but not known for certain, that basement terrains across these faults are similar and that no strong velocity variations occur laterally. With these conditions and inferences in mind, the Galway Lake area seems appropriate for a flat-layered velocity model. Shocks from the Galway Lake sequence were therefore used for application of the velocity inversion program as set forth herein.

Of 207 shocks in the Galway Lake sequence for which data are available, only the 95 which were recorded during the operation of the temporary stations were considered. For earthquakes recorded only by the permanent stations of the Mojave net, the closest station is about 20 km distant giving no practical control on the depths of the hypocenters. This point is emphasized by comparing the distribution of calculated depths during the time period of the portables with the distribution for the remainder of the time, Table II-1. In the absence of the portables and with only refraction arrivals available, 64% of the depths were placed in the limited range of 1.9 - 2.1 km. When selecting events for the inversion data set, as many of the deeper events as possible were chosen. This selection provides the maximum number of direct arrivals for depth control and the greatest variety of raypaths sampling the velocity layers of the model. Some events were discarded because of too few phase arrivals or obvious location difficulties as indicated by the residuals in their epicenter solutions.

Another consideration in selecting events was their geographic distribution. The widest possible distribution was sought to again provide the greatest variety in the raypaths. In particular, the selection of two earthquakes with very nearly the same location and depth should be avoided. Very few additional independent data are gained and the problem matrix tends to have an unstable matrix unless steps are taken to stabilize it. Because it is possible for two locations to migrate close to each other during iterations,

Table II-1

Percentage of Depths in Various Ranges

	0-1 km	1-2 km	2-3 km	3-4 km	≥4 km
Portables not operating	14	44	31	2	9
Portables operating	45	40	9	2	4

stabilization of the matrix is an essential part of the inversion algorithm.

Twenty events were sought because the program had been sized to accommodate about that number. But with the above criteria, only about 20 reasonably independent earthquakes could be chosen. The data set could be altered slightly by substituting some shallow events, but the distribution would not be changed appreciably. All of the events selected were relocated using only those stations that would be used for the inversion problem. All of the temporary stations were used. In addition, three of the permanent stations at distances up to about 55 km were included to close up angular gaps in coverage for some of the events. The events selected are given in Table II-2.

Inversion Starting With the HYPO71 Velocity Model

The hypocenters of Table II-2 constitute the locations portion of the initial trial model. The remainder of the model is made up of station delays and the velocity structure as determined by Fuis (personal communication, 1977). The initial station delays were estimated by Fuis using a feature of the HYPO71 program which averages the residuals for each station when a large number of locations are run. He based the initial velocity structure on refraction data from the Eagle Mountain quarry. The structure was then modified to include a thin low-velocity layer at the surface and a transition layer just above the halfspace. The HYPO71 velocity model is included in Table A2-1 of Appendix 2. S-wave velocities are not estimated independently,

Table II-2

Earthquakes Used for the Inversion Data Set

	Date	Time		Lat, N		Long, W		Dep, Km	Mag
	YYMMDD	HHMM	SEC	DEG	MIN	DEG	MIN		
1	750606	0137	43.25	34°	31.30	116°	29.10'	4.81	1.7
2	750606	0244	45.74	34	30.89	116	28.90	0.55	1.5
3	750606	1219	57.53	34	31.08	116	29.20	1.87	1.9
4	750607	0239	53.61	34	31.09	116	29.80	0.90	1.7
5	750607	0508	17.41	34	30.51	116	29.90	0.64	1.7
6	750607	0529	57.75	34	30.36	116	29.20	0.28	1.4
7	750607	1602	35.70	34	30.44	116	29.50	0.99	1.8
8	750608	1547	04.42	34	31.82	116	30.20	4.42	1.5
9	750608	1646	12.50	34	32.48	116	30.10	5.95	2.0
10	750608	1652	08.89	34	31.81	116	29.40	0.73	1.2
11	750608	1848	56.19	34	30.39	116	30.00	3.57	1.2
12	750608	2357	57.22	34	30.85	116	28.80	0.59	2.3
13	750611	0043	23.83	34	32.07	116	30.00	1.75	2.0
14	750612	0023	01.47	34	32.06	116	30.18	1.99	2.0
15	750612	0918	53.43	34	31.87	116	27.60	8.88	0.6
16	750613	0009	44.77	34	31.32	116	29.10	2.19	2.5
17	750613	0503	05.07	33	31.03	116	28.90	7.13	1.7
18	750613	0704	21.65	34	31.17	116	29.40	1.86	1.6
19	750614	1718	46.93	34	31.68	116	29.40	2.46	1.0
20	750614	2328	24.73	34	31.72	116	29.80	1.91	1.6

but taken as $V_s = V_p/\sqrt{3}$ (poisson's ratio of .25). Deeper velocities are not sampled by the source-station distribution of this data set.

The model variances ω_j^2 of equation (II-16) are used to control how freely the model parameters may be changed in attempting to fit the observed data. A small variance for a particular variable causes only small changes in that variable to be permitted. The relative values of each of the model variances specify the relative changes allowed at each iteration. If excessive changes in the model were permitted, the model conceivably might change erratically from one local RMS minimum to another or even become catastrophically unstable. If any particular model parameters are changing erratically during the iterations, this effect can be controlled with the variance for that parameter. If the entire model were changing erratically, then the tradeoff parameter θ could be used to reduce all of the changes. In either case, the change for each iteration is constrained, but the total change over many iterations might be large for some problems. For this problem, most of the model variances were selected to be compatible with the assumed precision of location results. Latitudes and longitudes are assumed to be correct within 0.5 km, depths within 1.0 km, and origin times within 0.2 sec. Station delays are common to all of the earthquakes and therefore should be determined more closely than origin times. A 0.05 sec variance for the station delays is approximately a $\sqrt{N}$ improvement over the origin times for 20 events. A variance of 0.01 km/sec was taken for the velocities because only small changes to "tune up" the velocities were anticipated.

The results of two early runs of the inversion problem are shown in Figure II-2. In the figure, the initial and final values for the layer velocities and station delays are tabulated at the left. On the right are the relocation vectors for each of the earthquakes. For the problem of Figure II-2(a), all of the phase data were utilized. The problem of Figure II-2(b) used only the P-wave data. There is a great difference in the relocation vectors for these two problems. In each case however, the vectors are essentially parallel and the relative locations have not been changed greatly. Other problems which are not shown, such as using S-waves only or using different initial velocities, also gave much the same results but with different vector trends. The westward component was consistent, but the latitude changes were erratic.

This parallelism of the vectors is similar to what might be expected if a set of shocks which were well-located with respect to each other were relocated using a "master" event. Different "master" events would lead to various vector trends. When using a "master" event the station residuals for the chosen "master" event are applied to the arrival times for all the remaining events before they are relocated. This analogy suggested that the station delays should be examined closely.

Changes in station delays as determined by the inversion program are plotted according to the geographic distribution of the stations in Figures II-3(a) and (b). These figures correspond to the two problems shown in Figures II-2(a) and (b). The shaded area indicates

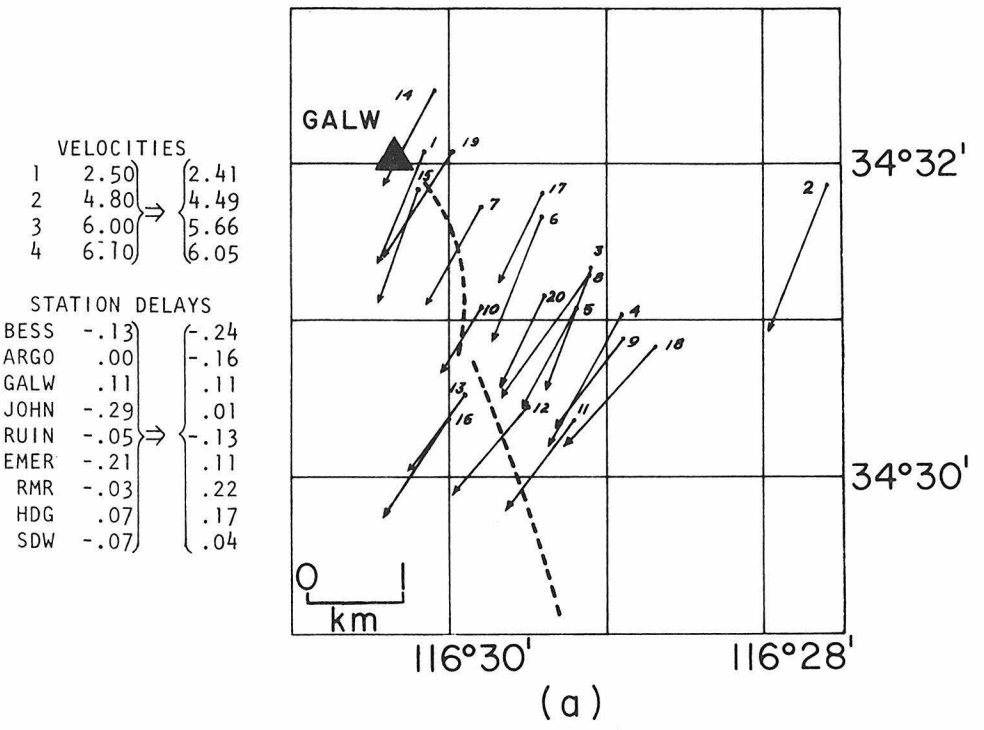

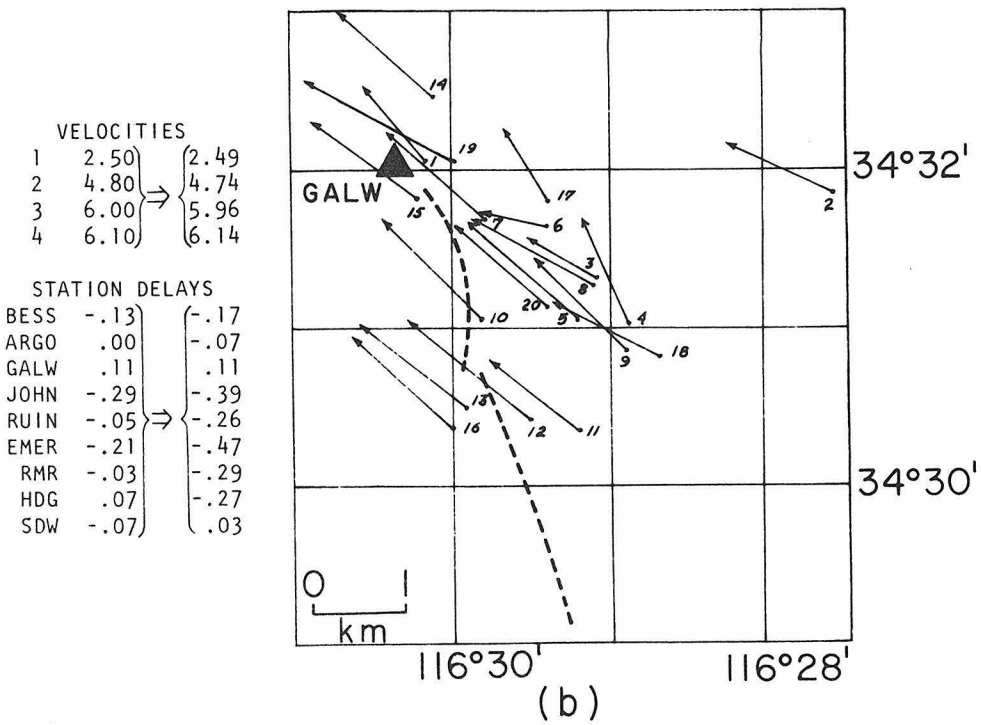

Figure II-2. Inversion results with HYP071 model before incorporating constraints on station delays. Vectors show changes in the epicenters. The differences between (a) which uses all the phase data and (b) which uses only P-waves are attributed to systematic bias introduced into the station delays.

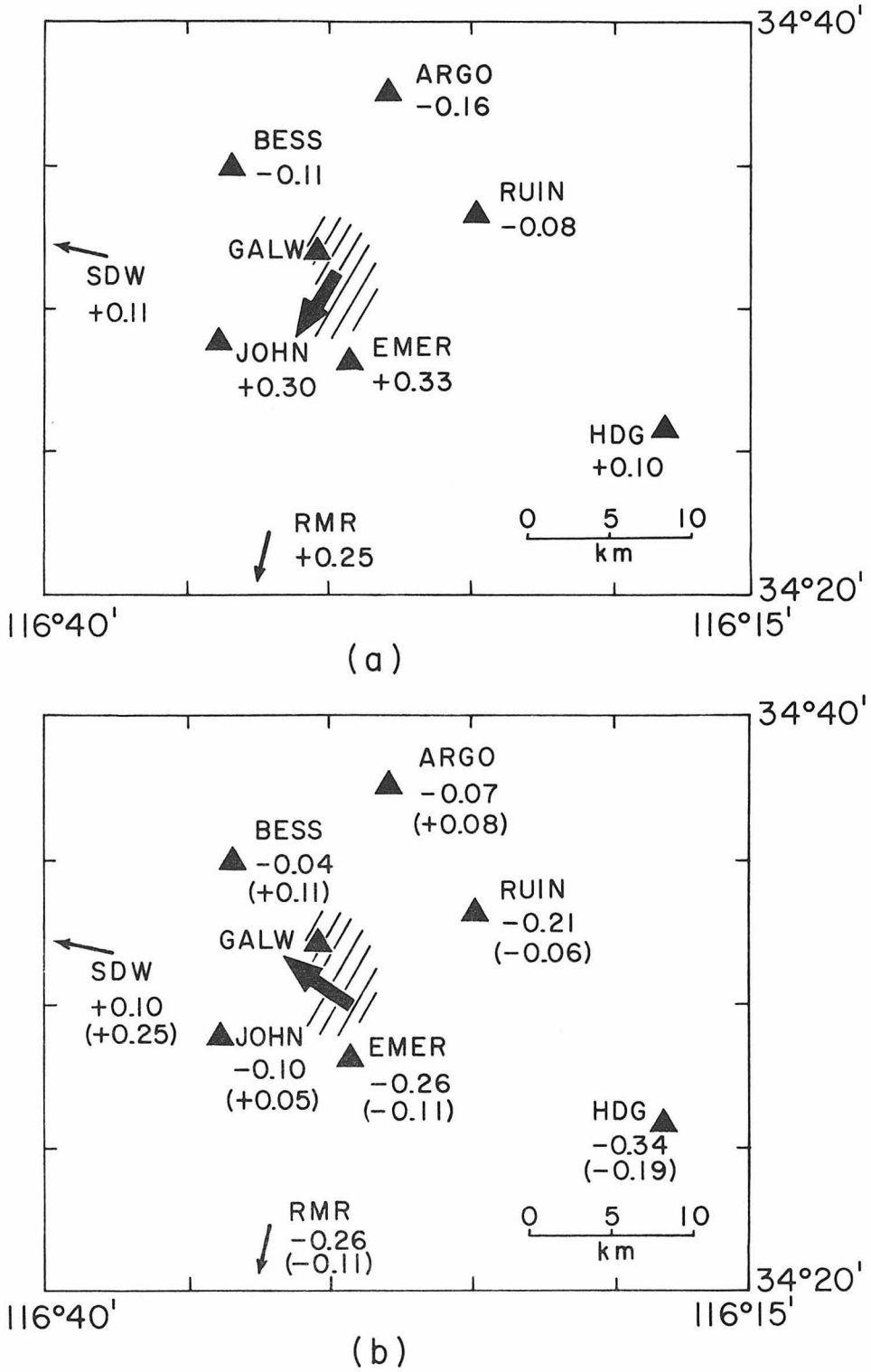

Figure II-3. Seismographic stations and the changes in station delays estimated by inversion for the problems shown in Figure II-2. Large arrows show the trends of the relocation vectors; the aftershock area is shaded. The changes are systematically larger in the directions of the relocation trends.

the extent of the aftershock area. In Figure II-3(a), the changes in delays are negative to the northeast of the earthquakes and positive to the southwest. The delay for GALW was fixed at its original value. The arrow in the shaded area shows the general trend of the relocation vectors. Figure II-3(b) is drawn similarly for the other illustrative problem, but includes also a second set of values in parentheses. The parenthetical values are the delay changes biased by +0.15 to show the geographical dependence more clearly. This geographical dependence must be an artifact introduced by the program since the effect is erratic and depends strongly on how the problem is set up.

The changes in station delays are more positive at stations which are in the general direction of the relocation vectors. Station delays are added to the phase times. Thus, these positive delays are in the correct sense to compensate the calculated travel times for epicenters which have been moved closer to the stations. The converse is true for stations in the opposite direction and having negative changes. Evidently there has been a freedom in the problem to trade-off between station residuals, in the geographic relation shown, and the average location of the earthquakes. The geographic dependence should not be exact in this data since valid station delay corrections are expected.

These changes in station delays can be thought of as defining a plane, by least-squares fit, which dips opposite to the induced trend of the relocation vectors. If this plane were constrained to be horizontal, then no bias would be introduced into the relocations by

changes in the station delays. The conditions to provide this constraint are contained in equations (II-21) as developed in the previous chapter. Each of the two constraint equations has a "datum" variance σ_i^2 associated with it which determines the significance of these equations in the total set of equations of matrix A. Several trial runs showed that a variance of 0.0001 was adequate to cause the removal of geographic bias in the station delays.

Running the inversion problem again and incorporating the constraint on station delay changes gave the results shown in Figure II-4 (a); complete results are listed in Table A2-2 of Appendix 2. The westward component of the relocation trend which had been common to the earlier runs is retained and very little change in latitudes is estimated. Station delays were adjusted somewhat by the routine, the greatest change being 0.16 sec. Changes in the station delays are shown in Figure II-4(b) demonstrating that the earlier geographic effect has been removed. All of the velocities were lowered, most by significant amounts of 0.25 - 0.38 km/sec. Many of the hypocenter depths were increased slightly, less than a kilometer, and origin times were made earlier by 0.1 - 0.2 sec. Depths on two events, numbers 9 and 12, were changed from 0.6 to 4.3 km and 1.0 to 3.5 km respectively. The RMS level of the residual times improved from 0.188 to 0.147 sec.

To test the stability of the solution, all of the initial trial epicenters were shifted 0.5 minutes to the north ($\sim$0.9 km) and 0.5 minutes to the west ($\sim$0.7 km). The results obtained using these

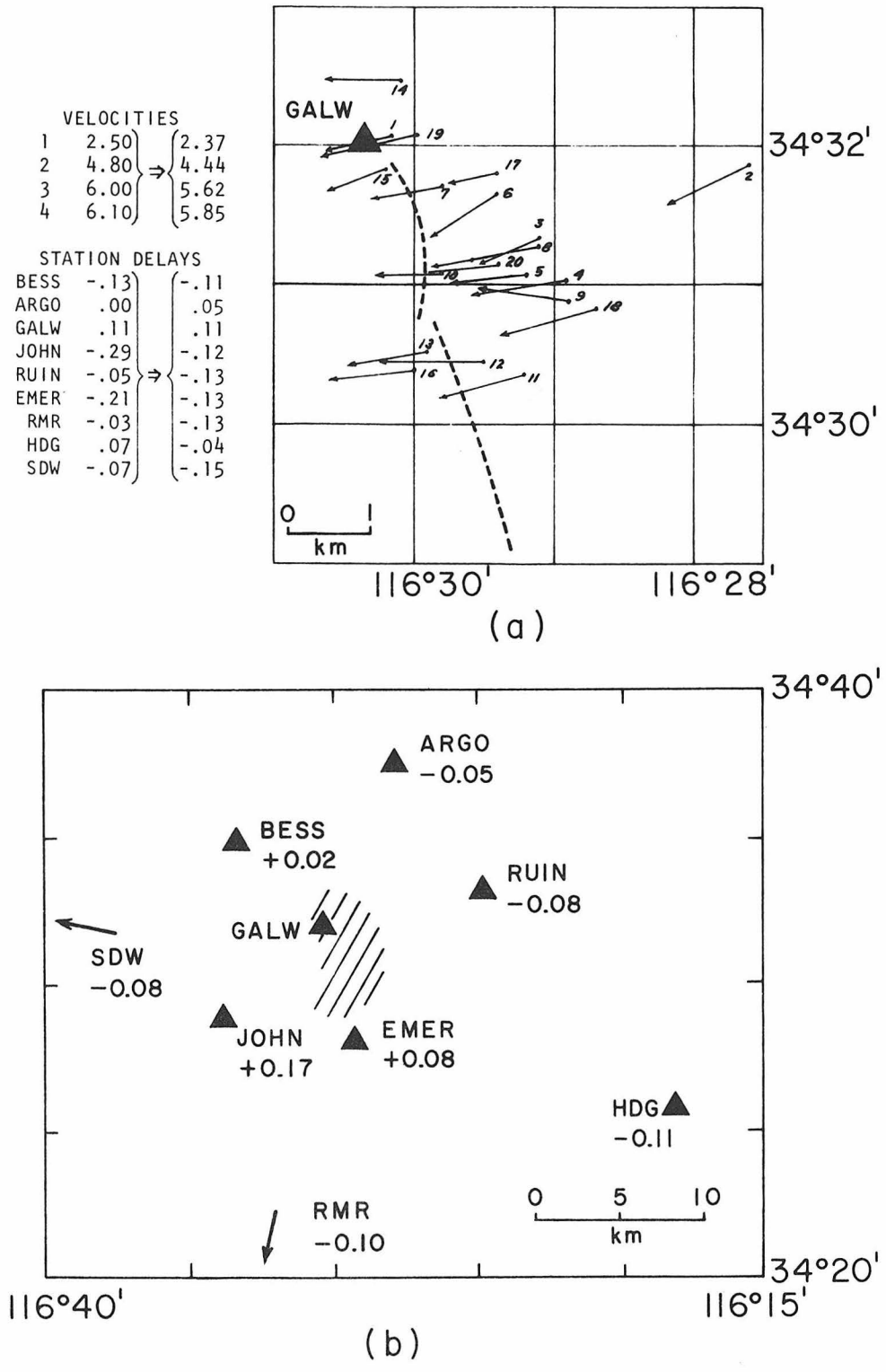

Figure II-4. (a) Inversion results with HYP071 model, and (b) changes in station delays when the systematic bias in delays is constrained.

shifted locations are shown in Figure II-5(a) and tabulated in Table A2-3 of Appendix 2. Figure II-5(b) shows the relocation differences between the results with and without the shifted initial locations. Velocities and station delays for the two problems are very nearly the same, no more than 0.02 km/sec difference in velocities or 0.04 sec in the delays.

The above results are somewhat misleading. Although the solutions for the epicenters and station delays are well-behaved and the RMS level of the residuals is convergent, the velocities are changing slowly and monotonically. The velocities are reduced by about 0.02 km/sec at each iteration. Velocity results of the two problems above are similar because both problems ran for 10 iterations. This behavior is caused partly by the small variances given to the velocity terms of the model. Small variances were chosen because the velocity model was considered to be reasonably good initially. Looking at the stepwise changes in hypocenter depths and the origin times shows that on the average the depths were pushed down slightly and the times made slightly earlier at each iteration. When epicenters are well surrounded by the recording stations, the first order effect of velocity changes is in the computed hypocenter depths. Evidently with this velocity model, the data set permits some trade-off between depths, times, and velocities. To test for ultimate convergence of this trade-off, a model with extremely low velocities was tried. From the surface downward, the layer velocities were 2.0, 3.6, 5.4, and 5.5 km/sec. For this new problem, the velocity increments were

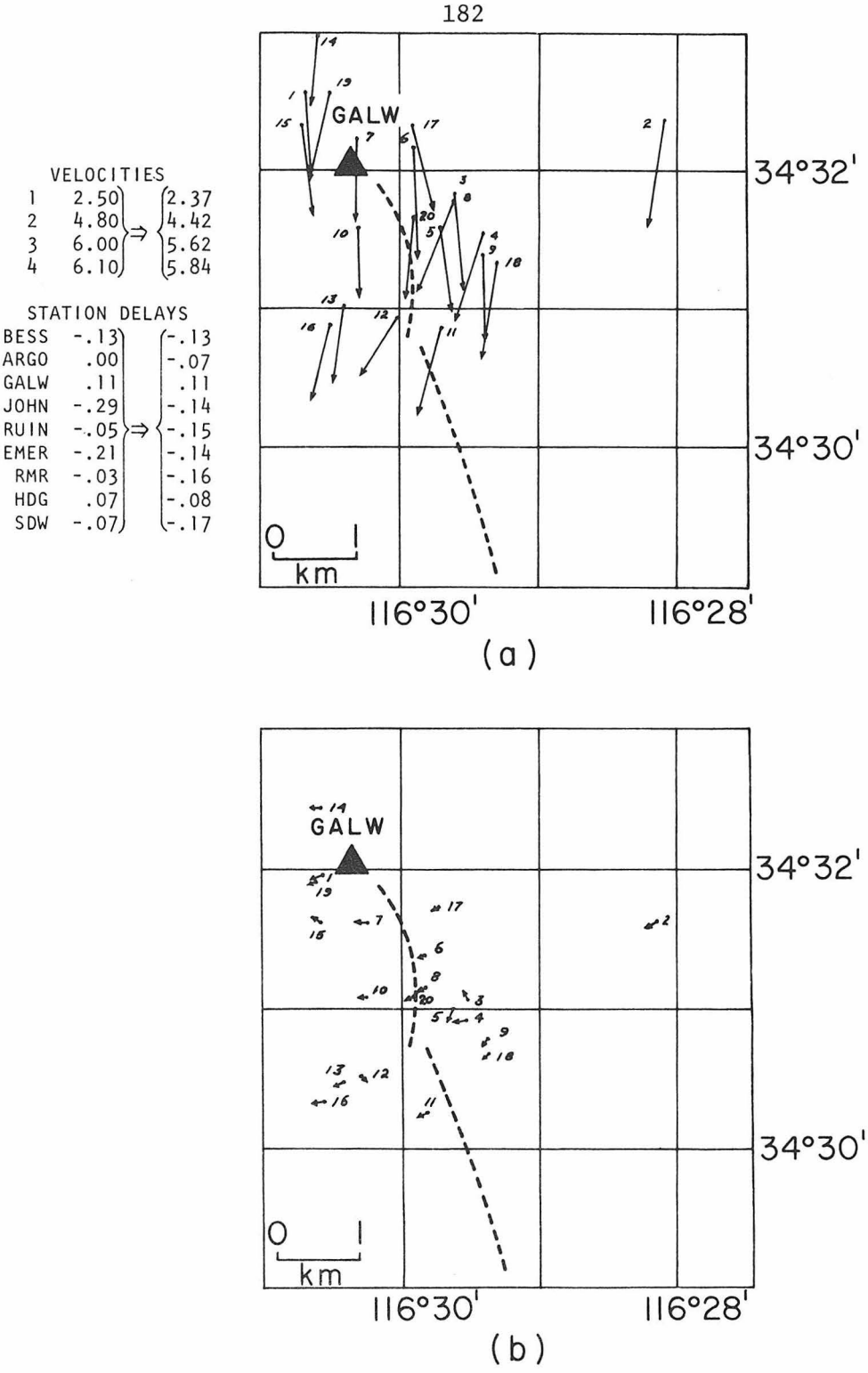

Figure II-5. (a) Inversion results with the HYP071 model when the initial epicenters were shifted to the northwest. (b) Differences in the final epicenters using the shifted and unshifted initial epicenters. Vectors point to the unshifted results.

initially negative, but were decreasing in magnitude and began changing signs after about 15 iterations showing no further significant changes. The final velocities were 1.96, 3.54, 5.57, and 5.84 km/sec, and the RMS level of residuals was 0.139 sec. These values are uniformly lower than the previous results: 2.37, 4.44, 5.62, and 5.85 km/sec. Locations were essentially the same as those shown in Figure II-4.

The model just described is the best model fitting the data in a least-squares sense (HYPO-71 layer structure). However, the velocities are suspiciously low relative to the refraction data of Fuis (personal comm., 1977) for the Eagle Mountain quarry and the velocity model given by Hadley and Kanamori (1977) for the Mojave region. Also, the behavior of the RMS level of the residuals from iteration to iteration shows that the data do not constrain the velocities particularly well for this layer structure. The RMS level of the residuals can be thought of as defining a multi-dimensional surface for which the model parameters are the coordinates of positions on the surface. The purpose of the inversion and iteration scheme is to locate the minimum point on the surface. The surface may have relative minima, and there is no way of knowing if a particular minimum is relative or absolute other than mapping the surface. Consider the RMS surface for the Galway Lake data and the HYPO71 model. A "section" through the surface taken so that velocities are constant would show a well-defined minimum relative to changes in epicenters and station delays. Relative minima are shallow and near the absolute minimum. This description is indicated because locations and delay parameters are usually near

their final values within a few iterations. Also, the final parameter values and RMS levels are similar for various problems. Conversely, a "section" showing the velocity dependence of the RMS surface would have a very broad minimum. Velocity values were slow to converge and RMS improvements were small.

A different and more physical insight into some features of the inversion problem comes from considering the travel-time surface defined by the velocity model. For points on the surfaces shown herein, the z coordinate is the source-receiver distance, x is the source depth, and y is the travel time for a first arrival. Sections parallel to the y-z plane are the usual travel-time curves. Sections parallel to the x-y plane show travel time as a function of depth for a fixed distance. Sections parallel to the x-z plane show wavefronts for a surface focus. The surface is conveniently displayed by contours of equal source distance plotted on the time-depth plane.

Figure II-6 shows travel-time surfaces for P and S waves for the HYPO71 velocity model. Each travel-time surface has a number of regions which are separated by dotted lines on the figures. Within each region, all of the first arrivals are of a single type: 1 indicates direct arrivals, 2 indicates refraction arrivals from the top of the second layer, etc. Regions representing refraction arrivals are planes and the boundaries between refraction regions must be straight lines. Regions representing direct arrivals are curved surfaces with the curvature greatest at zero distance and asymptotically approaching no curvature at great distance.

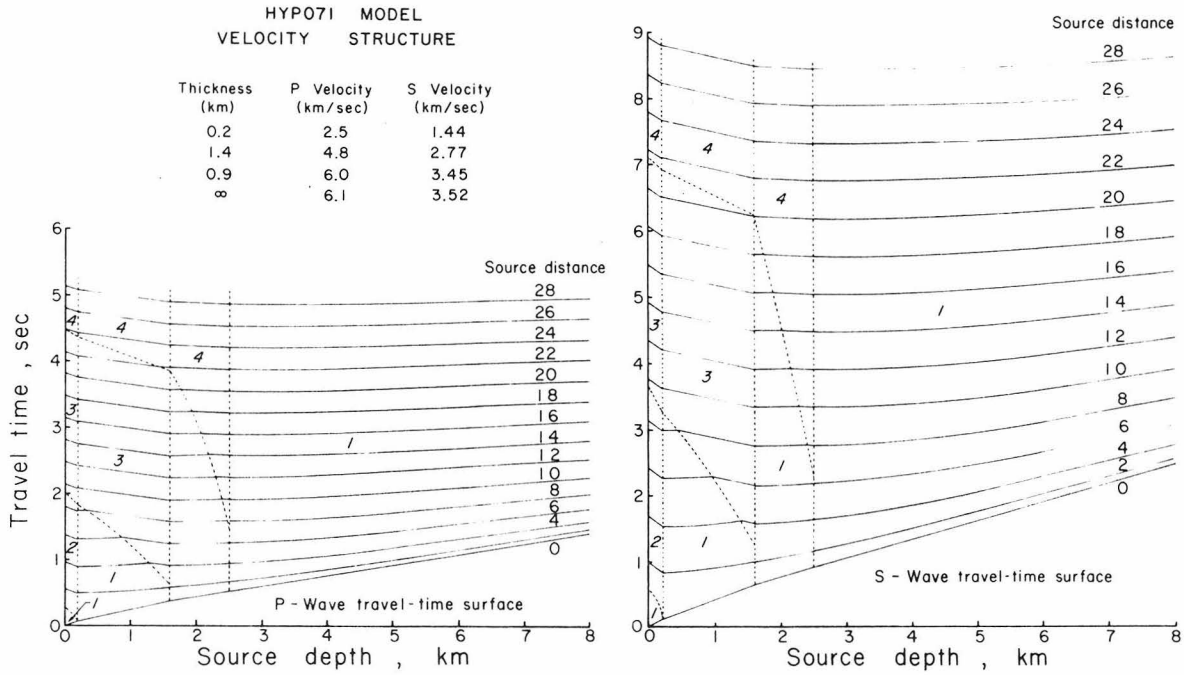

Figure II-6. Travel-time surfaces for P-waves and S-waves for the HYP071 velocity model. Contours show travel times as a function of depth for fixed source distances. Slanted numbers indicate types of first arrivals; 1 for direct wave, 2 for refraction from top of second layer, etc. Dotted lines separate regions with different types of arrivals.

These travel-time surfaces illustrate the nature of the difficulties in constraining velocities and hypocenter depths. Consider the P-wave contour for a distance of 6 km. There is only about 0.1 sec variation in arrival time as the depth is moved between 0.1 and 4.0 km. At other distances, the effect is less severe, but usually a range of very slow change exists. The contours for near distances, 0 to 2 km, clearly show how close-in stations can provide control for depth determination. Partial derivatives of travel-time with respect to depth are positive in the direct-wave regions and negative in the refracted-wave regions.

When locating a single earthquake using a given velocity function, the arrival times can be plotted as a line of points parallel to the time axis. The location procedure moves this line of points to give a least-squares fit to the travel-time surface. If the line of points lies completely within one of the refraction regions, the line could be moved freely along the contours without changing the fit. This property demonstrates the indeterminancy present if the data consist of only refractions from one layer. For the inversion problem herein, there are several lines of points, one for each earthquake, which can be moved. Also, the travel-time surface itself can be adjusted to provide a better fit. Because the depth estimation is poorly controlled, there is freedom to move the data points about. This possibility then allows various adjustments of the travel-time surface, i.e. the velocities. The geometrical constraints on epicenters provided by having stations well-distributed in azimuth are not present

in this representation of the travel-time surface. A higher dimensionality to include azimuths would be required.

The travel-time surfaces shown in Figure II-6 are defined by four velocities and three layer thicknesses. It is easy to see that the rather complicated nature of these surfaces would require many more terms for a polynomial approximation. For this reason, a polynomial approximation of the travel-time surface was not used in the implementation of the inversion scheme.

Inversion Starting with the H-K Velocity Model

Another initial velocity model for the Galway Lake area is taken from the work of Hadley and Kanamori (1977). They used regional earthquakes, accurately timed blasts, and P-delays to give a structure for the Mojave Desert. Their structure has been modified for the Galway Lake inversion problem by incorporating the same shallow low-velocity layer used in the HYPO71 velocity model. The resulting model will be referred to as the H-K velocity model. The thicknesses and velocities for the three layers from the surface downward are: 0.2 km and 2.3 km/sec, 4.3 km and 5.5 km/sec, 23.0 km and 6.2 km/sec. Deeper layers with velocities of 6.7 and 7.8 km/sec are not sampled at the distances represented by the Galway Lake data used. This model is also similar to that given by Kanamori and Hadley (1975). Initial station delays used with the H-K model are the same as those used for the HYPO71 model. The variances given to each of the model parameters are also the same as those used with the HYPO-71 model.

Relocation vectors obtained after 10 iterations from the initial H-K model are shown in Figure II-7(a). The complete results are listed in Table A2-4 of Appendix 2. A comparison of these results with those from the HYPO71 model (Figure II-4) is given in Figure II-7(b) which shows the differences between the two solutions. Most of the epicenters for both solutions have error ellipses of similar sizes and orientations. The error ellipse for one standard deviation for event 2 is shown in Figure II-7(b). The error ellipses are computed according to equations (A-3) given in Appendix 1. In general, the differences in epicenters for the two solutions is no greater than the semi-axes of their error ellipses.

For the H-K model, the parameters for locations and station delays generally converged rapidly during the first few iterations. The velocity values were incremented very slowly, except the size of the incremental steps decreased faster than for the HYPO-71 model.

To compare the effects of the two velocity structures more closely, the station delays were set equal to the previously determined delays and fixed. The results of the inversion program under these conditions is shown in Figure II-8(a) and listed in Table A2-5 of Appendix 2. The velocities obtained here are much the same as when the delays were free. The differences in relocation vectors (Figure II-8(b)) for these two models are about 1/2 to 2/3 of the error ellipse semi-axes. The error ellipse shown is for event number 2 but it is typical of the other ellipses. For the H-K model with delays fixed, the location parameters are adjusted rapidly during

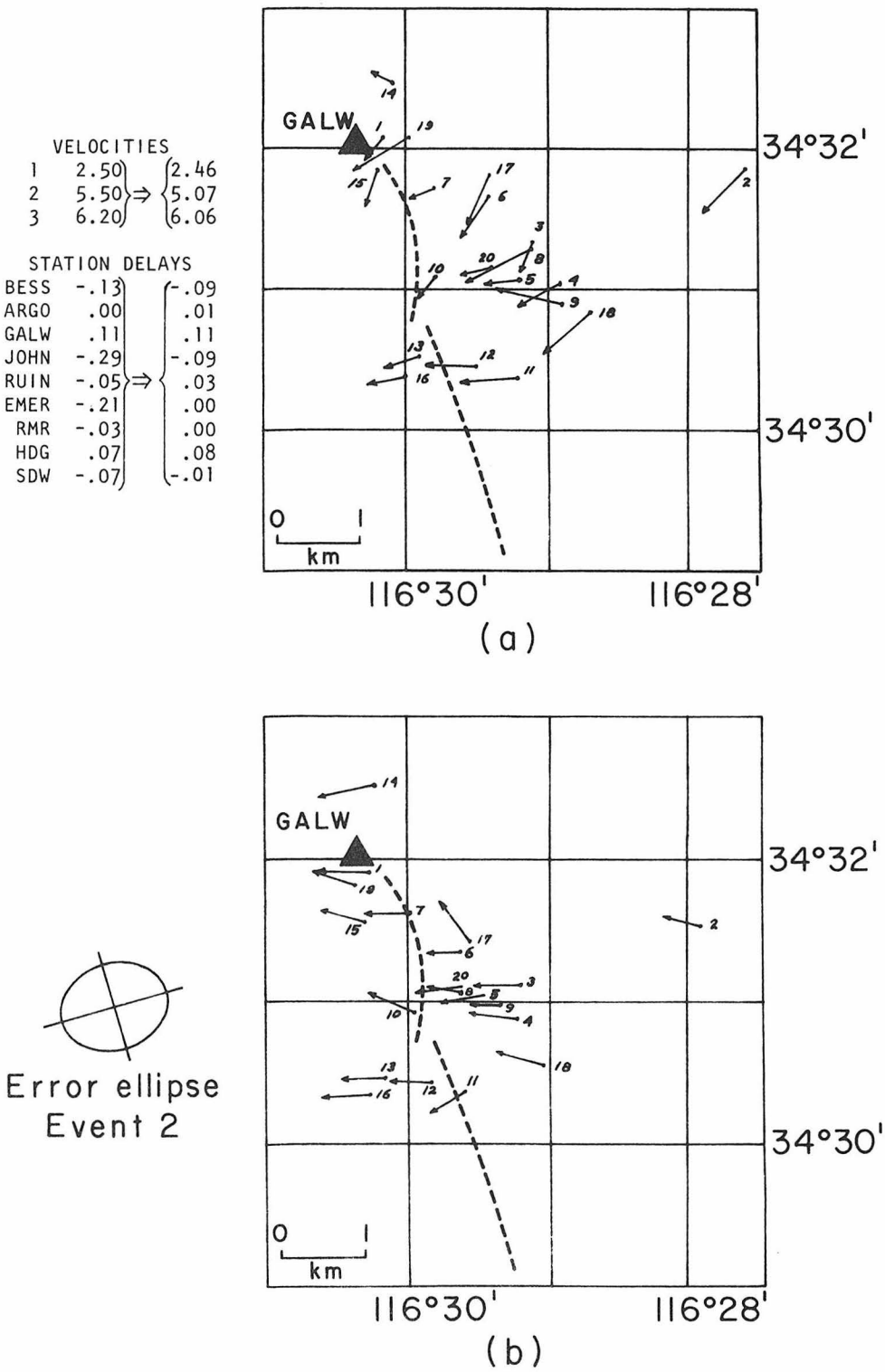

Figure II-7. (a) Inversion results with the H-K model. (b) Differences in the final epicenters using the H-K model and the HYP071 model. Vectors point to the HYP071 results. The error ellipse is typical of the other events.

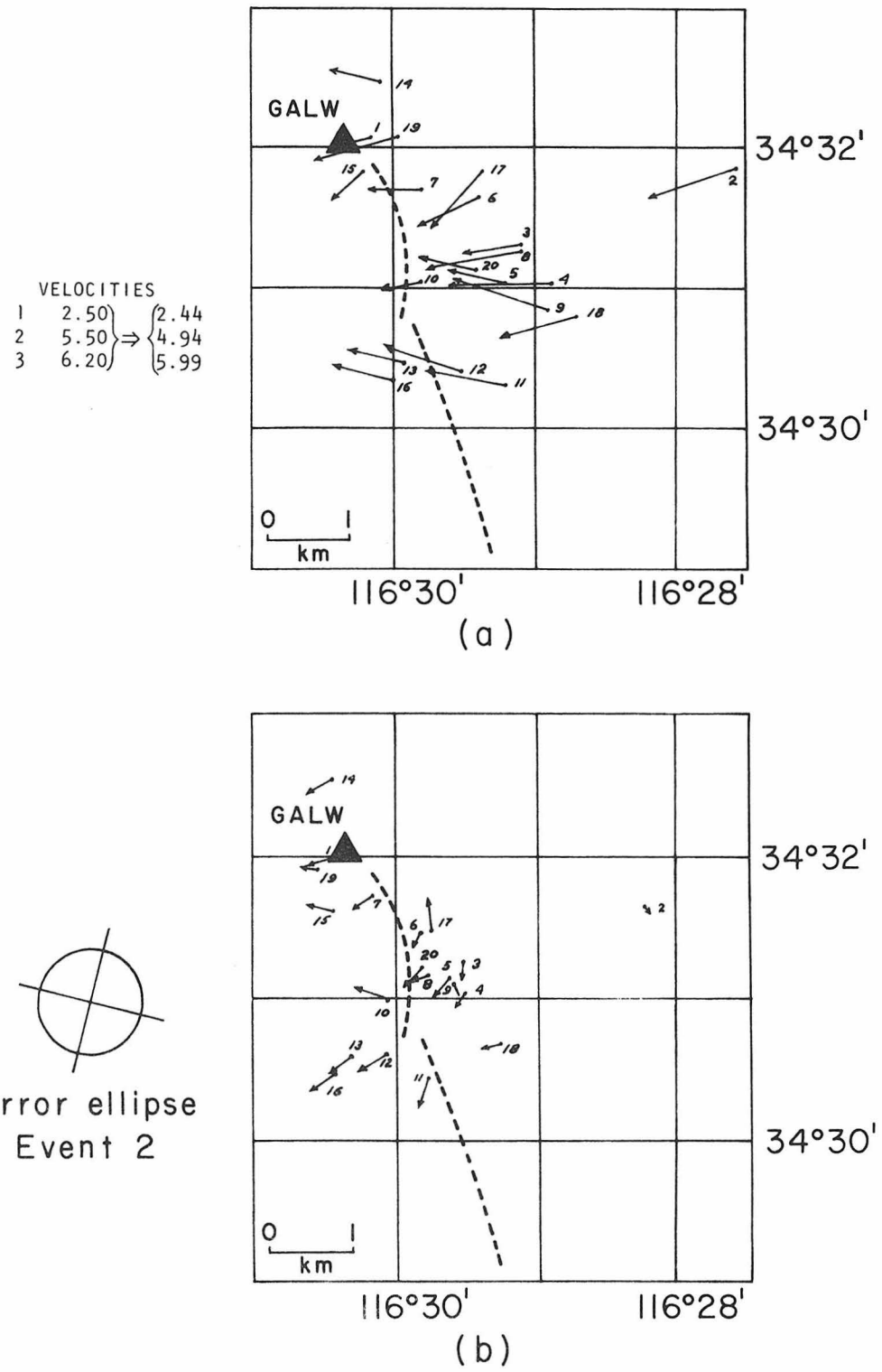

Figure II-8. (a) Inversion results with the H-K model, except station delays were fixed to the values estimated using the HYPO71 model. (b) Differences in the final epicenters using the H-K model with fixed delays and the HYPO71 model. Vectors point to the HYPO71 results. The error ellipse is typical of the other events.

the first three or four iterations, and then the increments become small. Velocities for the first and third layers are changed in the same manner as the location parameters. The velocity for the second layer is converging very slowly, and the behavior of the increments is much the same as observed for the HYPO-71 model. The second layer is the most significant to the model because it contains a predominant portion of each of the travel paths for the six near stations. Slight changes in the velocity are trading off with slight changes in depths and origin times. The travel-time surfaces for the H-K velocity structure are shown in Figure II-9. These surfaces are less complicated than those for the HYPO-71 model because there are fewer layers. The difficulty in controlling depths is similar here. Depth control is poor wherever the contours are parallel, or nearly so, to the depth axis. Poor depth control in turn causes poor control of the velocity estimates as discussed for the HYPO-71 model.

A number of problems were run testing various ways to improve the velocity estimates. All of the trials were unsuccessful in circumventing the broad poorly-defined RMS minimum relative to the velocity parameters. First, the trial locations were changed so that the epicenters required very little correction. Then the P and S arrival times at the GALW station were given very low variances which caused these times to be weighted much more heavily in the solution. The GALW station is no more than about 3 km distant from any of the epicenters. One run was made in which the depth changes were restricted for the first five iterations by using a very small model

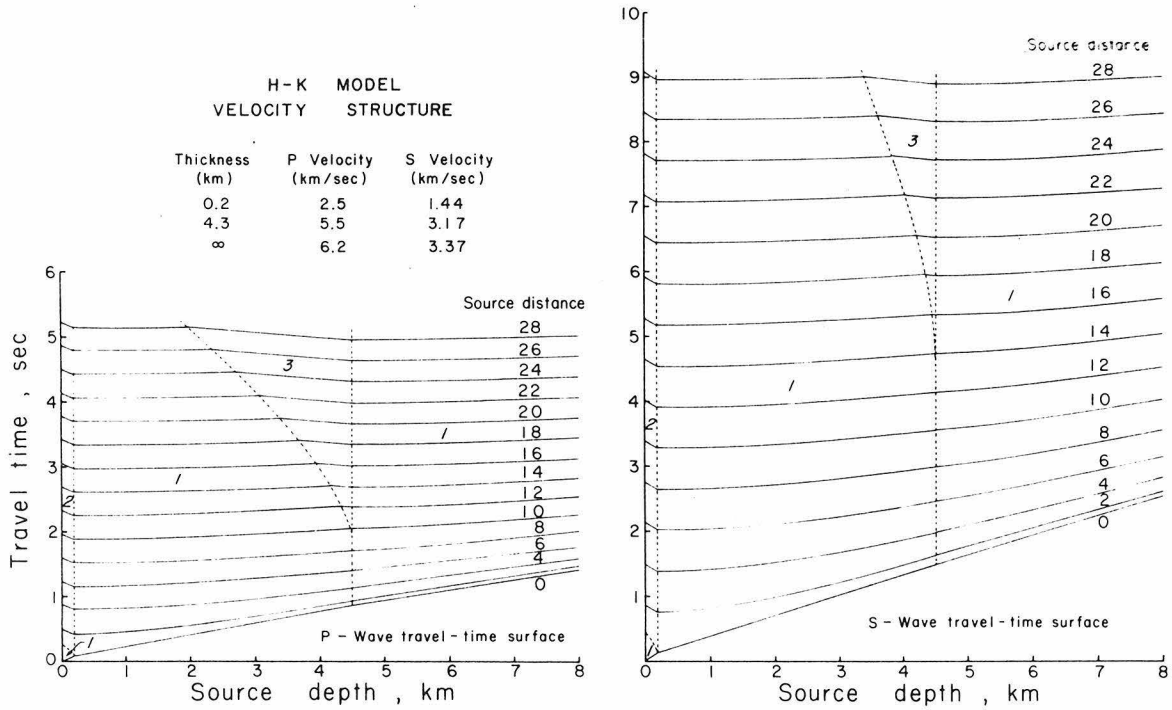

Figure II-9. Travel-time surfaces for P-waves and S-waves for the H-K velocity model. The notation is the same as for Figure II-6.

variance, and then the restriction was relaxed. This changed the path of convergence but not the final result after 10 iterations. Similar results were obtained by limiting the velocity changes for the first five iterations.

Inversion Starting with an Arbitrary Velocity Model

A velocity model with arbitrary layers was also used as an initial trial model for the inversion. This model, called the VEL-1 model, contains some features of both the HYPO71 and H-K models. The shallow low-velocity layer of the previous models was retained because this seems a reasonable way to allow for a weathered layer. A layer with a velocity of 6.2 km/sec beginning at a depth of 4.5 km was chosen to agree with the structure given by Hadley and Kanamori (1977). This velocity layer is desirable for the initial model since it represents an average velocity determined from regional data. Intermediate layers with intermediate velocities were added so that the velocities increased with depth. All of the parameters for the VEL-1 model are listed in Table A2-6 of Appendix 2. Station delays, hypocenter depths, and model variances are the same as used for the H-K model. Initial trial epicenters were shifted to locations close to those determined when using the previous models.

The final model obtained using the VEL-1 layer structure is listed in Table A2-7 of Appendix 2. Vectors showing the differences in epicenters between the VEL-1 and HYPO71 results are plotted in Figure II-10. The epicenter results here are essentially the same

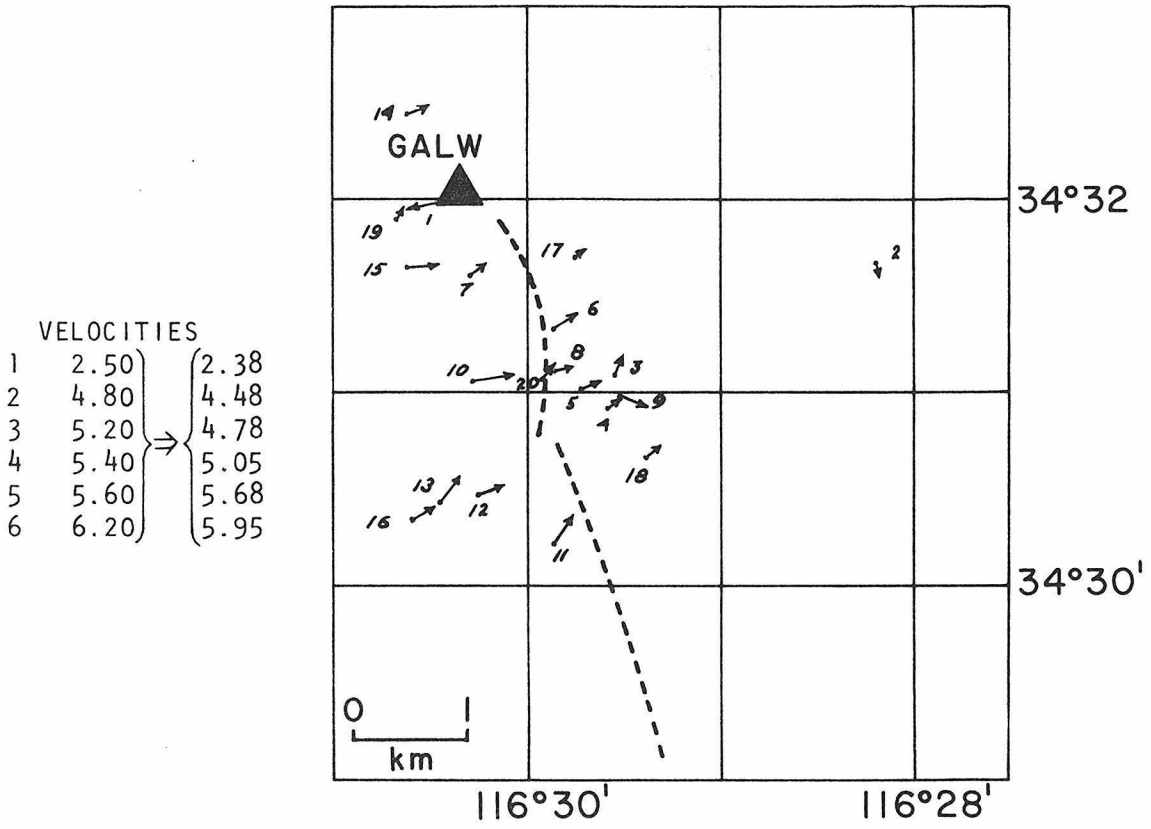

Figure II-10. Inversion results with the VEL-1 model. Initial epicenters were taken close to the expected results and delays were fixed to those estimated from the HYPO71 model. The vectors point from the VEL-1 results to the HYPO71 results.

as before. In common with the other velocity models, VEL-1 gives hypocenters which are deeper by 1-2 km than the starting depths. The velocities were lowered from their initial values (Figure II-10), and they did converge although rather slowly.

Travel-time surfaces for the VEL-1 model are shown in Figure II-11. Here the surfaces are complex because there are 6 layers in the model. The velocity determination for this model converged somewhat more quickly, 10-12 iterations, than did the estimations for the other models, 15-20 iterations. Of course, this model might be closer to the true velocity structure but there are no strong reasons to support this contention. The final RMS level of 0.138 sec is slightly lower than for the HYPO71 model, 0.147 sec, or the H-K model, 0.143 sec. The travel-time surface illustrates a heuristic explanation of the better convergence behavior. There are many regions on the travel-time surface for both direct arrivals and refracted arrivals. Then, the collection of partial derivatives with respect to depth for each earthquake is more likely to have both positive and negative terms. A set of derivatives with mixed signs is less likely to permit trade-offs with other parameters.

One interesting feature of this travel-time surface should be noted. Refraction arrivals from the top of the fifth layer are first arrivals for a limited source-depth range only, 3.0 - 3.5 km. If a normal refraction survey using near-surface sources were conducted, layer five would not be detected. Instead, layers four and five would be interpreted as a single layer with the velocity of layer

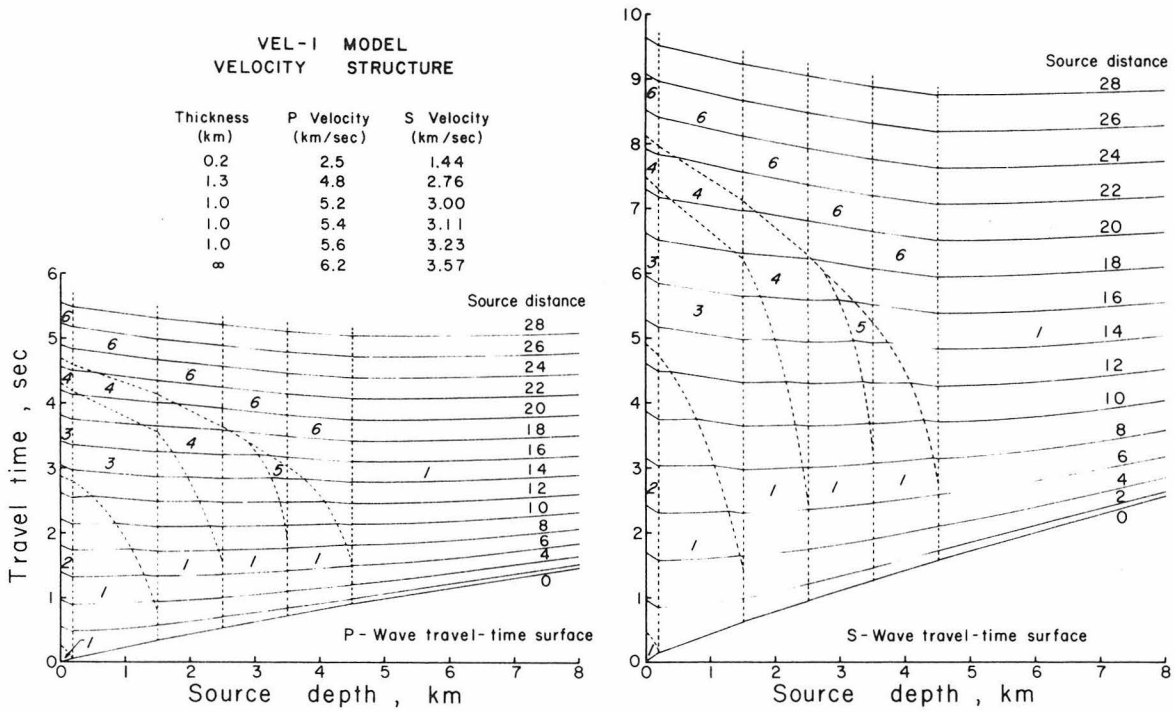

Figure II-11. Travel-time surfaces for P-waves and S-waves for the VEL-1 velocity model. The notation is the same as for Figure II-6.

four, and the depth to layer six would be underestimated slightly. Layer five is "hidden", it is never a first arrival from surface sources even though the velocities are monotonically increasing with depth.

Comparison of Velocity Estimates for the Three Models

The velocity model results from the three inversion problems for the Galway Lake data are shown in Figure II-12 along with two conventional models for the same region. Each of the velocity models estimated by a least-squares fit to the data has velocities consistently lower than those of the conventional models. As discussed earlier, the HYPO71 estimates are not very satisfying because of the very slow convergence of that problem. It should be noted that after the rapid corrections of the first several iterations for the HYPO71 model, the surface layer was 2.4 km/sec and the halfspace was 5.9 km/sec. These two values compare well with the final values of the other two problems. The H-K and VEL-1 structures differ only in the number of intermediate layers. The velocity estimates for the surface layer and the halfspace are the same. The velocity estimate for the intermediate layer of the H-K model, 4.9 km/sec, is very close to the weighted-average velocity of the intermediate layers of the VEL-1 structure, 5.0 km/sec.

Further experimentation with layer structure and resolution of layers is desirable in this kind of study. This was not pursued for the Galway Lake area because the data set proved to be only marginally effective in providing constraints on velocity models. A large number

Thickness	Fuis(1977) Velocity	HYPO71 Velocity	Thickness	Hadley and Kanamori (1977) Velocity	H-K Velocity	Thickness	VEL-1 Velocity
0.2 km	2.5 km/sec	2.0 km/sec	0.2 km	2.5 km/sec	2.4 km/sec	0.2 km	2.4 km/sec
1.4	4.8	3.5				1.3	4.5
0.9	6.0	5.6	4.3	5.5	4.9	1.0	4.8
	6.1	5.8				1.0	5.1
						1.0	5.7
				6.2	6.0		6.0
		RMS = .139			RMS = .143		RMS = .138

Figure II-12. Summary of Galway Lake Velocity Estimates

of similar models could be derived each having much the same RMS level of residuals. Even though one station, GALW, was generally at epicentral distances of 1-2 km, and three additional stations were at distances of 8-10 km, most of the earthquakes were too shallow for their depth estimates to be well-controlled. The difficulty in depth control translates directly into difficulty in velocity estimation.

A much better data set for the purpose of estimating shallow crustal velocity structure would result if several of the recording stations were very close to the epicenters. The Galway Lake data were adequate for locations, but more close-in stations were needed. These close-in stations should be at a distance equal to no more than one or two times the focal depths of the shocks. Even for areas such as the Mojave Desert or the Imperial Valley where local networks have station spacing on the order of 10-15 km, additional stations are needed for this type of velocity study. Sites for portable instruments should be distributed within an aftershock area rather than surrounding it, assuming a good local network is present already. Even if a velocity study is not contemplated, portable instruments should not be located in a circle concentric with the epicenters. In such a case, all source-receiver distances would be similar and all stations would have the same relations for depth control. A more random set of source-receiver distances is a better strategy because at least some stations may then help control depth estimates.

Two conclusions about the velocity structure in the Galway Lake

area can be drawn from these studies. The appropriate velocities in the upper few kilometers of the crust are lower than those used in the regional velocity models. This result is in agreement with Kanamori and Hadley (1975) who found similarly low velocities at shallow depths at sites southwest of Victorville in the Mojave Desert. They used detailed refraction surveys. Second, the regional velocity layer of 6.2 km/sec at a depth of 4.5 km (Hadley and Kanamori, 1977) has a lower velocity locally in the Galway Lake area. A value of 6.0 km/sec is indicated on the basis of the Galway Lake data.

The inversion technique discussed herein is moderately successful for the Galway Lake data. The usual velocity functions for the Mojave Desert are shown to be slightly high for Galway Lake and modified velocity functions are derived. The success is qualified as moderate because the velocities are not strongly constrained for this data. Application of the method has also demonstrated the nature of the shortcomings in this data set and made clear the criteria for applications to other areas. When precautions are taken to insure close-in stations, relative to focal depths, this inversion technique is a useful tool for estimating local velocity structures.

REFERENCES

Aki, K. (1965), Maximum likelihood estimate of b in the formula log N = a - bM and its confidence limits, Bull. Earthq. Res. Inst., 43, 237-239.

Aki, K. and W. H. K. Lee (1976), Determination of three-dimensional velocity anomalies under a seismic array using first P-arrival times from local earthquakes. Part I-a homogeneous initial model, Jour. Geophys. Res., 81, 4381-4399.

Allen, C. R. (1968), The tectonic environments of seismically active and inactive areas along the San Andreas fault system, in Proceedings of Conference on Geologic Problems of San Andreas Fault System, ed. by W. R. Dickinson and A. Grantz. Stanford Univ., Stanford, Calif.

Allen, C. R. (1974), Geologic criteria for evaluating seismicity, Bull. Geol. Soc. Am., 86, 1041-1057.

Allen, C. R. and J. M. Nordquist (1972), Foreshock, main shock, and larger aftershocks of the Borrego Mountain earthquake, in The Borrego Mountain Earthquake of April 9, 1968. U.S. Geol. Surv. Prof. Paper 787.

Allen, C. R., P. St Amand, C. F. Richter and J. M. Nordquist (1965), Relationship between seismicity and geologic structure in the southern California region, Bull. Seism. Soc. Am., 55, 753-797.

Atwater, Tanya (1970), Implications of plate tectonics for the cenozoic tectonic evaluation of western North America, Bull. Geol. Soc. Am., 81, 3513-3536.

Backus, G. E. and J. F. Gilbert (1967), Numerical application of a formalism for geophysical inverse problems, Geophys. Jour., 13, 247-276.

Backus, G. E. and J. F. Gilbert (1968), The resolving power of gross earth data, Geophys. Jour., 16, 169-205

Backus, G. E. and J. F. Gilbert (1969), Constructing P-velocity models to fit restricted sets of travel-time data, Bull. Seism. Soc. Am., 59, 1407-1414.

Backus, G. E. and J. F. Gilbert (1970), Uniqueness in the inversion of inaccurate gross earth data, Phil. Trans. Roy. Soc. London, Ser. A, 266, 123-192.

Beeby, D. J. and R. L. Hill (1975), Galway Lake fault, Calif. Geol., 28, 219-221.

Biehler, S., R. L. Kovach and C. R. Allen (1964), Geophysical framework of the northern end of Gulf of California structural province, Am. Assoc. Pet. Geol., Memoir 3, 126-143.

Bjerhammar, A. (1973), Theory of Errors and Generalized Matrix Inverses. Elsevier, New York.

Burchfiel, B. C. and G. A. Davis (1972), Structural framework and evolution of the southern part of the Cordilleran orogen, western United States, Am. Jour. Sci., 272, 97-118.

Crosson, R. S. (1976a), Crustal structure modeling of earthquake data 1. Simultaneous least squares estimation of hypocenter and velocity parameters, Jour. Geophys. Res., 81, 3036-3046.

Crosson, R. S. (1976b), Crustal structure modeling of earthquake data 2. Velocity structure of the Puget Sound region, Washington, Jour. Geophy. Res., 81, 3047-3054.

Davis, G. A. and B. C. Burchfiel (1973), Garlock fault: an intra-continental transform structure, Southern California, Geol. Soc. Am., 84, 1407-1422.

Dixon, W. J. and F. J. Massey Jr. (1957), Introduction to Statistical Analysis. McGraw-Hill, New York.

Eaton, J. P., M. E. O'Neil and J. N. Murdock (1970), Aftershocks of the 1966 Parkfield-Cholame, California, earthquake: a detailed study, Bull. Seis. Soc. Am., 60, 1151-1197.

Elders, W. A., R. W. Rex, Tsvi Meidav, P. T. Robinson and S. Biehler (1972), Crustal spreading in Southern California, Science, 178, 15-24.

Ellsworth, W. L., R. H. Campbell, D. P. Hill, R. A. Page, R. W. Alewine, T. C. Hanks, T. H. Heaton, J. A. Hileman, H. Kanamori, B. Minster and J. H. Whitcomb (1973), Point Mugu, California, earthquake of 21 February 1973 and its aftershocks, Science, 182, 1127-1129.

Flinn, E. A. (1960), Local earthquake location with an electronic computer, Bull. Seis. Soc. Am., 50, 467-470.

Friedman, M. E., J. H. Whitcomb, C. R. Allen and J. A. Hileman (1976), Seismicity of the Southern California region, 1 January 1972 to 31 December 1974. Seismological Laboratory, California Institute of Technology, Pasadena.

Fuis, G. S. (1976), Ground breakage and aftershocks of the M_L = 5.2 Galway Lake earthquake, June 1975, Mojave Desert, California, Trans. Am. Geophys. Union, 57, 954 (abstract).

Garfunkel, Z. (1972), A model for the young tectonics of the Mojave Desert, California, and its relations to adjacent regions (unpublished manuscript), Contribution No. 2166. Div. of Geol. and Planet. Sci., Calif. Inst. of Tech., Pasadena.

Gutenberg, B. (1932), Travel-time curves at small distances and wave velocities in Southern California, Gerl. Beitr. Z. Geophys., 35, 6-50.

Gutenberg, B. (1943), Earthquakes and structure in Southern California, Bull. Geol. Soc. Am., 54, 499-526.

Gutenberg, B. (1944a), Travel times of principal P and S phases over small distances in Southern California, Bull. Seism. Soc. Am., 34, 13-32.

Gutenberg, B. (1944b), Reflected and minor phases in records of near-by earthquakes in Southern California, Bull. Seism. Soc. Am., 34, 137-160.

Gutenberg, B. (1951a), Travel times from blasts in Southern California, Bull. Seism. Soc. Am., 41, 5-12.

Gutenberg, B. (1951b), Waves from blasts recorded in Southern California, Trans. Am. Geophys. Union, 33, 427-431.

Gutenberg, B. (1951c), Revised travel times in Southern California, Bull. Seism. Soc. Am., 41, 143-163.

Gutenberg, B. and C. F. Richter (1944), Frequency of earthquakes in California, Bull. Seism. Soc. Am., 34, 185-188.

Hadley, D. M. and H. Kanamori (1977). Seismic structure of the Transverse Ranges, California, Bull. Geol. Soc. Am., (in press).

Healy, J. H., W. W. Rubey, D. T. Criggs and C. B. Rayleigh (1968), The Denver earthquakes, Science, 161, 1301-1308.

Hileman, J. A., C. R. Allen and J. M. Nordquist (1973), Seismicity of the Southern California region, 1 January 1932 to 31 December 1972. Seismological Laboratory, California Institute of Technology, Pasadena.

Hill, D. P., Penelope Mowinckel and L. G. Peake (1975), Earthquakes, active faults and geothermal areas in the Imperial Valley, California, Science, 188, 1306-1308.

Hill, R. T. (1928), Southern California geology and Los Angeles earthquakes. Southern California Academy of Sciences, Los Angeles, California.

Holden, E. S. (1887), List of recorded earthquakes in California, Lower California, Oregon and Washington Territory. Univ. of Calif., Berkeley.

Holden, E. S. (1898), Catalog of earthquakes of the Pacific Coast from 1769 to 1897. Smithsonian Institution, Misc. Collections No. 1087.

Ikegami, R. (1967), On the secular variation of magnitude-frequency relation of earthquakes, Bull. Earthq. Res. Inst., 45, 327-338.

Ishimoto, M. and K. Iida (1939), Observations sur les seismes enregistres par le microseismographe construit dernierment (1), Bull. Earthq. Res. Inst., 17, 443-478 (in Japanese).

Jennings, C. W. (1973), State of California, preliminary fault and geologic map. Calif. Div. Mines, Prelim. Rept. 13.

Johnson, C. E. and D. M. Hadley (1976), Tectonic implications of the Brawley earthquake swarm, Imperial Valley, California, January 1975, Bull. Seism. Soc. Am., 66, 1133-1144.

Kanamori, H. and D. L. Anderson (1975), Theoretical basis of some emperical relations in seismology, Bull. Seism. Soc. Am., 65, 1073-1095.

Kanamori, H. and D. M. Hadley (1975), Crustal structure and temporal velocity change in southern California, Pure and Appl. Geoph., 113, 257-280.

Klein, F. W. (1976), Earthquake swarms and the semidiurnal solid earth tide, Geophys. Jour. Roy. Astr. Soc., 45, 245-295.

Lawson, A. C. (1908), The California earthquake of April 18, 1906, Report of the State Earthquake Investigation Commission. Carnegie Institution, Washington.

Lee, W. H. K. and J. C. Lahr (1971), HYPO71: a computer program for determining hypocenter, magnitude, and first-motion pattern of local earthquakes, U.S. Geol. Surv. Open File Report.

Levenberg, K. (1944), A method for the solution of certain non-linear problems in least squares, Quant. Appl. Math., 2, 164-168.

Lomnitz, C. and A. Hax (1966), Clustering in aftershock sequences, in The Earth Beneath the Continents. Am. Geophy. Union, Geophy. Monograph 10.

Lomnitz, C., F. Mooser, C. R. Allen, J. N. Brune and W. Thatcher (1970), Seismicity and tectonics of the northern Gulf of California region, Mexico, preliminary results, Geofisica Internacional, 10, 37-48.

Mathews, J. and R. L. Walker (1970), Mathematical Methods of Physics, Second Ed., W. A. Benjamin, Inc., New York.

McAdie, A. G. (1907), Catalog of Earthquakes of the Pacific coast from 1897 to 1906. Smithsonian Institution, Misc. Collections, No. 1721.

Minster, J. B., T. H. Jordan, P. Molnar and E. Hains (1974), Numerical modelling of instantaneous plate tectonics, Geophys. Jour. Roy. Astr. Soc., 36, 541-576.

Minster, J. F., J. B. Minster, M. Trevil and C. J. Allegre (1977), Systematic use of trace elements in igneous process, Part II, Inverse problem of the fractional crystallization process in volcanic suites, Cont. Mineral. Petrol., (in press).

Miyamura, S. (1962), Magnitude-frequency relation of earthquakes and its bearing on geotectonics, Proc. Japan Acad., 38, 27-30.

Nordquist, J. M. (1962), A special-purpose program for earthquake location with an electronic computer, Bull. Seism.Soc. Am., 52, 431-437.

Olsen, P. G. and A. G. Sylvester (1975), The Santa Barbara earthquake, 29 June, 1925, California Geology, 28, 123-131.

Palmer, H. N. (1916), California earthquakes during 1915, Bull. Seism. Soc. Am., 6, 8-25.

Peters, D. C. (1973), Hypocenter location and crustal structure inversion of seismic array travel-times, Ph. D. Thesis, University of Washington, Seattle.

Richter, C. F. (1955), Foreshocks and aftershocks, in Earthquakes in Kern County, California During 1952. Calif. Div. of Mines, Bull. 171.

Richter, C. F. (1958), Elementary Seismology. W. H. Freeman and Co., San Francisco.

Richter, C. F. (1969), Transversely aligned seismicity and concealed structures, Science, 166, 173-178.

Richter, C. F. (1971), Sporadic and continuous seismicity of faults and regions, in Recent Crustal Movements. Roy. Soc. of New Zealand, Bull. 9, 171-173.

Ryall, A., D. B. Slemmons and L. D. Gedney (1966), Seismicity, tectonism and surface faulting in the western United States during historic time, Bull. Seism. Soc. Am., 56, 1105-1135.

Scholz, C. H. (1968), The frequency-magnitude relation of microfracturing in rock and its relation to earthquakes, Bull. Seism. Soc. Am., 58, 399-416.

Sharp, R. V. (1972), Tectonic setting of the Salton trough, in The Borrego Mountain Earthquake of April 9, 1968. U. S. Geol. Surv. Prof. Paper 787.

Stewart, J. H. (1970), Upper precambrian and lower cambrian strata in the southern great basin California and Nevada. U. S. Geol. Surv, Prof. Paper 620.

Suyehiro, S. (1966), Differences between aftershocks and foreshocks in the relationship of magnitude to frequency of occurrence for the great Chilean earthquake of 1960, Bull. Seism. Soc. Am., 56, 185-200.

Suyehiro, S. (1969), Difference in the relationship of magnitude to frequency of occurrence between aftershocks and foreshocks for an earthquake of magnitude 5.1 in central Japan, Geophys., 20, 175-187.

Sylvester, A. G., S. W. Smith and C. H. Scholz (1970), Earthquake swarm in the Santa Barbara channel, California, 1968, Bull. Seism. Soc. Am., 60, 1047-1060.

Townley, S. D. and M. W. Allen (1939), Descriptive catalog of earthquakes of the Pacific Coast of the United States, 1769 to 1928, Bull. Seism. Soc. Am., 29, 1-297.

Utsu, T. (1965), A method for determining the value of b in a formula log n = a - bM showing the magnitude-frequency relation for earthquakes, Geophys. Bull. Hokkaido Univ., 13, 99-103 (in Japanese with English summary).

Utsu, T. (1967), Some problems of the frequency distribution of earthquakes in respect to magnitude, Geophys. Bull. Hokkaido Univ., Part I in 17, 85-112, Part II in 18, 53-69 (in Japanese with English summary).

Wesson, R. L., R. O. Burford and W. L. Ellsworth (1973), Relationship between seismicity, fault creep and crustal loading along the central San Andreas fault, in Proceedings of the Conference on Tectonic Problems of the San Andreas Fault System, ed. by R. L. Kovach and A. Nur, Stanford Univ., Stanford, Calif.

Wesson, R. L. and W. L. Ellsworth (1973), Seismicity preceding moderate earthquakes in California, Jour. Geophys. Res., 78, 8527-8546.

Whitcomb, J. H. (1976). Earthquake prediction: a hypothesis test, (unpublished manuscript).

Whitcomb, J. H., C. R. Allen, J. D. Garmany and J. A. Hileman (1973a), San Fernando earthquake series 1971: focal mechanisms and tectonics, Rev. Geophys. Space Phys., 11, 693-730.

Whitcomb, J. H., J. D. Garmany and D. L. Anderson (1973b), Earthquake prediction: variation of seismic velocities before the San Fernando earthquake, Science, 180, 632-635.

Wiggins, R. A. (1972), The general linear inverse problem: implication of surface waves and free oscillations for earth structure, Rev. Geophys. Space Phys., 10, 251-285.

Wood, H. O. (1916), California earthquakes (generatrices and history), Bull. Seism. Soc. Am., 6, 55-180.

Wyss, M. (1973), Toward a physical understanding of the earthquake frequency distribution, Jour. Roy. Astr. Soc., 31, 341-359.

Wyss, M. and W. H. K. Lee (1973), Time variations of the average earthquake magnitude in central California, in Proceedings of the Conference on Tectonic Problems of the San Andreas Fault System, edited by R. L. Kovach and A. Nur. Stanford Univ., Stanford, Calif.

Appendix 1

PROGRAM IMPLEMENTATION OF THE INVERSION PROBLEM

The computer codes for the inversion problem formulated herein were developed on both the Data General NOVA and the IBM 370 computers. Nearly all of the program development and testing was carried out on the NOVA with its 32K core. Use of the NOVA dictated several features of the program designed for economy of core usage. Although not strictly necessary on the IBM, many of these features were retained when the program was transferred. When a full problem with 20 earthquakes and 12 velocity parameters was run on the NOVA, running time became excessive. Much time was used by a large number of core-disk data transfers, and about half of the 90 minutes for a single iteration was taken by inversion of the 92-by-92 matrix. The same problem on the IBM requires about 30 seconds per iteration.

The most significant core-usage feature retained in the IBM version of the program is that the full matrix A of equation (II-18) is never formed explicitly. Matrix A could be as large as 100-by-300. The matrix $\cos\theta \left[A^T V^{-1} A\right] + \sin\theta \left[W^{-1}\right]$ of (II-18) has the general form shown in equation (A-1). Each submatrix L is a 4-by-4 matrix derived from partial derivatives of travel-time with respect to the location parameters for a single earthquake. Each submatrix M is a 4-by-N matrix derived from partial derivatives of travel-time with respect to the velocity model parameters for a single earthquake. N is the number of parameters in the velocity model. The entire matrix of (A-1), except for the submatrix M', can be built up earthquake by earthquake without ever forming the matrix A. This construction is

$$B = \begin{bmatrix} [L] & & 0 & & \overline{M} \\ & [L] & & & \overline{M} \\ & & [L] & & \overline{M} \\ & 0 & & \ddots & \vdots \\ & & & [L] & \overline{M} \\ \left[M^T\right] & \left[M^T\right] & \left[M^T\right] & \cdots \left[M^T\right] & \left[M'\right] \end{bmatrix} \qquad \text{(A-1)}$$

done by the subroutine PHASE2. The several earthquakes of a problem are coupled together through the common velocity model and this coupling appears in the submatrix M'. M' is produced by those columns of A that contain the velocity model derivatives. These velocity model vectors of A are built up as PHASE2 operates on each individual earthquake. Finally, PHASE3 computes the submatrix M', and the matrix of (A-1) is ready for inversion.

MAIN Program

The MAIN program is concerned primarily with setup of the problem, calling subroutines for calculations, and bookkeeping of the various intermediate results. Nearly all substantive calculations are done in subroutines. A generalized flowchart for the MAIN program is given in Figure A-1.

Input data for the program consist of parameters controlling the number of iterations, the value of the tradeoff parameter θ, a number of switches for optional printouts, the initial trial model, station data, and earthquake arrival times. The arrival times are

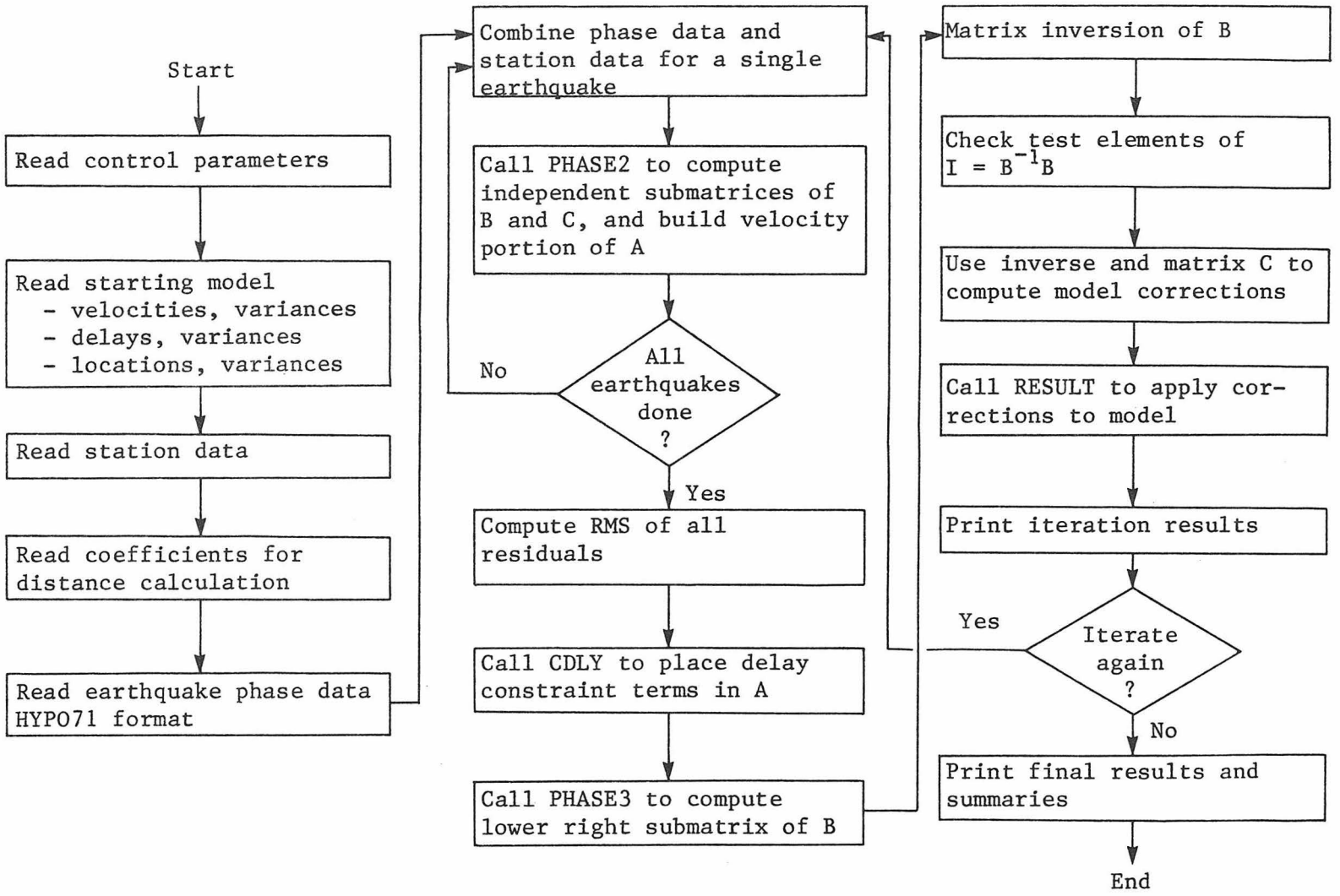

Figure A-1. Flow chart for MAIN program. B is the complete matrix for all earthquakes and has the form $B = \cos\theta\ A^T V^{-1} A + \sin\theta\ W^{-1}$. $C = \cos\theta\ A^T V^{-1} \delta T$.

read from punched card format compatible with that of HYPO71 (Lee and Lahr, 1971). Considerable flexibility in program usage is available through the tradeoff parameter θ, the model variances, and the data variances. Examination of the details of calculations at many intermediate points is possible by using the switches for optional printout. All of the input data are printed with the output so that results are easily documented. The results of each iteration are printed as well as a summary of how the model parameters and RMS residual have changed with each iteration.

On the flowchart of Figure A-1, matrix A corresponds to the matrix A in the equations of Chapter 6. Matrix B is the matrix which is inverted in the solution of the problem as noted for equation (II-22). The matrix inversion is a standard IBM subroutine using gaussian elimination and pivoting on the largest diagonal element at each step. Elements of the identity matrix calculated using the inverse are correct to about five decimal digits for a 92-by-92 matrix.

The program has no provision for automatically evaluating convergence of the solution. For a single earthquake location, convergence is usually considered satisfactory when the location parameters do not change by a significant amount, and there is no further significant reduction in the RMS of the residuals. These same criteria could be utilized for the joint problem of determining locations of many earthquakes and a velocity model. Closely monitoring the results of each iteration seemed more expedient because the program could be easily restarted if desirable.

Subroutine PHASE2 is discussed below. Subroutine CDLY evaluates the necessary coefficients for the station delay constraints as given in equation (II-21). These terms are then placed in the appropriate columns of the velocity model portion of the matrix A, lengthening the column vectors by 2. PHASE3 operates on these same column vectors to produce submatrix M', shown equation (A-1). Subroutine RESULT applies the corrections δm_i of the solution to the trial model. Location corrections in kilometers are converted to changes in longitude and latitude. Depths are prevented from going zero or negative. RESULT prints out the old model, the corrections, and the new model.

Subroutine PHASE2

This subroutine, whose generalized flowchart is shown in Figure A-2, constructs the L and M submatrices of matrix C as shown in equation (A-1) for each earthquake of the problem. Epicentral distances are calculated by subroutine DIST according to the method of Richter (1958, p. 701) giving results valid to 0.1 km out to distances of 500 km. DIST also provides azimuth from the earthquake to the recording station. Subroutine TTIM, discussed below, is called to compute travel times and partial derivatives for the A matrix. PHASE2 then uses the results to compute $B' = \cos\theta\left[A^T V^{-1} A\right] + \sin\theta\left[W^{-1}\right]$ which contains the submatrices L and M for a single earthquake. The portion of the RHS column vector, $C = \cos\theta\left[A^T V^{-1}\right]\delta T$, appropriate to each earthquake is also constructed.

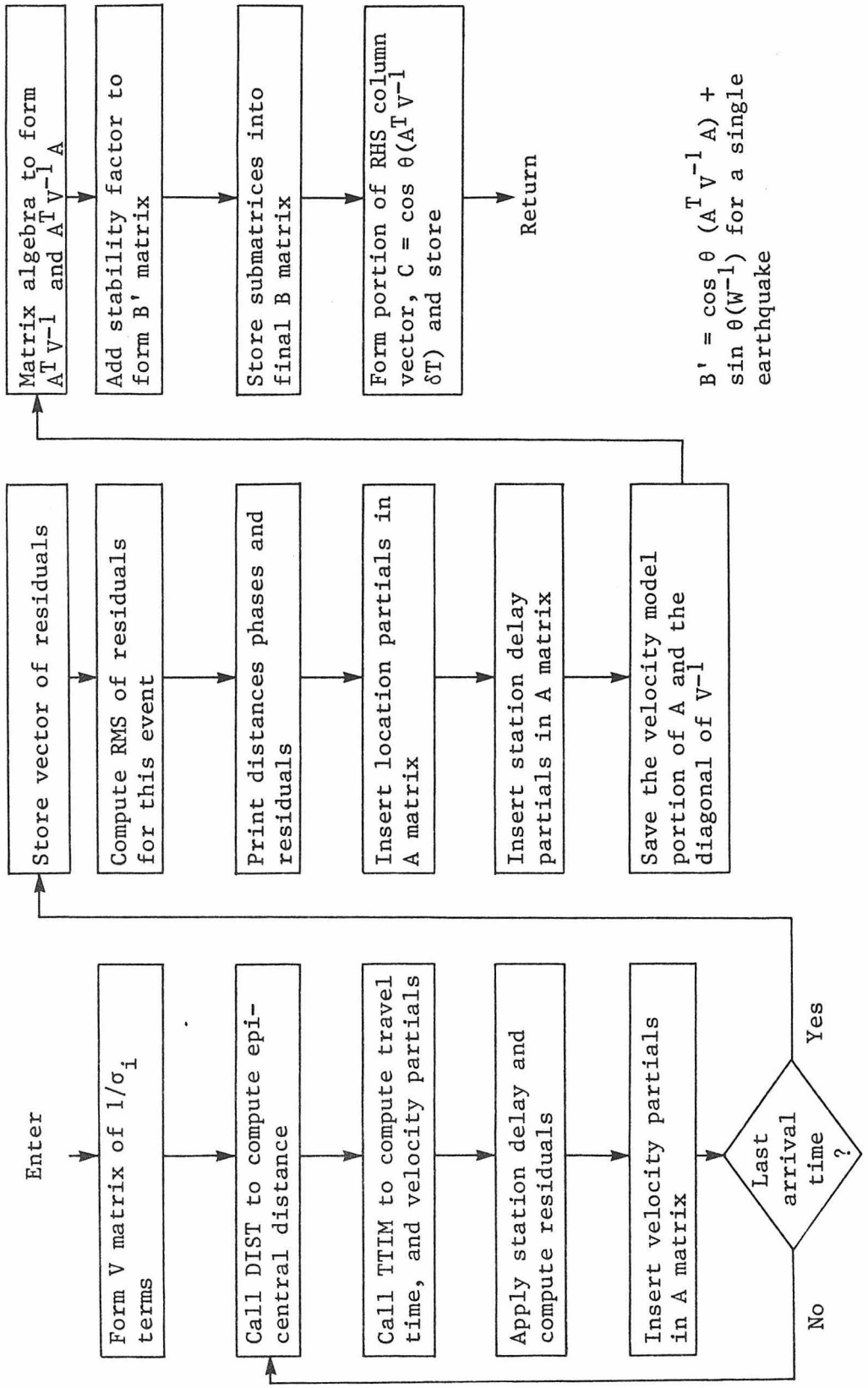

Figure A-2. Flow chart of subroutine PHASE2.

Subroutine TTIM

This subroutine represents the "forward" part of the inversion problem; it uses the given model parameters to produce calculated arrival times. Partial derivatives of these arrival times with respect to the model parameters are also computed. Possible refraction travel times are calculated analytically, but direct-wave travel times are estimated iteratively. A flowchart of TTIM is given in Figure A-3.

In the iteration, the sine of the takeoff angle is varied until the computed distance converges with the epicentral distance. Corrections to the sine are uniform until the sign of the distance error changes, then the corrections are calculated by Newton's method to hasten convergence. In cases where the takeoff angle is near $\pi/2$, such as a distant receiver and the hypocenter is just under a velocity interface, the iteration may not converge because of the limited numerical precision of the computer. For these cases, the travel-time curves are essentially linear and the travel time is found by interpolation of the results of the last two iterations. When travel times for all possible rays have been computed, the minimum time is selected. A ray identifier is also returned, 1 for a direct ray, 2 for a refraction off the top of the second layer, etc.

Partial derivatives of the travel times with respect to the location parameters are computed analytically for the refraction arrivals. The simple expressions are: $\partial T/\partial \Delta = 1/V_R$ and $\partial T/\partial h = \cos \theta_H/V_H$ where T is time, Δ is distance, V_R is velocity in the refracting layer, h is hypocentral depth, θ_H is the angle of incidence

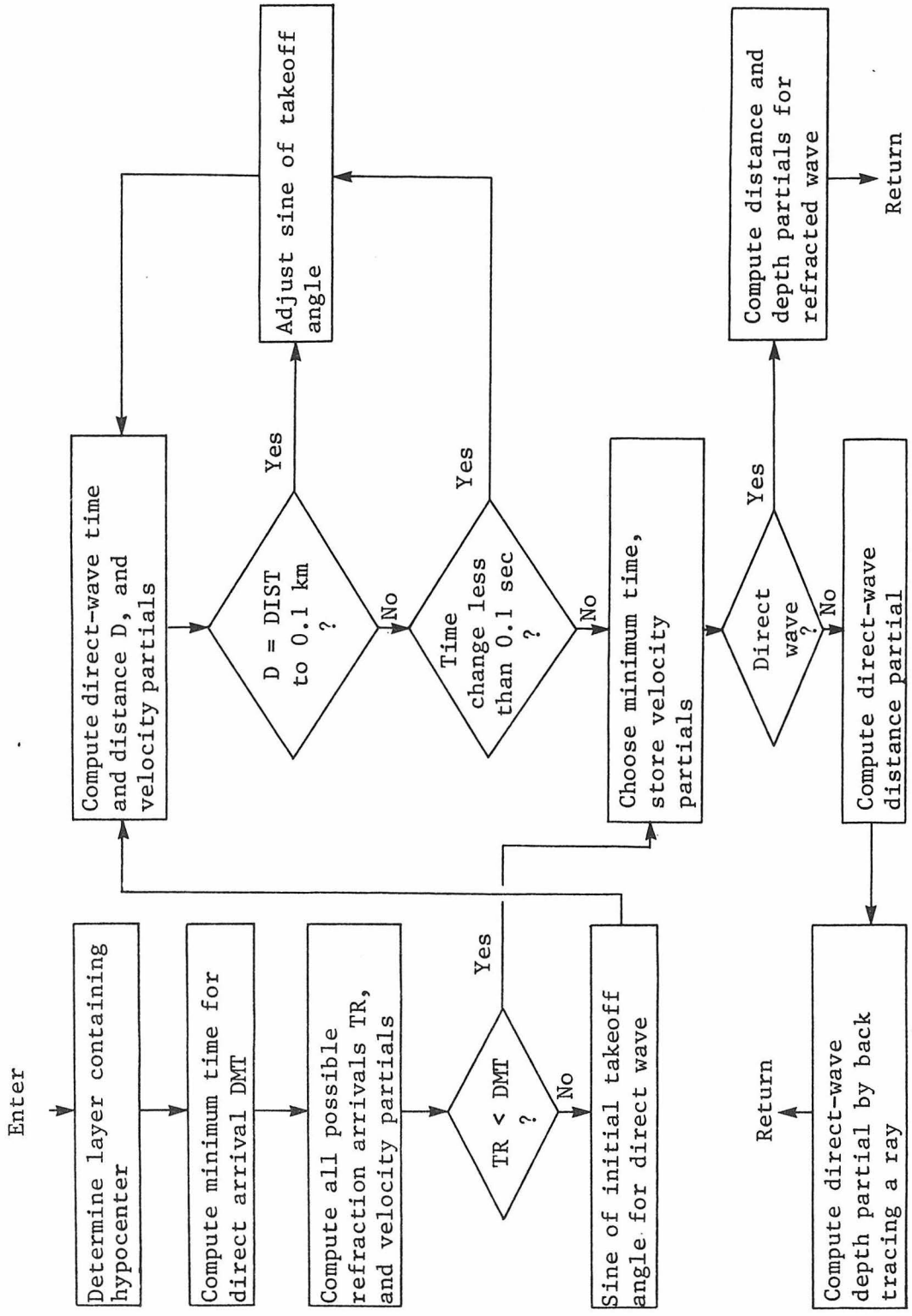

Figure A-3. Flow chart of subroutine TTIM.

and V_H is the velocity in the layer containing the hypocenter. For direct arrivals, numerical estimates are used. The distance partial for the direct ray is readily available from the times and distances of the final two iterations of computing the direct arrival. The depth partial for the direct ray is computed by changing the emergence angle of the ray very slightly and tracing the new ray through the epicentral distance to obtain a new depth.

Partial derivatives of the travel times with respect to the layer velocities are computed analytically for both refraction and direct arrivals using

$$\delta T = \int \frac{\delta V}{V^2} \, ds \qquad \text{(A-2)}$$

from Backus and Gilbert (1969). The integral is taken along the path of the ray. For this application, a layered velocity model, (A-2) reduces to $\partial T/\partial V_i = s_i/V_i^2$ where s_i is the distance traveled in the layer having velocity V_i. Using this form is convenient here because the travel path is easily known for the refraction arrivals and has been computed for the direct arrival.

Performance of the inversion program was checked out using synthetic data derived from the Galway Lake data to be studied. After each earthquake was located individually, the residual times were subtracted from the observed times to give a new set of test data that was error free. Using the test data <u>per se</u>, the program correctly

calculated zero changes in the model. Then, runs were made in which only a hypocenter location was changed, or only a station delay, or only a layer velocity. For perturbations of a delay or a velocity, the program corrected the perturbed element of the model quickly without making any significant changes in the remaining elements. For a perturbation of one hypocenter, the program restored the latitude and longitude, but undercorrected the depth somewhat, a one-km error, while making slight adjustments to the rest of the model parameters. Velocities were changed by about 0.05 km/sec, delays by about 0.05 sec, and other locations by about 0.04 km. These results reflect basic difficulties in depth control rather than program error.

The covariance matrix of the solution is given by $[\cos\theta(A^TV^{-1}A) + \sin\theta(W^{-1})]^{-1}$ from which error estimates may be obtained from expressions given by Bjerhammar (1973). Each diagonal term, such as Q_{xx} or Q_{yy}, is the variance of its corresponding model parameter. The off-diagonal terms, such as Q_{xy}, are the covariances between the two parameters and a useful indicator of the degree of dependence of the parameters. An error ellipse relating any two model parameters has λ_1 and λ_2 as semi-axes and α_1 as the angle to the λ_1 axis where

$$\lambda = \frac{Q_{xx} + Q_{yy}}{2} \pm \left[\frac{(Q_{xx} - Q_{yy})^2 + 4\,Q_{xy}^2}{4} \right]^{\frac{1}{2}} \qquad \text{(A-3)}$$

and

$$\tan 2\alpha_1 = \frac{2Q_{xy}}{Q_{xx} - Q_{yy}} .$$

If Q_{xy} is much smaller than Q_{xx} and Q_{yy}, then the error ellipse lies along one of the axes and the two parameters are relatively independent in the solution. If Q_{xx}, Q_{yy} and Q_{xy} are all of similar magnitude, the ellipse is highly elliptical and skewed at about 45^{o}. Then, the solution can tradeoff freely between the two parameters. This type of analysis can be extended to higher dimensions.

Appendix 2

NUMERICAL RESULTS

TABLE A2-1

HYPO71 INITIAL TRIAL MODEL

TRIAL LOCATIONS

EVENT	LAT DEG/MIN	LONG DEG/MIN	DEPTH KM	TIME SEC
1	34 32.06	116 30.18	1.47	1.99
2	34 31.87	116 27.60	8.88	53.43
3	34 31.32	116 29.10	2.19	44.77
4	34 31.03	116 28.90	7.13	5.07
5	34 31.08	116 29.20	1.87	57.53
6	34 31.68	116 29.40	2.46	46.93
7	34 31.72	116 29.80	1.91	24.73
8	34 31.30	116 29.10	4.81	43.25
9	34 30.89	116 28.90	0.55	45.74
10	34 31.09	116 29.80	0.90	53.61
11	34 30.36	116 29.20	0.28	57.75
12	34 30.44	116 29.50	0.99	35.70
13	34 30.51	116 29.90	0.64	17.41
14	34 32.48	116 30.10	5.95	12.50
15	34 31.82	116 30.20	1.77	4.42
16	34 30.39	116 30.00	3.57	56.19
17	34 31.81	116 29.40	0.73	8.89
18	34 30.84	116 28.80	0.59	57.22
19	34 32.07	116 30.00	1.75	23.83
20	34 31.17	116 29.40	1.86	21.65

TRIAL VELOCITIES

LAYER	THICKNESS KM	P-VEL KM/SEC	S-VEL KM/SEC
1	0.20	2.50	1.44
2	1.40	4.80	2.77
3	0.90	6.00	3.45
4	23.50	6.10	3.52

TRIAL STATION DELAYS

STATION	TIME SEC
BESS	-0.13
ARGO	0.0
GALW	0.11
JOHN	-0.29
RUIN	-0.05
EMER	-0.21
RMR	-0.03
HDG	0.07
SDW	-0.07

TABLE A2-2

HYPO71, DELAYS CONSTRAINED, FINAL MODEL

NEW LOCATIONS

EVENT	LAT DEG/MIN	LONG DEG/MIN	DEPTH KM	TIME SEC
1	34 31.92	116 30.61	2.35	1.84
2	34 31.60	116 28.19	8.36	53.37
3	34 31.12	116 29.52	2.50	44.65
4	34 30.92	116 29.57	7.25	4.92
5	34 31.00	116 29.73	3.00	57.36
6	34 31.37	116 29.87	2.98	46.76
7	34 31.61	116 30.30	2.63	24.56
8	34 31.13	116 29.87	5.46	43.08
9	34 31.01	116 29.55	4.32	45.75
10	34 31.07	116 30.27	0.96	53.77
11	34 30.22	116 29.83	0.95	57.63
12	34 30.50	116 30.25	3.48	35.61
13	34 30.47	116 30.46	1.39	17.30
14	34 32.45	116 30.61	6.71	12.30
15	34 31.66	116 30.61	2.22	4.26
16	34 30.33	116 30.60	4.18	56.01
17	34 31.71	116 29.76	1.50	8.84
18	34 30.65	116 29.38	1.35	57.14
19	34 31.91	116 30.65	2.34	23.66
20	34 31.08	116 29.93	2.89	21.49

NEW VELOCITIES

LAYER	THICKNESS KM	P-VEL KM/SEC	S-VEL KM/SEC
1	0.20	2.37	1.37
2	1.40	4.44	2.56
3	0.90	5.62	3.23
4	23.50	5.85	3.38

NEW STATION DELAYS

STATION	TIME SEC
BESS	-0.11
ARGO	-0.05
GALW	0.11
JOHN	-0.12
RUIN	-0.13
EMER	-0.13
RMR	-0.13
HDG	-0.04
SDW	-0.15

RMS RESIDUALS AT EACH ITERATION, 0-10, SEC

0.1879 0.1605 0.1688 0.1787 0.1554 0.1534
0.1514 0.1492 0.1522 0.1473 0.1470

TABLE A2-3

HYPO71, SHIFTED, FINAL MODEL

NEW LOCATIONS

EVENT	LAT DEG/MIN	LONG DEG/MIN	DEPTH KM	TIME SEC
1	34 31.93	116 30.62	2.21	1.85
2	34 31.60	116 28.21	8.26	53.39
3	34 31.13	116 29.54	2.35	44.66
4	34 30.93	116 29.60	7.19	4.94
5	34 30.99	116 29.63	2.53	57.41
6	34 31.37	116 29.87	2.84	46.78
7	34 31.61	116 30.32	2.47	24.58
8	34 31.13	116 29.89	5.38	43.10
9	34 30.78	116 29.39	1.69	45.74
10	34 31.08	116 30.29	0.90	53.78
11	34 30.24	116 29.86	0.92	57.65
12	34 30.51	116 30.27	3.35	35.63
13	34 30.48	116 30.48	1.31	17.31
14	34 32.44	116 30.64	6.61	12.33
15	34 31.66	116 30.61	2.13	4.28
16	34 30.34	116 30.62	4.08	56.03
17	34 31.72	116 29.76	1.44	8.85
18	34 30.66	116 29.40	1.29	57.15
19	34 31.90	116 30.67	2.04	23.68
20	34 31.08	116 29.94	2.75	21.51

NEW VELOCITIES

LAYER	THICKNESS KM	P-VEL KM/SEC	S-VEL KM/SEC
1	0.20	2.37	1.37
2	1.40	4.42	2.55
3	0.90	5.62	3.23
4	23.50	5.84	3.37

NEW STATION DELAYS

STATION	TIME SEC
BESS	-0.13
ARGO	-0.07
GALW	0.11
JOHN	-0.14
RUIN	-0.15
EMER	-0.14
RMR	-0.16
HDG	-0.08
SDW	-0.17

RMS RESIDUALS AT EACH ITERATION, 0-10, SEC

0.2681 0.1610 0.1585 0.1558 0.1539 0.1512
0.1505 0.1531 0.1506 0.1493 0.1461

TABLE A2-4

VEL-HK, DELAYS FREE, FINAL MODEL

NEW LOCATIONS

EVENT	LAT DEG/MIN	LONG DEG/MIN	DEPTH KM	TIME SEC
1	34 31.90	116 30.27	3.77	1.64
2	34 31.54	116 27.91	7.77	53.32
3	34 31.11	116 29.20	4.05	44.42
4	34 30.89	116 29.21	7.10	4.82
5	34 31.07	116 29.44	4.05	57.15
6	34 31.36	116 29.61	3.93	46.54
7	34 31.62	116 30.00	3.86	24.34
8	34 31.08	116 29.68	5.53	42.97
9	34 31.01	116 29.38	4.33	45.49
10	34 30.92	116 29.93	2.85	53.66
11	34 30.35	116 29.61	3.96	57.53
12	34 30.49	116 29.89	4.03	35.41
13	34 30.47	116 30.16	3.62	17.14
14	34 32.51	116 30.24	7.19	12.19
15	34 31.58	116 30.29	3.47	4.06
16	34 30.35	116 30.27	4.30	55.84
17	34 31.43	116 29.54	2.71	8.63
18	34 30.55	116 29.04	3.29	56.98
19	34 31.83	116 30.37	3.48	23.47
20	34 31.11	116 29.61	3.96	21.27

NEW VELOCITIES

LAYER	THICKNESS KM	P-VEL KM/SEC	S-VEL KM/SEC
1	0.20	2.46	1.42
2	4.30	5.07	2.92
3	23.00	6.06	3.29

NEW STATION DELAYS

STATION	TIME SEC
BESS	-0.09
ARGO	0.01
GALW	0.11
JOHN	-0.09
RUIN	0.03
EMER	0.0
RMR	0.0
HDG	0.07
SDW	-0.01

RMS RESIDUALS AT EACH ITERATION, 0-10, SEC

0.2406 0.1598 0.1529 0.1487 0.1470 0.1451
0.1443 0.1438 0.1434 0.1431 0.1427

TABLE A2-5

VEL-HK, DELAYS FIXED, FINAL MODEL

NEW LOCATIONS

EVENT	LAT DEG/MIN	LONG DEG/MIN	DEPTH KM	TIME SEC
1	34 31.99	116 30.43	3.63	1.70
2	34 31.64	116 28.21	7.71	53.40
3	34 31.25	116 29.51	3.99	44.50
4	34 31.02	116 29.61	6.90	4.92
5	34 31.14	116 29.61	3.91	57.22
6	34 31.46	116 29.82	3.88	46.61
7	34 31.71	116 30.16	3.72	24.41
8	34 31.17	116 29.76	5.02	43.05
9	34 31.10	116 29.58	4.27	45.56
10	34 31.00	116 30.08	2.75	53.73
11	34 30.44	116 29.76	3.77	57.60
12	34 30.60	116 30.05	3.93	35.48
13	34 30.58	116 30.31	3.51	17.20
14	34 32.53	116 30.44	6.62	12.29
15	34 31.62	116 30.43	3.28	4.12
16	34 30.47	116 30.42	4.21	55.91
17	34 31.48	116 29.73	2.60	8.69
18	34 30.68	116 29.25	3.33	57.05
19	34 31.90	116 30.54	3.35	23.54
20	34 31.22	116 29.80	3.88	21.34

NEW VELOCITIES

LAYER	THICKNESS KM	P-VEL KM/SEC	S-VEL KM/SEC
1	0.20	2.44	1.41
2	4.30	4.94	2.85
3	23.00	5.99	3.25

NEW STATION DELAYS

STATION	TIME SEC
BESS	-0.11
ARGO	-0.05
GALW	0.11
JOHN	-0.12
RUIN	-0.13
EMER	-0.13
RMR	-0.13
HDG	-0.04
SDW	-0.15

RMS RESIDUALS AT EACH ITERATION, 0-10, SEC

0.2570 0.1637 0.1591 0.1554 0.1513 0.1484
0.1467 0.1447 0.1440 0.1436 0.1430

TABLE A2-6

VEL-1 INITIAL TRIAL MODEL

TRIAL LOCATIONS

EVENT	LAT DEG/MIN	LONG DEG/MIN	DEPTH KM	TIME SEC
1	34 32.00	116 30.50	1.47	1.99
2	34 31.60	116 28.20	8.88	53.43
3	34 31.20	116 29.50	2.19	44.77
4	34 31.00	116 29.50	7.13	5.07
5	34 31.10	116 29.70	1.87	57.53
6	34 31.50	116 29.80	2.46	46.93
7	34 31.70	116 30.20	1.91	24.73
8	34 31.10	116 29.80	4.81	43.25
9	34 31.00	116 29.50	0.55	45.74
10	34 31.10	116 30.10	0.90	53.61
11	34 30.40	116 29.80	0.28	57.75
12	34 30.60	116 30.10	0.99	35.70
13	34 30.60	116 30.30	0.64	17.41
14	34 32.50	116 30.50	5.95	12.50
15	34 31.70	116 30.40	1.77	4.42
16	34 30.40	116 30.50	3.57	56.19
17	34 31.60	116 29.70	0.73	8.89
18	34 30.80	116 29.30	0.59	57.22
19	34 32.00	116 30.50	1.75	23.83
20	34 31.20	116 29.90	1.86	21.65

TRIAL VELOCITIES

LAYER	THICKNESS KM	P-VEL KM/SEC	S-VEL KM/SEC
1	0.20	2.50	1.44
2	1.30	4.80	2.76
3	1.00	5.20	3.00
4	1.00	5.40	3.11
5	1.00	5.60	3.23
6	25.00	6.20	3.57

TRIAL STATION DELAYS

STATION	TIME SEC
BESS	-0.15
ARGO	-0.09
GALW	0.11
JOHN	-0.18
RUIN	-0.16
EMER	-0.17
RMR	-0.18
HDG	-0.09
SDW	-0.19

TABLE A2-7

VEL-1 FINAL MODEL

NEW LOCATIONS

EVENT	LAT DEG/MIN	LONG DEG/MIN	DEPTH KM	TIME SEC
1	34 31.99	116 30.41	3.20	1.69
2	34 31.62	116 28.18	8.13	53.36
3	34 31.20	116 29.50	3.33	44.51
4	34 30.97	116 29.52	7.21	4.89
5	34 31.07	116 29.62	3.35	57.22
6	34 31.42	116 29.83	3.58	46.62
7	34 31.69	116 30.20	3.35	24.40
8	34 31.16	116 29.77	5.25	43.03
9	34 30.95	116 29.47	3.35	45.56
10	34 31.10	116 30.06	1.98	53.67
11	34 30.39	116 29.73	3.01	57.57
12	34 30.53	116 30.11	3.57	35.48
13	34 30.58	116 30.33	3.02	17.19
14	34 32.47	116 30.51	6.68	12.27
15	34 31.67	116 30.46	2.87	4.10
16	34 30.41	116 30.47	4.09	55.92
17	34 31.72	116 29.70	2.41	8.67
18	34 30.72	116 29.31	2.90	57.03
19	34 31.94	116 30.57	2.80	23.52
20	34 31.17	116 29.84	3.45	21.35

NEW VELOCITIES

LAYER	THICKNESS KM	P-VEL KM/SEC	S-VEL KM/SEC
1	0.20	2.38	1.37
2	1.30	4.48	2.58
3	1.00	4.78	2.75
4	1.00	5.05	2.91
5	1.00	5.68	3.28
6	25.00	5.95	3.43

NEW STATION DELAYS

STATION	TIME SEC
BESS	-0.11
ARGO	-0.05
GALW	0.11
JOHN	-0.12
RUIN	-0.13
EMER	-0.13
RMR	-0.13
HDG	-0.04
SDW	-0.15

RMS RESIDUALS AT EACH ITERATION, 0-10, SEC

0.2106 0.1504 0.1451 0.1431 0.1417 0.1409
0.1403 0.1399 0.1390 0.1387 0.1382